# Nonlinear Wave Interactions with Submerged Obstacles With or Without Current

by

Yuming Liu

BS, Civil Engineering, Hohai University, China, 1985
MS, Coastal Engineering, The University of Florida, 1988

Submitted to the Department of Ocean Engineering
in partial fulfillment of the requirements for the degree of

Doctor of Philosophy in Hydrodynamics

at the

MASSACHUSETTS INSTITUTE OF TECHNOLOGY

May 1994



Author .....
Department of Ocean Engineering
April 11, 1994

Certified by .....
Dick K.P. Yue
Associate Professor of Ocean Engineering
Thesis Supervisor

Accepted by .....
A. Douglas Carmichael
Chairman, Departmental Committee on Graduate Students

# Nonlinear Wave Interactions with Submerged Obstacles With or Without Current

by

Yuming Liu

Submitted to the Department of Ocean Engineering
on April 11, 1994, in partial fulfillment of the
requirements for the degree of
Doctor of Philosophy in Hydrodynamics

## Abstract

We study the nonlinear interactions of surface waves with general two- and three-dimensional bodies which are either stationary, or undergoing imposed oscillatory or steady motions. Despite the success of linearized theory for a wide variety of wave-body problems, nonlinear effects are important and even essential for many applications. These include cases when the leading-order answer from linearized theory is trivial or singular, and when the solution is dominated by strong resonant or coupled nonlinear interactions. Through analyses and numerical simulations, this thesis addresses three general and related classes of problems for which such nonlinear effects are of theoretical interest and practical importance to naval architecture and coastal engineering. For simplicity of the numerical simulation — a high-order spectral method using free-surface Fourier basis functions is employed — we consider only submerged bodies or bottom variations.

A significant problem for which linearized theory predicts trivial (zero) result is the horizontal drift force on a submerged circular cylinder. By including nonlinearities up to third order, we quantify a *negative* drift force which is in good agreement with experiments. Surprisingly, this force is a result of quadratic interaction between the first- and third-order (first-harmonic) waves rather than self-interaction of the second-order (second-harmonic) waves. Similar interactions also play a major role for three-dimensional bodies. A systematic study is performed for submerged spheroids where it is shown that nonlinear mean effects generally oppose linearized predictions and, for slender geometries, can be comparable in magnitude. Thus, the mean pitch moment in head seas, for example, can be positive, negative or zero depending on wave steepness and submergence.

When forward speed is present, nonlinear effects of the seakeeping problem become more critical because of the dependence of wave radiation on forward speed. In particular, at critical frequency corresponding to $\tau \equiv \omega_e U/g = 1/4$, the group velocities of two of the wave components vanish, the associated energy can no longer be radiated away, and classical analysis predicts an unbounded solution. By considering the full geometry rather than a point source, we obtain an analytic proof that the

linear solution is in fact *bounded* for a general class of submerged and surface-piercing geometries. Further analyses establish also the important consequence that transient effects associated with body accelerations actually decay an order of magnitude *faster* than classical-theory predictions. We confirm these findings by detailed numerical simulations. Despite the above, linear results near critical frequency are still unrealistically large. When nonlinear interactions are included, a third-order change in the dispersion relationship is found to produce appreciable corrections to the motion coefficients. Such corrections are shown to be *first-order* in wave steepness.

Nonlinear effects must also be considered when resonance occurs. We investigate this by considering Bragg reflection of waves by an undulated bottom. The high-order spectral method is extended for this case to confirm existing theoretical and experimental results for linear and subharmonic Bragg resonances. When wave nonlinearities are included, we discover a new *superharmonic* Bragg mechanism for reflected and transmitted waves associated with quartet interactions between the free surface and the bottom.

This thesis addresses the important nonlinear effects in wave interactions with submerged bodies in the context of potential theory. With the use of free-surface Chebyshev or Legendre basis functions, the present high-order spectral method can be generalized to surface-intersecting bodies.

Thesis Supervisor: Dick K.P. Yue
Title: Associate Professor of Ocean Engineering

# Acknowledgments

I wish to express my sincere appreciation and gratitude to my advisor, Professor. D.K.P. Yue, for his continuous guidance, stimulation, and encouragement throughout this study. I also direct my thanks to Professors J.N. Newman, M.S. Triantafyllou, and H. Schmidt for their patience in reviewing this thesis.

The financial support was provided by K.C. Wong Education Foundation Ltd. of Hong Kong, the National Science Foundation, and the Office of Naval Research (grants N00014-89-J-1713 and N00014-94-1-0142). It is gratefully acknowledged. Some computations were performed on a Cray Y-MP at POPS Supercomputer Center, and on a Cray-2S at Cray Research, Inc.

Finally I would like to thank my wife, Yujia Huang, for her endless understanding and support.

# Contents

# List of Figures

# List of Tables

# Chapter 1

# Introduction

The nonlinear interaction of surface waves with a body and/or bottom topography is a fundamental problem of theoretical interest and practical importance in naval architecture, offshore and coastal engineering. When a circular cylinder is fixed under the free surface in the presence of waves, for example, it has been observed in experiments (Salter *et al.* 1976; Longuet-Higgins 1977; Inoue & Kyozuka 1984; Miyata *et al.* 1988) that the body experiences a negative horizontal drift force which is not predicted by linearized potential theory (Maruo 1960; Ogilvie 1963). The existence of such negative drift force can be attributed to high-order free-surface effects (Liu *et al.* 1992). The accurate prediction of this force is of evident importance to the design of mooring lines of underwater pipebridges. For a submerged spheroid in head seas, the inclusion of strong nonlinear wave effects can change the direction of the mean pitch moment from bow-down to bow-up (Lee & Newman 1991; Liu & Yue 1994a). Because of no restoring force, a large rotation of the spheroid can be resulted from even a small steady moment if it acts on the body for a sufficiently long period of time. Thus, the understanding of nonlinear effects of this problem should be critical for the operation of submarines and underwater vehicles. In addition, it has been known that second-order difference- and sum-frequency wave excitations may cause large subharmonic resonant motions of moored vessels or offshore platforms (*e.g.* Ogilvie 1983; Emmerhoff & Sclavounos 1992; Newman 1993) and 'springing' (superharmonic resonance) of tension-leg platforms (TLP's) (*e.g.* Ogilvie 1983; Kim

& Yue 1988). Recently, the third-order wave effect (*e.g.* Newman 1994) has also been found to play a major role for the occurrence of 'ringing' of offshore structures in deep water (Jefferys 1993; Stokka 1994). For ship-motion problems, on the other hand, it is well known that classical theories (*e.g.* Haskind 1954; Havelock 1958; Newman 1978) fail to provide any satisfactory predictions at the critical frequency where two of the wave components are resonant. To suppress resonance and obtain reasonable answers there, the third-order free-surface effects must be included (Dagan & Miloh 1982; Akylas 1984; Liu & Yue, 1994c). In nearshore areas, wave motions are generally known to be highly nonlinear due to the effect of bottom topography (Mei 1983). When surface waves propagate over an undulated bottom, in particular, large resonant reflection can be caused from both linear and high-order Bragg resonances (Davies & Heathershaw 1984; Mei 1985; Guazzelli *et al.* 1992; Liu & Yue 1994d). Such resonance mechanisms in wave-bottom interactions provide an important alternative for the protection of beaches. In open seas, significant energy transfer among different wave components (Philips 1960; Longuet Higgins 1962) occurs due to quartet or quintet wave resonances. This nonlinear resonant effect is of obvious significance to the prediction of the spectrum of ocean waves (*e.g.* Hasselmann 1962, 1963a, 1963b; Resio & Perrie 1991).

Despite the importance of nonlinear wave-body/bottom interaction problems, a general analytical method or numerical scheme which can account for nonlinear boundary effects accurately and efficiently is not available yet. Most existing nonlinear solutions have so far been obtained through numerical simulations. A commonly used numerical scheme for the study of wave-body/bottom interactions is the boundary-integral-equation method (BIEM) using wave-source Green's function (Mei 1978; Korsmeyer *et al.* 1988; Lee *et al.* 1991). Because no Green's function satisfies the nonlinear free-surface boundary conditions, the discretization of the entire free surface is generally necessary. This leads to a linear system involving a large number of unknowns (typically $N = O(10^{4\sim5})$) and its solution requires $O(N^{2\sim3})$ computational efforts in general. The associated numerical error due to boundary discretizations is typically of $O(\Delta^{1\sim2})$, where $\Delta$ represents the size of boundary elements (panels). For

practical problems, the required minimum computational burden may not be afforded by available computational facilities. In the study of nonlinear wave kinematics using a quadratic-boundary-element method, for example, the use of $O(1000)$ elements on the free-surface in a doubly-periodic domain requires $O(100)$ Cray-Y/MP cpu hours in order to observe wave overturning phenomena (Xu & Yue 1992). In addition to the BIEM, the finite-difference and finite-volume methods are also used for solving nonlinear wave-body/bottom problems. Compared to the BIEM, these methods need to discretize the whole fluid domain and the number of total unknowns involved is even much larger. Overall, the success of these numerical methods employing direct surface or volume discretizations has so far been limited to two-dimensional or axisymmetric problems (*e.g.* Longuet-Higgins & Cokelet 1976; Vinje & Brevig 1981; Dommermuth & Yue 1987a). Based on the assumption of weak nonlinearity and mode-coupling idea, a high-order spectral method (Dommermuth & Yue 1987b) has recently been demonstrated to be effective for the study of nonlinear wave-wave interactions. However, the usefulness of this method is limited to moderately steep waves.

In summary, nonlinear boundary effects are critical even in the absence of viscosity for many wave-body/bottom applications. These include cases when the leading-order prediction from linearized theory is trivial or singular, and when the solution is dominated by strong resonant or coupled nonlinear interactions. Due to the limitation of theoretical and computational capabilities, the understanding of such significant nonlinear effects has been far from satisfactory.

This thesis focuses on the study of nonlinear wave interactions with general two- and three-dimensional bodies which are either stationary, or undergoing imposed oscillatory or steady motions. Through analyses and numerical simulations, we address three general and related classes of nonlinear problems of theoretical interest and practical importance to naval architecture and coastal engineering: (1) mean wave effects on a body at zero forward speed; (2) the behaviour of seakeeping solution near the critical frequency; (3) Bragg resonant reflection of surface waves by bottom ripples. For the numerical formulation, a high-resolution nonlinear spectral method

is extended to include bodies. For simplicity, free-surface Fourier spectral functions are employed and submerged bodies are considered. The major finding and results include: (i) the quantification of the negative horizontal drift force on a submerged circular cylinder; (ii) nonlinear solutions of the mean wave force and pitch moment on a submerged spheroid; (iii) a formal proof that the linear seakeeping solution at the critical frequency is bounded for a general class of submerged and surface-piercing bodies; (iv) an analysis to show that the decay rate of linear transients associated with body accelerations is actually an order of magnitude faster than classical theory predictions; (v) nonlinear solutions for the motion coefficients of the seakeeping problem near the critical frequency; (vi) the discovery of a new superharmonic Bragg mechanism for reflected and transmitted waves associated with quartet resonant interactions between the surface and the bottom.

### (I) The negative horizontal drift force on a submerged circular cylinder

A problem for which linearized theory fails to provide the leading-order prediction is the mean wave force on a fixed submerged circular cylinder. In this case, it has been known that the horizontal drift force vanishes up to second-order in wave steepness according to linearized potential theory (Maruo 1960; Ogilvie 1963). This result is in contrast to experimental observations (*e.g.* Salter *et al.* 1976) that a free cylinder just awash experiences a negative drift force which causes it to move towards the wavemaker. Longuet-Higgins (1977) suggested that this negative drift force can most likely be attributed to wave breaking. The measurements of Miyata *et al.* (1988) and Inoue & Kyozuka (1984) do not support all of Longuet-Higgins' predictions. They found that as the cylinder was moved closer to the free surface, which led to more intense breaking, the negative horizontal drift force was actually reduced and ultimately reversed sign. Such disagreement between predictions and measurements leads to a presumption that the negative horizontal drift force is due to high-order potential effects.

According to a regular perturbation analysis beyond the second-order, the next possible contribution to the mean force is fourth-order due to quadratic interactions

of high-order potentials, which include self-interactions of the second-order zeroth- and second-harmonic waves, and quadratic interaction of the first- and third-order first-harmonic waves. For a submerged body in deep water, in general, locked waves are small compared to free waves at the second-order. Thus the effect of the zeroth-harmonic wave should be unimportant compared to that of the other two harmonics. On the other hand, the second-harmonic (free) wave becomes considerable only when the body is very close to the free surface because it decays with depth much faster than the first-harmonic wave. To corroborate with the measurements of Miyata *et al.* (1988) and Inoue & Kyozuka (1984), we deduce that the negative drift force must be a result of the quadratic interaction of the first- and third-order first-harmonic waves rather than the self-interaction of the second-order second-harmonic waves which may actually reduce this force. Such intuitive deduction is fully confirmed by our fourth-order potential-flow calculations (in chapter 3) which agree well with the laboratory experiments of Miyata *et al.* (1988).

### (II) The mean force and moment on a submerged spheroid

The question then arises as to whether nonlinear interactions play an equally important role for a three-dimensional body. To address this, we consider the mean force and moment on a spheroid. Under beam sea conditions, there is no horizontal drift force according to the strip theory prediction (for circular sections). If the three-dimensional effect is included, a positive second-order horizontal drift force is expected in principle, which vanishes as the body aspect ratio increases. When strong nonlinear interactions are involved, a fourth-order negative horizontal drift force can also be anticipated for a near-surface spheroid. Thus, three-dimensional and nonlinear effects produce opposing horizontal drift forces. For a given spheroid in an ambient wave field, there must be a particular depth at which the total horizontal drift force is identically zero.

In head seas, the slender body theory (*e.g.* Lee & Newman 1971) predicts that the vertical drift force is dominated by the 'IB' interaction between the incident wave (I) and the body disturbance (B), whereas the mean pitch moment vanishes as the

'IB' interaction is symmetric about the midbody section. A three-dimensional panel method solution (Lee & Newman 1991), however, reveals the presence of a positive (bow-down) mean pitch moment which is due to the quadratic (BB) interaction of the body disturbance itself. Such non-zero mean pitch moment has strong dependence on body slenderness. For a high aspect-ratio spheroid near the free surface, nonlinear wave effects can thus be expected to be critical.

Through careful initial-value simulations, in chapter 4, we obtain accurate nonlinear solutions for the mean force and pitch moment on the body including complete fourth-order corrections. In particular, it is found that when nonlinear free-surface effects are included, the mean pitch moment changes its direction from bow-down to bow-up as the incident wave steepens or when the submergence is decreased. Like the horizontal drift force in beam seas, for a given sea state and body aspect ratio, a submergence can be found at which the mean pitch moment is minimized. Significantly, we are able to establish a simple formula to estimate that depth.

### (III) The classical seakeeping solution near the critical frequency

When forward speed is present, nonlinear effects of the seakeeping problem become even more critical because of the effect of the forward speed on the radiation of wave energy. Of particular interest is the case where the group velocities of two of the wave components vanish so the associated energy can no longer be radiated away. This happens at the particular value of the frequency ($\omega$) and forward speed ($U$) combination $\tau = U\omega/g = \frac{1}{4}$, where $g$ is the gravitational acceleration. Before detailed nonlinear simulations are performed, it is necessary to perceive the linear solution completely.

For a single source, it is well known that the Green's function becomes unbounded at $\tau = \frac{1}{4}$ (Haskind 1954; Wehausen & Laitone 1960). Physically, this may be explained in terms of the group velocities (in still water) of two components of the accompanying wave which approach $U$ as $\tau \to \frac{1}{4}$ (from below). The associated energy can no longer be radiated away, and the amplitudes of these wave components tend to grow indefinitely. Since the problem for a general body can, in principle, be represented by

an appropriate distribution of such sources, it is widely accepted that the resulting seakeeping problem must likewise be singular at $\tau = \frac{1}{4}$ (*e.g.* Dagan & Miloh 1982). This appears also to be confirmed by existing approximate theories and calculations (*e.g.* Havelock 1958; Newman 1959; Wu & Eatock Taylor 1988) suggesting that this difficulty may be inherent in the linearized problem.

With careful numerical calculations for the case of submerged circular and elliptical cylinders, Grue & Palm (1985) and Mo & Palm (1987) recently offered strong numerical evidence that the amplitudes of the resonant upstream and downstream waves approach the same finite limit as $\tau \to \frac{1}{4}$. Since their equations are singular at $\tau = \frac{1}{4}$, they consider the problem undetermined at this limiting value. Through an asymptotic analysis, in chapter 5, we offer a formal proof in the frequency domain that the linear solution of the seakeeping problem is finite if and only if a certain geometric condition is satisfied. This is in contrast to existing theories based upon the single source result. For a submerged body, a necessary and sufficient condition is that the body must have non-zero volume. For a surface-piercing body, a sufficient condition is derived which has a geometric interpretation similar to that of John (1950). As an illustration, we provide an analytic (closed-form) solution for the case of a submerged circular cylinder oscillating near $\tau = \frac{1}{4}$, which compares well with the calculations of Grue & Palm (1985). Also, we identify the underlying difficulties of existing approximate theories and numerical computations near $\tau = \frac{1}{4}$, and offer a simple remedy for the latter.

### (IV) The time-dependence of the wave resistance of a body

An immediate implication of the frequency-domain result is the time-dependence of the force on a body due to an initial change in the velocity. This is directly related to the question of how rapidly transients associated with the abrupt motions of a floating body decay. The rate at which transient oscillations vanish and measurements taken is of some concern in model tests especially for unsteady and local effects. The question of the behavior of transients comes up also in almost all numerical simulations in the time domain and directly affects our ability to extract steady-state predictions for

resistance problems and to obtain meaningful results for general seakeeping problems.

Despite the obvious importance, this problem appears to have been addressed only for the idealized case of a single translating source of *known* strength. Havelock (1949) considered the two-dimensional problem of the wave resistance of a submerged circular cylinder impulsively started from rest. By approximating the body as a point dipole of constant strength, he derived a closed-form solution for the wave resistance. The significant finding is that for a given forward speed $U$, the resistance oscillates about the steady value with the frequency $\omega_c = g/4U$, and the oscillation decays only like $t^{-\frac{1}{2}}e^{i\omega_c t}$ as $t \to \infty$. This result was extended to three dimensions by Wehausen (1964) who considered a constant source started abruptly and obtained that the unsteady resistance vanishes like $t^{-1}e^{i\omega_c t}$ as $t \to \infty$.

The frequency-domain result suggests that with the removal of the $\tau = \frac{1}{4}$ singularity, the actual decay rate of transients must necessarily be an order of magnitude faster than the single-source predictions of Havelock (1949) and Wehausen (1964) for a body which satisfies the requisite geometric condition. In chapter 6, this is proved in a thorough analysis of the time-dependence of the wave resistance of a body starting from rest. The exact decay rate is found to be respectively proportional to $t^{-\frac{3}{2}}$ and $t^{-2}$ for two- and three-dimensional bodies in contrast to $t^{-\frac{1}{2}}$ and $t^{-1}$ derived by approximating a body using constant sources at a particular point or on a special plane. These results are confirmed by our detailed numerical simulations.

### (V) Nonlinear wave radiation near the critical frequency

Due to weak wave radiation near the cut-off, the linear solution is still very large and varies sharply near $\tau = \frac{1}{4}$. Nonlinear effects must then play a prominent role especially through corrections in group velocities of resonant waves. For a single source, the third-order change in the dispersion relation due to free-surface nonlinearity has been shown to be critical in suppressing the first-order resonance at the critical frequency and obtaining a finite solution (Dagan & Miloh, 1982). In principle, such nonlinear effects should also be contemplated for a real physical body. To address this, in chapter 7, we consider nonlinear wave radiation of a submerged circular cylinder

which moves forward while undergoing small oscillations.

With long-time simulations, steady-state (limit-cycle) solutions for the radiation force on the body can be obtained. When nonlinear interactions are included, the group velocities of resonant waves near $\tau = \frac{1}{4}$ retain a significant change which is found to be first-order in wave steepness. Because of this, the nonlinear steady-state solution is reached much faster than the linear solution in initial-value simulations. Like that for a single source, the inclusion of the third-order free-surface nonlinearity is demonstrated to produce appreciable corrections to the motion coefficients near the critical frequency. Such corrections are shown to be first-order in wave steepness.

### (VI) Nonlinear wave reflection by an undulated bottom

Finally we consider a problem for which nonlinear effects are amplified due to a near-periodic placement of weak scatterers. Because of strong Bragg resonance, large reflection can occur for surface waves travelling over undulated bottom topography. Laboratory experiments of Davies & Heathershaw (1984) confirm this prediction and suggest a possible practical application of this mechanism for the protection of beaches. For mild wave and bottom slopes, reflection at or near Bragg resonance is well predicted by perturbation theory based on multiple scales and the assumption of linearized surface waves (Mei 1985).

For moderate to large wave and/or bottom steepnesses, higher-order Bragg resonances must also occur due to nonlinear interactions between surface waves and bottom undulations. Of especial interests are the second-order Bragg resonances which result from second-order bottom or free-surface effects. In principle, they could be understood as the quartet wave resonance, which is well known in ocean wave hydrodynamics (Philips 1960), with certain wave components replaced by bottom undulations. Depending on the inclusion of bottom or free-surface nonlinearity, there can be different types of second-order Bragg resonances.

The significance of the second-order Bragg resonance due to bottom nonlinearity has been demonstrated in experiments of Guazzelli *et al.* (1992). For a bottom containing unidirectional doubly-sinusoidal ripples, they observed significant Bragg

reflection corresponding to differences of the bottom ripple wavenumbers even for small undulation amplitudes. Moreover, this nonlinear resonant reflection can be comparable in magnitude (although not at the same frequency) to that due to linear Bragg effect. Since this phenomenon is a result of high-order bottom effects, it cannot be predicted by the theory of Mei (1985).

When free-surface nonlinearity is included, the second-order Bragg resonance corresponding to sums or differences of incident wave frequencies can also exist. The simplest case for such resonance is when a single normally-incident wave travels over a horizontal bottom with uniformly-sinusoidal ripples. Under the quartet condition (with the incident wave counted twice), a large superharmonic (double-frequency) wave can be reflected or transmitted. Due to this high-order Bragg resonance, significant energy transfer from low to high frequency occurs in a spectrum of ocean waves. Despite its apparent importance in the development of wave spectra in coastal zones, this nonlinear resonance mechanism has not been addressed yet.

In chapter 8, we extend the nonlinear spectral method for this problem and accurately calculate Bragg resonant reflection by undulated bottom topography including nonlinear effects of the free surface and bottom. For both normal and oblique incidences, our numerical solutions confirm existing theoretical and experimental results for linear and subharmonic Bragg resonances. Significantly, we are able to examine the second-order Bragg resonance due to free-surface nonlinearity. For surface waves propagating over a horizontal rippled bottom with uniformly sinusoidal undulations, as an example, we obtain accurate predictions for the resonant superharmonic reflected waves. For moderate bottom slope and wave steepness, the present numerical result agrees well with the regular perturbation theory prediction.

### (VII) The high-order spectral method

For numerical work in this thesis, we employ an efficient high-resolution computational method which is an extension of the high-order spectral method of Dommermuth & Yue (1987b) for nonlinear gravity wave-wave interactions. This method allows interactions between surface waves and the body/bottom up to an arbitrary

order $M$ in wave steepness, and exhibits exponential convergence with respect to M and the number of spectral modes $N$. With fast transform techniques, the computational effort is only linearly proportional to $M$ and $N$. The efficiency and accuracy of the present nonlinear spectral method provides a computational capability for high-resolution calculations not readily available using other numerical methods employing direct surface or volume discretizations. The mathematical formulation and numerical issues associated with the extension of the high-order spectral method to wave-body interaction problems are summarized in chapter 2, while those for wave-bottom interactions are separately given in chapter 8.

This thesis is composed of a total of nine chapters. The development of the numerical method is presented in chapter 2. Except in chapters 5 and 6 where the effect of the critical frequency to the classical linear seakeeping solution is addressed, the understanding of basic nonlinear mechanisms in wave-body/bottom interactions is focused in chapters 3, 4, 7 and 8. Conclusions are drawn in chapter 9. For clarity, major symbols are used consistently and equations, tables, and figures are numbered in terms of chapter number. For convenience, figures for each chapter are located after the last page of the text of that particular chapter. References and appendices are placed at the end of the entire thesis.

# Chapter 2

# The high-order spectral method for nonlinear wave-body interactions

In this chapter, we extend a high-order spectral method which was originally developed for nonlinear wave-wave interactions (Dommermuth & Yue 1987b, hereafter denoted by DY) to the study of nonlinear wave interactions with a submerged body. The present method accounts for the nonlinear interactions among $N_F$ wave modes on the free surface and $N_B$ source modes on the body up to an arbitrary order $M$ in wave steepness. By using fast-transform techniques, the operational count per time step is only linearly proportional to $M$ and $N_F$ (typically $N_F >> N_B$). For a (closed) submerged body in moderately steep waves, exponential convergence with respect to $M$, $N_F$ and $N_B$ is obtained.

The high-order spectral method developed by DY is formally based on the Zakharov equation (Zakharov 1968; Crawford *et al.* 1981) / mode-coupling (Phillips 1960; Benney 1962) idea. The method models interactions up to an arbitrary order $M$ in wave steepness and follows the evolution of a large number (typically $N \sim 10^3$ per dimension) of wave modes through a pseudo-spectral (Fornberg & Whitham 1978) treatment of the nonlinear free-surface conditions. The method exhibits exponential convergence with respect to $M$ and $N$ for waves up to $\sim 80\%$ ($kA \sim 0.35$) of Stokes

limiting steepness (beyond this the convergence is only algebraic), and its efficacy for a variety of wave interaction problems is now well established (see also Dommermuth & Yue 1987c).

This method can be generalized to nonlinear wave-body interactions. At each time step, the nonlinear boundary-value problem is solved up to a specified order $M$ in wave steepness by using perturbation expansions and the spectral method. Given surface elevation and potential, the nonlinear problem is expanded into a sequence of linear boundary-value problems for the perturbation potentials $\Phi^{(m)}, m = 1, \cdots, M$, with Dirichlet and Neumann conditions imposed on mean positions of the free surface and body. The solution for the potential at each order is represented in terms of global free-surface and body basis (spectral) functions. The unknown modal amplitudes are determined by invoking the free-surface and body boundary conditions. The basis functions can be suitably constructed in terms of singularity distributions on the mean free surface and body. For simplicity, free-surface Fourier basis functions are used and submerged bodies are considered. The convergence of the solution with respect to the numbers of free-surface and body spectral modes, $N_F$ and $N_B$, as well as the perturbation order $M$ is exponentially rapid. By using fast transform techniques, the computational effort per time step is linearly proportional to $M$ and $N_F$. The efficiency and accuracy of this high-order spectral method provides a computational capability for high-resolution calculations not readily available using other numerical methods employing direct surface or volume discretizations.

In §2.1, the general initial-boundary-value problem for wave-body problems is reviewed. The numerical formulation for the high-order spectral method including a submerged body is summarized in §2.2, and the implementation of the method is presented in §2.3. After systematically discussing sources of numerical errors in §2.4, we finally establish a simple relation (in §2.5) between results obtained using the present time-domain approach and that by the frequency-domain perturbation methods.

## 2.1 The general initial-boundary-value problem

Consider nonlinear wave interactions with a submerged body in a uniform current. A Cartesian coordinate system is chosen with the origin at the mean water level, the $x$-axis pointing into the current of speed, $-U$, and the $z$-axis positive upwards.

The fluid is assumed homogeneous, incompressible, inviscid, and its motion irrotational. The flow can be described by a velocity potential:

$$\Phi^*(\mathbf{x}, z, t) = \bar{\phi}(\mathbf{x}, z) + \Phi(\mathbf{x}, z, t) \tag{2.1}$$

where $\mathbf{x} = (x, y)$ is a vector in the horizontal plane, $\bar{\phi}$ represents a certain base flow, and $\Phi$ is the wave disturbance. The potential, $\Phi$, satisfies Laplace's equation within the fluid and the normal velocity vanishes on the bottom, $\Phi_z = 0$ on $z = -h_0$. Here the water depth $h_0$ is assumed to be constant (and the problem with variable bottom configurations is separately studied in chapter 8). The kinematic and dynamic boundary conditions to be satisfied at the instantaneous free surface $z = \eta(\mathbf{x}, t)$ are respectively given by:

$$\left.\begin{aligned} &\eta_t + \nabla_{\mathbf{x}}\eta \cdot \nabla_{\mathbf{x}}\Phi - \Phi_z = \bar{\phi}_z - \nabla_{\mathbf{x}}\eta \cdot \nabla_{\mathbf{x}}\bar{\phi}\,, \\ &\Phi_t + g\eta + \nabla\bar{\phi} \cdot \nabla\Phi + \tfrac{1}{2}(\nabla\Phi \cdot \nabla\Phi) = -\tfrac{1}{2}\nabla\bar{\phi} \cdot \nabla\bar{\phi} \end{aligned}\right\} \tag{2.2}$$

for zero atmospheric pressure, where $\nabla_{\mathbf{x}} \equiv (\partial/\partial x, \partial/\partial y)$ denotes the horizontal gradient, and $g$ is the gravitational acceleration. The kinematic boundary condition applied on the body, $S_B(t)$, can be written as:

$$\Phi_n = -\bar{\phi}_n + \mathbf{V}(t) \cdot \mathbf{n} \qquad \text{on} \qquad S_B(t) \tag{2.3}$$

where $\mathbf{n} = (n_x, n_y, n_z)$ is the unit normal out of the body, $\mathbf{V}$ represents the instantaneous body velocity. For initial conditions, the velocity potential $\Phi(\mathbf{x}, 0)$ and the surface elevation $\eta(\mathbf{x}, 0)$ are prescribed. This completes the initial-boundary-value problem for $\Phi$. For calculations, we impose periodic boundary conditions in both

horizontal directions.

The pressure on the body is determined according to Bernoulli's equation:

$$\frac{P(\mathbf{x},z,t)}{\rho} = -\Phi_t - \nabla\bar{\phi}\cdot\nabla\Phi - \frac{1}{2}\nabla\Phi\cdot\nabla\Phi - \frac{1}{2}\nabla\bar{\phi}\cdot\nabla\bar{\phi} + \frac{1}{2}U^2 \tag{2.4}$$

where $\rho$ is the fluid density. The instantaneous force on the body is obtained by direct integration of (2.4).

## 2.2 Formulation of the high-order spectral method

In this section, we employ the time-domain perturbation scheme to develop an efficient high-order spectral method for solving the initial-boundary-value problem for $\Phi$.

Following Zakharov (1968), we define the surface potential

$$\Phi^s(\mathbf{x},t) = \Phi(\mathbf{x},\eta(\mathbf{x},t),t)\,, \tag{2.5}$$

where the free surface $z = \eta(\mathbf{x},t)$ is assumed to be continuous and single-valued. Upon using chain rules

$$\Phi_t(\mathbf{x},\eta,t) = \Phi^s_t(\mathbf{x},t) - \Phi_z(\mathbf{x},\eta,t)\eta_t\,, \quad \text{and} \tag{2.6}$$

$$\nabla_{\mathbf{x}}\Phi(\mathbf{x},\eta,t) = \nabla_{\mathbf{x}}\Phi^s(\mathbf{x},t) - \Phi_z(\mathbf{x},\eta,t)\nabla_{\mathbf{x}}\eta\,, \tag{2.7}$$

we can rewrite the free surface boundary conditions (2.2) as:

$$\left.\begin{aligned} &\eta_t + \nabla_{\mathbf{x}}\eta\cdot\nabla_{\mathbf{x}}\Phi^s - (1+\nabla_{\mathbf{x}}\eta\cdot\nabla_{\mathbf{x}}\eta)\Phi_z(\mathbf{x},\eta,t) \\ &\qquad\qquad = \bar{\phi}_z(\mathbf{x},\eta) - \nabla_{\mathbf{x}}\eta\cdot\nabla_{\mathbf{x}}\bar{\phi}(\mathbf{x},\eta)\,, \\ &\Phi^s_t + g\eta + \tfrac{1}{2}\nabla_{\mathbf{x}}\Phi^s\cdot\nabla_{\mathbf{x}}\Phi^s - \tfrac{1}{2}(1+\nabla_{\mathbf{x}}\eta\cdot\nabla_{\mathbf{x}}\eta)\Phi_z^2(\mathbf{x},\eta,t) \\ &\qquad\qquad = -\tfrac{1}{2}\nabla\bar{\phi}(\mathbf{x},\eta)\cdot\nabla\bar{\phi}(\mathbf{x},\eta)\,. \end{aligned}\right\} \tag{2.8}$$

An apparent advantage of using (2.8) instead of (2.2) as free-surface boundary cond-

tions is that given the initial values of $\eta$ and $\Phi^s$, (2.8) can be readily integrated in time for the new values of $\eta$ and $\Phi^s$ provided that the surface vertical velocity $\Phi_z(\mathbf{x}, \eta, t)$ can be obtained from the boundary-value problem.

In order to solve the boundary-value problem, we assume that $\eta$ and $\Phi$ are $O(\epsilon)$ quantities, where $\epsilon$, a small parameter, is a measure of the wave steepness. We then expand $\Phi$ in a perturbation series in $\epsilon$ up to order $M$:

$$\Phi(\mathbf{x}, z, t) = \sum_{m=1}^{M} \Phi^{(m)}(\mathbf{x}, z, t)\,, \tag{2.9}$$

where $()^{(m)}$ denotes a quantity of $O(\epsilon^m)$. We further expand each $\Phi^{(m)}$ evaluated on $z = \eta$ in Taylor series about $z = 0$, so that

$$\Phi^s(\mathbf{x}, t) \equiv \Phi(\mathbf{x}, \eta, t) = \sum_{m=1}^{M} \sum_{\ell=0}^{M-m} \frac{\eta^\ell}{\ell!} \frac{\partial^\ell}{\partial z^\ell} \Phi^{(m)}(\mathbf{x}, 0, t). \tag{2.10}$$

The method we develop will, in principle, be able to account for nonlinearities up to an arbitrary order $M$ in $\epsilon$. In practice, however, (2.10) places a limit on the maximum steepness of the free surface we can consider. In particular, the validity and convergence of (2.10) is limited by the radius of convergence (from $z = 0$) of $\Phi$, which cannot extend beyond the first singularity in the analytic continuation of $\Phi$ above $z = \eta$.

At a given instant time, $\eta$ and $\Phi^s$ can be obtained by the nonlinear evolution equations (2.8). Thus, we can treat (2.10) as a Dirichlet boundary condition for the unknown $\Phi$. Expanding (2.10) and collecting terms at each order, we obtain a sequence of boundary conditions for the unknown $\Phi^{(m)}$ on $z = 0$:

$$\begin{aligned} &\Phi^{(1)}(\mathbf{x}, 0, t) = \Phi^s\,, \\ &\Phi^{(m)}(\mathbf{x}, 0, t) = -\sum_{\ell=1}^{m-1} \frac{\eta^\ell}{\ell!} \frac{\partial^\ell}{\partial z^\ell} \Phi^{(m-\ell)}(\mathbf{x}, 0, t), \qquad m = 2, 3, \cdots, M. \end{aligned} \tag{2.11}$$

For small body motions, the kinematic boundary condition (2.3) applied on the body

$S_B(t)$ can also be expanded in Taylor series about its mean position $\bar{S}_B$:

$$\Phi_n + \bar{\phi}_n + (S_B(t) - \bar{S}_B) \cdot (\nabla\Phi_n + \nabla\bar{\phi}) + \cdots = \mathbf{V}(t) \cdot \mathbf{n} \quad \text{on} \quad \bar{S}_B \tag{2.12}$$

where $S_B(t) - \bar{S}_B = O(\epsilon)$ is the body displacement from its mean position. After substituting (2.9) into (2.12) and collecting terms at each order, a sequence of body boundary conditions for the unknown $\Phi^{(m)}$ applied on $\bar{S}_B$ are obtained:

$$\left.\begin{aligned} \Phi_n^{(1)} &= -\bar{\phi}_n - (S_B(t) - \bar{S}_B) \cdot \nabla\bar{\phi} + \mathbf{V}(\mathbf{t}) \cdot \mathbf{n}\,, \\ \Phi_n^{(m)} &= f(\bar{\phi}, \Phi^{(\ell)}, \ell = 1, 2, \cdots, m-1)\,, \quad m = 2, \cdots, M. \end{aligned}\right\} \tag{2.13}$$

The Dirichlet and Neumann conditions (2.11) and (2.13), in addition to being doubly-periodic in the horizontal plane and $\Phi_z^{(m)} = 0$ on $z = -h_0$, define a sequence of boundary-value problems for $\Phi^{(m)}, m = 1, 2, \cdots, M$, in the domain $z \leq 0$.

As in a typical mode-coupling approach, we represent each $\Phi^{(m)}$ as an expansion of coupled free-surface and body basis functions:

$$\Phi^{(m)}(\mathbf{x}, z, t) = \sum_{n=0}^{\infty} \mu_n^{(m)}(t)\Psi_{Fn}(\mathbf{x}, z) + \sum_{n=0}^{\infty} \sigma_n^{(m)}(t)\Psi_{Bn}(\mathbf{x}, z) \tag{2.14}$$

where $\mu_n^{(m)}(t)$ and $\sigma_n^{(m)}(t)$ denote the unknown modal amplitudes. The basis functions $\Psi_{Fn}(\mathbf{x}, z)$ and $\Psi_{Bn}(\mathbf{x}, z)$ are defined to be harmomic within the fluid and periodic in $\mathbf{x}$, and satisfy the bottom boundary condition. With this construction, (2.14) satisfies Laplace's equation and all the boundary conditions with the exception of those on the mean free surface and the body. Substituting (2.14) into (2.11) and (2.13) for each order, the modal amplitudes $\mu_n^{(m)}(t)$ and $\sigma_n^{(m)}(t)$ are determined successively for $m = 1, \ldots, M$, in terms of the known surface elevation $\eta(\mathbf{x}, t)$ and potential $\Phi^S(\mathbf{x}, t)$.

After the boundary-value problems for $\Phi^{(m)}$ are solved up to the desired order $M$, the vertical velocity on the free surface is given by

$$\Phi_z(\mathbf{x}, \eta, t) = \sum_{m=1}^{M} \sum_{\ell=0}^{M-m} \frac{\eta^\ell}{\ell!} \frac{\partial^{\ell+1}}{\partial z^{\ell+1}} \Phi^{(m)}(\mathbf{x}, 0, t). \tag{2.15}$$

The vertical derivatives here (and in (2.11)) are obtained in terms of the modal amplitudes:

$$\Phi_z^{(m)}(\mathbf{x},0,t) = \sum_{n=0}^{\infty} \mu_n^{(m)}(t) \frac{\partial}{\partial z} \Psi_{Fn}(\mathbf{x},0) + \sum_{n=0}^{\infty} \sigma_n^{(m)}(t) \frac{\partial}{\partial z} \Psi_{Bn}(\mathbf{x},0) \,. \tag{2.16}$$

Thereafter, higher derivatives are found by using Laplace's equation (*e.g.*, $\Phi_{zz}^{(m)} = -\Phi_{xx}^{(m)} - \Phi_{yy}^{(m)}$, $\Phi_{zzz}^{(m)} = -(\Phi_z^{(m)})_{xx} - (\Phi_z^{(m)})_{yy}, \ldots$), and the $(x,y)$-derivatives are easily evaluated in the spectral space. The evolution equations (2.8) can then be integrated for the new values of $\Phi^S$ and $\eta$. The process is repeated starting from initial conditions. The potential on the body is available from (2.14), and the pressure on the body $S_B(t)$ can be evaluated according to (2.4).

Note that the basis functions $\Psi_{Fn}$ and $\Psi_{Bn}$, in general, depend on the body geometry and the periodic domain. A straightforward way to construct these functions is to treat them as the influences of certain singularity distributions on the mean free surface and the body. For high-resolution calculations and minimum computational effort, in practice, we make them orthogonal so that the convergence of (2.14) is exponentially rapid with increasing the numbers of spectral modes.

## 2.3 Implementation

The time simulation of the nonlinear wave-body problem up to an arbitrary order $M$ consists of three main steps. Beginning from initial values for $\Phi^S$ and $\eta$, at each successive time step: (i) solve the boundary-value problem for the perturbation velocity potentials $\Phi^{(m)}(\mathbf{x},z,t)$, $m = 1,\ldots,M$; (ii) evaluate the vertical velocity at the free surface $\Phi_z(\mathbf{x},\eta,t)$; and (iii) integrate the evolution equations (2.8) forward for $\Phi^S(\mathbf{x},t+\Delta t)$ and $\eta(\mathbf{x},t+\Delta t)$; and the process is repeated.

In practice, the numbers of free-surface and body spectral modes are truncated at some suitable numbers, say, $N_F$ for $\Psi_{Fn}$ and $N_B$ for $\Psi_{Bn}$. Given the boundary-value problems for $\Phi^{(m)}$, $m = 1,\ldots,M$, the modal amplitudes $\mu_n^{(m)}(t)$, $n = 0,\ldots,N_F$, and $\sigma_n^{(m)}(t)$, $n = 0,\ldots,N_B$, are determined by satisfying the Dirichlet and Neumann con-

ditions at $N_F$ and $N_B$ control points on the mean free surface and body respectively. The resulting $N_F + N_B$ linear equations can be formally represented as:

$$\left.\begin{aligned} [C_{\mu\mu}]\mu^{(m)} + [C_{\mu\sigma}]\sigma^{(m)} &= \{f^{(m)}\} \\ [C_{\sigma\mu}]\mu^{(m)} + [C_{\sigma\sigma}]\sigma^{(m)} &= \{B^{(m)}\}\,, \end{aligned}\right\} \tag{2.17}$$

where $[C_{\mu\mu}]$, $[C_{\mu\sigma}]$, $[C_{\sigma\mu}]$, and $[C_{\sigma\sigma}]$ are respectively the $N_F \times N_F$, $N_F \times N_B$, $N_B \times N_F$, and $N_B \times N_B$ modal influence matrices given in terms of the basis functions; and $\mu^{(m)}$, $\sigma^{(m)}$, the vectors of the unknown modal amplitudes $\mu_n^{(m)}$, $n = 0, \ldots, N_F$, and $\sigma_n^{(m)}$, $n = 0, \ldots, N_B$. Solving these equations, we obtain, again formally:

$$\left.\begin{aligned} \sigma^{(m)} &= [T_{\sigma f}]\{f^{(m)}\} + [T_{\sigma b}]\{B^{(m)}\} \\ \mu^{(m)} &= [T_{\mu f}]\{f^{(m)}\} + [T_{\mu\sigma}]\sigma^{(m)}\,, \end{aligned}\right\} \tag{2.18}$$

where $[T_{\sigma f}]$ $(N_B \times N_F)$, $[T_{\sigma b}]$ $(N_B \times N_B)$, $[T_{\mu f}]$ $(N_F \times N_F)$, and $[T_{\mu\sigma}]$ $(N_F \times N_B)$, are related to the inverses of the influence matrices in (2.17).

Once $\mu^{(m)}$ and $\sigma^{(m)}$ are obtained, the perturbation vertical velocities at the control points on the free surface follow from (2.16), which take the form:

$$\{\Phi_z^{(m)}\} = [W_\mu]\mu^{(m)} + [W_\sigma]\sigma^{(m)}\,, \tag{2.19}$$

where $[W_\mu]$ $(N_F \times N_F)$, and $[W_\sigma]$ $(N_F \times N_B)$ are known matrices given by (2.16) in terms of the basis functions.

In practice, the boundary-value problems are solved using a pseudo-spectral approach, wherein all the spatial derivatives are evaluated in the spectral representation, while nonlinear products (such as those in (2.11)) are computed in physical space at the discrete control points. The rapid transformations between the representations are effected by fast-Fourier transforms (FFT's).

It is important to note that in the present high-order method, the $[T]$ and $[W]$ matrices in (2.18) and (2.19) are functions of the mean geometry only. Therefore, they

are independent of time and need to be evaluated only once for the entire simulation. More significantly, since for typical applications (especially for three-dimensional problems), $N_F >> N_B$, in the spectral approach, the $N_F \times N_F$ matrices $[T_{\mu f}]$ and $[W_\mu]$ need not be explicitly realized as the contributions $[T_{\mu f}]\{f^{(m)}\}$ and $[W_\mu]\mu^{(m)}$ can be evaluated in $O(N_F \ln N_F)$ operations via FFT. Consequently, the net computational effort is approximately proportional to $N_F$ and not $N_F^2$. Specifically, the total operational count of the method is $[O(MN_F \ln N_F) + O(MN_F N_B)]$ per time step, with an initial set-up effort of $[O(N_B^2 N_F) + O(N_B^2 N_F \ln N_F)]$.

With the surface vertical velocities thus obtained from (2.19) and (2.15), the nonlinear evolution equations (2.8) can be integrated as a coupled set of nonlinear ODE's. We employ the fourth-order Runge-Kutta (RK4) scheme which requires twice as many evaluations as the commonly used multi-step predictor-corrector (*e.g.*, the Adams-Bashforth-Moulton, ABM) methods of the same order but has a somewhat lower global truncation error and a larger stability region (see, *e.g.*, Dommermuth *et al.* 1988).

## 2.4 Error considerations

The main sources of computational error for the present high-order wave-body simulations are: (i) errors due to truncation in the numbers of spectral modes $N_F$, $N_B$, and the perturbation order $M$; (ii) error due to the finite (periodic) computational domain for a given simulation time, $T_S$; (iii) amplification of round-off and truncation errors; (iv) aliasing errors of the pseudo-spectral method; (v) errors due to numerical time integration; and (vi) for estimates of mean and harmonic force coefficients etc., errors due to the finite simulation time, $T_S$, of the initial-value problem.

### 2.4.1 Errors due to truncation of modes $N_F, N_B$, and order $M$

For sufficiently smooth $\eta$ and $\Phi^s$, the numerical error in the spectral representations of $\Phi^{(m)}$, $m = 1, \cdots, M$, vanishes exponentially as $N_F$ and $N_B \to \infty$. Similarly, for mild

nonlinearities, the truncation errors after order $M$ is $O(\epsilon^{M+1})$, and the convergence is exponential with increasing $M$. As pointed out after (2.10), such convergence ceases beyond a certain wave steepness. For regular Stokes waves, the maximum wave steepness for exponential convergence of the method is found to be $\epsilon = kA \sim .35$ (see DY Table 1). The corresponding maximum local slope is $\epsilon_L \equiv (\partial\eta/\partial x)_{max} \sim .38$. In the presence of a submerged body, the incident Stokes wave steepness $\epsilon$ is neither the limiting nor useful parameter due to local wave steepening over the body. Using $\epsilon_L$ instead, our present calculations with a body confirm the result of DY based on Stokes waves. It is important to point out that converged results (not necessarily exponentially fast) for large local slopes up to $\epsilon_L \sim 1.5$ can and have been obtained in the present simulations (see also DY figures 2 and 5).

### 2.4.2 Error due to the finite computational domain

For a computational domain fixed relative to wavelength and body dimension, the solution in the near field of the body will eventually be distorted due to 'reflections' from the periodic boundaries as the simulation time $T_S$ is increased. This error is avoided by successively increasing the sizes of the periodic domain until the quantities of interest no longer vary. We remark that with the $O(N_F)$ efficiency of the present method, the computation cost increases only linearly with the area of the computational domain.

### 2.4.3 Amplification of round-off and truncation errors

In any computational model without dissipation, nonlinear interactions cause energy in the lower modes to cascade to higher modes which eventually accumulates at the highest wavenumbers retained in the model. As pointed out in DY, this is accompanied by an amplification of numerical error in the modal amplitudes which increases with the mode number. This combined effect is the root cause of large wavenumber instabilities in our nonlinear simulations. To avoid such instabilities, we follow DY

and apply an ideal numerical low-pass filter in the Fourier space:

$$\Lambda_I(n,\gamma) = \begin{cases} 1 & \text{for } n \leq \gamma N_F \\ 0 & \text{for } n > \gamma N_F \end{cases} . \tag{2.20}$$

Typically, we apply $\Lambda_I$ with $\gamma = 0.8$ to the spectra of $\eta$ and $\Phi^s$ every five time steps.

### 2.4.4 Aliasing errors

In a pseudo-spectral approach, the product $h{=}f{\cdot}g$, represented respectively by Fourier modes $h_n$, $f_n$, $g_n$, $n \leq N$, are performed in physical space at equally-spaced points. This results in aliasing errors due to the finite Fourier representations. It is well known that the best approximation (in the mean square sense) to the product is the so-called alias-free sum (*e.g.*, Orszag 1971). To obtain this, we double the number of Fourier modes and the number of collocation points to $2N$, calculate the product $H = FG$, as before in physical space, where $(F_n, G_n) = (f_n, g_n)$ for $|n| \leq N$ and $(F_n, G_n) = (0,0)$ for $N < |n| \leq 2N$, and define the alias-free product, $h$, by $h_n = H_n$ for $|n| \leq N$. For products involving two or more terms, the multiplication is done successively where each factor is made alias-free before multiplying by the next term.

### 2.4.5 Errors due to numerical time integration

The fourth-order Runge-Kutta (RK4) scheme we use is conditionally stable for the linearized equation for $g\kappa_{max}\Delta t^2 \leq 8$, where $\kappa_{max}$ is the maximum grid (Nyquist) wavenumber. This should be a necessary condition for the nonlinear problem. The local truncation error of RK4 is $O(\Delta t^5)$, so that the global truncation error for $T_S = O(1)$ is fourth-order in $\Delta t$.

### 2.4.6 Errors in the estimation of mean and limit-cycle force coefficients

One of the main interests in the study of wave-body interactions is the mean and harmonic force components on the body. To obtain them from the initial-value simulation, we define for definiteness

$$F_n(\tau_0) = \frac{1}{T}\int_{\tau_0}^{\tau_0+T} F(t)e^{-in\omega t}dt\ , \tag{2.21}$$

where $F(t)$ is the time-dependent force on the body, $T$ the fundamental period (of the incident wave), $\omega = 2\pi/T$, and $\tau_0$ a time interval selected so that limit-cycle values are obtained. The (rapid) convergence of $\bar{F}$ with $\tau_0$ is an important and desired property.

## 2.5 Relation to frequency-domain perturbation results

Although the present approach is strictly a time-domain (initial-value problem) one, and steady and harmonic amplitudes are obtained via harmonic analysis of the limit-cycle time histories, these results can be related in a direct way to the linear and higher-order components of perturbation methods in the frequency domain. In a typical frequency-domain approach, the time dependence is factored out explicitly and the velocity potential written as:

$$\Phi = \sum_{n=0}^{\infty} \Re(\tilde{\phi}_n e^{in\omega t})\ , \tag{2.22}$$

where $\omega = 2\pi/T$. Each $\tilde{\phi}_n$ is then expanded in a perturbation series in the wave steepness, $\epsilon$:

$$\tilde{\phi}_n = \sum_{m=1}^{\infty} \epsilon^m \tilde{\phi}_n^{(m)}\ , \tag{2.23}$$

and the boundary-value problems for $\tilde{\phi}_n^{(m)}$ are solved. In the present method, the initial-boundary-value problem for $\Phi(\mathbf{x}, z, t)$ is integrated accurately to the specified order $M$ in $\epsilon$. Despite the truncation at $M$ (cf. (2.9) and (2.10)), the presence of the nonlinear terms in (2.8) eventually causes all time harmonics to be present in $\Phi$, in fact in each $\Phi^{(m)}$. Upon reaching limit cycle, the (complex) amplitudes of these harmonics are then extracted via Fourier decomposition:

$$\phi_n^{(m)} = \frac{1}{T}\int_{\tau_0}^{\tau_0+T} \Phi^{(m)}(t) e^{-in\omega t} dt \,, \qquad n = 1, 2, \ldots; \quad m = 1, 2, \ldots, M \,. \tag{2.24}$$

It should be pointed out that, in general, $\phi_n^{(m)}$, $n > m$ (and also $n = 0$, $m = 1$), are small as expected but do not vanish. In the high-order time-domain approach, there is no *direct* relationship between $m$-th order terms in (2.24) and those in (2.23) (cf. (2.11)). For direct comparisons then, it is useful to define the amplitude:

$$\phi_n^{<M>} = \sum_{m=1}^{M} \phi_n^{(m)} \,, \qquad n = 1, 2, \ldots \,, \tag{2.25}$$

where $M$ is the order of the simulation. Note that the magnitude of $\phi_n^{<M>}$ is $O(\epsilon^n)$, except for $\phi_0^{<M>}$ which is of second order. With this notation, then, the amplitudes in (2.23) and (2.25) are related by:

$$\left.\begin{aligned} &\tilde{\phi}_0^{(2)} = \phi_0^{<2>} + O(\epsilon^3) \\ &\tilde{\phi}_n^{(n)} = \phi_n^{<M>} + O(\epsilon^{n+1}) \,, \qquad n > 0 \,, \text{ and } M \geq n \,; \end{aligned}\right\} \tag{2.26}$$

while such simple relationships cannot, in general, be written for the amplitudes in (2.24). Similar formulae and results apply also to other quantities such as forces, wave amplitudes, etc. We remark that, in some sense, the present results are more 'physical' in that they correspond directly to what one might measure in a laboratory.

## 2.6 Conclusions

Based on time-domain perturbation expansions and using mode-coupling approach, a high-order spectral method is developed for the study of nonlinear wave-body interactions. The method accounts for the nonlinear interactions among $N_F$ wave modes on the free surface and $N_B$ source modes on the body up to an arbitrary order $M$ in wave steepness. By using fast-transform techniques, the operational count per time step is only linearly proportional to $M$ and $N_F$ (typically $N_F >> N_B$). For a (closed) submerged body in moderately steep waves, the exponential convergence with respect to $M$, $N_F$, and $N_B$ is obtained. The efficiency and accuracy of the spectral method provides a computational capability for high-resolution calculations not readily available using other numerical methods employing direct surface or volume discretizations.

In chapters 3-7, we apply this method to investigate nonlinear interactions between surface waves with submerged bodies. In chapter 8, this method is extended to the study of nonlinear wave-bottom interactions. The finite-depth effect can be easily included by the present method. This is considered in appendix C. With slight modification in the implementation, the present efficient computational method can be used to simulate the evolution of an ocean wave field including long-short wave interactions. For this purpose, some analytical results for the calculation of free-surface vertical velocity are summarized in Appendix D.

Finally we point out that for a general nonlinear problem, it is known that a sinusoidal forcing may not necessarily lead to a steady periodic response at the driving frequency in the limit of large time (*e.g.* Aranha *et al.* 1982). This implies that the solution obtained using the frequency-domain approach may be unrealistic. From this point of view, the time-domain approach would be superior to the frequency-domain scheme for general wave-body/bottom problems.

# Chapter 3

# Nonlinear wave diffraction by a submerged circular cylinder

As a special application of the high-order spectral method, in this chapter, we study the nonlinear diffraction of Stokes waves by a fixed and submerged circular cylinder. This is a special nonlinear problem for which the horizontal drift force on the cylinder vanishes up to second-order in wave steepness according to linearized potential theory. By including high-order free surface effects, we show that the horizontal drift force is negative and of fourth-order in magnitude. This prediction agrees well with experimental measurements. It is found that the dominant contribution of this force is due to the quadratic interaction of first- and third-order first-harmonic waves rather than the self-interaction of second-order second-harmonic waves, which in fact reduces the negative drift force.

Wave diffraction by a submerged circular cylinder is a well studied problem for which a number of established theoretical, computational and experimental results are available. Using conformal mapping, Dean (1948) found, to leading order in wave steepness, that a circular cylinder held fixed under waves does not reflect waves, and transmitted waves merely experience a change in phase but not amplitude. Ursell (1950), using a multipole expansion, found the complete linear solution and showed that it was unique. Following Ursell's approach, Ogilvie (1963) showed that the linear potential leads to a mean (second-order) vertical force but that the horizontal mean

force at second order vanishes identically. This result agrees with the prediction from a far-field formula of Maruo (1960), but is in contrast to experimental observations (*e.g.*, Salter *et al.* 1976) that a free cylinder just awash experiences a negative drift force which causes it to move towards the wavemaker.

Longuet-Higgins (1977) suggested that this negative drift force can be attributed mostly to wave breaking, and, to a lesser degree, to the second-harmonic component of the transmitted wave. The measurements of Miyata *et al.* (1988) and Inoue & Kyozuka (1984) do not support all of Longuet-Higgins' predictions. They found that as the cylinder was moved closer to the free surface, which led to more intense breaking, the negative horizontal drift force was actually reduced and ultimately reversed sign. Using a Stokes expansion, Vada (1987) solved the second-order (frequency-domain) diffraction problem but was unable to calculate all the terms (at fourth order) of the non-vanishing mean horizontal force, since third-order potentials are involved (see §3.3.4). For the second-order oscillatory forces, however, Vada's results were in good agreement with the measurements of Chaplin (1984), thereby confirming Chaplin's suggestion that inviscid flow models would be good for Keulegan-Carpenter numbers less than about two for second-order forces. As pointed out by Chaplin, however, this is not necessarily true for first-order forces (see §3.3.3).

A number of fully-nonlinear (time-domain) computations of this problem were also attempted. Vinje & Brevig (1981) used the mixed Eulerian-Lagrangian method of Longuet-Higgins & Cokelet (1976) to study the forces acting on a cylinder under a breaking wave, but their results were only qualitative. Using a similar method, Cointe (1989) obtained higher-order harmonic forces and transmission coefficients but did not focus on the question of the mean horizontal drift force. Stansby & Slaouti (1983) used the method of Zaroodny & Greenberg (1973) to study the forces on cylinders under waves and found that steady-state was rapidly approached. No conclusions were made, however, regarding the steady forces.

For the reflected and transmitted waves, the theoretical prediction of Dean (1948) and Ursell (1950) of no leading-order reflected waves was confirmed by the measurements of Chaplin (1984) to even higher order for mild waves. Grue (1991) performed

a careful set of experiments which showed that the transmitted waves are, however, significantly affected by nonlinear wave interactions over the submerged body. Motivated by these results, there are a number of recent theoretical demonstrations (Friis 1990; McIver & McIver 1990; Wu 1991) of the fact that the reflection coefficient is identically zero to second order. The most general result to date is the work of Palm (1991), who proved that the leading order component of any harmonic of the reflected wave also vanishes. These analytical results and experimental observations are confirmed by our numerical computations of high-order (up to $M = 3$) reflected and transmitted waves in §3.3.2

We use the high-order spectral method to solve the present nonlinear wave-body interaction problem up to the order $M = 4$ in the incident wave slope. Extensive convergence tests are performed and presented in §3.2. In §3.3, numerical computations for nonlinear diffraction of a submerged circular cylinder are presented and compared to available measurements and theoretical predictions. Results are given for the nonlinear mean and harmonic amplitudes of the diffracted waves and oscillatory forces, with a special emphasis on the horizontal drift force on the cylinder.

## 3.1 Computational issues

Consider the wave diffraction by a submerged circular cylinder in deep water. The high-order spectral method is used to solve this problem up to an arbitrary order $M$. With initial-value simulations, we obtain the transient solutions for the nonlinear forces on the body and the high-order diffracted wave field. The frequency harmonic amplitudes are extracted via the Fourier transform of steady-state time histories.

For numerical computations, we choose a global Cartesian coordinate system $(x, z)$ which is located at the mean water level directly above the cylinder center with $z$ positive upward and $x$ positive in the direction of wave propagation. A local cylindrical coordinate system $(r, \theta)$ is placed at the center of the cylinder, which is at a depth $H$ below the mean water level. Thus, $r^2 = x^2 + (z + H)^2$ and $\theta$ is measured counter-clockwise from positive $x$.

For the zero speed problem, the base flow is chosen to be $\bar{\phi} = 0$. In the horizontal direction, periodic boundary conditions are imposed far upstream and downstream, say at $x = \pm L$. On the body, normal velocity vanishes:

$$\Phi_r^{(m)}(R, \theta, t) = 0 \qquad m = 1, \cdots, M \tag{3.1}$$

for $0 \leq \theta < 2\pi$, where $R$ is the radius of the cylinder. The velocity potential at each order $m = 1, \ldots, M$ is represented in terms of global free-surface and body basis functions, $\Psi_{Fn}$ and $\Psi_{Bn}$. The modal amplitudes are determined through the imposition of Dirichlet and Neumann conditions on the mean free surface and the body. For $N_F$ free-surface and $N_B$ body modes, the convergence of the solution with $N_F$, $N_B$ and $M$ is exponentially rapid. This spectral accuracy allows us to obtain high-resolution results for nonlinear quantities such as the forth-order negative horizontal drift force on the body.

### 3.1.1 The basis functions

To construct the basis functions $\Psi_{Fn}(x, z)$ and $\Psi_{Bn}(x, z)$, we distribute dipoles $\mu(x)$ over the mean free surface, and sources $\sigma(\theta)$ on the circular cylinder. Since $\mu(x)$ and $\sigma(\theta)$ are $2L$- and $2\pi$-periodic in $x$ and $\theta$ respectively, we expand them as Fourier series:

$$\mu(x) = \sum_{n=0}^{\infty} \mu_n e^{in\pi x/L}, \qquad \sigma(\theta) = \sum_{n=0}^{\infty} \sigma_n e^{in\theta}, \tag{3.2}$$

where real parts of the complex quantities are implied. The basis functions can then be considered as the influences of the $n$-th mode dipole and source distributions on the mean free surface and body respectively. In terms of the Fourier integrals, they can formally be expressed as:

$$\Psi_{Fn}(x, z) = \int_{-L}^{L} e^{in\pi x'/L} G_{z'}(x, z; x', 0) dx', \tag{3.3}$$

$$\Psi_{Bn}(x, z) = \int_{0}^{2\pi} e^{in\theta'} G(r, \theta; R, \theta') R d\theta', \tag{3.4}$$

where $G(x,z;x',z')$ is the $2L$-periodic source potential in two dimensions:

$$G(x,z;x',z') = \frac{1}{2}\log\left[\sin^2(\frac{x-x'}{2L/\pi}) + \sinh^2(\frac{z-z'}{2L/\pi})\right]. \tag{3.5}$$

### 3.1.2 Numerical implementation

The time simulation of the present nonlinear problem up to an arbitrary order $M$ consists of three main steps. Beginning from the initial values for $\Phi^s$ and $\eta$, at each successive time step: (i) solve the boundary-value problem for the perturbation velocity potentials $\Phi^{(m)}(x,z,t), m = 1,\cdots,M$; (ii) evaluate the vertical velocity at the free-surface $\Phi_z(x,\eta,t)$; and (iii) integrate the evolution equations (2.8) forward for $\Phi^s(x,t+\Delta t)$ and $\eta(x,t+\Delta t)$; and the process is repeated.

In solving the boundary-value problem, in practice, the series in (3.2) and (2.14) are truncated at suitable numbers, $N_F$ and $N_B$. For sufficiently smooth surface elevation $\eta$ and potential $\Phi^s$, the convergence of (3.2) and (2.14) with respect to $N_F$ and $N_B$ is exponential. $N_F$ and $N_B$ control points on the mean free surface and the body are equally spaced in $x$ and $\theta$ so that the rapid transformations between spectral and physical representations can be effected by the FFT's. Thus, the computational effort is linearly proportional to $N_F$ only (usually $N_F \gg N_B$).

For the time integration of the nonlinear evolution equations (2.8), the fourth-order Runge-Kutta scheme is used. The resulting global error is expected to be $O(\Delta t/T)^4$. As initial conditions, we choose *exact* deep-water Stokes waves of steepness $\epsilon = kA$ ($2A \equiv \eta_{max} - \eta_{min}$), wavelength $\lambda = 2L/N_w$, *i.e.*, $N_w$ complete waves in the periodic domain $[-L,L]$, and period $T$. To calculate the initial values $\eta(x,0)$ and $\Phi^S(x,0)$, we follow Schwartz (1974), but solve the mapping (Schwartz' Eqs. 2.6) by direct numerical iterations.

## 3.2 Numerical convergence tests

Before focusing on the nonlinear solution of the wave-body problem, we first perform systematic numerical tests to verify the accuracy and convergence of the present

| $N_w$ | $M=2$ | $M=3$ | $M=4$ |
|---|---|---|---|
| 8 | -1.0650 | -1.0750 | -1.0800 |
| 16 | -1.0784 | -1.0876 | -1.0907 |
| 32 | -1.0800 | -1.0890 | -1.0920 |

Table 3.1: Convergence of the normalized horizontal drift force, $\bar{F}_x/\rho g A^2\epsilon^2$, on a submerged circular cylinder with increasing number of wavelengths $N_w$ of the periodic domain and for different order $M$. $kA$=0.04, $kR$=0.4, $H/R = 2$; and $N_F$=64$N_w$, $N_B$=256, $T/\Delta t$=64, $\tau_0$=5$T$.

| $N_B$ | $M=2$ | $M=3$ | $M=4$ |
|---|---|---|---|
| 64 | -1.0656 | -1.0845 | -1.0880 |
| 128 | -1.0778 | -1.0869 | -1.0900 |
| 256 | -1.0784 | -1.0876 | -1.0907 |

Table 3.2: Convergence of the normalized horizontal drift force, $\bar{F}_x/\rho g A^2\epsilon^2$, on a submerged circular cylinder with increasing number of body modes $N_B$ and order $M$. $kA$=0.04, $kR$=0.4, $H/R = 2$; and $N_w$=16, $N_F$=64$N_w$, $T/\Delta t$=64, $\tau_0$=5$T$.

method. For specificity, we consider only the horizontal (mean) drift force $\bar{F}_x$ on the submerged circular cylinder. This offers a severe test on the accuracy of the high-order method since the horizontal drift force is zero up to second order (Ogilvie 1963) and its magnitude is (at most) fourth-order in the incident wave steepness.

Table 3.1 shows the results for the horizontal drift force for increasing $N_w$, keeping $kA$, $kR$ and $kH$ fixed. For $N_w$=16, $\bar{F}_x$ shows convergence up to three significant figures. The convergence with number of body modes, $N_B$, keeping $N_F$ and other parameters fixed, is shown in table 3.2. For a given order $M$, $\bar{F}_x$ converges to its limit exponentially fast as $N_B$ is increased, although $N_B$ needs to be sufficiently large for the exponential convergence with $M$ to take place.

Similar rapid convergence with respect to the number of free-surface modes, $N_F$, and with order $M$ is displayed in table 3.3 for a range of incident wave steepness, $\epsilon = kA$. Again, the exponential convergence with $N_F$ is achieved for any $M$, while that with $M$ requires first that $N_F$ is adequately large. When the maximum local slope, $\epsilon_L$, of the free surface (typically above the cylinder) exceeds $\sim$ 0.4, however,

| $\epsilon$ | $N_F/N_w$ | $M=2$ | $M=3$ | $M=4$ |
|---|---|---|---|---|
| .04 | 32 | -1.0479 | -1.0520 | -1.0550 |
| | 64 | -1.0784 | -1.0876 | -1.0907 |
| | 128 | -1.0804 | -1.0898 | -1.0930 |
| .08 | 32 | -.9399 | -.9617 | -.9717 |
| | 64 | -1.0083 | -1.0435 | -1.0561 |
| | 128 | -1.0072 | -1.0432 | -1.0588 |
| .12 | 32 | -.8276 | -.8713 | -.8885 |
| | 64 | -.8977 | -.9722 | -1.0079 |
| | 128 | -.9102 | -.9643 | -.9910 |
| .16 | 32 | -.7365 | -.8152 | -.8427 |
| | 64 | -.7512 | -.8620 | -.9438 |

Table 3.3: Convergence of the normalized horizontal drift force, $\bar{F}_x/\rho g A^2\epsilon^2$, on a submerged circular cylinder with number of free-surface modes $N_F$ and order $M$ for different incident slopes $\epsilon = kA$. $kR$=0.4, $H/R = 2$; and $N_w$=16, $N_B$=256, $T/\Delta t$=64, $\tau_0$=5$T$.

the convergence becomes only algebraic. This has occurred, for example, for the case of $\epsilon$=.16 in table 3.3.

We next show the approach to the steady-state limit (limit-cycle) of the forces on the cylinder by considering the convergence of (2.21) with $\tau_0$. This is shown in table 3.4 for different order $M$. The steady-state limit is reached rapidly after $\tau_0 \sim 2T$. Finally, we show the convergence of the numerical time integration with $\Delta t$ in table 3.5. The expected $O(\Delta t/T)^4$ global error is obtained provided that the solution to

| $\tau_0/T$ | $M=2$ | $M=3$ | $M=4$ |
|---|---|---|---|
| 0 | -5.8477 | -5.9392 | -5.9414 |
| 1 | -.9742 | -.9811 | -.9821 |
| 2 | -1.0724 | -1.0847 | -1.0869 |
| 3 | -1.0877 | -1.0919 | -1.0941 |
| 4 | -1.0662 | -1.0916 | -1.0926 |
| 5 | -1.0784 | -1.0876 | -1.0907 |

Table 3.4: Convergence of the normalized horizontal drift force, $\bar{F}_x/\rho g A^2\epsilon^2$, on a submerged circular cylinder with duration of simulation $\tau_0$ and order $M$. $kA$=0.04, $kR$=0.4, $H/R = 2$; and $N_w$=16, $N_F$=64$N_w$, $N_B$=256, $T/\Delta t$=64.

| $T/\Delta t$ | $M=2$ | $M=3$ | $M=4$ |
|---|---|---|---|
| 32 | -1.0766 | -1.0862 | -1.0893 |
| 48 | -1.0775 | -1.0868 | -1.0900 |
| 64 | -1.0784 | -1.0876 | -1.0907 |

Table 3.5: Convergence of the normalized horizontal drift force, $\bar{F}_x/\rho g A^2\epsilon^2$, on a submerged circular cylinder with integration time step $\Delta t$ and order $M$. $kA$=0.04, $kR$=0.4, $H/R=2$; and $N_w$=16, $N_F$=64$N_w$, $N_B$=256, $\tau_0$=5$T$.

the boundary-value problem itself is sufficiently accurate.

Unless otherwise stated, for all subsequent computations, we use $N_w$=16, $N_B$=256, $N_F$=64$N_w$, $\tau_0$=5$T$, and $\Delta t = T/64$. Based on the foregoing numerical tests, we anticipate the maximum error for $\bar{F}_x$ to be less than 1%.

In addition to these convergence tests, all our computations are checked for the conservation of volume, $\int_{-L}^{L}\eta dx$, or alternatively the vanishing of the volume flux, $\int_{-L}^{L}\eta_t dx$; as well as the invariance of the total energy:

$$\int_{S_F}\Phi^S\Phi_n^S ds+\int_{-L}^{L}\eta^2 dx\ , \tag{3.6}$$

where $\Phi_n^S$ is the normal velocity on the free surface $S_F$, and the first and second terms are proportional respectively to the kinetic and potential energies. For all later results we present, the volume flux is within $\sim 10^{-5}$, and the volume and total energy do not deviate by more than 1% from their initial values.

The force on the cylinder can also be obtained by applying the momentum theorem:

$$\frac{\vec{F}}{\rho}=\int_0^{2\pi}\Phi_t\mathbf{n}Rd\theta+\frac{d}{dt}\int_{S_F}\Phi\mathbf{n}ds\ , \tag{3.7}$$

where the unit normal vector $\mathbf{n}$ is positive into the fluid domain. In all cases, the force from (3.7) compares well with that obtained by direct integration of the pressure (2.4) over the body surface. For the fourth order horizontal drift force in §3.3.4, for example, the difference between the two is always less than 1%.

| | Ogilvie (1963) | Vada (1987) | Present Results |
|---|---|---|---|
| $F_{x1}/\rho gRA$ | 1.15 | 1.15 | 1.1406 ($M$=1) |
| $F_{x2}/\rho gA^2$ | — | .28 | 0.2754 ($M$=2) |
| $T_2/kA$ | — | 2.65 | 2.7025 ($M$=2) |

Table 3.6: Comparisons between existing frequency-domain and the present time-domain results for the (normalized) first- and second-harmonic horizontal force and the second-harmonic transmission coefficients. $kR$=0.4, $H/R = 2$ and $kA$=0.08.

## 3.3 Numerical Results

We consider the diffraction of Stokes waves by a fixed, submerged circular cylinder. We present results for the high-order diffracted wave amplitudes, the oscillatory force coefficients, and finally the mean forces on the cylinder. Comparisons to theoretical, computational and experimental results are made whenever they are available.

### 3.3.1 Verification of the relation between time- and frequency-domain perturbation results

With the present high-order time-domain approach, the steady and harmonic amplitudes are obtained via Fourier analysis of the limit-cycle time histories. As discussed in §2.5, they can be directly related to the results obtained from the frequency-domain perturbation methods by a simple formula (2.26). To verify the relationship, table 3.6 shows the correspondences (2.26) for the normalized harmonic forces and transmission coefficient. The frequency-domain values are taken from Ogilvie (1963) (first order) and Vada (1987) (second order). The discrepancies between the present time-domain and existing frequency-domain results are indeed of $O(\epsilon)$ or less. This confirms the relation in (2.26).

### 3.3.2 Diffracted waves

For the diffraction of surface waves by a submerged circular cylinder in deep water, Dean (1948) and Ursell (1950) show that the linear potential produces no reflected

waves and all incoming waves are transmitted downstream. This is confirmed experimentally by Chaplin (1984), suggesting further that the reflected waves may be small even to higher order. Recently, Palm (1991) proves analytically that the leading order part (at order $m$) of wave mode of frequency $m\omega$ is not reflected. For the transmitted wave, however, experiments by Grue (1991) show that the amplitudes are significantly affected by the nonlinear interactions between the cylinder and the free surface. Here we compare the high-order spectral method predictions of the reflected and transmitted wave amplitudes to these analytical and experimental results.

Expecting the reflected wave amplitude to be at most $O(\epsilon^2)$, we write the free surface elevation far upstream of the cylinder as:

$$\begin{aligned}\eta(x,t) = {} & a_1\cos(kx-\omega t) + \frac{1}{2}ka_1^2\cos 2(kx-\omega t) + \frac{3}{8}k^2a_1^3\cos 3(kx-\omega t) \\ & + a_1'\cos(kx+\omega t+\delta_1') + a_2'\cos(4kx+2\omega t+\delta_2') + a_3'\cos(9kx+3\omega t+\delta_3') \\ & + O(\epsilon^4)\,, \qquad\qquad x<0\,. \end{aligned} \tag{3.8}$$

Similarly, far downstream we write:

$$\begin{aligned}\eta(x,t) = {} & b_1\cos(kx-\omega t+\delta_1) + \frac{1}{2}kb_1^2\cos 2(kx-\omega t+\delta_1) \\ & + \frac{3}{8}k^2b_1^3\cos 3(kx-\omega t+\delta_1) + b_2\cos(4kx-2\omega t+\delta_2) \\ & + b_3\cos(9kx-3\omega t+\delta_3) + O(\epsilon^4)\,, \qquad x>0\,. \end{aligned} \tag{3.9}$$

The reflection and transmission coefficients for each harmonic are defined accordingly by $R_1 = a_1'/a_1$, $R_2 = a_2'/a_1$, $R_3 = a_3'/a_1$, and $T_1 = b_1/a_1$, $T_2 = b_2/a_1$, $T_3 = b_3/a_1$, etc.

In numerical simulations, we record the time series of the free-surface elevation at a location far upstream (at $x = -8R$), and another far downstream ($x = 8R$), the latter corresponding to the measurement position of Grue (1991). At these positions, the limit cycle for the surface elevation up to third harmonics is approached after typically $\tau_0/T \sim$ 7–8. (The simulations themselves are typically stopped after $\sim 10T$ before any appreciable effects due to images of the periodic boundaries are felt.) The harmonic amplitudes of the transmitted and reflected waves are then obtained via

| | $n=M=1$ | $n=M=2$ | $n=M=3$ |
|---|---|---|---|
| $R_n^{<M>}$ | 0.0250 | 0.0025 | 0.0003 |

Table 3.7: Harmonic amplitudes of the reflection coefficient for the diffraction of Stokes waves by a submerged circular cylinder, $kA$=0.05, $kR$=0.4 and $H/R = 2$. The numerical parameters are $N_w$=16, $N_F$=64$N_w$, $N_B = 256$, $T/\Delta t = 64$, and $\tau_0 = 9T$.

Fourier analysis of the limit-cycle time histories at these two locations.

To study the effect of nonlinearity on wave reflection and transmission, we first fix $kR = 0.4$ and $kH = 0.6$, and consider the dependence of $R_n$ and $T_n$ on the incident wave slope $kA$. For the reflected wave amplitudes, the dominant contribution for each $n > 0$ harmonic is at order $m = n$, i.e., $\tilde{R}_n^{(n)}$. In view of (2.26), this can be estimated to leading order by $R_n^{<n>}$. Table 3.7 shows a typical example for $kA = 0.05$. It is seen that $R_n^{<n>}$, $n = 1, 2, 3$, is at most of $O(\epsilon^n)$ and is at least one order higher than the transmission coefficients (which are $O(1)$). These (limited) results provide a direct numerical confirmation of the analytical predictions of Palm (1991).

The dependence of the first-harmonic transmission coefficient, $T_1$, on incident wave steepness $\epsilon = kA$ is shown in figure 3-1. For linear theory, $T_1 \equiv 1$ and is not a function of $\epsilon$. However, the measurements of Grue (1991) show that $T_1$ in fact decreases appreciably from 1 as $\epsilon$ increases. Our converged numerical results confirm this nonlinear dependence quantitatively up to $\epsilon \sim 0.08$. (Beyond $\epsilon \sim 0.08$, extensive wave breaking over the cylinder is reported by Grue (1991). For clarity, these experimental data points are omitted from this and subsequent figures.) From figure 3-1, we also conclude that it is necessary to include third-order ($M = 3$) contributions to correctly account for the behavior of $T_1$.

Figure 3-2 shows the comparisons for the second-harmonic transmission coefficient $T_2$ among our high-order numerical results, Vada (1987)'s second-order frequency-domain computations, and Grue (1991)'s experimental data. The strong nonlinear interactions over the cylinder result in a significant reduction of $T_2$ from the second-order perturbation result (which predicts a linear dependence on $\epsilon$). Although our numerical results show some indication of convergence at $M$=4, comparison to the

measured data indicates that even higher order effects are present in $T_2$ for near-breaking conditions.

Figure 3-3 summarizes the dependence of transmitted wave amplitudes on $\epsilon = kA$ for this case ($kR = 0.4$, $kH = 0.6$). Also shown are our predictions for $T_3$ and $T_4$ which have been obtained for the first time. It is interesting to note that as $\epsilon$ increases beyond $\sim$0.055, $T_2$ decreases while $T_3$ continues to grow, so that for steep waves ($\epsilon >\sim .065$) $T_3$ becomes greater than $T_2$. A direct experimental confirmation for these very high harmonics, however, may be difficult and has not yet been obtained. We caution that the present results for $T_3$ and $T_4$ have been obtained up to $M$=4 only. Although the dominant components are included, higher values of $M$ may lead to some reductions of their amplitudes (cf. figure 3-2).

Finally, we study the dependence of $T_n$ on the body submergence $H/R$ by fixing $kR = 0.4$, $kA = 0.08$ and consider varying $kH$. The numerical results for $T_1$ and $T_2$ are shown in figure 3-4. For this case, two experimental points at $H/R$=1.5 and 2 are available from Grue (1991). For large $H/R$, $T_1$ approaches 1 rapidly, while $T_2$ decreases monotonically. The coefficients are overpredicted by these asymptotes, however, as the cylinder approaches the surface and nonlinear effects evidently become important. This is seen from the differences among the results for $M = 2$, 3, and 4. Indeed, comparison with experimental data suggests that even higher-order interactions play a role.

### 3.3.3 Oscillating forces

As demonstrated in table 3.4, limit cycle for the force time history is reached rapidly after $\tau_0/T \sim 3$. The amplitudes of the force harmonics are then obtained using Fourier analysis (with $\tau_0/T$=5).

Figure 3-5 shows the comparisons for the first-harmonic horizontal force amplitude $F_{x1}$ among our high-order ($M = 4$) numerical results, linear (potential flow) analytic solution (Ogilvie 1963), and experimental measurements of Chaplin (1984). Following Chaplin, we plot $F_{x1}$ here as a function of the Keulegan-Carpenter number defined as $K_C = \pi e^{-kH} A/R$, which is based on linear deep water waves. Comparing just the

theoretical and computed results, it is remarkable that the first-harmonic amplitude is affected very little by nonlinear effects at least up to $K_C \sim 1$. On the other hand, as suggested by Chaplin, effects of (clockwise) circulation around the cylinder result in a sharp decrease of $F_{x1}$ for $K_C >\sim 0.5$ (possible effects of flow separation and wave breaking also cannot be ruled out). Our numerical results also show a reduction due to nonlinear diffraction but the magnitude is small compared to that due to circulation or real fluid effects.

In direct contrast to the first-harmonic force, circulation does not appear to affect the higher-harmonic forces as shown in figure 3-6 for $F_{x2}$ and $F_{x3}$. The higher-order (potential flow) results are in excellent agreement with Chaplin's data up to $K_C \sim 1$, beyond which the effects of wave breaking most likely are important. The computed data also readily confirm the expected quadratic and cubic dependencies respectively of $F_{x2}$ and $F_{x3}$ on the Keulegan-Carpenter number.

### 3.3.4 Mean forces

We finally turn to the steady (drift) forces on the cylinder which is the main focus of this study.

First, we show the dependence of mean forces on body submergence by varying $kH$ with fixed $kR = 0.4$ and $kA = 0.12$. This is shown in figures 3-7 and 3-8 where our high-order calculations using $M = 2, 3, 4$ are compared with the measurements of Miyata *et al.* (1988). The horizontal drift force $\bar{F}_x$, figure 3-7, is negative (against the direction of wave propagation) with a magnitude which increases, as expected, with decreasing submergence. Except for relatively shallow submergence, $H/R <\sim 1.75$, the numerical predictions agree well with measurements. Since our computations do not account for wave breaking, it is evident that nonlinear diffraction effects rather than wave breaking is the dominant cause of the negative drift force. For $H/R <\sim 1.75$, extensive wave breaking is observed in the experiments, and the magnitude of the negative drift force is smaller compared to the diffraction results. This provides some evidence that the presence of wave breaking may lead to positive mean horizontal forces on the cylinder.

For the mean uplift force $\bar{F}_z$, figure 3-8, our numerical results compare well with both the second-order analytic solution (Ogilvie 1963) and the measurements of Miyata *et al* (1988). Higher-order interactions and wave breaking effects are evidently less important for the vertical mean force.

It is clear that since $\bar{F}_x$=0 up to second order in wave steepness (Ogilvie 1963), the next available contribution is at most fourth order. Likewise, one may expect a fourth-order correction to the second-order $\bar{F}_z$. These expectations are confirmed by our calculation of the mean forces for varying incident wave slopes $kA$ (fixing $kR = 0.4$ and $kH = 2.0$). Figure 3-9 shows the numerical results ($M$=2,3,4) for $\bar{F}_x$ and $\bar{F}_z$ which have been normalized by their expected leading-order magnitudes proportional to $\epsilon^4$ and $\epsilon^2$ respectively. As expected, these normalized values approach constant asymptotes for small $kA$. For the mean uplift force, this asymptote is well predicted by the second-order value based on the (analytic) first-order potential only. Hereafter, we concentrate on the 'truly' nonlinear horizontal drift force.

To assist us in understanding the horizontal drift force results, it is useful to obtain an estimate based on the conservation of energy and linear horizontal momentum. We neglect wave reflection (cf. §3.3.2) and consider the incident/transmitted wave amplitudes far up/down stream of the body. Let $a_n$ and $b_n$ be the $n$-th harmonic of the incident and transmitted wave amplitudes respectively. Following Longuet-Higgins (1977), we further assume that all $a_n$, $b_n$, $n = 1, 2, \ldots$ are of the same order of magnitude and consider only 'bi-linear' interactions. With this assumption, application of the conservation of horizontal momentum yields an expression for the horizontal drift force which, to leading order, is given by:

$$\bar{F}_x = \frac{\rho g}{4} \sum_{n=1} (a_n^2 - b_n^2) \,. \tag{3.10}$$

From the conservation of energy, $a_n$ and $b_n$ are related by

$$\sum_{n=1} a_n^2/n = \sum_{n=1} b_n^2/n. \tag{3.11}$$

For Stokes incident waves, the first-harmonic amplitude $a_1$ is much greater than all

other harmonics, so that we can neglect all $a_n$, $n > 1$ terms in (3.10) and (3.11). Substituting (3.11) into (3.10), we obtain finally

$$\bar{F}_x = -\frac{\rho g}{4} \sum_{n=2} b_n^2 (n-1)/n. \tag{3.12}$$

Equation (3.12) provides a way to estimate $\bar{F}_x$ given the transmitted wave harmonic amplitudes, and is a generalization of a result of Longuet-Higgins (1977) who included the first ($b_2$) term only. Note that in view of the 'bi-linear' assumption, higher-order interaction terms involving different harmonics (especially in the transmitted waves) are neglected in (3.10) and (3.11). Therefore (3.12) must be considered only as an approximate formula valid primarily for small wave steepness.

The prediction using (3.12) based on computed transmitted wave amplitudes is compared to that obtained by direct pressure integration in figure 3-10, where $\bar{F}_x$ is plotted as a function of $kA$. For small wave slopes, $kA <\sim 0.03$, (3.12) with only $b_2$ provides an adequate estimate. As $kA$ increases further beyond $\sim$0.05, $b_2$ reaches its maximum (cf. figure 3-3) and consequently also the estimated drift force based on $b_2$, while the actual $\bar{F}_x$ continues to increase. The prediction based on (3.12) is improved if third harmonic transmitted waves are taken into account, and the discrepancy is not appreciable until after $kA \sim 0.05$. Not completely unexpected, applications of (3.12) with even higher transmitted wave harmonics included (not shown) do not produce appreciable further improvements unless wave reflection and higher-order interactions are also considered. In so far as independent ways are used to obtain $\bar{F}_x$, figure 3-10 can be considered a further validation of our predictions of the fourth-order negative drift force.

In the context of a frequency-domain perturbation approach, we see from the expression for the pressure on the body (2.4) that steady forces must be due to quadratic interactions of the perturbation potentials $\tilde{\phi}_n^{(m)}$. Specifically, the horizontal drift force on the circular cylinder is given, up to fourth order in the wave slope, by:

$$\bar{F}_x \sim \int_0^{2\pi} d\theta \, R \cos\theta \, (\nabla\tilde{\phi}_1^{(1)} \cdot \nabla\tilde{\phi}_1^{(1)*}$$

$$+2\nabla\tilde{\phi}_1^{(1)}\cdot\nabla\tilde{\phi}_1^{(3)*}+\nabla\tilde{\phi}_2^{(2)}\cdot\nabla\tilde{\phi}_2^{(2)*}+\nabla\tilde{\phi}_0^{(2)}\cdot\nabla\tilde{\phi}_0^{(2)*}+\text{c.c.})\,, \quad (3.13)$$

where * denotes complex conjugate, and "c.c." the complex conjugate of the preceding terms. Equation (3.13) is obtained by direct integration of the pressure over the cylinder and taking time average.

As shown by Ogilvie (1963), the first term in (3.13), which is second order, has no contribution to the mean force, so that the drift force results from the remaining three fourth-order terms. For later convenience, we denote the 2nd, 3rd and 4th terms in (3.13) by $\bar{F}_{11}$, $\bar{F}_{22}$, and $\bar{F}_{00}$ respectively. With the present accurate high-order (albeit time-domain) results, it is possible to deduce the respective contributions of $\bar{F}_{11}$, $\bar{F}_{22}$, and $\bar{F}_{00}$ to $\bar{F}_x$. (We solve the problem up to $M$=3, obtain the steady-state potential $\Phi^{<3>}$, from which we determine the amplitudes $\phi_0^{<3>}$, $\phi_1^{<3>}$, and $\phi_2^{<3>}$ via harmonic analysis. Using (2.26), we calculate $\bar{F}_{22}$ and $\bar{F}_{00}$ to *leading* (fourth) order using $\phi_2^{<3>}$ and $\phi_0^{<3>}$ instead of $\tilde{\phi}_2^{(2)}$ and $\tilde{\phi}_0^{(2)}$. Finally, since there is no drift force due to $\tilde{\phi}_1^{(1)}$ (and there is no $\tilde{\phi}_1^{(2)}$), we deduce that $\bar{F}_{11}$ is produced by the self-interaction of $\phi_1^{<3>}$.)

The drift force components $\bar{F}_{11}$, $\bar{F}_{22}$, and $\bar{F}_{00}$ are plotted in figure 3-11 as functions of $H/R$. As expected, all three components have magnitudes which diminish with body submergence. Overall, the magnitude of $\bar{F}_{00}$ is much smaller than $\bar{F}_{11}$ and $\bar{F}_{22}$ which implies that the self-interaction of zeroth-harmonic waves has negligible effect on $\bar{F}_x$. More importantly, we note that for any body submergence, $\bar{F}_{22}$ is non-negative, while $\bar{F}_{11}$ is always negative and much greater in magnitude. Thus, the *negative* horizontal drift force is a result of the *difference* between these two magnitudes. An immediate consequence of this is that one indeed needs to solve the third order perturbation problem to obtain $\bar{F}_x$, and a frequency-domain solution up to and including $\tilde{\phi}^{(2)}$, for example, is inadequate, and in fact would produce the wrong sign for the horizontal drift force!

One advantage of having identified the components in (3.13) is that one can now deduce how $\bar{F}_x$ would, in principle, attenuate with body submergence. Specifically, for small $kR$, we expect the self-interaction of first-harmonic waves (first- and third-order) to decay as $\bar{F}_{11}\sim e^{-4kH}$; while that for second-harmonic waves as $\bar{F}_{22}\sim e^{-8kH}$.

These are qualitatively confirmed in figure 3-11 (although the actual attenuation rates are somewhat slower probably due to the effect of finite body radius.) By accounting for these submergence dependencies (and magnitudes) of $\bar{F}_{11}$ and $\bar{F}_{22}$, it is evident that *in general* $\bar{F}_x$ is negative and dominated by $\bar{F}_{11}$ except possibly for small submergence. As $kH$ decreases, $\bar{F}_{22}$ increases more rapidly than $\bar{F}_{11}$, so that at very shallow submergence, the magnitude of the negative drift force may be reduced appreciably by $\bar{F}_{22}$. This is in qualitative agreement with the experimental observations of Miyata *et al.* (1988) and Inoue & Kyozuka (1984).

Finally, we point out that by considering the radiation stress (Longuet-Higgins 1977), the horizontal drift force is related to the mean set-down above the cylinder. Figure 3-12 plots the separate contributions to the mean set-down associated with $\bar{F}_{22}$ and $\bar{F}_{11}$. The corresponding time-averaged pressure distributions on the cylinder associated with these two interactions are also shown. The larger (smaller) downstream mean set-down for $\bar{F}_{22}$ ($\bar{F}_{11}$) and the distribution of the mean pressure provide immediate qualitative confirmation of the positive (negative) sign and magnitude of its contribution to $\bar{F}_x$. (Note that this is not inconsistent with figure 3-10 since $b_1$ depends on $\tilde{\phi}_1^{(3)}$.)

When the body submergence is sufficiently small and/or the incident wave steepness is sufficiently large, wave breaking above the cylinder must be expected and the present method and results are no longer applicable. It has been suggested (Longuet-Higgins 1977) that wave breaking provides the *dominant* contribution to the negative drift force. This is not completely supported by measurements (for example, Miyata *et al* 1988) which indicate that as the body submergence is reduced and wave breaking therefore enhanced, the magnitude of the negative drift force may, in fact, decrease. Although the present method is not valid for breaking (and near breaking) waves, our results compare well with experimental data (not in the breaking range) and explain the potential flow mechanism for the negative drift force. Not insignificantly, we are also able to offer an explanation for the observed decrease of its magnitude with small submergence (due to $\bar{F}_{22}$) which may be manifest even in the presence of intensifying wave breaking.

## 3.4 Conclusions

The efficient high-order spectral method has been employed to study nonlinear wave diffraction by a submerged circular cylinder. Extensive convergence tests are carried out to validate the accuracy and its dependence on the computational parameters. Results are presented for the harmonic amplitudes of the transmitted and reflected waves, and the mean and harmonic amplitudes of the forces on the cylinder. Corroborations with theoretical and computational predictions and experimental measurements are made whenever they are available. The comparisons are in uniformly good agreement. Of special interest is our quantification of the horizontal drift force which is fourth order in the incident wave steepness and negative. It is shown that the dominant contribution of this force is a result of the interaction between first- and third-order first-harmonic waves. The effect of similar nonlinear interactions on a three-dimensional body will be investigated in the next chapter.

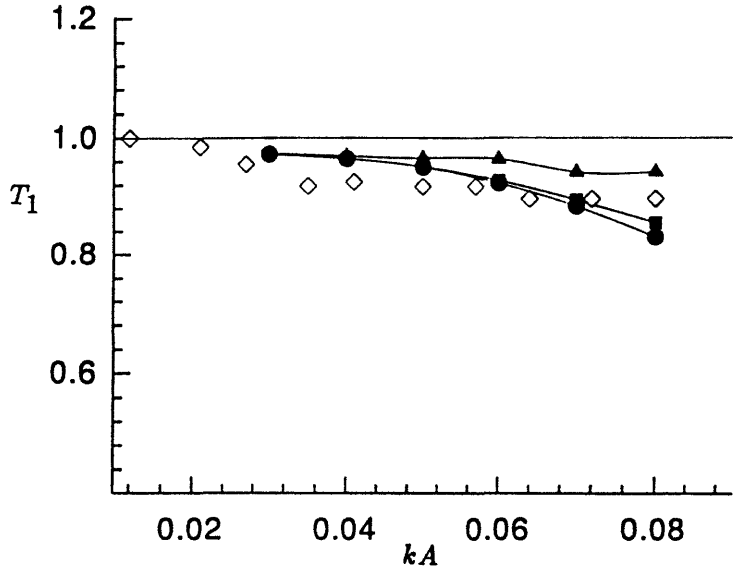


Figure 3-1: Dependence of the first-harmonic wave transmission coefficient $T_1$ on the incident wave slope $kA$. Experiments (Grue 1991) (◇); linear solution (——); and present high-order results for $M = 2$ (▲), $M = 3$ (■), and $M = 4$ (●). ($kR = 0.4, H/R = 1.5$.)

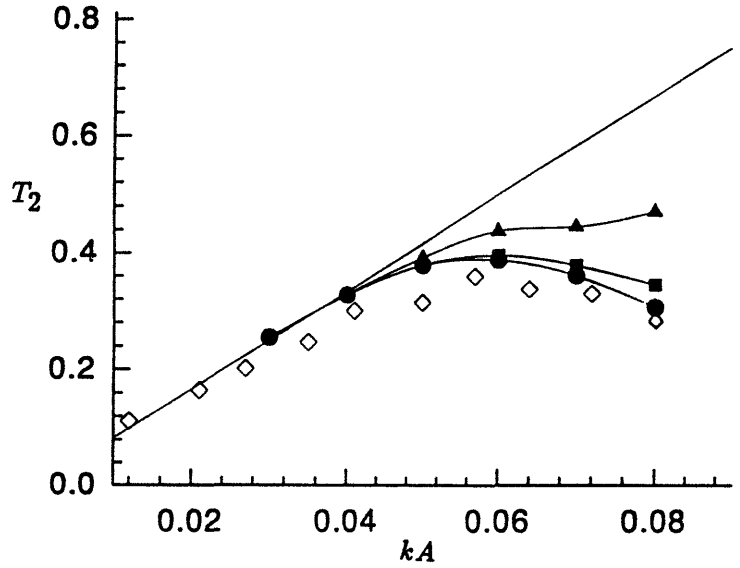


Figure 3-2: Dependence of the second-harmonic wave transmission coefficient $T_2$ on the incident wave slope $kA$. Experiments (Grue 1991) (◇); second-order computation (Vada 1987) (——); and present high-order results for $M = 2$ (▲), $M = 3$ (■), and $M = 4$ (●). ($kR = 0.4, H/R = 1.5$.)

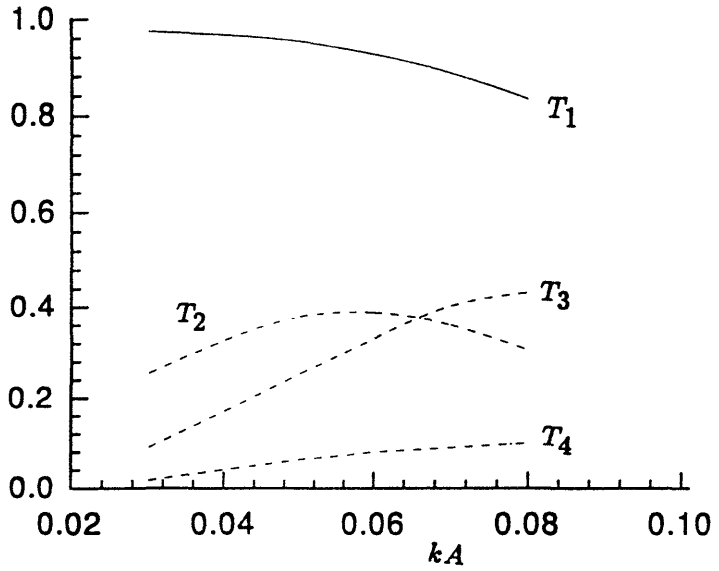


Figure 3-3: High-order spectral solution ($M = 4$) of harmonic wave transmission coefficients $T_1, T_2, T_3, T_4$ as a function of incident wave slope $kA$. ($kR = 0.4, H/R = 1.5$.)

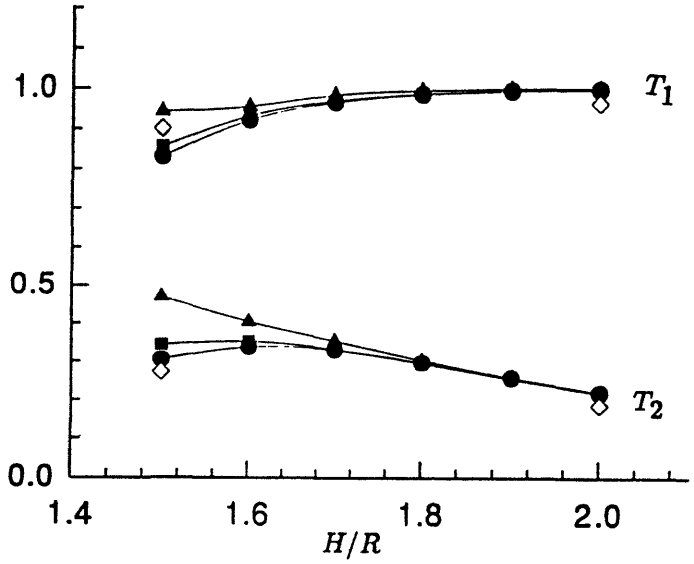


Figure 3-4: Dependence of the first- and second-harmonic wave transmission coefficients on the body submergence $H/R$. Experiments (Grue 1991) (◇); and present high-order results for $M = 2$ (▲), $M = 3$ (■), and $M = 4$ (●). ($kR = 0.4, kA = 0.08$.)

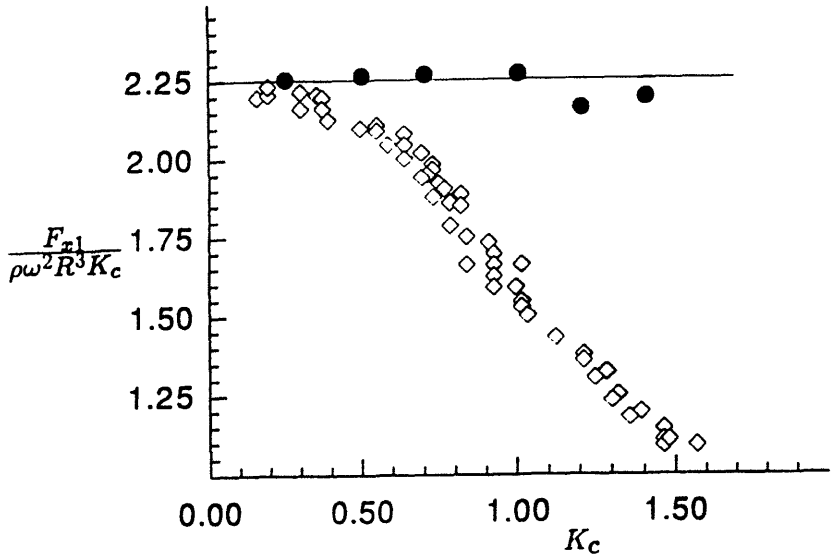


Figure 3-5: The first-harmonic horizontal force $F_{x1}$ as a function of Keulegan-Carpenter number $K_c$. Experiments (Chaplin 1984) ($\diamond$); linear result (Ogilvie 1963) (——); and present high-order results for $M = 4$ ($\bullet$). ($kR = 0.21, H/R = 2.0$.)

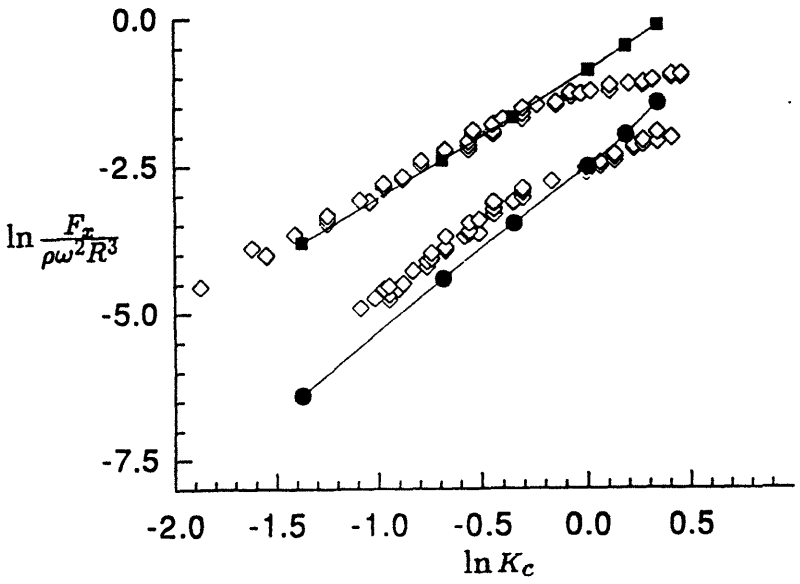


Figure 3-6: The second- and third-harmonic horizontal forces $F_{x2}$, $F_{x3}$ as a function of Keulegan-Carpenter number $K_c$. Experiments (Chaplin 1984) ($\diamond$); and present high-order results with $M = 4$ for $F_{x2}$ ($\blacksquare$) and $F_{x3}$ ($\bullet$). ($kR = 0.21, H/R = 2.$)

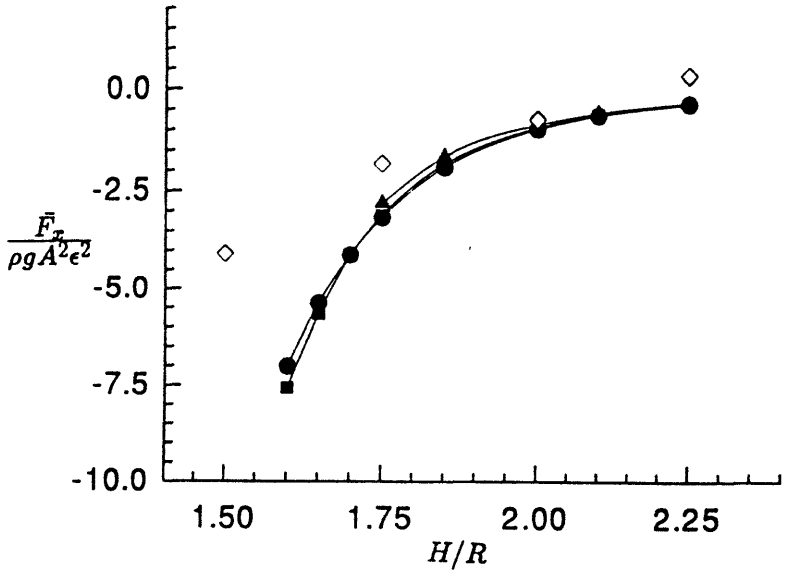


Figure 3-7: Horizontal drift force as a function of body submergence. Experiments (Miyata et al. 1988) (◇); and present high-order results for $M = 2$ (▲), $M = 3$ (■), and $M = 4$ (●). ($kR = 0.4, \epsilon = kA = 0.12$.)

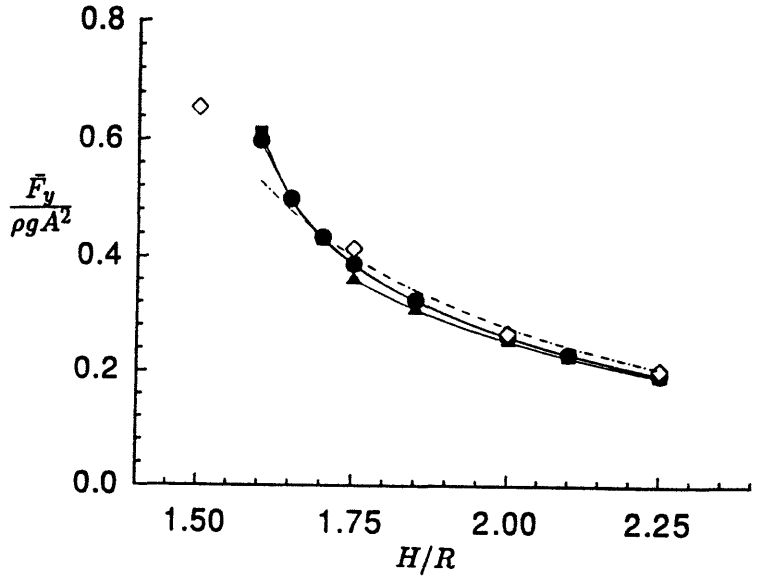


Figure 3-8: Vertical drift force as a function of body submergence. Experiments (Miyata et al. 1988) (◇); linear potential solution (Ogilvie 1963) (— · —); and present high-order results for $M = 2$ (▲), $M = 3$ (■), and $M = 4$ (●). ($kR = 0.4, \epsilon = kA = 0.12$.)

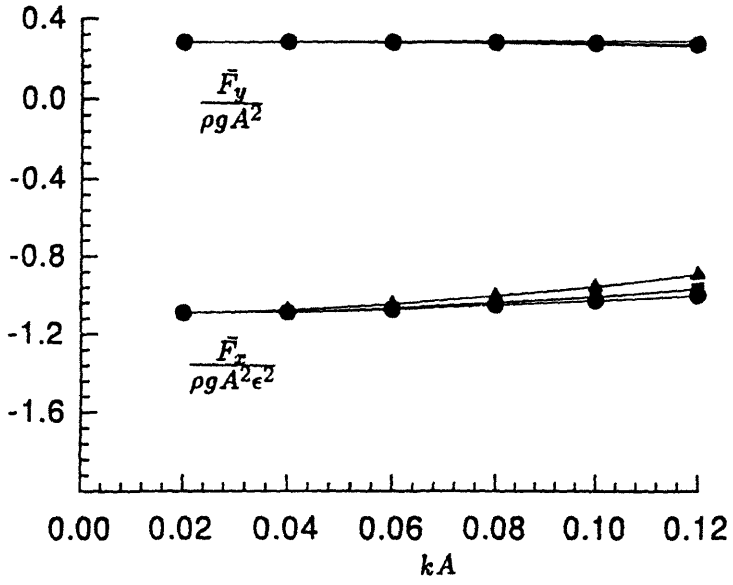


Figure 3-9: Dependence of the horizontal and vertical drift forces on the incident wave slope $\epsilon = kA$. $M = 2$ (▲), $M = 3$ (■), and $M = 4$ (●). ($kR = 0.4, H/R = 2.$)

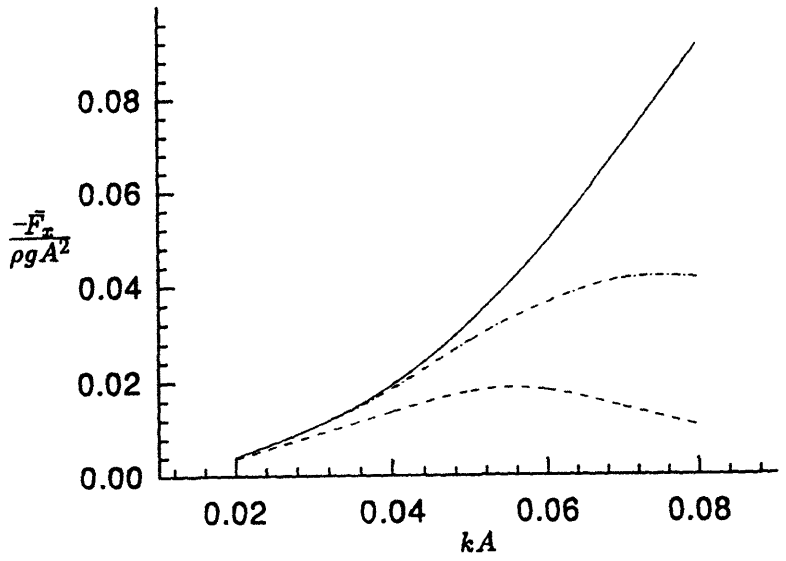


Figure 3-10: Comparison of the horizontal drift force as a function of wave slope $kA$. The results are from direct high-order simulation with $M = 4$ (——); Eq. (3.12) using $b_2$ only (- - -); and Eq. (3.12) including $b_2$ and $b_3$ (— · —). ($kR = 0.4, H/R = 1.5.$)

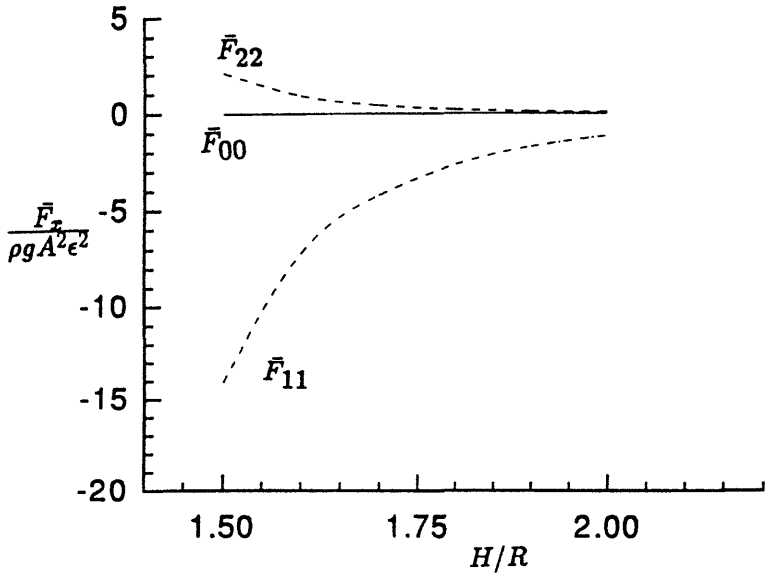


Figure 3-11: Contributions of the three fourth-order components $\bar{F}_{00}, \bar{F}_{11}, \bar{F}_{22}$ to the mean horizontal drift force as a function of submergence $H/R$. ($kR = 0.4, \epsilon = kA = 0.04$.)

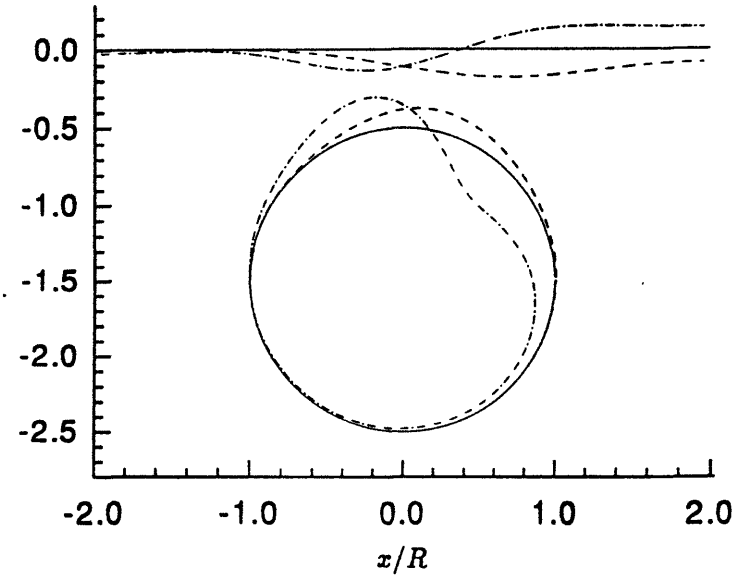


Figure 3-12: Separate contributions associated with the self-interactions of the first-harmonic $(\,)_{11}$ and second-harmonic $(\,)_{22}$ waves to the mean free surface: $\bar{\eta}_{11}/kA^2$ (— · —); $\bar{\eta}_{22}/kA^2$ (- - -); and the mean pressure on the cylinder surface: $5\bar{p}_{11}/\rho gkA^2$ (— · —); $5\bar{p}_{22}/\rho gkA^2$ (- - -). Pressure is plotted positive into the body. ($kR = 0.4, H/R = 1.5, kA = 0.04$.)

# Chapter 4

# The mean force and pitch moment on a submerged spheroid

After finding significant and strong high-order free-surface effects on a two-dimensional submerged body, in this chapter, we investigate nonlinear wave interactions with a three-dimensional body. To illustrate interaction mechanisms, we consider wave diffraction by a submerged spheroid and especially focus on the study of nonlinear solutions for the steady force and moment on the body.

Compared to unsteady components, the steady force and moment are usually small in magnitude, and thus have no significant influence on body oscillations. However, they can be important when considering drifting motions of the body. Especially for a submerged body, since there is no hydrostatic restoring force in both vertical and horizontal planes, a large excursion or rotation of the body can result from even a very small wave-induced steady force or moment if it acts over a sufficiently long period of time. This large drifting motion may be of even greater significance than oscillatory motion for the operation of submarines and underwater vehicles.

For a submerged spheroid in beam seas, there is no horizontal drift force according to the strip theory prediction. If the three-dimensional effect is included, a positive second-order horizontal drift force is expected in principle, which diminishes as the body becomes more slender. When strong nonlinear interactions are involved, it is known that there can be a negative drift force even on a two-dimensional submerged

circular cylinder (chapter 3). Such nonlinear effect can of course also be anticipated for a near-surface spheroid. Thus, linear three-dimensional and nonlinear effects produce opposing horizontal drift forces. For a given spheroid in an ambient wave field, there must be a particular submergence where the total horizontal drift force is identically zero.

In head seas, the slender body theory (*e.g.* Lee & Newman 1971) predicts that the vertical drift force is dominated by the 'IB' interaction between the incident wave (I) and the body disturbance (B), whereas the mean pitch moment vanishes since the 'IB' interaction is symmetric about the midbody section. A three-dimensional panel method solution (Lee & Newman 1991), however, reveals the presence of a non-zero mean pitch moment which is primarily due to the quadratic (BB) interaction of the body disturbance itself. Such non-zero mean pitch moment has strong dependence on slenderness of the body and vanishes rapidly as the aspect ratio of the body increases. For a high aspect-ratio spheroid near the free surface, we generally expect nonlinear wave effects to be dominant for the mean pitch moment on the body.

We here employ the high-order spectral method (developed in chapter 2) to solve the present nonlinear wave-body problem up to order $M = 3$ in the incident wave slope. Nonlinear solutions (§4.3) including complete fourth-order corrections for the steady force and moment on the spheroid are obtained. It is found that when nonlinear wave effects are included, the mean pitch moment changes its direction from bow-down to bow-up as the incident wave steepens or when the submergence is decreased. Similar to the horizontal drift force in beam seas, for a given sea state and body aspect ratio, a submergence can be found at which the mean pitch moment vanishes. Through systematic study of the dependences of the linear solution and high-order corrections on effective parameters, a simple formula is established to estimate this special depth.

## 4.1 Computational issues

We consider the diffraction of nonlinear gravity waves by a fixed, submerged spheroid in deep water. The center of the body is submerged a distance $H$ beneath the mean free surface. For convenience, we denote the major and minor axes of the spheroid by $a$ and $b$. The high-order spectral method is employed to solve this wave-body problem by accounting for nonlinear free-surface effects up to an arbitrary order $M$ in wave steepness. Through accurate initial-value simulations, we obtain high-resolution transient solutions for the nonlinear force and moment on the body. The harmonic components are obtained via the Fourier transforms of steady-state time histories.

As in two dimensions, the base flow is chosen to be $\bar{\phi}(\mathbf{x}, z) = 0$. On the body, the condition of zero normal velocity ($\Phi_n = 0$) is applied. For a three-dimensional body, we impose doubly-periodic boundary conditions at $x = \pm L$ and $y = \pm W$ in the horizontal plane. As initial conditions, the surface elevation $\eta(\mathbf{x}, 0)$ and potential $\Phi^s(\mathbf{x}, 0)$ are prescribed from Stokes waves.

With the high-order spectral method, at each time step, the nonlinear boundary-value problem is decomposed into a sequence of linear boundary-value problems for perturbation potentials $\Phi^{(m)}$, $m = 1, \cdots, M$ by expanding the nonlinear free-surface boundary conditions about the mean free surface $z = 0$. These linear problems are successively solved up to the specified order $M$ in wave steepness using global basis functions expansions. After obtaining the free-surface vertical velocity $\Phi_z(\mathbf{x}, \eta, 0)$, the overall problem is integrated in time via (2.8) starting from initial conditions.

### 4.1.1 The basis functions

To construct the basis functions $\Psi_{Fn}$ and $\Psi_{Bn}$, as in two dimensions, we distribute dipoles $\mu(\mathbf{x})$ on the mean free surface ($z = 0$) and sources $\sigma(\theta, \varphi)$ on the body, where $(\theta, \varphi)$ are respectively the polar and azimuthal angles of a point on the body with respect to its center. Noting that the dipole distribution is periodic in both $x$ and $y$,

we can expand $\mu(\mathbf{x})$ in double Fourier series:

$$\mu(\mathbf{x}) = \sum_p \sum_q \mu_{pq} e^{i\pi(px/L+qy/W)} \ . \tag{4.1}$$

As a single-valued function, $\sigma(\theta, \varphi)$ can be periodic in either $\theta$ or $\varphi$. In order to retain rapid convergence for the expansion of $\sigma$, it is necessary to use a representation whose exponential convergence does not depend on the end conditions. Here, we choose to expand $\sigma$ in a Fourier-Chebyshev expansion:

$$\sigma(\theta, \varphi) = \sum_k \sum_\ell \sigma_{k\ell} T_\ell(1 - 2\theta/\pi) e^{ik\varphi} \ . \tag{4.2}$$

Similarly to that in two dimensions, the basis functions $\Psi_{Fn}$ and $\Psi_{Bn}$ can be considered as the influences of the $pq$-th mean free-surface dipole and $k\ell$-th body source distributions, respectively. In terms of double-Fourier and Chebyshev-Fourier integrals, they can be formally expressed as:

$$\Psi_{Fn} \equiv \Psi_{Fpq}(\mathbf{x}, z) = \int_{-L}^{L} \int_{-W}^{W} G_{z'}(\mathbf{x}, z; \mathbf{x}', 0) e^{i\pi(px'/L+qy'/W)} dx' dy' \ , \tag{4.3}$$

and

$$\Psi_{Bn} \equiv \Psi_{Bk\ell}(\mathbf{x}, z) = \int \int_{S_B} G(\theta, \varphi; \theta', \varphi') T_\ell(1 - 2\theta'/\pi) e^{ik\varphi'} ds' \tag{4.4}$$

where $G$ is the doubly-periodic Rankine source potential. With such construction for the basis functions, the convergence of the perturbation potentials in (2.14) is exponential with respect to the number of spectral modes.

### 4.1.2 Doubly-periodic Green function

The Green function $G(\mathbf{x}, z; \mathbf{x}', z')$ represents the velocity potential at the point $(\mathbf{x}, z)$ due to a sequence of periodic Rankine sources located at $(x' + 2jL, y' + 2nW, z')$. Here the integers $j$ and $n$ take any positive and negative values as well as zero. In a series

representation, $G$ can be formally expressed as:

$$G(\mathbf{x},z;\mathbf{x}',z) = \sum_{j=-\infty}^{\infty}\sum_{n=-\infty}^{\infty}\{[(x+2jL-x')^2+(y+2nw-y')^2+(z-z')^2]^{-1/2} \\ -[(jL)^2+(nW)^2]^{-1/2}\}+[(x-x')^2+(y-y')^2+(z-z')^2]^{-1/2} \quad (4.5)$$

where $|j|+|n|>0$. Note that due to slow convergence with respect to $j$ and $n$, in practice, the series in (4.5) cannot be directly summed. For an efficient evaluation of $G$, we follow Newman (1992) and rewrite the Green function $G$ as a summation of single-periodic Green functions $g_n$, $n=0,\pm1,\cdots$. Here $g_n$ represents the potential resulting from a single-periodic array of sources in the $y$-direction. Then we expand each $g_n$ in a series involving trigonometric functions of $y-y'$ and modified Hankel functions of $R_n=[(x-x'+2nL)^2+(z-z')^2]^{1/2}$. Such expansions converge rapidly with increasing $n$ except when $R_n \leq \min(2L,2W)$. To complement this, we use two-dimensional Chebyshev expansions in $y-y'$ and $R_n$ for $R_n < \min(2L,2W)$. With these effective series expansions, the computational effort for the calculation of $G$ as well as its derivatives with the accuracy of $O(10^{-6})$ is only $O(10)$ times more than that for a single Rankine source.

### 4.1.3 Numerical implementation

The numerical procedure for the time simulation of three-dimensional nonlinear wave-body interactions is identical to that in two dimensions (cf. §3.1.2) except for a slight difference in distributing free-surface and body control points.

In three-dimensional calculations, the numbers of free-surface and body spectral modes are truncated at $N_F = N_x N_y$ and $N_B = N_\theta N_\varphi$, respectively. Since the basis functions are orthogonal, the convergence of (2.14) is exponentially rapid with respect to $N_F$ and $N_B$. On the mean free surface, $N_F$ control points are uniformly spaced in the $x-$ and $y-$directions with $\Delta x = 2L/N_x$ and $\Delta y = 2W/N_y$. On the body, $N_B$ control points are collocated at the zeros of $T_{N_\theta}(1-2\theta/\pi)$ while equally spanned in $\varphi$ with $\Delta\varphi = 2\pi/N_\varphi$. With these distributions of control points, the transform between the spectral and physical representations can be effected by the use of the

| $N_w$ | $M=1$ | $M=2$ | $M=3$ |
|---|---|---|---|
| 4 | .09210 | .05390 | .05450 |
| 8 | .09761 | .05677 | .05745 |
| 16 | .09802 | .05707 | .05752 |

Table 4.1: Convergence of the normalized mean pitch moment, $\bar{M}_y/\rho g b^2 A^2$, on a submerged spheroid in head seas with increasing the number of wavelengths $N_w$ of the doubly-periodic domain and for different order $M$. $kA$=0.05, $ka = \pi/2$, $\gamma = 0.1$, $H/a = 0.2$; and $N_x = N_y = 16N_w$, $N_\varphi = N_\theta = 8$, $T/\Delta t$=64, $\tau_0$=5$T$.

FFT's. The computational effort required is merely a linear function of the number of spectral modes $N_F$ (in general $N_F \gg N_B$).

## 4.2 Convergence tests

The main sources of the computational error for the present high-order wave-body simulations are: (i) errors due to the truncation in the numbers of Fourier and Chebyshev spectral modes $N_x, N_y, N_\varphi, N_\theta$, and the perturbation order $M$; (ii) error due to the finite (periodic) computational domain for a given simulation time $T_S$; (iii) amplification of round-off and truncation errors; (iv) aliasing errors of the pseudo-spectral method; (v) errors due to numerical time integration; and (vi) for estimates of mean force and moment coefficients etc., errors due to the finite simulation time, $T_S$, of the initial-value problem.

To verify the accuracy and convergence of the present method, we conduct systematic numerical tests for the mean pitch moment $\bar{M}_y$ on a submerged spheroid in head seas. For numerical calculations, the body parameters are chosen to be: the major radius $ka = \pi/2$, the slenderness $\gamma = b/a = 0.1$, and the submergence $H/a$=0.2.

We first test the convergence of the solution with increasing size of the computational domain. For a square computational domain ($L = W$), table 4.1 shows the results for the mean pitch moment for increasing $N_w$, keeping $kA$, $ka$, $\gamma$ and $H/a$ fixed. For $N_w$=8, it is seen that $\bar{M}_y$ converges up to three significant figures.

For sufficiently smooth $\eta$ and $\Phi^s$, the numerical errors in the (Fourier and Cheby-

| $(N_\varphi, N_\theta)$ | $M=1$ | $M=2$ | $M=3$ |
|---|---|---|---|
| (4,8) | .07510 | .03699 | .03850 |
| (8,8) | .09761 | .05677 | .05745 |
| (16,8) | .09801 | .05692 | .05760 |
| (8,4) | .06350 | .06537 | .06643 |
| (8,8) | .09761 | .05677 | .05745 |
| (8,16) | .09820 | .05647 | .05662 |

Table 4.2: Convergence of the normalized mean pitch moment, $\bar{M}_y/\rho g b^2 A^2$, on a submerged spheroid in head seas with number of body mode $N_B = N_\theta N_\varphi$ and order $M$. $kA$=0.05, $ka = \pi/2$, $\gamma = 0.1$, $H/a = 0.2$; and $N_w = 8$, $N_x = N_y = 16N_w$, $T/\Delta t$=64, $\tau_0$=5$T$.

| $N_x/N_w$ | $M=1$ | $M=2$ | $M=3$ |
|---|---|---|---|
| 8 | .14343 | .13890 | .14192 |
| 16 | .09761 | .05677 | .05745 |
| 32 | .09810 | .05662 | .05677 |

Table 4.3: Convergence of the normalized mean pitch moment, $\bar{M}_y/\rho g b^2 A^2$, on a submerged spheroid in head seas with number of free-surface mode $N_F = N_x N_y$ and order $M$. $kA$=0.05, $ka = \pi/2$, $\gamma = 0.1$, $H/a = 0.2$; and $N_w = 8$, $N_y = N_x$, $N_\varphi = N_\theta = 8$, $T/\Delta t$=64, $\tau_0$=5$T$.

shev) spectral representations of $\eta$, $\Phi^s$, and $\Phi^{(m)}, m = 1, \cdots, M$ vanish exponentially as $N_F = N_x N_y$ and $N_B = N_\theta N_\varphi$ are increased. Similarly, for mild nonlinearities, the truncation errors after order $M$ is $O(\epsilon^{M+1})$, and the convergence is also exponential with increasing $M$. The convergence with the number of body modes, $N_B = N_\theta N_\varphi$, keeping $N_F = N_x N_y$, and other parameters fixed, is shown in table 4.2. At a given order $M$, $\bar{M}_y$ converges to its limit exponentially fast as $N_\theta$ and $N_\varphi$ are increased.

Similar rapid convergence with respect to the number of free-surface modes, $N_F$, as well as order $M$ is displayed in table 4.3. As in two dimensions, we must note that such fast convergence ceases when the maximum local surface wave slope $\epsilon_L \equiv (\partial\eta/\partial x)_{max}$ (usually occuring on the top of the body) exceeds its limit .38. It is important to point out that beyond this limit, converged results (not necessarily exponentially fast) for large local slopes up to $\epsilon_L \sim 1.5$ can still be obtained.

In general, the steady-state limit (limit-cycle) in three dimensions is reached quicker than that in two dimensions. For the mean pitch moment on the spheroid, we note that the required simulation time is typically about $(2 \sim 3)T$. The global truncation error for $T_S = O(1)$ is fourth-order in $\Delta t$ due to the use of the fourth-order Runge-Kutta scheme for the numerical time integration.

Unless otherwise stated, for all subsequent computations, we use $N_w$=8, $N_x = N_y$=$16N_w$, $N_\varphi = N_\theta$=16, $\tau_0$=$5T$, and $\Delta t = T/64$. Based on the foregoing numerical tests, we anticipate the maximum error for $\bar{M}_y$ to be less than 1%.

In addition to these convergence tests, all our computations are checked for the conservation of volume, as well as the invariance of the total energy. For all of following results we present, the volume and total energy do not deviate by more than 1% from their initial values.

## 4.3 Numerical Results

We consider the nonlinear diffraction of Stokes waves by a submerged spheroid. The spectral method is applied to solve this problem up to third order ($M = 3$) in wave steepness. Nonlinear solutions for the mean (drift) and harmonic force and moment coefficients are obtained. In addition to further validation of the present method, we focus on the study of nonlinear solutions with a special emphasis on the mean pitch moment on the body.

### 4.3.1 Comparisons to frequency-domain solutions

To further verify the solution by the present time-domain approach, we make direct comparisons to the linear and high-order components of perturbation methods in the frequency domain.

For a submerged stationary sphere, we accurately calculate the wave force on the body including high-order free-surface effects using the present efficient computational method. The harmonic amplitudes are compared to the theoretical and numerical results of Wu & Eatock Taylor (1987) and Kim & Yue (1989). Both results of Wu

| $ka$ | Wu & Eatock Taylor | Kim & Yue | $M = 1$ | $M = 2$ |
|---|---|---|---|---|
| 0.5 | 1.6474 | 1.6497 | 1.6423 | 1.6344 |
| 1.0 | 1.3929 | 1.4003 | 1.3889 | 1.3898 |
| 1.5 | 0.8703 | 0.8752 | 0.8689 | 0.8682 |
| 2.0 | 0.5047 | 0.5078 | 0.5047 | 0.5039 |

Table 4.4: Comparisons between existing frequency-domain and the present time-domain results for the first-harmonic vertical force coefficient $|F_z^{(1)}|/\rho g a^2 A$. $H/a = 1.5$ and $\epsilon = kA$=0.03.

| $ka$ | Kim & Yue | $M = 2$ | $M = 3$ |
|---|---|---|---|
| 0.5 | .3921 | .3625 | .3716 |
| 1.0 | .2563 | .2460 | .2492 |
| 1.5 | .1302 | .1214 | .1253 |
| 2.0 | .0641 | .0572 | .0581 |

Table 4.5: Comparisons between existing frequency-domain and the present time-domain results for the second-harmonic vertical force coefficient $|F_z^{(2)}|/\rho g a A^2$. $H/a = 1.5$ and $\epsilon = kA$=0.03.

& Eatock and Kim & Yue are directly obtained in the frequency domain. Specifically, Wu & Eatock Taylor analytically solved the linearized problem for a submerged spheroid by expanding the source distribution on the body in a series of Legendre functions, while Kim & Yue solved the complete second-order problem for an axisymmetric body using a panel method. For the case of $H/a = 1.5$, the comparisons for the first- and second-harmonic vertical forces are respectively shown in tables 4.4 and 4.5 for a range of incident wavelength $ka$. The agreements among results by different methods are very good and thus confirm the accuracy of first- and second-order potentials of the present method. In particular, the discrepancies between results obtained by the present time-domain method and that by the frequency-domain approaches for normalized force amplitudes are all seen to be within the limit of $O(\epsilon)$. This further supports the relation in (2.26).

We remark that with the use of sufficiently many panels, the results of Kim & Yue (1989) in tables 4.4 and 4.5 are accurate to the third decimal place.

### 4.3.2 Mean pitch moment in head seas

Under head-sea conditions, the incident wave is assumed to propagate in the negative $x$-direction, parallel to the body axis. The bow of the spheroid is referred to the end ($x = a$) which faces the incoming waves. This definition is important for later discussion regarding to the sign of the mean pitch moment.

We consider a spheroid with a major axis of $ka = \pi/2$, a slenderness of $\gamma = 0.1$, and a submergence of $H/a = .2$, and carry out the computations up to $M = 3$ by varying the surface wave slope $kA$. The results for the mean pitch moment with $M = 1, 2$ and 3 are displayed in figure 4-1, where the linear (frequency-domain) panel-method solution of Lee & Newman (1991) is also shown. It is seen that the linear solution ($M = 1$), denoted by $\bar{M}_{11}$, agrees well with that of Lee & Newman (1991) and is always positive (bow-down). After including high-order potential effects ($M = 2, 3$), we surprisingly find that the total mean pitch moment, $\bar{M}_y$, changes its direction from bow-down to bow-up as the incident waves steepen. This implies that quadratic interactions among high-order potentials must contribute a significant bow-up pitch moment.

For a slender body, it is generally expected that the mean pitch moment is dominated by the distribution of the vertical drift force $\bar{F}_z(x)$, while the effect of the horizontal drift force is relatively small and can be neglected. To assist us in understanding the mean pitch moment results, we split the vertical drift force into a symmetric part, $\bar{F}_{zs}(x)$, and an asymmetric part, $\bar{F}_{za}(x)$, with respect to the mid-body section ($x = 0$). Clearly, the mean pitch moment is due to the action of $\bar{F}_{za}$, but not $\bar{F}_{zs}$. For the case of $kA = .14$, the distributions of $\bar{F}_{zs}$ and $\bar{F}_{za}$ are depicted in figure 4-2 where the linear solution, $(\bar{F}_z)_{11}$, and the nonlinear correction, $(\bar{F}_z)_{NL}$ are presented separately. We clearly see that $(\bar{F}_{za})_{NL}$ is comparable to $(\bar{F}_{za})_{11}$ in magnitude, and the resulting pitch moments should also be comparable, i.e. $\bar{M}_{NL} \sim \bar{M}_{11}$. Furthermore, $(\bar{F}_{za})_{NL}$ and $(\bar{F}_{za})_{11}$ are seen to have opposite sign, and the total mean pitch moment is thus a result of the difference between $\bar{M}_{NL}$ and $\bar{M}_{11}$.

In the following, we establish a simple formula for the estimation of the total mean pitch moment on the body by analyzing the dependences of the solution on effective

factors such as wave steepness, submergence and slenderness.

First we identify the associated potential interactions with both the linear and nonlinear solutions. To do that, we write the mean pressure on the body up to fourth-order in the wave slope as:

$$\frac{\bar{P}}{\rho} = (\nabla\tilde{\phi}_1^{(1)} \cdot \nabla\tilde{\phi}_1^{(1)*} + 2\nabla\tilde{\phi}_1^{(1)} \cdot \nabla\tilde{\phi}_1^{(3)*} + \nabla\tilde{\phi}_2^{(2)} \cdot \nabla\tilde{\phi}_2^{(2)*} + \nabla\tilde{\phi}_0^{(2)} \cdot \nabla\tilde{\phi}_0^{(2)*} + c.c.)\,. \quad (4.6)$$

From (4.6), we see that the steady moment is due to quadratic interactions of the perturbation potentials, $\tilde{\phi}_n^{(m)}$. Specifically, the linear solution $\bar{M}_{11}$ results from the first term in (4.6) which represents the self-interaction of the linear potential $\tilde{\phi}_1^{(1)}$. The nonlinear correction (up to fourth-order), $\bar{M}_{NL}$, is produced by the remaining three terms in (4.6) which are the result of quadratic interactions among high-order potentials. For the convenience of later discussions, these high-order potential effects are denoted by $\bar{M}_{13}$, $\bar{M}_{22}$, and $\bar{M}_{00}$, respectively.

Based on the perturbation analysis, it is clear that $\bar{M}_{11}$ is of second-order in the wave slope. This is confirmed by the linear solution ($M = 1$) in figure 4-1, where normalized $\bar{M}_{11}$ is nearly constant. Since the first-order first-harmonic potential $\tilde{\phi}_1^{(1)}$ is known to attenuate with body submergence like $e^{-kH}$, the linear solution $\bar{M}_{11}$ which is due to the self-interaction of $\tilde{\phi}_1^{(1)}$, is generally expected to be proportional to $e^{-2kH}$ particularly for small bodies. According to the slender body solution derived by Lee & Newman (1971), $\bar{M}_{11}$ is a result of the self-interaction of the body disturbance and is asymptotically proportional to $\gamma^4$. Upon factoring out these leading dependences on the wave slope, body submergence, and slenderness, the linear solution for the mean pitch moment can be written as

$$\bar{M}_{11} = C(ka, kH, \gamma)\gamma^4(kA)^2 e^{-2kH}(\rho g a^4) \quad (4.7)$$

where the dimensionless coefficient $C$ needs to be determined through simulations. For a finite three-dimensional body, we anticipate that the coefficient $C$ has slow dependences on body submergence $kH$ and slenderness $\gamma$.

In principle, all three components $\bar{M}_{13}$, $\bar{M}_{22}$, and $\bar{M}_{00}$ due to high-order potential

effects are fourth-order in the wave slope, and so is their sum, $\bar{M}_{NL}$. By separating $\bar{M}_{NL}$ from the total mean pitch moment $\bar{M}_y$, we plot $\bar{M}_{NL}$, normalized by $(kA)^4$, as a function of the wave slope in figure 4-3. As expected, these normalized values approach a constant asymptote for small $kA$.

Without the presence of a body, it is well-known that there are no second-order waves in deep water. We therefore believe that the inclusion of a submerged slender spheroid will not generate significantly large second-order zeroth- and second-harmonic waves unless the body is very close to the free surface. As a result, $\bar{M}_{00}$ and $\bar{M}_{22}$ should be negligibly small compared to $\bar{M}_{13}$. In figure 4-4, we make comparisons among these three components by varying body submergence. Overall, we see that the magnitude of $\bar{M}_{00}$ is much smaller than that of $\bar{M}_{22}$ and $\bar{M}_{13}$. This confirms our expectation that the self-interaction of zeroth-harmonic waves has negligible effect on $\bar{M}_y$. Except for very small body submergence, figure 4-4 shows that $\bar{M}_{22}$ is also negligible compared to $\bar{M}_{13}$. This is due to the fact that the second-harmonic wave decays with body submergence much faster than the first-harmonic wave in general. Therefore, it is reasonable to consider $\bar{M}_{NL}$ as dominated by the quadratic interaction between first- and third-order (first-harmonic) waves, i.e. $\bar{M}_{NL} \approx \bar{M}_{13}$.

The first-order first-harmonic potential $\tilde{\phi}_1^{(1)}$ is known to attenuate with body submergence like $e^{-kH}$. The dominant part of the third-order first-harmonic potential $\tilde{\phi}_1^{(3)}$ can be considered to arise as a result of nonlinear interactions of three first-order first-harmonic waves so that $\tilde{\phi}_1^{(3)}$ should decay as $e^{-3kH}$ in principle. The other nonlinear interactions involving free second-harmonic waves all decay faster than $e^{-3kH}$ and thus can be neglected for deep submergence. For small bodies, therefore, the interaction between $\tilde{\phi}_1^{(1)}$ and $\tilde{\phi}_1^{(3)}$ is expected to attenuate with body submergence like $\bar{M}_{13} \sim e^{-4kH}$.

Based on the slender body solution of Lee & Newman (1971), the interaction between the incident wave (I) and the body disturbance (B) produces the dominant part of the vertical drift force which is of second-order in $\gamma$, but no mean pitch moment since the interaction itself is symmetric with respect to the midbody section of the spheroid. In principle, there in no reason to show that the fourth-order interaction

(IBIB) is also symmetric. We thus consider this interaction to give the dominant contribution to the fourth-order mean pitch moment $\bar{M}_{NL}$ which then should have $\gamma^4$ dependence on slenderness. All other possible effective interactions have slenderness dependence higher than $\gamma^4$ and can be neglected for a high aspect-ratio body. Such deduction is confirmed by our numerical results of $\bar{M}_{11}$ and $\bar{M}_{13}$ (normalized by $\gamma^4$) shown in figure 4-5, which approach to constant asymptotes as $\gamma$ is decreased.

After anticipating leading dependences on the wave slope, body submergence and slenderness, the leading nonlinear correction to the mean pitch moment is then given by

$$\bar{M}_{NL} \approx \bar{M}_{13} = D(ka, kH, \gamma)\gamma^4(kA)^4 e^{-4kH}(\rho g a^4) \tag{4.8}$$

Where $D$ is a dimensionless coefficient and has slow dependences on $kH$ and $\gamma$ for a finite three-dimensional body.

After the establishment of solution forms for $\bar{M}_{11}$ and $\bar{M}_{NL}$, the total mean pitch moment on the spheroid can be written as:

$$\bar{M}_y = \bar{M}_{11} + \bar{M}_{NL} = \bar{M}_{11}[1 - E(ka)e^{-2kH}(kA)^2] \tag{4.9}$$

where the coefficient $E$ is given by $-D/C$. Although the coefficients $C$ and $D$ have slow dependences on $\gamma$ and $kH$, we find through systematic numerical simulations that their ratio $(-E)$ is nearly independent of $\gamma$ and $kH$. To understand the influence of $\gamma$ on $E$, we plot in figure 4-6 the ratio of $\bar{M}_{13}$ and $\bar{M}_{11}$ as a function of $\gamma$. It is seen that $\bar{M}_{13}/\bar{M}_{11}$ is almost constant for three different submergences. This indicates that the coefficient $E$ has no significant dependence on $\gamma$. As for the effect of the body submergence $kH$, the results for $e^{2kH}\bar{M}_{13}/\bar{M}_{11}$ are shown in figure 4-7 as a function of $kH$ for three different incident wavelength $ka$. It is seen that the quantity $e^{2kH}\bar{M}_{13}/\bar{M}_{11}$ is roughly constant, which implies that the body submergence $kH$ has no significant influence on the coefficient $E$.

The importance of equation (4.9) is that the nonlinear solution including fourth-order corrections for the mean pitch moment $\bar{M}_y$ can be determined provided that the linear solution $\bar{M}_{11}$ and the coefficient $E$ are known. Since the evaluation of the

linear solution and the coefficient $E$ are relatively simple, (4.9) greatly reduces the calculations for estimating the general nonlinear solution of the mean pitch moment. In figure 4-8, we provide a set of results for the coefficient $E$ as a function of $ka$, which are obtained by using the present high-resolution spectral method.

For a body in a given ambient sea state, a special interest of practical significance is to determine the position where the mean pitch moment vanishes. Such position is critical for the operation of submarines and underwater vehicles. Based on (4.9), the condition for $\bar{M}_y = 0$ is found to be:

$$1 - E(ka)e^{-2kH}(kA)^2 = 0 \tag{4.10}$$

which is independent of body slenderness $\gamma$. Given $ka$ and $kA$, equation (4.10) gives a particular submergence $kH$ at which the mean pitch moment is identically zero.

### 4.3.3 Mean horizontal force in beam seas

We now turn to study the horizontal drift force on the spheroid in beam seas. The incident wave is assumed to propagate in the positive $y$-direction, parallel to the minor axis of the body.

Under beam sea conditions, the second-order horizontal drift force does not vanish in contrast to strip theory predictions (for circular sections). In the presence of three-dimensional effects, a positive second-order drift force can be expected in principle. When strong nonlinear interactions (due to steep incident waves or shallow submergence) are involved, it is known that there can be a negative drift force on a two-dimensional submerged circular cylinder (in chapter 3). For high-aspect ratio spheroids, this effect can of course also be anticipated. Thus, like the mean pitch moment in head seas, three-dimensional and (higher-order) nonlinear effects produce opposing horizontal drift forces on the spheroid.

In figure 4-9, we plot our converged numerical results with the order $M = 1$, 2 and 3 for the horizontal drift force on the body as a function of the incident wave slope at a fixed body submergence. As expected, the horizontal drift force changes

its sign from positive to negative as the incident wave slope is increased if nonlinear free-surface effects are included ($M = 2$ and 3). For a fixed incident wave steepness, the dependence of the horizontal drift force on the submergence is displayed in figure 4-10, where again for a given wave steepness, there exists a depth at which the steady horizontal force vanishes. Like that for a submerged two-dimensional circular cylinder, the negative drift force on the spheroid is believed to be a result of the quadratic interaction between the first- and third-order first-harmonic waves.

## 4.4 Conclusions

In this chapter, the high-order spectral method is employed to study nonlinear wave diffraction by a fixed and submerged spheroid. Of particular interest is to understand the high-order potential effects to the steady force and moment on the body. If nonlinear free-surface effects are included, we find that the mean pitch moment in head seas and the horizontal drift force in beam seas change their directions as the surface waves steepen or when the body is moved closer to the free surface. Through systematic numerical computations, the dominant nonlinear correction for both the mean pitch moment and horizontal force is found to be a result of the quadratic interaction between first- and third-order (first-harmonic) waves. Significantly, we find that the linear solution and high-order corrections are generally of opposite signs so that for given body aspect ratio and ambient surface waves, there is a particular submergence at which the mean pitch moment or horizontal drift force vanishes. For the mean pitch moment, in particular, we establish a simple formula to estimate this special position, which should be useful for the operation of submarines and underwater vehicles.

Having found interesting and significant nonlinear wave effects on a fixed submerged body, we will address the question of how wave-body interactions are affected by forward speed of the body in the subsequent three chapters.

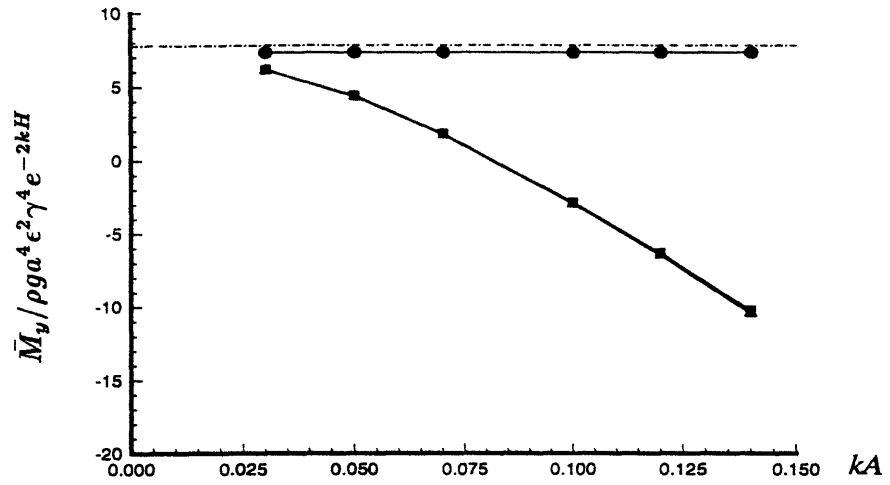


Figure 4-1: The mean pitch moment as a function of the incident wave slope. Panel method solution of Lee & Newman (1991) (— · —), and present numerical solutions for $M = 1$ (●), $M = 2$ (▲) and $M = 3$ (■). ($\epsilon = kA$, $ka = \pi/2$, $\gamma = 0.1$, $H/a = 0.2$.)

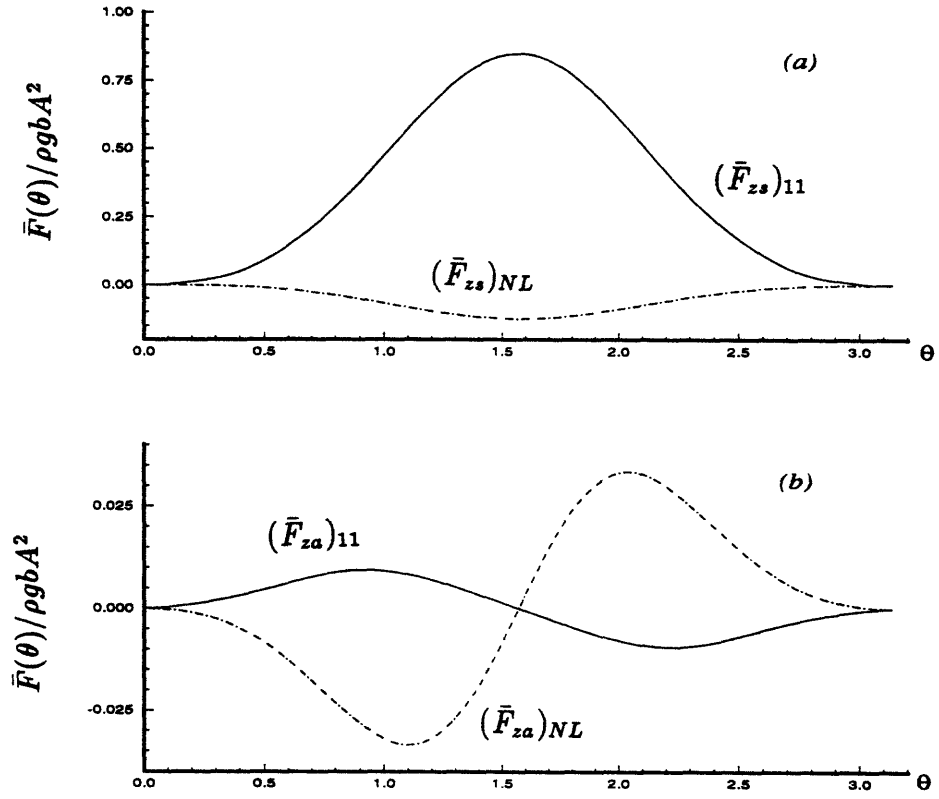


Figure 4-2: (a) symmetric and (b) asymmetric vertical drift force on the submerged spheroid. linear solution (——) and nonlinear corrections (— · —). $\theta = (0, \pi) \equiv$ (stern, bow). ($\epsilon = kA$=0.14, $ka = \pi/2$, $\gamma = 0.1$, $H/a = 0.2$.)

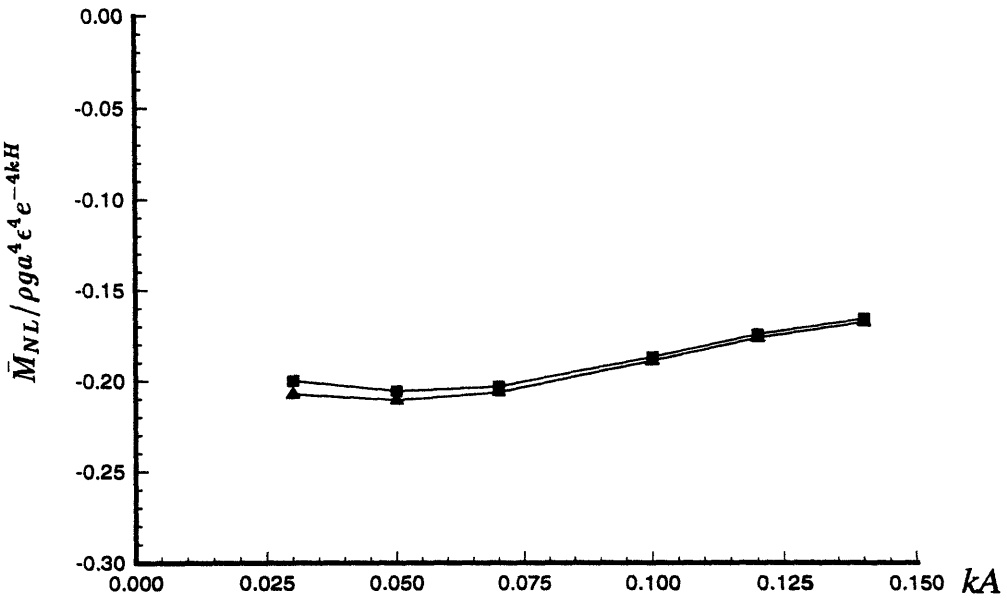


Figure 4-3: Dependence of the mean pitch moment due to nonlinear corrections on the incident wave slope. $M = 2$ (▲), $M = 3$ (■). ($\epsilon = kA$, $ka = \pi/2$, $\gamma = 0.1$, $H/a = 0.2$.)

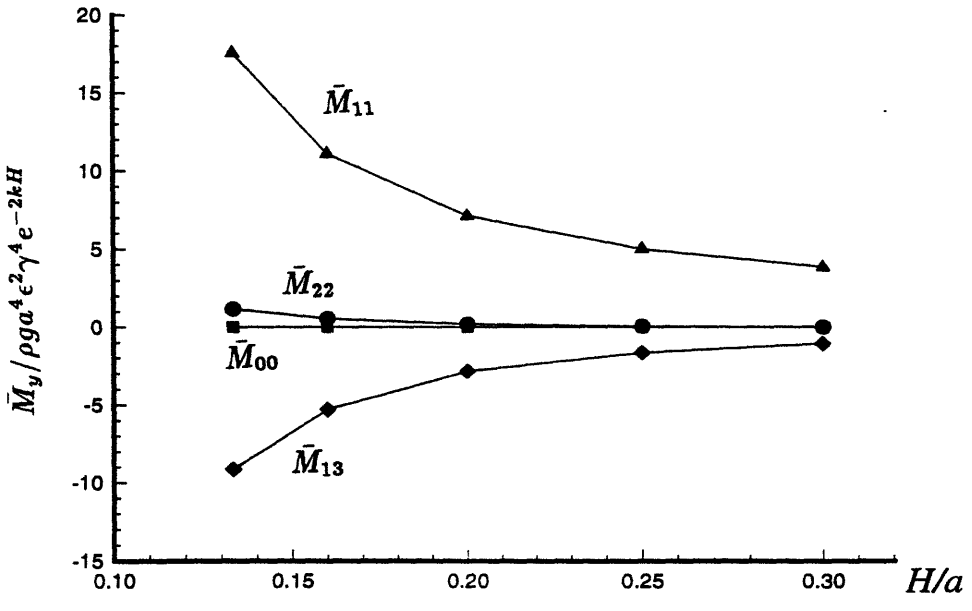


Figure 4-4: Components of the mean pitch moment as a function of submergence $H/a$. $\bar{M}_{11}$ (▲), $\bar{M}_{00}$ (■), $\bar{M}_{22}$ (●), and $\bar{M}_{13}$ (◆). ($\epsilon = kA = 0.05$, $ka = \pi/2$, $\gamma = 0.1$.)

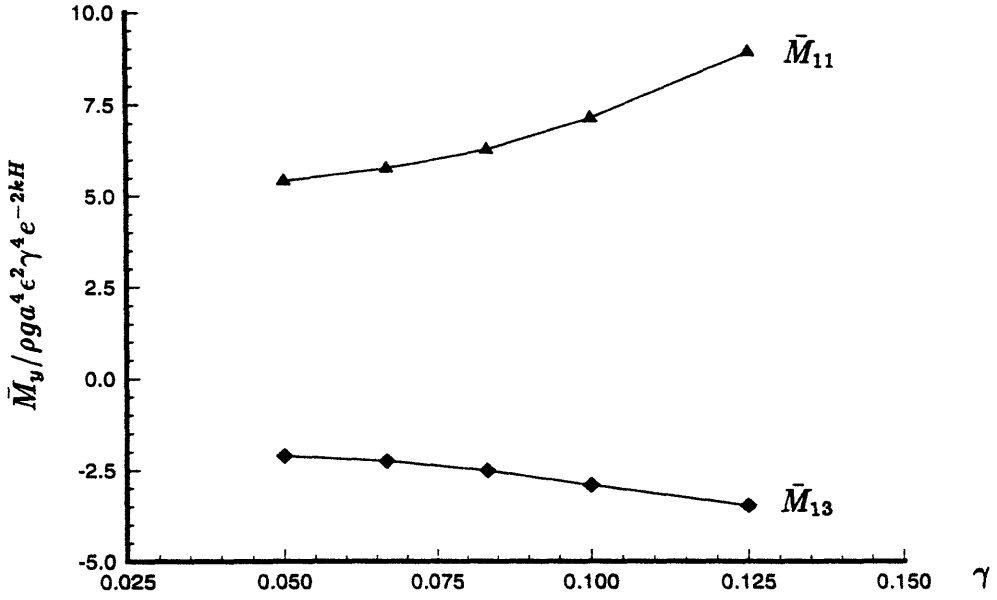


Figure 4-5: Dependence of the mean pitch moment on body slenderness $\gamma$. $\bar{M}_{11}$ (▲) and $\bar{M}_{13}$ (◆). ($\epsilon = kA = 0.05$, $ka = \pi/2$, $H/a = 0.2$.)

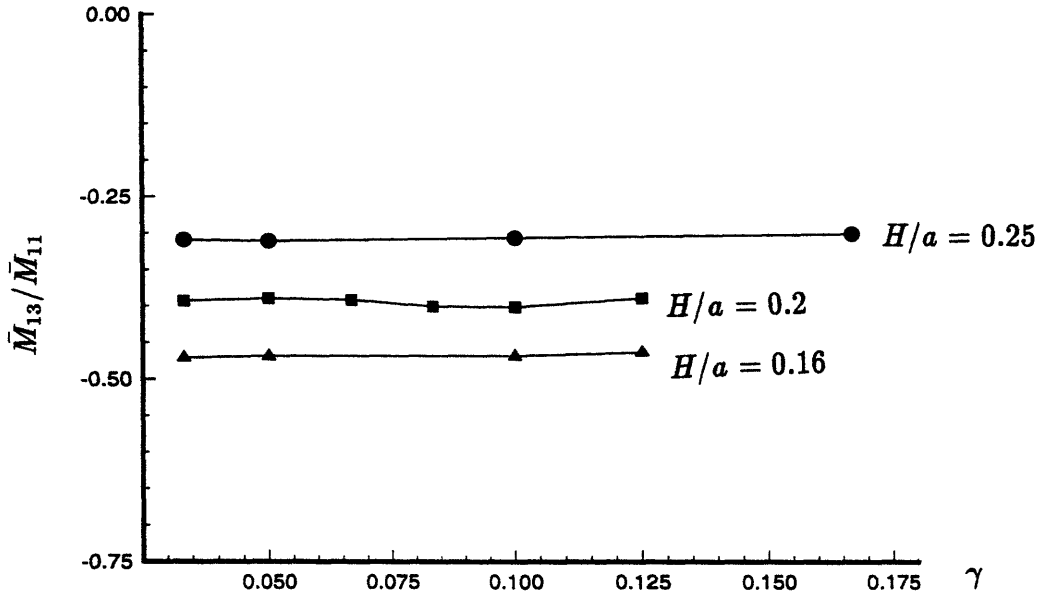


Figure 4-6: The ratio between linear solution $\bar{M}_{11}$ and nonlinear correction $\bar{M}_{13}$ as a function of body slenderness at different submergence. $H/a$=0.16 (▲), $H/a$=0.2 (■), and $H/a$=0.25 (●). ($kA = 0.05$, $ka = \pi/2$.)

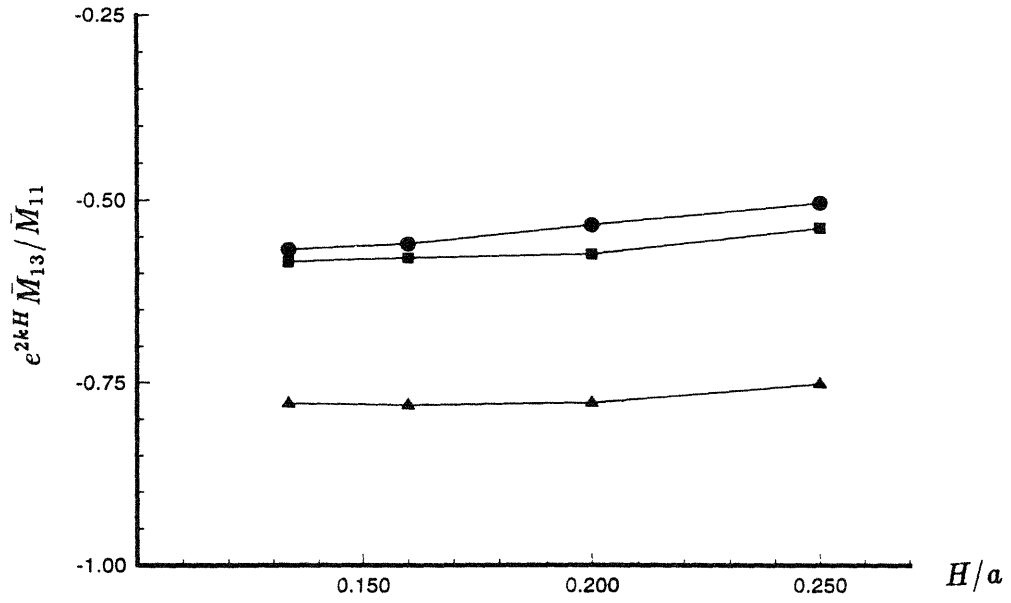


Figure 4-7: The ratio between linear solution $\bar{M}_{11}$ and nonlinear correction $\bar{M}_{13}$ as a function of submergence for different incident wavelength. $ka = 0.5\pi$ (▲), $ka = 0.75\pi$ (■), and $ka = \pi$ (●). ($kA = 0.05$, $\gamma = 0.1$.)

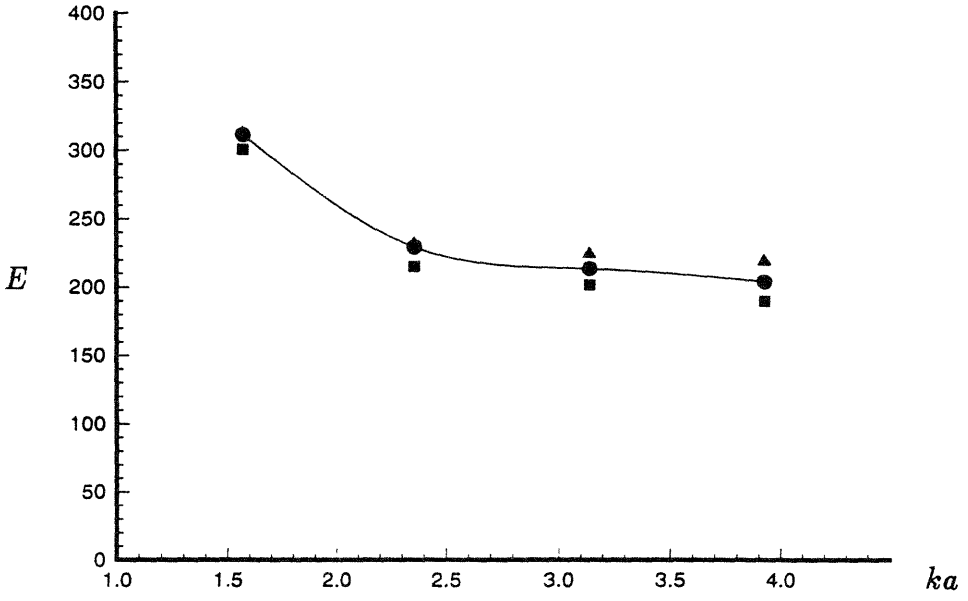


Figure 4-8: Dimensionless Coefficient $E$ as a function of incident wavelength $ka$. $H/a$=0.16 (▲), $H/a$=0.2 (●), and $H/a$=0.25 (■).

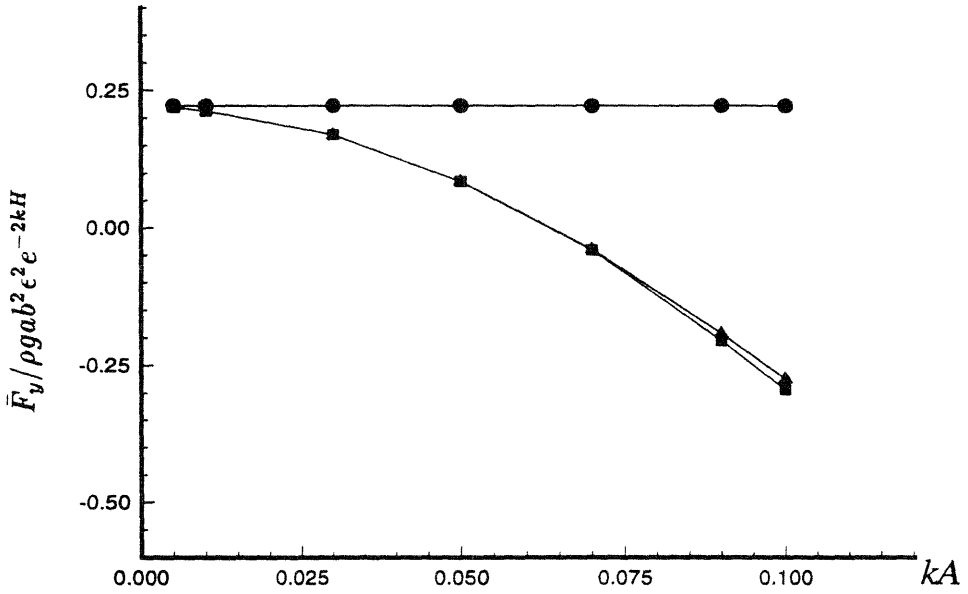


Figure 4-9: The horizontal drift force as a function of the incident wave slope. $M = 1$ (●), $M = 2$ (▲), $M = 3$ (■). ($\epsilon = kA$, $ka = \pi$, $\gamma = 0.1$, $H/a = 0.2$.)

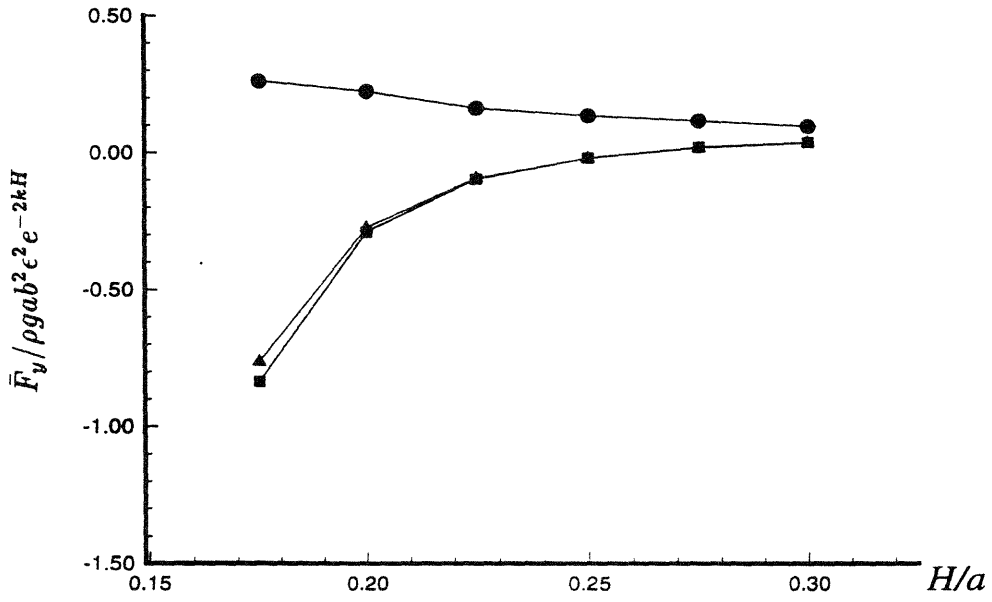


Figure 4-10: The horizontal drift force as a function of body submergence. $M = 1$ (●), $M = 2$ (▲), $M = 3$ (■). ($\epsilon = kA = 0.1$, $ka = \pi$, $\gamma = 0.1$.)

# Chapter 5

# Classical seakeeping solution near the critical frequency $\tau \equiv \frac{U\omega}{g} = \frac{1}{4}$

Compared to that of the zero-speed problem, nonlinear effects of the seakeeping problem become even more critical because forward speed of a body can influence the radiation of wave energy. Of particular interest is the case where the group velocities of certain wave components vanish so that the associated energy can no longer be radiated away and is thus accumulated in the near field of the body. This happens at the particular value of the frequency ($\omega$) and forward speed ($U$) combination $\tau \equiv U\omega/g = \frac{1}{4}$, where $g$ is the gravitational acceleration.

Before detailed nonlinear simulations are performed, in this chapter, we theoretically show that the linear solution of the seakeeping problem is finite if and only if a certain geometric condition is satisfied. This is contrary to the existing theories based upon the single source result. For a submerged body, a necessary and sufficient condition is that the body must have non-zero volume. For a surface-piercing body, a sufficient condition is derived which has a geometric interpretation similar to that of John (1950). As an illustration, we provide an analytic (closed-form) solution for the case of a submerged circular cylinder oscillating near $\tau = \frac{1}{4}$. Finally, we identify the underlying difficulties of existing approximate theories and numerical computations near $\tau = \frac{1}{4}$, and offer a simple remedy for the latter.

The linearized problem is classically solved by approximating the body with a dis-

tribution of singularities typically taking advantage of the slenderness (or thinness) of the body (*e.g.* Hanaoka 1957; Havelock 1958; Newman 1959; Maruo 1967; Ogilvie & Tuck 1969; and Newman 1978, which also contains an extensive review). Satisfactory predictions can generally be obtained except in the neighborhood of the critical frequency $\tau \equiv U\omega/g = \frac{1}{4}$. Despite a substantial body of work for the general linearized problem, the nature of the solution near this critical frequency for a realistic body has not been satisfactorily resolved.

For a single source, it is well known that the Green's function becomes unbounded at $\tau = \frac{1}{4}$ (Haskind 1954; Wehausen & Laitone 1960). Physically, this may be explained in terms of the group velocities (in still water) of certain components of the accompanying wave which approach $U$ as $\tau \to \frac{1}{4}$ (from below). The associated energy can no longer be radiated away, and the amplitudes of these wave components tend to grow indefinitely. Since the problem for a general body can, in principle, be represented by an appropriate distribution of such sources, it is widely accepted that the resulting seakeeping problem must likewise be singular at $\tau = \frac{1}{4}$ (*e.g.* Dagan & Miloh 1982). This appears also to be confirmed by existing approximate theories and calculations (*e.g.* Newman 1959; Wu & Eatock Taylor 1988) suggesting that this difficulty may be inherent in the linearized problem.

The present work is motivated in a large part by careful numerical calculations for the case of submerged circular and elliptical cylinders by Grue & Palm (1985) and Mo & Palm (1987). For the submerged circle, Grue & Palm (1985) offered strong numerical evidence that the amplitudes of the resonant upstream and downstream waves approach the same finite limit as $\tau \to \frac{1}{4}$. They were able to support this by examining the coefficients of an infinite set of equations which resulted from Fourier discretizations of the source strengths on the circle. Since their equations are singular at $\tau = \frac{1}{4}$, they considered the problem undetermined at this limiting value. Similar finite results were obtained for the submerged ellipse near $\tau = \frac{1}{4}$ by Mo & Palm (1987). From these results, they again reasoned that the amplitudes should be finite as $\tau \to \frac{1}{4}$.

Here we offer a formal proof that a finite solution exists at $\tau = \frac{1}{4}$ for a general

class of bodies. In particular, a simple necessary and sufficient geometric condition is found for such finite solutions. This condition depends on and must be satisfied for all possible values of the frequency $\omega$ but is not a function of $U$. When the body is submerged, the condition is satisfied if and only if the body has non-zero volume (*e.g.* a submerged cylinder but not a point source or dipole). For a body intersecting the free surface, sufficient conditions can be obtained by considering deviations of the body from a vertically uniform geometry of the same waterplane and draft. The resulting condition has a similar geometric interpretation as that of John (1950) in another context (the uniqueness of the solution of the floating body motion problem without forward speed).

For analyses in this chapter, we concentrate only on the neighborhood of $\delta^2 \equiv |1-4\tau| \ll 1$. The linearized boundary-value problem and the behavior of the Green's function near $\tau = \frac{1}{4}$ are reviewed in §5.1. We reformulate this problem as source-distribution boundary-integral equations on the body for both submerged (§5.2) and surface intersecting bodies (§5.3) and discuss the solutions as $\tau \to \frac{1}{4}$. It is shown that the solutions are bounded for a general class of geometries satisfying an integral condition with simple geometric interpretations. As an illustration, we consider in §5.4 the special case of a submerged circular cylinder and obtain a closed-form (finite) solution for motions in the neighborhood of $\tau = \frac{1}{4}$.

For simplicity and the sake of closed-form answers, we present the problem mainly in two dimensions although similar results and geometric conditions follow directly for three-dimensional bodies. This is outlined in §5.5. Finally, in the discussions, §5.6, we identify the difficulties inherent in existing approximate theories and in direct numerical solutions of the integral equations as $\tau \to \frac{1}{4}$. In the latter case, a simple remedy is provided based on an alternative form of the integral equation valid for small $\delta^2$.

## 5.1 The boundary-value problem and Green function

We consider the generalized Kelvin-Neumann problem (Haskind 1946) of a two-dimensional body translating with constant forward speed $U$ parallel to the undisturbed free surface in deep water while at the same time undergoing small oscillatory motion and/or encountering small amplitude waves at frequency $\omega$. A Cartesian coordinate system $o-xz$ is chosen fixed with the mean position of the body, with $o-x$ in the undisturbed free surface, $x$ pointing in the direction of forward speed, and $z$ positive upwards. The fluid is assumed inviscid and incompressible, and the motion irrotational. The flow can be described by a velocity potential:

$$\Phi^*(x,z,t) = \bar{\phi}(x,z) + \Phi(x,z,t) = \bar{\phi}(x,z) + \Re\{\phi(x,z)e^{i\omega t}\} \tag{5.1}$$

where $\bar{\phi}$ is the potential due to the steady forward motion of the body, and $\Phi$ the unsteady potential associated with the body oscillations and/or incident waves. We focus on the unsteady potential $\Phi$ and do not further concern ourselves with $\bar{\phi}$ which is related to the steady wave resistance problem.

The time independent potential $\phi$ satisfies Laplace's equation within the fluid and vanishes at large depth, $\nabla\phi \to 0$ as $z \to -\infty$. For small amplitude incident waves or body motions, the linearized free-surface condition is

$$(i\omega - U\frac{\partial}{\partial x})^2\phi + g\frac{\partial\phi}{\partial z} = 0\ , \qquad \text{on} \quad z = 0\ . \tag{5.2}$$

The kinematic boundary condition applied at the mean position of the wetted body surface, $S_B$, can be written as

$$\frac{\partial\phi}{\partial n} = f(x,z)\ , \qquad \text{on} \quad S_B\ , \tag{5.3}$$

where $\mathbf{n} = (n_x, n_z)$ is the unit normal out of the body. In (5.3), the forcing term $f(x,z)$ is given in terms of the imposed body oscillations and incident wave as well

as the so-called "$m$-terms" due to the steady potential $\bar{\phi}$ (*e.g.* Newman 1978). The boundary-value problem for $\phi$ is complete with the imposition of an appropriate radiation condition, in this case a physical requirement that only waves with group velocity greater than (less than) the forward speed can be present far up (down) stream of the body.

At this point, we should remark that a general uniqueness theory for the boundary-value problem with the free-surface condition (5.2) is as yet unavailable. Despite this, the solution of the present problem has been pursued in a large number of studies (see, *e.g.* Newman 1978). For submerged bodies in steady motion, the Kelvin-Neumann problem is shown (with some restrictions, see Kochin 1937; Dern 1980) to possess a unique solution. We are unable to extend this result and simply postulate the uniqueness of the stated problem at least for the general case when $\tau \neq \frac{1}{4}$.

We define a Green function, $G(x,z;x',z')$, which is harmonic everywhere in the fluid except at $(x',z')$ where it is source like. In addition, $G$ satisfies the linearized free surface condition (5.2), the radiation condition, and vanishes at large depth. Physically, $G$ represents the potential due to a translating point source, velocity $U$, with a pulsating strength, frequency $\omega$.

The solution for $G$ was obtained by Haskind (1954), which we rewrite as follows:

$$G(x,z;x',z') = G_0 + G_1 + G_2 + G_3 + G_4 \tag{5.4}$$

where

$$G_0 = \frac{1}{2}\{\ln[(x-x')^2+(z-z')^2] - \ln[(x-x')^2+(z+z')^2]\}\,, \tag{5.5}$$

$$G_1 = \frac{i\pi}{\sqrt{1-4\tau}} e^{k_1[-i(x-x')+(z+z')]} + \frac{1}{\sqrt{1-4\tau}} \int_0^\infty \frac{1}{m-k_1} e^{m[-i(x-x')+(z+z')]} dm\,, \tag{5.6}$$

$$G_2 = \frac{i\pi}{\sqrt{1-4\tau}} e^{k_2[-i(x-x')+(z+z')]} - \frac{1}{\sqrt{1-4\tau}} \int_0^\infty \frac{1}{m-k_2} e^{m[-i(x-x')+(z+z')]} dm\,, \tag{5.7}$$

$$G_3 = \frac{-i\pi}{\sqrt{1+4\tau}} e^{k_3[i(x-x')+(z+z')]} + \frac{1}{\sqrt{1+4\tau}} \int_0^\infty \frac{1}{m-k_3} e^{m[i(x-x')+(z+z')]} dm\,, \tag{5.8}$$

$$G_4 = \frac{i\pi}{\sqrt{1+4\tau}} e^{k_4[i(x-x')+(z+z')]} - \frac{1}{\sqrt{1+4\tau}} \int_0^\infty \frac{1}{m-k_4} e^{m[i(x-x')+(z+z')]} dm\,, \tag{5.9}$$

and Cauchy principal-value integrals are indicated. In the above, we define $\tau \equiv U\omega/g$ and the four wavenumbers are defined by

$$k_{1,2} = \frac{\kappa}{8\tau^2}(1 - 2\tau \pm \sqrt{1-4\tau}) \; ; \qquad k_{3,4} = \frac{\kappa}{8\tau^2}(1 + 2\tau \pm \sqrt{1+4\tau}) \; ; \tag{5.10}$$

where $\kappa \equiv 4\omega^2/g$.

The far-field wave behaviour can be readily seen from (5.10). For $\tau < \frac{1}{4}$, all four wavenumbers are real and the $k_1$, $k_3$, and $k_4$ waves propagate downstream (behind the body), while the $k_2$ wave appears upstream. For $\tau > \frac{1}{4}$, $k_3$ and $k_4$ are still real, whereas $k_1$ and $k_2$ become complex. As a result, the $k_3$ and $k_4$ waves remain downstream, while the $k_1$ and $k_2$ waves are evanescent.

Our interest is in the neighborhood of $\tau = \frac{1}{4}$, where $k_1$ and $k_2$ approach a common value, and $G_1$ and $G_2$ become singular. Physically, this corresponds to the $k_1$ and $k_2$ waves merging into a single wave with group velocity equal to $U$. For a *single* source, the energy of this wave can not radiate away to infinity resulting in an unbounded build up of energy, at least in the context of linearized theory (see Dagan & Miloh 1982). The key finding of this chapter is that for an *actual* physical body, the wave sources of non-trivial strength may combine in such a way that the total solution remains finite as $\tau \to \frac{1}{4}$. We prove that this is indeed the case subject to a necessary and sufficient condition on the geometry of the body.

For convenience, we define $\delta^2 \equiv |1 - 4\tau|$. For $\delta^2 \ll 1$, we have from (2.10):

$$k_{1,2} = \kappa[1 + O(\delta)] \; , \qquad \delta^2 \ll 1 \; . \tag{5.11}$$

In the following, we consider asymptotic expansions valid for $\kappa|\vec{x} - \vec{x'}|\delta = o(1)$ as $\delta \to 0$. Note that the limit of $|\vec{x}| \to \infty$ such that $\kappa|\vec{x} - \vec{x'}|\delta \to \infty$ while $\delta \ll 1$ requires special care and is taken up in Appendix A.

From (5.6), (5.7), we write

$$G_1 + G_2 = \frac{2\pi i}{\delta} e^{\kappa[-i(x-x')+(z+z')]} + G' + O(\delta) \; , \qquad \delta^2 \ll 1 \; . \tag{5.12}$$

In (5.12), $G' = O(1)$ results from the principal-value integrals in (5.6) and (5.7), and is given by

$$\frac{1}{4}G' + 1 = \kappa[-i(x-x') + (z+z')]e^{\kappa[-i(x-x')+(z+z')]} \int_{-\kappa}^{\infty} \frac{1}{m} e^{m[-i(x-x')+(z+z')]} dm \ . \quad (5.13)$$

## 5.2 Submerged bodies

We construct a solution of the problem in terms of a source distribution (Brard 1972):

$$\phi(x,z) = \int_{S_B} \sigma(x',z') G(x,z;x',z') ds' \ , \quad (5.14)$$

where $\sigma(x',z')$ is the source strength distribution on the body. Clearly, (5.14) satisfies all the conditions of the boundary-value problem except for that on the body. Imposing the body boundary condition (5.3), we obtain an integral equation for the unknown source strength $\sigma$:

$$\pi\sigma(x,z) + \int\!\!\!\!\!\!- _{S_B} \sigma(x',z') \frac{\partial}{\partial n} G(x,z;x',z') ds' = f(x,z) \ , \qquad (x,z) \in S_B. \quad (5.15)$$

As with the original boundary-value problem, we assume that a unique solution to (5.15) exists in general for $\tau \neq \frac{1}{4}$. As $\tau \to \frac{1}{4}$, the kernel of (5.15) becomes unbounded everywhere due to the presence of $G_1$ and $G_2$. Our interest is in this neighborhood, so that for $\delta^2 \ll 1$, we substitute the asymptotic behaviour of $G_1 + G_2$ in (5.12) into (5.15) and rewrite the integral equation as

$$\begin{aligned} \pi\sigma(x,z) \ &+ \ \frac{2\pi\kappa}{\delta}(n_x + in_z) e^{\kappa(-ix+z)} \int_{S_B} \sigma(x',z') e^{\kappa(ix'+z')} ds' \\ &+ \ \int\!\!\!\!\!\!- _{S_B} \sigma(x',z') \tilde{G}_n(x,z;x',z') ds' = f(x,z) + O(\delta) \ , \qquad \delta^2 \ll 1 \ , \quad (5.16) \end{aligned}$$

where the principal-value integral involving $\tilde{G} \equiv G' + G_0 + G_3 + G_4$ is continuous as $\tau \to \frac{1}{4}$.

We now define the Kochin function

$$\alpha_1 \equiv \int_{S_B} \sigma(x,z) e^{\kappa(ix+z)} ds \ , \tag{5.17}$$

and rewrite (5.16) as

$$\begin{aligned} \sigma(x,z) = & - \frac{2\kappa\alpha_1}{\delta}(n_x + in_z)e^{\kappa(-ix+z)} \\ & - \frac{1}{\pi}\int_{S_B} \sigma(x',z')\tilde{G}_n(x,z;x',z')ds' + \frac{f(x,z)}{\pi} + O(\delta) \ , \qquad \delta^2 \ll 1 \ . \end{aligned} \tag{5.18}$$

The forcing function $f$, which is due to the incident and steady Kelvin waves as well as imposed body motions is, in general, finite and assumed to be $O(1)$.

To determine the magnitude of $\alpha_1$, we substitute $\sigma$ in (5.18) into (5.17), and solve for $\alpha_1$. After using the divergence theorem, we obtain

$$\alpha_1 = \frac{\delta}{\pi(\delta + 2i\kappa\Gamma)}[\mathcal{F} - \int_{S_B} \sigma(x',z')P_1(x',z')ds'] + O(\delta^2) \ , \tag{5.19}$$

where the kernel $P_1$ is given by

$$P_1(x',z') = \int_{S_B} e^{\kappa(ix+z)} \frac{\partial}{\partial n}(G' + G_0)ds \ , \tag{5.20}$$

and the constants $\mathcal{F}$ and $\Gamma$ are given by

$$\mathcal{F} = \int_{S_B} f(x,z)e^{\kappa(ix+z)}ds, \tag{5.21}$$

$$\Gamma = \int_{S_B} (-in_x + n_z)e^{2\kappa z}ds. \tag{5.22}$$

$\mathcal{F}$ and $P_1$ are independent of $\delta$ and can be at most $O(1)$. In (5.22), $\Gamma$ is a function of the body geometry only for a given frequency $\kappa$.

Depending on the body geometry, there are now two possibilities. If $\Gamma \neq 0$, we substitute (5.19) back into (5.18) to obtain a new integral equation for $\sigma$:

$$\pi\sigma(x,z) \ - \ \frac{(n_x + in_z)}{\delta/2\kappa + i\Gamma} e^{\kappa(-ix+z)} \int_{S_B} \sigma(x',z')P_1(x',z')ds'$$

$$+ \quad \fint_{S_B} \sigma(x',z')\tilde{G}_n(x,z;x',z')ds' = F(x,z) + O(\delta) \,, \tag{5.23}$$

where

$$F(x,z) = f(x,z) - \mathcal{F}\frac{(n_x + in_z)}{\delta/2\kappa + i\Gamma} e^{\kappa(-ix+z)} = O(1) \,. \tag{5.24}$$

The kernels in (5.23) are bounded and continuous as $\tau \to \frac{1}{4}$. Thus (5.23) is regular and, for sufficiently smooth $S_B$, has a bounded solution $\sigma = O(1)$ except possibly at an enumerable number of discrete values of $\kappa$ for which the Fredholm determinant vanishes (*e.g.* Ursell 1968. For steady motions and two- and three-dimensional submerged bodies these are shown to be absent for sufficiently small Froude numbers, Kochin 1937). This is a difficulty associated with the general problem and not specifically with the limit $\delta \to 0$. Since our interest is in the latter, we do not consider this possibility any further. From (5.19), it is also clear that $\alpha_1 = O(\delta)$ for $\Gamma \neq 0$.

We remark that for arbitrary geometries, (5.23) can be solved in general by direct numerical means for the finite solution. The velocity potential is finite as $\tau \to \frac{1}{4}$ and is given by

$$\phi(x,z) = \frac{2\pi i\alpha_1}{\delta} e^{\kappa(-ix+z)} + \int_{S_B} \sigma(x',z')\tilde{G}(x,z;x',z')ds' + O(\delta) \,, \tag{5.25}$$

which is bounded for $\Gamma \neq 0$. Note that in view of the approximation in (5.12), (5.25) is strictly valid for $\kappa|\vec{x} - \vec{x'}|\delta = o(1)$. The potential in this case is in fact finite everywhere even for $|x| \to \infty$ (see Appendix A).

If $\Gamma = 0$, then from (5.19), $\alpha_1$ is at least $O(1)$. It follows from (5.18) that $\sigma = O(\delta^{-1})$ which becomes unbounded as $\delta \to 0$.

In summary, then, a finite solution to the problem exists as $\tau \to \frac{1}{4}$ if and only if

$$\Gamma \equiv \int_{S_B} (-in_x + n_z)e^{2\kappa z} ds \neq 0 \,, \tag{5.26}$$

which is a condition that depends on the geometry $S_B$ and the frequency $\kappa = 4\omega^2/g$ only. If $\Gamma = 0$ for any frequency $\kappa$, then a forward speed $U^2 = g/4\kappa$ can always be found for which the solution becomes unbounded. Physically, (5.26) represents a

requirement that the resonant wave components must not be orthogonal to the body boundary condition.

With the use of divergence theorem, we obtain immediately

$$\Gamma = 2\kappa \iint_B e^{2\kappa z} dS \ , \tag{5.27}$$

where $B$ is the (mean) body section. Since the integrand in (5.27) is positive definite, $\Gamma \neq 0$ if and only if the (submerged) body has non-zero cross-section area. The known singular solution for a point source turns out to be a special case of $\Gamma = 0$.

## 5.3 Surface intersecting bodies

An analogous result can be obtained for the case where the body intersects the free surface. We assume (locally) vertical intersections, and again write the potential in terms of a body surface source distribution (*e.g.* Ursell 1980)

$$\phi(x,z) = \int_{S_B} \sigma(x',z') G(x,z;x',z') ds' - \ell[\sigma_- G(x,z;x_-,0) + \sigma_+ G(x,z;x_+,0)] \ , \tag{5.28}$$

where $\ell \equiv U^2/g$, and $\sigma_\pm$ represent the source strengths at the two intersection points, $x = x_\pm$.

For $\delta^2 \ll 1$, we proceed as before and write

$$\begin{aligned} \pi\sigma(x,z) = -\frac{2\pi\kappa\alpha_2}{\delta}(n_x + in_z)e^{\kappa(-ix+z)} - \fint_{S_B} \sigma(x',z')\tilde{G}_n(x,z;x',z')ds' \\ + \ell[\sigma_-\tilde{G}_n(x,z;x_-,0) + \sigma_+\tilde{G}_n(x,z;x_+,0)] + f(x,z) + O(\delta) \ , \end{aligned} \tag{5.29}$$

where the Kochin function $\alpha_2$ is defined to be

$$\alpha_2 = \int_{S_B} \sigma(x,z) e^{\kappa(ix+z)} ds - \ell[\sigma_- e^{i\kappa x_-} + \sigma_+ e^{i\kappa x_+}] \ . \tag{5.30}$$

Again, it is clear from (5.29) that $\sigma = O(1)$ if $\alpha_2 \leq O(\delta)$. Otherwise, $\sigma$ becomes unbounded as $\tau \to \frac{1}{4}$.

Substituting (5.29) into (5.30), we have

$$\alpha_2 = \frac{\delta}{(\delta + 2i\kappa\Gamma)\pi}[\mathcal{F} + \mathcal{Q} - \int_{S_B} \sigma(x', z')P_2(x', z')ds'] + O(\delta^2)\,, \tag{5.31}$$

where the kernel $P_2$ is given by

$$P_2(x', z') = \oint_{S_B} \tilde{G}_n(x, z; x', z')e^{\kappa(ix+z)}ds\,, \tag{5.32}$$

and the constant $\mathcal{Q}$ is defined as

$$\mathcal{Q} = \int_{S_B} \ell[\sigma_- \tilde{G}_n(x, z; x_-, 0) + \sigma_+ \tilde{G}_n(x, z; x_+, 0)]e^{\kappa(ix+z)}ds - \pi\ell[\sigma_- e^{i\kappa x_-} + \sigma_+ e^{i\kappa x_+}]. \tag{5.33}$$

$\mathcal{F}$, $\mathcal{Q}$ and $P_2$ are independent of $\delta$ and can be at most $O(1)$. If $\Gamma = 0$, $\alpha_2 = O(1)$ and $\sigma = O(\delta^{-1})$, and no finite solution exists as $\tau \to \frac{1}{4}$. If $\Gamma \neq 0$, $\alpha_2 = O(\delta)$ and $\sigma = O(1)$ and we may substitute (5.31) back into (5.29) to obtain a new integral equation for $\sigma$:

$$\begin{aligned}\pi\sigma(x, z) - \frac{(n_x + in_z)}{\delta/2\kappa + i\Gamma}e^{\kappa(-ix+z)} \int_{S_B} \sigma(x', z')P_2(x', z')ds' \\ + \oint_{S_B} \sigma(x', z')\tilde{G}_n(x, z; x', z')ds' - \ell[\sigma_- \tilde{G}_n(x, z; x_-, 0) + \sigma_+ \tilde{G}_n(x, z; x_+, 0)] \\ = F(x, z) + Q(x, z) + O(\delta)\,,\end{aligned} \tag{5.34}$$

where

$$Q(x, z) = -\frac{n_x + in_z}{\delta/2\kappa + i\Gamma}e^{\kappa(-ix+z)}\mathcal{Q}\,. \tag{5.35}$$

Now, every term in (5.34) is finite as $\tau \to \frac{1}{4}$, so that (5.34) is regular and a bounded solution for $\sigma$ can be obtained, after which the Kochin function $\alpha_2$ can be determined from (5.31). The problem is thus solved with

$$\begin{aligned}\phi(x, z) &= \frac{2\pi i\alpha_2}{\delta}e^{\kappa(-ix+z)} + \int_{S_B} \sigma(x', z')\tilde{G}(x, z; x', z')ds' \\ &- \ell[\sigma_- \tilde{G}(x, z; x_-, 0) + \sigma_+ \tilde{G}(x, z; x_+, 0)] + O(\delta)\,,\end{aligned} \tag{5.36}$$

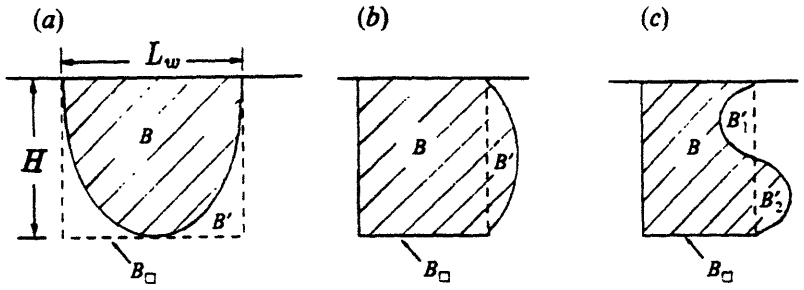


Figure 5-1: Geometric condition for a body intersecting the free surface. (a) $B' < 0$; (b) $B' > 0$; (c)$-B'_2 = B'_1 < 0$.

which is finite.

As with the submerged case, the necessary and sufficient condition for a finite solution is (5.26), *i.e.*, $\Gamma \neq 0$. Use of the divergence theorem here yields

$$\Gamma = 2\kappa \iint_B e^{2\kappa z} dS - L_w \,, \tag{5.37}$$

where $L_w = x_+ - x_> 0$ is the waterline width of the body. Let us divide the mean body section $B$ into two parts: $B = B_\square + B'$, where $B_\square$ is the rectangle with width $L_w$ and depth $H$ equal to the maximum draft of the body, and $B'$ the difference between $B$ and $B_\square$ (see figure 5-1). The double integral over $B_\square$ can be evaluated yielding

$$\Gamma = 2\kappa \iint_{B'} e^{2\kappa z} dS - L_w e^{-2\kappa H}. \tag{5.38}$$

If the body $B$ is completely enclosed by $B_\square$, $B'$ is negative and so also the negative integral over $B'$ in (5.38). Whence $\Gamma$ is negative definite and $B \subset B_\square$ is a sufficient condition for (5.26).

If $B \not\subset B_\square$ (for example, figure 5-1b), the integral over $B'$ may be positive, and a value of $\kappa$ may exist for which $\Gamma = 0$. To illustrate this further, consider the case of a circular cylinder, radius $R$, which intersects the free surface (for simplicity still

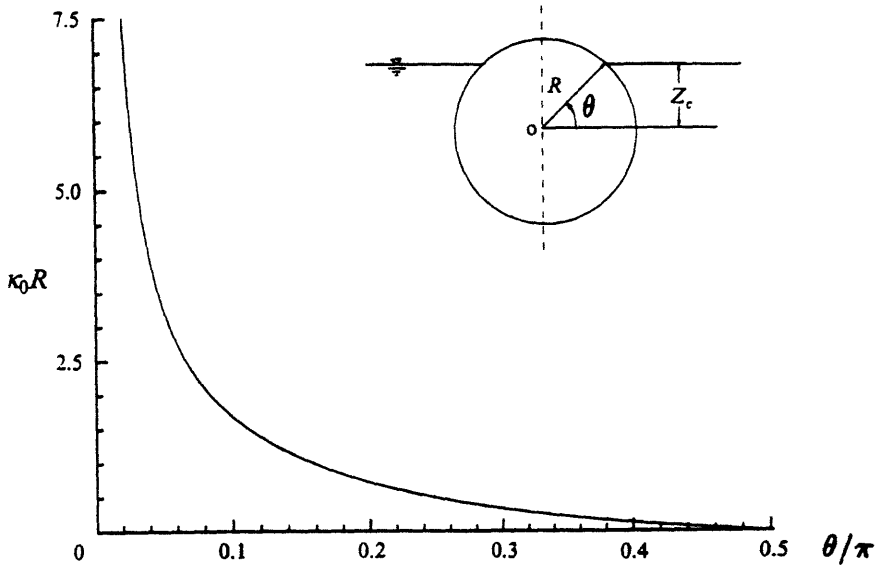


Figure 5-2: Dimensionless frequency $\kappa_0 R$ for $\Gamma = 0$ as a function of the submergence of a floating circle.

assuming the body to be *locally* vertical at the intersection points). If the center of the cylinder $z_c$ is above the free surface, $z_c > 0$, then $B \subset B_\square$ and $\Gamma$ is negative definite. If the cylinder is completely submerged, $z_c < -R$, then from (5.27), $\Gamma$ is positive definite. For the intermediate case of $-1 < z_c/R < 0$, however, (5.38) shows that $\Gamma$ is negative for $\kappa = 0$ but increases monotonically with $\kappa$ and eventually changes sign. For any $z_c/R \in (-1, 0)$, there exists a particular value of the frequency $\kappa = \kappa_0 > 0$ for which $\Gamma = 0$. It follows that a finite solution does not exist at that frequency and at a forward speed corresponding to $\tau = \frac{1}{4}$ given by $U_0^2 = g/4\kappa_0$. Figure 5-2 shows a plot of $\kappa_0 R$ as a function of $\theta \equiv \sin^{-1}(-z_c/R)$ for this case. Note that $\kappa_0 R \sim -\ln\theta/\theta$ as $\theta \to 0$.

The sufficient condition on the geometry, $B \subset B_\square$, is similar to that of John (1950) for the motions of a floating body (without forward speed) which requires that for every point of the mean free surface (in this case $x \notin [x_-, x_+]$), the entire vertical segment below it must not intersect the mean body. The actual requirement of $\Gamma \neq 0$

is, however, more general (less restrictive) and admits, for example, a geometry such as that depicted in figure 5-1c.

## 5.4 Application to a submerged circular cylinder

As an illustration, we consider the special case of a translating and oscillating submerged circular cylinder near $\tau = \frac{1}{4}$. Grue & Palm (1985) investigated this problem computationally using a source distribution (*cf.* (5.15)) represented by Fourier series. They obtained solutions very close to $\tau = \frac{1}{4}$ although the kernel of their integral equation becomes everywhere singular as $\tau \to \frac{1}{4}$ (*cf.* (5.16)). In this section, we obtain the finite solution to this problem in the neighborhood of $\tau = \frac{1}{4}$ ($\delta^2 \ll 1$). In particular, we provide closed-form asymptotic solutions for the far-field amplitudes of the $k_1$ and $k_2$ waves (which have a common finite value at $\tau = \frac{1}{4}$).

A local cylindrical coordinate system $(r, \theta)$ is placed at the center of the cylinder, which is at a depth $H$ below the mean water level. Thus, $r^2 = x^2 + (z+H)^2$ and $\theta$ is measured counterclockwise from positive $x$. The geometry parameter $\Gamma$ for a circular cylinder can be found in closed form

$$\Gamma = 2\pi R e^{-2\kappa H} I_1(2\kappa R) \,, \tag{5.39}$$

in which $R$ is the radius of the cylinder and $I_1$ the modified Bessel function of the first kind.

For a circular cylinder, we can easily prove the following relationship

$$\oint_{S_B} \sigma(x', z') \frac{\partial G_0}{\partial n} ds' = \int_{S_B} \sigma(x', z') ds' \,. \tag{5.40}$$

Since no fluid crosses the surface of the rigid body, the net source vanishes. As a result, there is no $G_0$ term in $\tilde{G}$ nor in the kernel $P_1$. Given the forcing function $F$, the solution to the integral equation (5.23) must, in general, be obtained numerically. For relatively deep submergence, $\kappa H$, however, the problem simplifies. In particular, the amplitudes of the $k_{1,2}$ waves can be obtained in closed form and interestingly do

not explicitly depend on the source strength $\sigma$.

The Kochin function, $\alpha_1$, is calculated from (5.19). Since the kernel $P_1$ (without $G_0$) diminishes with submergence $\kappa H$ like $e^{-3\kappa H}$ (*cf.* (5.20)), the second term in (5.19) can be neglected for large submergence:

$$\alpha_1 \simeq \frac{\mathcal{F}\delta}{\pi(\delta + 2i\kappa\Gamma)} \tag{5.41}$$

which is $O(e^{\kappa H})$ since $\Gamma = O(e^{-2\kappa H})$ from (5.39). To determine the potential, we substitute $\tilde{G} = G' + G_3 + G_4$ into (5.25). Since $G'$ diminishes as $e^{-\kappa H}$ for sources on the cylinder, its contribution to the $\kappa$ wave is small compared to that due to $\alpha_1$ which is proportional to $e^{\kappa H}$. The potential field is then given by

$$\phi(x,z) = \frac{2i\mathcal{F}}{\delta + 2i\kappa\Gamma} e^{\kappa(-ix+z)} + \int_{S_B} \sigma(x',z')(G_3 + G_4)ds' + O(\delta)\,. \tag{5.42}$$

From the dynamic free surface condition, the surface elevation $\eta$ is given by

$$\eta(x) = -\frac{1}{g}(i\omega - U\frac{\partial}{\partial x})\phi(x,0)\,. \tag{5.43}$$

The wave elevations far upstream and downstream of the body are

$$\eta = A_2 e^{-ik_2 x}\,, \qquad x \to +\infty\,, \tag{5.44}$$

$$\eta = A_1 e^{-ik_1 x} + A_3 e^{ik_3 x} + A_4 e^{ik_4 x}\,, \qquad x \to -\infty\,, \tag{5.45}$$

with the wave amplitudes given from (5.42) by,

$$A_{1,2} = 2\mathcal{F}\frac{(\omega + Uk_{1,2})}{g(\delta + i2\kappa\Gamma)} + O(\delta)\,, \tag{5.46}$$

$$A_{3,4} = \mp\frac{2\pi(\omega - Uk_{3,4})}{g\sqrt{1+4\tau}} \int_{S_B} \sigma(x,z) e^{k_{3,4}(-ix+z)} ds + O(\delta)\,. \tag{5.47}$$

From (5.46), it is clear that $A_{1,2}$ are independent of the source strength $\sigma$. Thus, the amplitudes of the $k_1$ and $k_2$ waves are explicit and do not require the solution of the integral equation (5.23).

In principle, it is necessary to solve the steady problem first to provide for the body boundary condition $f(x,z)$. Again for relatively deep submergence, we neglect the free surface effect and write the potential for steady flow past the circular cylinder as that around a dipole

$$\bar{\phi}(x,z) = -Ux(1+\frac{R^2}{r^2}) \,. \tag{5.48}$$

Considering only the radiation problem, $f$ is then given by

$$f(\theta) = \xi_x(i\omega\cos\theta + \frac{2U}{R}\cos 2\theta) + \xi_z(i\omega\sin\theta + \frac{2U}{R}\sin 2\theta) \,, \tag{5.49}$$

where $\xi_x$ and $\xi_z$ are respectively the amplitudes of the sway and heave motions of the body.

For the calculation of the coefficient $\mathcal{F}$, we first replace $(x,z)$ by its corresponding cylindrical coordinates $(r,\theta)$, and expand the exponential in (5.21) in Taylor series. The integration over $\theta$ can be readily carried out yielding

$$\mathcal{F} = \pi\kappa R^2 e^{-\kappa H}(\omega+\kappa U)(-\xi_x + i\xi_z) \,, \tag{5.50}$$

which is the limiting value for $\mathcal{F}$ with $\delta^2 \ll 1$. For somewhat larger $\delta$, the accuracy of (5.50) is improved by simply replacing the wave number $\kappa$ with $k_{1,2}$ respectively for $A_{1,2}$. (This is equivalent to factoring out $e^{k_{1,2}z}$ rather than $e^{\kappa z}$ in (5.12).) Substituting $\mathcal{F}$ and $\Gamma$ into (5.46), we obtain finally

$$\frac{A_{1,2}}{i\xi_x+\xi_z} = \frac{2\pi k_{1,2}Re^{-k_{1,2}H}}{-i\sqrt{1-4\tau}+4\pi\kappa RI_1(2\kappa R)e^{-2\kappa H}}(\frac{1\pm\sqrt{1-4\tau}}{2F_r})^2 + O(\delta) \,, \tag{5.51}$$

where $F_r \equiv U/\sqrt{gR}$ is the Froude number.

Equation (5.51) is consistent with the known result for a submerged circular cylinder that the far-field waves generated by unit sway or heave motion have the same amplitude but are shifted in phase by $\frac{\pi}{2}$.

Figure 5-3 plots (5.51) for $A_{1,2}$ as a function of $\tau$ for the parameters $H/R = 2$ and $F_r = 0.4$. The limiting value of $A_{1,2}/(i\xi_x+\xi_z)$ as $\tau \to \frac{1}{4}$ is 4.018.... These parameter values for $H/R$ and $F_r$ coincide with one of the two computed cases by Grue & Palm

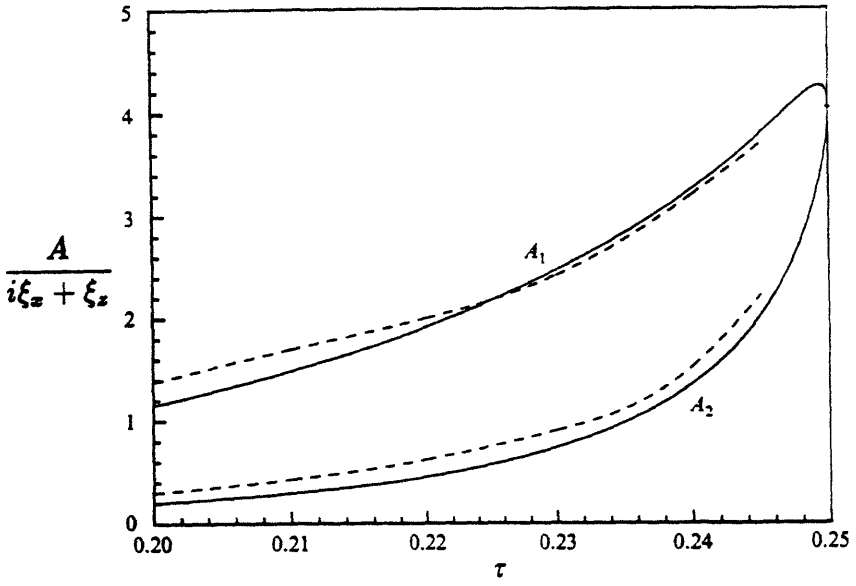


Figure 5-3: Amplitudes of the $k_1$ (upper branch) and $k_2$ (lower branch) waves radiated by the heave and sway oscillations of a submerged circular cylinder as a function of $\tau \equiv U\omega/g$. Asymptotic solution (5.51) (——); direct numerical calculations (Grue & Palm 1985) (- - -). ($F_\tau = U/(gR)^{\frac{1}{2}}$=0.4, $H/R$=2.)

(1985) for which they provide values for $\tau$ very close to $\frac{1}{4}$. For comparison, their numerical values are reproduced in figure 5-3. The comparison both in terms of the magnitudes and asymptotic slopes is quite satisfactory for this moderate submergence.

Finally, we consider the value of $A_{1,2}$ at $\tau = \frac{1}{4}$ as a function of wave frequency $\kappa R$ ($= (2F_\tau)^{-2}$). Evaluating (5.51) at $\tau = \frac{1}{4}$, we obtain

$$\frac{A_{1,2}}{(i\xi_x + \xi_z)} = \frac{\kappa R e^{\kappa H}}{2I_1(2\kappa R)} \,. \tag{5.52}$$

Figure 5-4 shows a plot of this limiting amplitude normalized by $e^{-\kappa H}$. As a check, at the other value of $F_\tau = 1.0$ ($\kappa R = 0.25$) computed by Grue and Palm (1985), the extrapolated value at $\tau = \frac{1}{4}$ from their curves again agrees well with the value of $A_{1,2}/(i\xi_x + \xi_z) = 0.799...$ given by (5.52). For low frequency (and large $U$), (5.52) has the limit of $\frac{1}{2}$ as $\kappa R \to 0$ — a surprisingly simple result. For high frequency, $\kappa R \gg 1$, the amplitude vanishes exponentially, $A_{1,2}e^{-\kappa H}/(i\xi_x + \xi_z) \sim \sqrt{\pi}(\kappa R)^{3/2}e^{-2\kappa R}$.

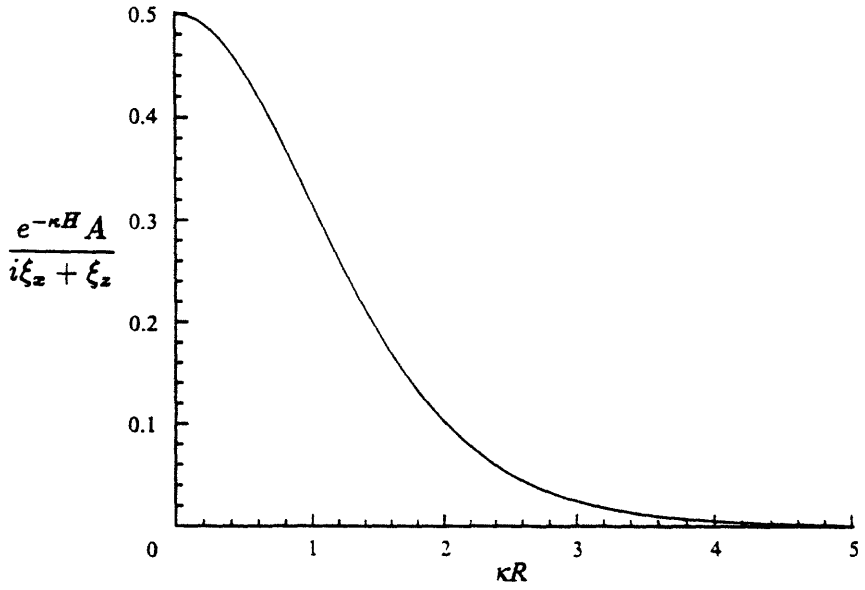


Figure 5-4: Limiting amplitude at $\tau \equiv U\omega/g = \frac{1}{4}$ of the $k_{1,2}$ waves due to the forced heave and sway oscillations of a submerged circular cylinder as a function of the dimensionless frequency $\kappa R$. $(H/R = 2.)$

## 5.5 Generalization to three dimensions

The foregoing analyses and results can be generalized to three dimensions. The key requirement is the separability of the dependence on $\vec{x}$ and $\vec{x'}$ in the leading-order term of the Green's function for $\delta^2 \ll 1$ (*cf.* (5.12)) leading to the factoring of the Kochin functions $\alpha_1$ and $\alpha_2$ (*cf.* (5.18), (5.29)).

The three-dimensional Green function for this problem (*e.g.* Wehausen & Laitone 1960) can be rewritten for $\tau < \frac{1}{4}$ as

$$G(x,y,z;x',y',z') = \frac{1}{r} - \frac{1}{r_1} + \frac{2}{\pi}\int_0^{\frac{\pi}{2}} \frac{d\theta}{\sqrt{1-4\tau\cos\theta}} \int_0^{\infty} (\frac{1}{k-k_1} - \frac{1}{k-k_2})\chi(\theta,k)dk$$
$$+\frac{2}{\pi}\int_{\frac{\pi}{2}}^{\pi} \frac{d\theta}{\sqrt{1-4\tau\cos\theta}} \int_0^{\infty} (\frac{1}{k-k_3} - \frac{1}{k-k_4})\chi(\theta,k)dk\ , \qquad (5.53)$$

in which

$$\begin{matrix} r \\ r_1 \end{matrix} = [(x-x')^2 + (y-y')^2 + (z \mp z')^2]^{\frac{1}{2}}\ , \qquad (5.54)$$

$$\chi(\theta,k) = k\cos[k(y-y')\sin\theta]e^{k[(z+z')-i(x-x')\cos\theta]}\ , \tag{5.55}$$

$$k_{1,2} = \kappa\frac{1-2\tau\cos\theta \mp \sqrt{1-4\tau\cos\theta}}{8\tau^2\cos^2\theta}\ . \tag{5.56}$$

The wave numbers $k_3$ and $k_4$ have solutions of the same form as $k_1$ and $k_2$. To satisfy the radiation condition at infinity, the integration paths for $k$ over the singularities in (5.53) are defined as $k_1 - i\epsilon$, $k_2 + i\epsilon$, $k_3 - i\epsilon$, $k_4 - i\epsilon$ as $\epsilon \to 0_+$. After the use of the Plemelj formula, the $k$ integrals reduce to Cauchy principle-value integrals plus the contribution from the four singularities at $k_1$, $k_2$, $k_3$ and $k_4$. As $\tau \to \frac{1}{4}$, the term $(1-4\tau\cos\theta)^{-\frac{1}{2}}$ becomes unbounded along $\theta = 0$. Thus $G$ is dominated by the integration near $\theta = 0$, *i.e.*,

$$\begin{aligned} G(x,y,z;x',y',z') = {} & \frac{2}{\pi}\int_0^\epsilon \frac{d\theta}{\sqrt{1-4\tau\cos\theta}} \fint_0^\infty (\frac{1}{k-k_1} - \frac{1}{k-k_2})\chi(\theta,k)dk \\ & - 2i\int_0^\epsilon \frac{\chi(\theta,k_1)+\chi(\theta,k_2)}{\sqrt{1-4\tau\cos\theta}}d\theta + O(1) \qquad \text{as } \tau \to (\tfrac{1}{4})_-\ . \end{aligned} \tag{5.57}$$

It can be shown that the double integral in (5.57) remains finite as $\tau \to \frac{1}{4}$. By expanding $\cos\theta$ in Taylor series about $\theta = 0$, the single integral can be carried out yielding finally

$$G(x,y,z;x',y',z') = i8\sqrt{2}\kappa\ln(\sqrt{1-4\tau})e^{\kappa[(z+z')-i(x-x')]} + O(1) \qquad \text{as } \tau \to (\tfrac{1}{4})_-\ . \tag{5.58}$$

The result is identical for $\tau \to (\frac{1}{4})_+$ and can be obtained similarly by considering this limit for the expression of $G$ for $\tau > \frac{1}{4}$.

We now note that the dependence of $G$ on $\vec{x}$, $\vec{x'}$ in (5.58) is identical to (5.12) for the two-dimensional case. The analyses in §§5.1, 5.2 thus follow directly leading to geometric conditions (5.27) and (5.37) for submerged and surface-intersecting bodies respectively. The integrands remain *identical*, but now the integrals are to be performed over the mean *two-dimensional* surface of the body. For (5.37), the waterline width $L_w$ is now replaced by the waterplane area of the body.

## 5.6 Discussions

The present findings can be motivated somewhat by physical arguments. Although the single source (Green function) becomes unbounded everywhere as $\tau \to \frac{1}{4}$, the distribution of such sources on the body satisfies a finite forcing. Physically, this requires that the Kochin function $\alpha_1/\delta$, which measures the net contribution of the sources at a fixed point, remains finite (*i.e.*, $\alpha_1 \leq O(\delta)$) as $\delta \to 0$. The necessary and sufficient condition for this to be true for a given body is the geomatric condition $\Gamma \neq 0$, a function of the frequency $\kappa$ but not of $U$. We reason that $\Gamma \neq 0$ is in effect a requirement that the Green's function (in fact just the resonant $k_{1,2}$ waves) is not orthogonal to the boundary condition on the body.

We note that the present problem is a classical one for which a number of approximate theories (*e.g.* Havelock 1958; Newman 1959; Dagan & Miloh 1981) exist, all of which indicate that the solution to the problem is singular as $\tau \to \frac{1}{4}$. The apparent contradiction with the present finding turns out to be the result of a common feature of the existing theories, namely, that the body boundary condition is enforced only in an approximate manner.

Consider, for example, a submerged circular cylinder represented by a single dipole Green function $G_x$ at the center. For $\tau$ not near $\frac{1}{4}$, the error in the normal velocity on the body surface is $\epsilon \sim e^{-2\kappa H}$ which vanishes as the body submergence increases. For $\delta^2 \ll 1$, however, $\epsilon \sim e^{-2\kappa H}/\delta$ since $G_{xn} \sim O(\delta^{-1})$, and the approximation is unacceptable as $\tau \to \frac{1}{4}$ for any finite $\kappa H$. Interestingly, for a point-like body, which may be a valid approximation for a very deeply submerged object, $\Gamma = 0$ according to (5.27). The solution at $\tau = \frac{1}{4}$ is then in fact unbounded and is consistent with existing results.

It is noteworthy that existing numerical solutions to this problem (*e.g.* Grue & Palm 1985; Wu & Eatock Taylor 1988) have likewise met with difficulties close to $\tau = \frac{1}{4}$. The computational difficulty arises from a direct solution of the integral

equation (5.15) as $\tau \to \frac{1}{4}$. From (5.16) and dividing by $(n_x + in_z)e^{\kappa(-ix+z)}/\delta$, we have

$$2\pi\kappa \int_{S_B} \sigma(x',z')e^{\kappa(ix'+z')}ds' + \frac{e^{\kappa(ix-z)}\delta}{n_x+in_z}[\pi\sigma(x,z) + \int\!\!\!\!\!\!-_{S_B} \sigma(x',z')\tilde{G}_n(x,z;x',z')ds'] = \frac{e^{\kappa(ix-z)}\delta}{n_x+in_z}f(x,z) + O(\delta^2)\,. \qquad (5.59)$$

In a typical numerical solution, (5.59) is discretized by subdividing $S_B$ into $N$ segments, and local basis functions are assumed for the source strength $\sigma$ over each segment, say resulting in $N$ unknown values for $\sigma$. Eq. (5.59) is then colocated at $N$ selected points (say one in each segment) resulting in a system of $N$ linear equations for the $N$ unknowns. The resulting coefficient matrix may be formally expressed as

$$([A_1] + [A_2]\delta) + O(\delta^2)\,, \qquad (5.60)$$

where $[A_1]$ and $[A_2]$ are the $N \times N$ influence matrices corresponding to the first and second terms respectively on the left side of (5.59) and are formally independent of $\delta$. As $\tau \to \frac{1}{4}$, (5.60) reduces to $[A_1] + O(\delta)$. From (5.59), it is clear that $[A_1]$ is not a function of the field point $\vec{x}$. Thus, the coefficient matrix has identical rows regardless of the position of the collocation points and is singular. The nature of the computational difficulty in the solution of (5.59) for $\delta^2 \ll 1$ is hence clear.

It is useful to point out that our analysis in §§5.1, 5.2 provides a simple remedy to the computational problem. For $\tau$ near the critical frequency, the numerical difficulties are easily avoided by solving the regular equations (5.23) for a submerged body or (5.34) for a surface-piercing body in favor of the singular equation (5.15).

## 5.7 Conclusions

We consider a floating or submerged body in deep water translating parallel to the undisturbed free surface with a steady velocity $U$ while undergoing small oscillations at frequency $\omega$. It is known that for a single source, the solution becomes singular at the resonant frequency given by $\tau \equiv U\omega/g = \frac{1}{4}$. In this chapter, we show that for

a general body, a finite solution exists as $\tau \to \frac{1}{4}$ *if and only if* a certain geometric condition (which depends only on the frequency $\omega$ but *not* on $U$) is satisfied. For a submerged body, a necessary and sufficient condition is that the body must have non-zero volume. For a surface-piercing body, a sufficient condition is derived which has a geometric interpretation similar to that of John (1950). As an illustration, we provide an analytic (closed-form) solution for the case of a submerged circular cylinder oscillating near $\tau = \frac{1}{4}$. Finally, we identify the underlying difficulties of existing approximate theories and numerical computations near $\tau = \frac{1}{4}$, and offer a simple remedy for the latter.

An immediate implication of the above result is the time-dependence of the force on a body due to an initial change in the velocity, which will be focused in the next chapter.

# Chapter 6

# The time dependence of the wave resistance of a body

An immediate and important extension of the finding in the preceding chapter is the time-dependence of the force on a body due to an initial change in the velocity. Based again on a single source starting from rest and maintaining constant strength, it is known (Havelock 1949; Wehausen 1964) that the wave resistance displays a slowly-decaying time oscillation at the frequency $\omega_c$ corresponding to $\tau = \frac{1}{4}$. Our frequency-domain result (chapter 5) suggests that with the removal of the $\tau = \frac{1}{4}$ singularity, the actual decay must in fact be faster for a body which satisfies the requisite geometric condition. In this chapter, we will prove this and derive the exact decay rate based on a thorough analysis of the time-dependence of the wave resistance of a body starting from rest.

The question of how rapidly transients associated with the abrupt motions of a floating body decay is one of fundamental theoretical interest as well as practical importance. The rate at which transient oscillations vanish and measurements taken is of some concern in model tests especially for unsteady and local effects. The question of the behavior of transients comes up also in almost all numerical simulations in the time domain and directly affects our ability to extract steady-state predictions for resistance problems and to obtain meaningful results for general seakeeping problems.

Despite its obvious importance, the problem appears to have been addressed only

for the idealized case of a single translating source of *known* strength. Havelock (1949) considered the two-dimensional problem of the wave resistance of a submerged circular cylinder started impulsively from rest. By approximating the body as a point dipole of constant strength, he derived a closed-form solution for the wave resistance. The significant finding is that for a given forward speed $U$, the resistance oscillates about the steady value with frequency $\omega_c = g/4U$, and the oscillation decays only like $t^{-\frac{1}{2}}e^{i\omega_c t}$ as $t \to \infty$. This result was extended to three dimensions by Wehausen (1964) who considered a constant source started abruptly and obtained that the unsteady resistance vanishes like $t^{-1}e^{i\omega_c t}$ as $t \to \infty$.

The above results can be understood by considering the associated classical seakeeping problem in the frequency domain, wherein it is known that (for a single source) the solution is in fact singular at the frequency $U\omega_c/g = \frac{1}{4}$ (Haskind 1954). In the preceding chapter, we just showed that for an actual body the solution at the critical frequency is finite for a general class of bodies (*admissible* bodies) subject to a single geometric condition. An immediate consequence of this finding is that the decay rate of transients must necessarily be an order of magnitude faster than the single-source predictions of Havelock (1949) and Wehausen (1964) for this class of geometries.

Here we consider the starting from rest to steady speed of a general body. The initial-boundary-value problem is reviewed in §6.1. To solve the problem, we use a transient source distribution on the wetted surface of the body, where in general the singularity strengths are unsteady and part of the solution of the problem. Our analyses (§§6.2, 6.3) show that for *admissible* bodies, the transient decay rate is indeed more rapid than for constant strength isolated singularities, with the unsteady wave resistance in two and three dimensions decaying respectively like $O(t^{-1}, t^{-\frac{3}{2}}e^{i\omega_c t})$ and $O(t^{-2}, t^{-2}e^{i\omega_c t})$ as $t \to \infty$. As a theoretical verification, we rederive these results (§6.4) using the Fourier method (e.g. Ursell 1964) based on the frequency-domain solution of the classical seakeeping problem. For a submerged circular cylinder and a Wigley hull, these results are further confirmed by carefully controlled numerical simulations in the time domain (§6.5).

## 6.1 The initial-boundary-value problem

We take a right-handed Cartesian coordinate system $o-xyz$ with the $(x,y)$-plane in the undisturbed free surface, the $x$-axis pointing in the direction of forward speed, and the $z$-axis vertically upwards. This system moves forward at constant speed $U$ and is fixed on a body at $t = 0$, which is started impulsively from rest. The fluid is assumed to be incompressible, homogeneous and inviscid, and its motion irrotational. The flow can be described by a velocity potential:

$$\Phi^*(\vec{x},t) = -Ux + \Phi(\vec{x},t) \tag{6.1}$$

where $\Phi$ represents the body disturbance in the flow. The potential, $\Phi$, satisfies Laplace's equation within the fluid and vanishes at deep water, $\nabla\Phi \to 0$ as $z \to -\infty$. Assuming the amplitudes of waves generated by the forward motion of the body are small, the free surface condition for $\Phi$ can be linearized and it follows that

$$\left(\frac{\partial}{\partial t} - U\frac{\partial}{\partial x}\right)^2 \Phi + g\frac{\partial \Phi}{\partial z} = 0\,, \qquad \text{on} \quad z = 0\,. \tag{6.2}$$

The kinematic boundary condition applied on the wetted body surface, $S_B$, can be written as:

$$\frac{\partial \Phi}{\partial n} = \begin{cases} Un_x & t > 0, \\ 0 & \text{otherwise,} \end{cases} \qquad \text{on} \quad S_B\,, \tag{6.3}$$

where $\mathbf{n} = (n_x, n_y, n_z)$ is the unit normal out of the body. At the time $t = 0$, the zero initial conditions are prescribed

$$\Phi(\vec{x},0) = \Phi_t(\vec{x},0) = 0, \qquad \text{for } z \le 0\,. \tag{6.4}$$

The velocity potential $\Phi$ is defined completely after imposing the radiation condition that no waves can appear at far upstream of the body at any time.

The general uniqness theory for this initial-boundary-value problem is as yet unavailable. Despite this fact, considerable amount of efforts have been devoted to find

the solution both theoretically and numerically (e.g. Havelock 1949; Lunde 1951; Wehausen 1964; Lin & Yue 1990; Bingham 1994). It should be noted that the large time limit of the present problem tends to the well-known steady Kelvin-Neumann problem for which, a unique solution has been shown (Kochin 1937; Dern 1980) to exist in the case of submerged bodies. We are unable to extend this result and simply postulate the uniqueness of the present problem for general bodies.

For a general body, the exact solution of the stated problem is very difficult to be obtained without the use of numerical techniques. In the following sections, we seek to understand transient behaviours of the solution at large time through systematic asymptotic analyses in both the time domain and the frequency domain. The determination of the decay rate of the transient solution is of theoretical interest and practical importance for experimental measurements of the wave resistance of a body and time-domain numerical simulations of the seakeeping problem.

## 6.2 Time-domain analyses

In this section, we solve the stated problem (§6.1) directly in the time domain and derive the explicit time-dependence of the solution through large-time asymptotic analyses. Based on the source formulation, the potential $\Phi$ is constructed in terms of an instantaneous wave source distribution over the wetted body surface. The unknown source strength at any point on the body at any time is determined by an integral equation resulting from the imposition of the body boundary condition. Based on large-time expansions of single-source potentials, the time-dependence of the source distribution can be determined from the integral equation. After obtaining the solution for the source strength, the transient solution of the velocity potential $\Phi$ follows directly.

For the sake of clarity, in this section, we present our analyses in detail only for two-dimensional submerged bodies. The extension to surface-intersecting and three-dimensional bodies is straightforward and will be outlined in the next section (§6.3).

### 6.2.1 Single-source potential

Consider a source of variable strength, $\sigma(t)$, located at $\vec{x'}$. The resulting velocity potential, denoted by $\Psi(\vec{x}, \vec{x'}, \sigma(t))$, is defined to be harmonic everywhere in the fluid except at the source position. In addition, $\Psi$ satisfies the linearized free surface condition (6.2) as well as the radiation condition, and vanishes at large depth. It is noted that $\Psi$ is identical to the conventional Green's function (Havelock 1949) if $\sigma(t)$ is constant.

The general solution of $\Psi$ can be derived by making use of classical transform techniques (for details, see Wehausen & Laitone 1960). In two dimensions, we write $\Psi$ in a conventional form:

$$\Psi(\vec{x}, \vec{x'}, \sigma(t)) = \sigma(t) \ln\left(\frac{r}{r_1}\right)$$

$$-2g\int_0^\infty \mathrm{d}k \frac{\mathrm{e}^{k(z+z')}}{(gk)^{\frac{1}{2}}} \int_{-\infty}^t \sigma(\tau) \cos[k(x-x') + kU(t-\tau)] \sin[(gk)^{\frac{1}{2}}(t-\tau)]\, \mathrm{d}\tau \quad (6.5)$$

where $r^2, r_1^2 = (x-x')^2 + (z \mp z')^2$. For convenience in analytical manipulation, we rewrite (6.5) in a more convenient form by expressing the trigonometric functions in complex exponential form

$$\Psi(\vec{x}, \vec{x'}, \sigma(t)) = \sigma(t) \ln\left(\frac{r}{r_1}\right)$$

$$+ \mathrm{i}\frac{g}{2} \int_0^\infty \frac{\mathrm{d}k}{(gk)^{\frac{1}{2}}} \mathrm{e}^{k\psi + \mathrm{i}[kU + (gk)^{\frac{1}{2}}]t} \int_{-\infty}^t \sigma(\tau) \mathrm{e}^{-\mathrm{i}[kU + (gk)^{\frac{1}{2}}]\tau}\, \mathrm{d}\tau + \text{c.c.}$$

$$- \mathrm{i}\frac{g}{2} \int_0^\infty \frac{\mathrm{d}k}{(gk)^{\frac{1}{2}}} \mathrm{e}^{k\psi + \mathrm{i}[kU - (gk)^{\frac{1}{2}}]t} \int_{-\infty}^t \sigma(\tau) \mathrm{e}^{-\mathrm{i}[kU - (gk)^{\frac{1}{2}}]\tau}\, \mathrm{d}\tau + \text{c.c.} \quad (6.6)$$

where $\psi = \mathrm{i}(x-x') + (z+z')$ and c.c. denotes the complex conjugate of the preceding terms. Changing variable with $k = m^2$ and manipulating the range of integration a

bit, it follows that

$$\Psi(\vec{x},\vec{x'},\sigma(t)) = \sigma(t)\ln\left(\frac{r}{r_1}\right)$$

$$+\mathrm{i}2g^{\frac{1}{2}}\int_0^\infty \mathrm{d}m\,\mathrm{e}^{m^2\psi+\mathrm{i}(m^2U+mg^{\frac{1}{2}})t}\int_{-\infty}^t \sigma(\tau)\mathrm{e}^{-\mathrm{i}(m^2U+mg^{\frac{1}{2}})\tau}\,\mathrm{d}\tau + \text{c.c.}$$

$$-\mathrm{i}g^{\frac{1}{2}}\int_{-\infty}^\infty \mathrm{d}m\,\mathrm{e}^{m^2\psi+\mathrm{i}(m^2U-mg^{\frac{1}{2}})t}\int_{-\infty}^t \sigma(\tau)\mathrm{e}^{-\mathrm{i}(m^2U-mg^{\frac{1}{2}})\tau}\,\mathrm{d}\tau + \text{c.c.}\,. \quad (6.7)$$

In order to find the explicit time-dependence of the velocity potential $\Phi$ in the near field of the body, it is necessary to first asymptotically expand $\Psi$ for $\frac{|\vec{x}-\vec{x'}|}{Ut} = o(1)$ as $t \to \infty$. For a given function of $\sigma(t)$, in principle, the expansion of $\Psi$ can be obtained from (6.7) by using the method of steepest decent. In the following, we summarize three major expansions of $\Psi$ for specially-anticipated source functions, which are useful for later analyses. The detailed derivation of these expansions is shown in appendix B.

**Case I: $\sigma(t) = q_0 = 1$ for $t > 0$ and $q_0 = 0$ elsewhere**

For a source with constant strength at $t > 0$, the potential $\Psi$ at large time can be expanded as:

$$\Psi(\vec{x},\vec{x'},q_0) = \bar{G}(\vec{x},\vec{x'}) + C_0\frac{\mathrm{e}^{-\mathrm{i}\omega_c t}}{t^{\frac{1}{2}}}\mathrm{e}^{\kappa\psi} + \text{c.c.} + O\left(\frac{\mathrm{e}^{-\mathrm{i}\omega_c t}}{t^{\frac{3}{2}}}\right) \qquad \text{as } t\to\infty \qquad (6.8)$$

where the wave number $\kappa = g/(4U^2)$, the constant $C_0 = 8(\frac{\pi U}{g})^{\frac{1}{2}}\,\mathrm{e}^{\mathrm{i}\frac{\pi}{4}}$, and the time-independent function $\bar{G}$ is given by

$$\bar{G}(\vec{x},\vec{x'}) = \ln(rr_1) + 2\pi\mathrm{e}^{k_0(z+z')}\sin k_0(x-x') + 2\int_0^\infty \frac{\cos k(x-x')}{k-k_0}\mathrm{e}^{k(z+z')}\,\mathrm{d}k \quad (6.9)$$

with $k_0 = 4\kappa$.

**Case II:** $\sigma(t) = \tilde{\sigma}(t) \neq 0$ **for** $t \in (0, t_0)$ **and** $\tilde{\sigma}(t) = 0$ **elsewhere**

If a source is suddenly brought into the existence at $t = 0$ and taken out of the fluid at $t = t_0$, the resulting potential $\tilde{\Psi}$ at large time can be expanded as:

$$\tilde{\Psi}(\vec{x}, \vec{x'}, \tilde{\sigma}(t)) = \tilde{W}(\vec{x'}) \frac{e^{-i\omega_c t}}{t^{\frac{1}{2}}} e^{\kappa\psi} + \text{c.c.} + O\left(\frac{1}{t}, \frac{e^{-i\omega_c t}}{t^{\frac{3}{2}}}\right) \qquad \text{as } t \to \infty \qquad (6.10)$$

where $\tilde{W}$ is independent of time and is given by

$$\tilde{W}(\vec{x'}) = \left(\frac{g\pi}{U}\right)^{\frac{1}{2}} e^{-i\frac{\pi}{4}} \int_0^{t_0} \tilde{\sigma}(\tau) e^{i\omega_c \tau} \, d\tau \, . \qquad (6.11)$$

**Case III:** $\sigma(t) = q_1 = t^{-\frac{1}{2}} e^{-i\omega_c t}$ **for** $t > t_0$ **and** $q_1 = 0$ **elsewhere**

If a source is brought into the fluid at $t = t_0$ with variable strength given by $t^{-\frac{1}{2}} e^{-i\omega_c t}$, the resulting potential at large time can be expanded as:

$$\Psi(\vec{x}, \vec{x'}, q_1) = C_1 e^{-i\omega_c t} e^{\kappa\psi} + \bar{C}_1 \frac{e^{-i\omega_c t}}{t^{\frac{1}{2}}} e^{\kappa\psi} + \hat{C}_1 \frac{e^{i\omega_c t}}{t^{\frac{1}{2}}} e^{\kappa\psi^*}$$

$$+ H(\vec{x}, \vec{x'}) \frac{e^{-i\omega_c t}}{t^{\frac{1}{2}}} + O\left(\frac{1}{t}, \frac{e^{-i\omega_c t}}{t}\right) \qquad \text{as } t \to \infty \qquad (6.12)$$

where $*$ denotes the complex conjugate and the constants $C_1$, $\bar{C}_1$, and $\hat{C}_1$ are respectively given by

$$C_1 = e^{-i\frac{\pi}{4}} (k_0 U)^{\frac{1}{2}} \sum_{n=0}^{\infty} \frac{\Gamma(n + \frac{1}{2})}{(2n+1)n!} \, , \qquad \bar{C}_1 = -2e^{-i\frac{\pi}{4}} (\pi k_0 U t_0)^{\frac{1}{2}} \, , \qquad (6.13)$$

and

$$\hat{C}_1 = e^{i\frac{\pi}{4}} (2\pi)^{\frac{1}{2}} W_2(k_0 U/2) \, . \qquad (6.14)$$

The regular function $H(\vec{x}, \vec{x'})$ is independent of time and is given by

$$H(\vec{x}, \vec{x'}) = \ln\left(\frac{r}{r_1}\right) + i\sqrt{2}\pi \left(e^{m_1^2 \psi^*} - e^{m_2^2 \psi^*}\right) + k_0^{\frac{1}{2}} \left\{ -2 \int_0^{\infty} \frac{e^{m^2 \psi}}{(m + k_0^{\frac{1}{2}}/2)^2} \, dm \right.$$

$$- \oint_0^\infty \frac{e^{m^2\psi^*}}{(m+m_1)(m-m_2)}\,dm + \int_{\mathcal{L}} \frac{e^{m^2\psi^*}}{(m-m_1)(m+m_2)}\,dm \Bigg\} \qquad (6.15)$$

where $m_{1,2} = k_0^{\frac{1}{2}}(\sqrt{2} \pm 1)/2$, and $\oint$ indicates the path of integration to go below the pole. The contour $\mathcal{L}$ extends from $-\infty$ to $+\infty$ in the complex $m$-plane and is indented to pass below the pole at $m = m_1$ and above the pole at $m = -m_2$.

### 6.2.2 Submerged bodies

For a submerged body moving in the direction of $ox$ with constant forward speed $U$, the solution can be constructed in terms of a continuous source distribution (Havelock 1949; Lunde 1951):

$$\Phi(\vec{x}, t) = \int_{S_B} \Psi(\vec{x}, \vec{x'}, \sigma(\vec{x'}, t))\,ds' \,, \qquad (6.16)$$

where $\sigma(\vec{x'}, t)$ represents the source distribution on the body. Since the solution eventually reaches the steady state, in general, we can decompose the source strength $\sigma(\vec{x'}, t)$ into steady and unsteady components:

$$\sigma(\vec{x'}, t) = \bar{\sigma}(\vec{x'}) + \check{\sigma}(\vec{x'}, t) \qquad (6.17)$$

in which the time-dependent part $\check{\sigma}$ is expected to vanish at large time. After substituting (6.17) into (6.16), the velocity potential $\Phi$ can be expressed as:

$$\Phi(\vec{x}, t) = \int_{S_B} \bar{\sigma}(\vec{x'})\Psi(\vec{x}, \vec{x'}, q_0)\,ds' + \int_{S_B} \Psi(\vec{x}, \vec{x'}, \check{\sigma}(\vec{x'}, t))\,ds' \,. \qquad (6.18)$$

To find the asymptotic solution of $\Phi$ at large time, it is clear from (6.18) that it is necessary to construct the asymptotic expansion of the single-source potential $\Psi$. For doing this, the time dependence of the unsteady source $\check{\sigma}$ must be known in advance.

In order to derive the asymptotic expansion of the unsteady source distribution, we further split $\check{\sigma}$ into two parts:

$$\check{\sigma}(\vec{x'}, t) = \tilde{\sigma}(\vec{x'}, t) + \hat{\sigma}(\vec{x'}, t) \qquad (6.19)$$

where $\tilde{\sigma}$ is assumed to be a continuous function of the time for $t \in (0, t_0)$ and vanishes for $t > t_0$, while $\hat{\sigma}$ is identically zero for $t \in (0, t_0)$ and decays as $t \to \infty$. Due to such decompositions, the velocity potential in (6.18) can then be rewritten as:

$$\Phi(\vec{x}, t) = \int_{S_B} \bar{\sigma}(\vec{x'}) \Psi(\vec{x}, \vec{x'}, q_0)\, \mathrm{d}s' + \int_{S_B} \tilde{\Psi}(\vec{x}, \vec{x'}, \tilde{\sigma}(t))\, \mathrm{d}s' + \int_{S_B} \Psi(\vec{x}, \vec{x'}, \hat{\sigma}(\vec{x'}, t))\, \mathrm{d}s' \,. \tag{6.20}$$

By substituting the asymptotic expansions of $\Psi(\vec{x}, \vec{x'}, q_0)$ and $\tilde{\Psi}$ into (6.20), it follows that

$$\begin{aligned} \Phi(\vec{x}, t) = & \int_{S_B} \bar{\sigma}(\vec{x'}) \bar{G}(\vec{x}, \vec{x'})\, \mathrm{d}s' + \int_{S_B} \Psi(\vec{x}, \vec{x'}, \hat{\sigma}(\vec{x'}, t))\, \mathrm{d}s' \\ & + \frac{\alpha_1 \mathrm{e}^{-\mathrm{i}\omega_c t}}{t^{\frac{1}{2}}} \mathrm{e}^{\kappa(\mathrm{i}x+z)} + \text{c.c.} + O\left(\frac{1}{t}, \frac{\mathrm{e}^{-\mathrm{i}\omega_c t}}{t^{\frac{3}{2}}}\right) \qquad \text{as } t \to \infty \end{aligned} \tag{6.21}$$

in which the Kochin function $\alpha_1$ is defined by

$$\alpha_1 = \int_{S_B} \left[ C_0 \bar{\sigma}(\vec{x'}) + \tilde{W}(\vec{x'}) \right] \mathrm{e}^{\kappa(-\mathrm{i}x' + z')}\, \mathrm{d}s' \,. \tag{6.22}$$

Clearly, the solution constructed in (6.21) satisfies all conditions of the initial-boundary-value problem except for that on the body. Imposing the body boundary condition (6.3) to (6.21), an integral equation for the unknown source strengths is obtained:

$$\begin{aligned} & \pi[\bar{\sigma}(\vec{x}) + \hat{\sigma}(\vec{x}, t)] + \fint_{S_B} \bar{\sigma}(\vec{x'}) \frac{\partial}{\partial n} \bar{G}(\vec{x}, \vec{x'})\, \mathrm{d}s' + \fint_{S_B} \frac{\partial}{\partial n} \Psi(\vec{x}, \vec{x'}, \hat{\sigma}(\vec{x'}, t))\, \mathrm{d}s' \\ & + \frac{\mathrm{e}^{-\mathrm{i}\omega_c t}}{t^{\frac{1}{2}}} \alpha_1 \kappa (\mathrm{i} n_x + n_z) \mathrm{e}^{\kappa(\mathrm{i}x+z)} + \text{c.c.} = U n_x + O\left(\frac{1}{t}, \frac{\mathrm{e}^{-\mathrm{i}\omega_c t}}{t^{\frac{3}{2}}}\right) \qquad \text{as } t \to \infty \end{aligned} \tag{6.23}$$

for any $\vec{x}$ on the body. Because the time-dependent terms in the equation decay for large time, (6.23) can be separated into steady-state and time-dependent components:

$$\pi \bar{\sigma}(\vec{x}) + \fint_{S_B} \bar{\sigma}(\vec{x'}) \bar{G}_n(\vec{x}, \vec{x'})\, \mathrm{d}s' = U n_x \,, \tag{6.24}$$

and

$$\pi\hat{\sigma}(\vec{x},t)+\fint_{S_B}\Psi_n(\vec{x},\vec{x'},\hat{\sigma}(\vec{x'},t))\,\mathrm{d}s'$$
$$+\frac{\mathrm{e}^{-\mathrm{i}\omega_c t}}{t^{\frac{1}{2}}}\alpha_1\kappa(\mathrm{i}n_x+n_z)\mathrm{e}^{\kappa(\mathrm{i}x+z)}+\mathrm{c.c.}=O\left(\frac{1}{t},\frac{\mathrm{e}^{-\mathrm{i}\omega_c t}}{t^{\frac{3}{2}}}\right)\qquad\text{as } t\to\infty \quad (6.25)$$

for $\vec{x}\in S_B$.

Equation (6.24) governs the steady source $\bar{\sigma}$ which is associated with the well-known Kelvin-Neumann problem. The solution of (6.24) has been investigated by many researchers both theoretically and numerically (e.g. Wehausen 1973; Nakos & Sclavounos 1990). Since our focus is on the unsteady solution, we here just simply assume the existence of a unique finite solution for $\bar{\sigma}$ and will not consider equation (6.24) any further.

Equation (6.25) governs the unsteady source $\hat{\sigma}$ at large time. Based on (6.25) and the large-time expansion of $\Psi(\vec{x},\vec{x'},q_1)$, we deduce that in general, the unsteady source $\hat{\sigma}$ must formally take the following asymptotic expansion in time:

$$\hat{\sigma}(\vec{x'},t)=\mathrm{Re}\left\{\sigma_1(\vec{x'})\frac{\mathrm{e}^{-\mathrm{i}\omega_c t}}{t^{\frac{1}{2}}}\right\}+O\left(\frac{1}{t},\frac{\mathrm{e}^{-\mathrm{i}\omega_c t}}{t^{\frac{3}{2}}}\right)\qquad\text{as } t\to\infty \qquad (6.26)$$

where $\sigma_1$ is complex. In the following, however, we shall show that subject to a body geometric condition, $\sigma_1(\vec{x'})$ is identically zero for any $\vec{x'}$ on the body.

Now we substitute (6.26) back into (6.25) and obtain

$$\mathrm{Re}\left\{\pi\sigma_1(\vec{x})\frac{\mathrm{e}^{-\mathrm{i}\omega_c t}}{t^{\frac{1}{2}}}+\fint_{S_B}\sigma_1(\vec{x'})\Psi_n(\vec{x},\vec{x'},q_1)\,\mathrm{d}s'\right\}$$
$$+\frac{\mathrm{e}^{-\mathrm{i}\omega_c t}}{t^{\frac{1}{2}}}\alpha_1\kappa(\mathrm{i}n_x+n_z)\mathrm{e}^{\kappa(\mathrm{i}x+z)}+\mathrm{c.c.}=O\left(\frac{1}{t},\frac{\mathrm{e}^{-\mathrm{i}\omega_c t}}{t}\right)\qquad\text{as } t\to\infty\,. \quad (6.27)$$

Substituting the asymptotic expansions of $\Psi(\vec{x},\vec{x'},q_1)$ into (6.27), it follows that

$$\frac{\mathrm{e}^{\mathrm{i}\omega_c t}}{t^{\frac{1}{2}}}\beta_1\kappa(-\mathrm{i}n_x+n_z)\mathrm{e}^{\kappa(-\mathrm{i}x+z)}+\frac{\mathrm{e}^{-\mathrm{i}\omega_c t}}{t^{\frac{1}{2}}}\{\pi\sigma_1(\vec{x})$$

$$+ \oint_{S_B} \sigma_1(\vec{x}') \, H_n(\vec{x}, \vec{x}') \, \mathrm{d}s' + \beta_2 \kappa (\mathrm{i} n_x + n_z) \mathrm{e}^{\kappa(\mathrm{i}x+z)} \Big\} = O\left(\frac{1}{t}, \frac{\mathrm{e}^{-\mathrm{i}\omega_c t}}{t}\right) \quad (6.28)$$

as $t \to \infty$, where the constants $\beta_1$ and $\beta_2$ are Kochin functions respectively defined by

$$\beta_1 = \alpha_1^* + \hat{C}_1 \int_{S_B} \sigma_1(\vec{x}') \mathrm{e}^{\kappa(\mathrm{i}x'+z')} \, \mathrm{d}s' \quad (6.29)$$

and

$$\beta_2 = \alpha_1 + (C_1 t^{\frac{1}{2}} + \bar{C}_1) \int_{S_B} \sigma_1(\vec{x}') \mathrm{e}^{\kappa(-\mathrm{i}x'+z')} \, \mathrm{d}s' \, . \quad (6.30)$$

By identifying the coefficients of each time harmonic in (6.28), we have

$$\beta_1 \kappa (-\mathrm{i} n_x + n_z) \mathrm{e}^{\kappa(-\mathrm{i}x+z)} = 0 \, , \quad (6.31)$$

and

$$\pi \sigma_1(\vec{x}) + \oint_{S_B} \sigma_1(\vec{x}') \, H_n(\vec{x}, \vec{x}') \, \mathrm{d}s' = -\beta_2 \kappa (\mathrm{i} n_x + n_z) \mathrm{e}^{\kappa(\mathrm{i}x+z)} \quad (6.32)$$

as $t \to \infty$.

Since (6.31) needs to be satisfied for any $\vec{x}$ on the body, it immediately follows that the Kochin function $\beta_1$ must vanish.

Notice that integral equations (6.30) and (6.32) are coupled for unknowns $\alpha_1$ and $\sigma_1$. To decouple these equations and find the solution of $\sigma_1$, we follow the procedure employed in §5.2. First, we rewrite (6.32) as:

$$\sigma_1(\vec{x}) = -\frac{1}{\pi} \oint_{S_B} \sigma_1(\vec{x}') \, H_n(\vec{x}, \vec{x}') \, \mathrm{d}s' - \frac{\beta_2 \kappa}{\pi} (\mathrm{i} n_x + n_z) \mathrm{e}^{\kappa(\mathrm{i}x+z)} \, . \quad (6.33)$$

We then substitute (6.33) into (6.30) and solve for the Kochin function $\beta_2$ to obtain

$$\beta_2 = \frac{1}{\pi + (C_1 t^{\frac{1}{2}} + \bar{C}_1) \kappa \Gamma} \left[ \pi \alpha_1 - (C_1 t^{\frac{1}{2}} + \bar{C}_1) \int_{S_B} \sigma_1(\vec{x}') P_1(\vec{x}') \, \mathrm{d}s' \right] \quad (6.34)$$

where the kernel $P_1$ is given by

$$P_1(\vec{x}') = \oint_{S_B} \mathrm{e}^{\kappa(-\mathrm{i}x+z)} H_n(\vec{x}, \vec{x}') \, \mathrm{d}s \quad (6.35)$$

and the geometric constant $\Gamma$ is given by (5.22).

Depending on the body geometry, there are two possibilities. If $\Gamma \neq 0$, we substitute (6.34) back into (6.32) to obtain a new integral equation for $\sigma_1$:

$$\pi\sigma_1(\vec{x}) + \fint_{S_B} \sigma_1(\vec{x'})\, H_n(\vec{x},\vec{x'})\, \mathrm{d}s' - \frac{\mathrm{i}n_x + n_z}{\Gamma} \mathrm{e}^{\kappa(\mathrm{i}x+z)} \int_{S_B} \sigma_1(\vec{x'}) P_1(\vec{x'})\, \mathrm{d}s' = 0 \quad (6.36)$$

as $t \to \infty$. Note that equation (6.36) is homogeneous and its kernels are regular. According to the Fredholm theorem, (6.36) possesses a trivial solution except possibly at an enumerable number of discrete values of $\kappa$ for which the Fredholm determinant vanishes and nontrivial homogeneous solutions can exist. Since our major interest is on the general problem, we will not be particularly concerned with this possibility. It then follows that if $\Gamma \neq 0$, $\sigma_1(\vec{x}) = 0$ for any $\vec{x}$ on the body and thus $\hat{\sigma}(\vec{x},t) = O(t^{-1}, t^{-\frac{3}{2}}\mathrm{e}^{-\mathrm{i}\omega_c t})$ from (6.26) as $t \to \infty$.

From (6.32), it is clear that the constant $\beta_2$ must be identically zero as $t \to \infty$. This leads to the Kochin function $\alpha_1 = 0$ according to (6.30), which also follows from (6.29). In this case, the velocity potential $\Phi$ in (6.21) reduces to:

$$\Phi(\vec{x},t) = \int_{S_B} \bar{\sigma}(\vec{x'})\bar{G}(\vec{x},\vec{x'})\, \mathrm{d}s' + \int_{S_B} \Psi(\vec{x},\vec{x'},\hat{\sigma}(\vec{x'},t))\, \mathrm{d}s' + O\left(\frac{1}{t}, \frac{\mathrm{e}^{-\mathrm{i}\omega_c t}}{t^{\frac{3}{2}}}\right) \qquad (6.37)$$

where $\hat{\sigma}(\vec{x'},t) = O(t^{-1}, t^{-\frac{3}{2}}\mathrm{e}^{-\mathrm{i}\omega_c t})$ as $t \to \infty$.

Following the above procedure with $\hat{\sigma}(\vec{x'},t) = O(t^{-1}) + O(t^{-\frac{3}{2}}\mathrm{e}^{-\mathrm{i}\omega_c t})$, we can further show that at the order $t^{-1}$, there is a monotonically decaying term but no oscillatory term $O(t^{-1}\mathrm{e}^{-\mathrm{i}\omega_c t})$ in the expansion of the potential $\Phi$. Thus we can rewrite (6.37) as:

$$\Phi(\vec{x},t) = \int_{S_B} \bar{\sigma}(\vec{x'})\bar{G}(\vec{x},\vec{x'})\, \mathrm{d}s' + O\left(\frac{1}{t}, \frac{\mathrm{e}^{-\mathrm{i}\omega_c t}}{t^{\frac{3}{2}}}\right) \qquad \text{as } t \to \infty \qquad (6.38)$$

which indicates that the transient potential vanishes in the same way as the unsteady source distribution $\hat{\sigma}$.

If $\Gamma = 0$, the substitution of (6.34) into (6.32) gives

$$\pi\sigma_1(\vec{x}) + \fint_{S_B} \sigma_1(\vec{x'})\, H_n(\vec{x},\vec{x'})\, \mathrm{d}s' + \alpha_1\kappa(\mathrm{i}n_x + n_z)\, \mathrm{e}^{\kappa(\mathrm{i}x+z)}$$

$$= \frac{\kappa}{\pi}(C_1 t^{\frac{1}{2}} + \bar{C}_1)(\mathrm{i}n_x + n_z)\mathrm{e}^{\kappa(\mathrm{i}x+z)} \int_{S_B} \sigma_1(\vec{x'}) P(\vec{x'})\, \mathrm{d}s' + O\left(\frac{1}{t^{\frac{1}{2}}}\right) \qquad (6.39)$$

as $t \to \infty$. Note that the right-hand side of (6.39) becomes unbounded for $\sigma_1 \neq 0$ as $t \to \infty$ and the solution of $\sigma_1$ depends on the constant $\alpha_1$. In general, we can only have $\alpha_1 \neq 0$ for discussing the solution of $\sigma_1$. From (6.39), $\sigma_1$ must be at least $O(1)$ for $\alpha_1 \neq 0$. As a result, the unsteady potential $\Phi$ due to $\hat{\sigma}$ must be larger than $O(1)$ as $t \to \infty$. This implies that if $\Gamma = 0$, the steady-state solution does not exist for the original initial-boundary-value problem based on linearized theory. It is remarked that such solution behaviour was also found by De Prima & Wu (1956) and Akylas (1984) for water waves generated by a moving disturbance which has a constant magnitude but oscillates in time at the critical frequency $\omega_c$.

In summary, we conclude that for a submerged two-dimensional body, the transient potential due to an initial acceleration of the body decays like $O(t^{-1}, t^{-\frac{3}{2}}\mathrm{e}^{-\mathrm{i}\omega_c t})$ as $t \to \infty$ if $\Gamma \neq 0$. On the other hand, no steady-state solution exists if $\Gamma = 0$. Note that according to Bernoulli's equation (2.4), the wave resistance of the body has the same leading time dependence as the velocity potential.

For a submerged body, as discussed in §5.2, the condition $\Gamma \neq 0$ corresponds to the requirement that the body has non-zero volume.

## 6.3 Generalizations

In this section, we extend the time-domain analysis of the preceding section to surface-intersecting and three-dimensional bodies.

### 6.3.1 Surface-intersecting bodies

As with the demonstration for the frequency-domain problem (§§5.2, 5.3), the transient analysis (§6.2) for submerged bodies can be generalized to surface-intersecting bodies with the extra complication of a waterline integral.

By assuming (locally) vertical intersections, we again write the velocity potential

in terms of a body surface source distribution (e.g. Ursell 1980)

$$\Phi(\vec{x},t) = \int_{S_B} \Psi(\vec{x},\vec{x'},\sigma(\vec{x'},t))\,\mathrm{d}s' - \ell[\Psi(\vec{x},\vec{x'}_-,\sigma_-) + \Psi(\vec{x},\vec{x'}_+,\sigma_+)]\,, \qquad (6.40)$$

where $\ell \equiv U^2/g$, and $\sigma_\pm$ represent the source strengths at the two intersection points, $\vec{x'} = (x'_\pm, 0)$. Based on (6.40) and following the same procedure as in §6.2.2 for submerged bodies, we can show that the unsteady potential in (6.40) decays like $O(t^{-1}, t^{-\frac{3}{2}}e^{i\omega_c t})$ if the surface-piercing body satisfies the geometric condition $\Gamma \neq 0$. Otherwise, the steady state of the original initial-boundary-value problem may not exist.

For surface-piercing bodies, the evaluation of the constant $\Gamma$ as well as the geometric interpretation of the condition $\Gamma \neq 0$ are discussed in detail in §5.3 and thus omitted here.

### 6.3.2 Three-dimensional bodies

The analytical procedure in §6.2.2 can be directly applied to a three-dimensional body. Upon decomposing the source strength $\sigma$ into three components $\bar{\sigma}$, $\tilde{\sigma}$, and $\hat{\sigma}$, the velocity potential can be represented as the sum of their influences:

$$\Phi(\vec{x},t) = \int_{S_B} \bar{\sigma}(\vec{x'})\,\Xi(\vec{x},\vec{x'},q_0)\mathrm{d}s' + \int_{S_B} \tilde{\Xi}(\vec{x},\vec{x'},\tilde{\sigma}(t))\mathrm{d}s' + \int_{S_B} \Xi(\vec{x},\vec{x'},\hat{\sigma}(\vec{x'},t))\mathrm{d}s'\,. \quad (6.41)$$

where $\Xi$ represents the three-dimensional single-source potential (e.g. Wehausen & Laitone 1960). Like that for $\Psi$, the large-time expansion of $\Xi$ can also be obtained by using the method of steepest decent for given source functions. For three source functions used in following analyses, the resutls are presented in appendix B.

After substituting the larg-time expansions of $\Xi(\vec{x},\vec{x'},q_0)$ and $\tilde{\Xi}(\vec{x},\vec{x'},\tilde{\sigma}(t))$, equation (6.41) can be rewritten as:

$$\Phi(\vec{x},t) = \int_{S_B} \bar{\sigma}(\vec{x'})\bar{\mathcal{G}}(\vec{x},\vec{x'})\,\mathrm{d}s' + \int_{S_B} \Xi(\vec{x},\vec{x'},\hat{\sigma}(\vec{x'},t))\,\mathrm{d}s'$$

$$+ \frac{\alpha_1 e^{-i\omega_c t}}{t} e^{\kappa(ix+z)} + \text{c.c.} + O\left(\frac{1}{t^2}, \frac{e^{-i\omega_c t}}{t^2}\right) \qquad \text{as } t \to \infty \qquad (6.42)$$

where the Kochin function $\alpha_1$ is defined by

$$\alpha_1 = \int_{S_B} \left[\mathcal{C}_0 \bar{\sigma}(\vec{x'}) + \bar{\mathcal{W}}(\vec{x'})\right] e^{\kappa(-ix'+z')} \, ds' \, . \qquad (6.43)$$

Based on the integral equation for the unknown source distribution $\hat{\sigma}(\vec{x'}, t)$ and using the large-time expanion of $(\Xi(\vec{x}, \vec{x'}, q_1)$ (in appendix B), we proceed as in §6.2.2 and can show that If $\Gamma \neq 0$, the source strength $\hat{\sigma} = O(t^{-2}, t^{-2}e^{-i\omega_c t})$ and the Kochin function $\alpha_1 = 0$ as $t \to \infty$. In this case, the potential $\Phi$ in (6.42) can be rewritten as:

$$\Phi(\vec{x}, t) = \int_{S_B} \bar{\sigma}(\vec{x'}) \bar{\mathcal{G}}(\vec{x}, \vec{x'}) \, ds' + O\left(\frac{1}{t^2}, \frac{e^{-i\omega_c t}}{t^2}\right) \qquad \text{as } t \to \infty \, . \qquad (6.44)$$

If $\Gamma = 0$, no steady-state solution can be obtained based on linearized theory.

## 6.4 Frequency-domain analyses

In this section, we apply the Fourier method to rederive the solution (§§6.2, 6.3) obtained by the time-domain asymptotic analysis.

With the inverse Fourier transform, we can write the potential $\Phi$ as:

$$\Phi(\vec{x}, t) = \frac{1}{2\pi} \int_0^\infty \phi(\vec{x}, \omega) e^{i\omega t} \, d\omega + \text{c.c.} \qquad (6.45)$$

where $\phi$ is the Fourier transform of $\Phi$. From (6.45), it is clear that the potential $\Phi$ at large time is dominated by the integration in the neighbourhood of the end point $\omega = 0$ and the singularities of $\phi$ on the positive $\omega$-axis.

In order to determine $\phi$, we apply the Fourier operator $\int_0^\infty e^{-i\omega t} \cdots dt$ to the governing equations of the initial-boundary-value problem of $\Phi$ (§6.1). After taking account of initial conditions, a complete boundary-value problem for $\phi$ is obtained, which is identical to the classical seakeeping problem with the body boundary condition given

by

$$\frac{\partial \phi}{\partial n} = n_x U \left[\pi\delta(\omega) + \frac{1}{\mathrm{i}\omega}\right] \qquad \text{on } S_B \tag{6.46}$$

where $\delta(\omega)$ is the dirac delta function. Based on (6.46), we can write $\phi$ as:

$$\phi(\vec{x},\omega) = U\left[\pi\delta(\omega) + \frac{1}{\mathrm{i}\omega}\right]\phi_0(\vec{x},\omega) \tag{6.47}$$

where $\phi_0$ represents the solution with the body forcing $\frac{\partial \phi_0}{\partial n} = n_x$.

For the seakeeping problem, it is known that $\phi_0$ is generally regular except at the critical frequency, $\omega_c = g/4U$, where the single-source solution (Green function) (Haskind 1954; Wehausen & Laitone 1960) is singular. By using a source distribution on the submerged body surface and through systematic asymptotic analyses, in chapter 5, we showed that $\phi_0$ is actually bounded at the critical frequency if the body satisfies the geometric condition $\Gamma \neq 0$. Despite this, the integration in (6.45) near the critical frequency may still dominate the time oscillation of $\Phi$ at large time due to the nonsmoothness of $\phi_0$. By neglecting exponentially small contributions, we can thus rewrite (6.45) as:

$$\Phi(\vec{x},t) = \frac{U}{2\pi}\left\{\int_0^{\epsilon} + \int_{\omega_c-\epsilon}^{\omega_c+\epsilon}\right\}\left[\pi\delta(\omega) + \frac{1}{\mathrm{i}\omega}\right]\phi_0(\vec{x},\omega)\mathrm{e}^{\mathrm{i}\omega t}\,\mathrm{d}\omega + \text{c.c.} \qquad \text{as } t \to \infty \tag{6.48}$$

where $\epsilon$ is a positive small number. To evaluate the integrals in (6.48), it is necessray to have the explicit dependence of $\phi_0$ on the frequency $\omega$.

### 6.4.1 Two-dimensional bodies

For a two-dimensional body satisfying the condition $\Gamma \neq 0$, the asymptotic solution near the critical frequency can be derived according to (5.25) and (5.36). If $\Gamma \neq 0$, we obtain the solution for $\phi_0$ which can be expressed in a symbolic form:

$$\phi_0(\vec{x},\omega) = \frac{f(\vec{x})}{(\omega_c-\omega)^{\frac{1}{2}} + \kappa\Gamma D} + \text{smaller terms} \qquad |\omega-\omega_c| \ll 1 \tag{6.49}$$

where the function $f$ and the constant $D$ are independent of frequency $\omega$. Note that $\phi_0$ is clearly bounded, but its first $\omega$-derivative possesses a square-root singularity at $\omega = \omega_c$.

In order to establish the expansion of $\phi_0$ at low frequency, we first asymptotically expand the wave-source Green function (Haskind 1954) about $\omega = 0$ to obtain:

$$G(\vec{x}, \vec{x'}, \omega) = \bar{G}(\vec{x}, \vec{x'}) + \omega E(\vec{x}, \vec{x'}) + O(\omega^2) \qquad \omega \ll 1 \tag{6.50}$$

where the function $E$ is regular and independent of $\omega$. Based on the source formulation, it can be easily shown that $\phi_0$ must take the similar expansion:

$$\phi_0(\vec{x}, \omega) = \phi_{00}(\vec{x}) + \omega \phi_{01}(\vec{x}) + O(\omega^2) \qquad \omega \ll 1 \tag{6.51}$$

where $\bar{\phi}_{00}$ and $\phi_{01}$ are also independent of $\omega$.

By substituting (6.49) and (6.51) into (6.48) and employing integration by parts and the method of steepest decent, we obtain that if $\Gamma \neq 0$,

$$\Phi(\vec{x}, t) = \frac{U\phi_{00}(\vec{x})}{2} + O\left(\frac{1}{t}\right) + O\left(\frac{e^{-i\omega_c t}}{t^{\frac{3}{2}}}\right) \qquad \text{as } t \to \infty\,. \tag{6.52}$$

Here we note that the unsteady potential in (6.52) decays in the same way as that in (6.38) obtained using the direct time-domain analysis (§6.2).

### 6.4.2 Three-dimensional bodies

For a three-dimensional body, we follow the procedure outlined in §5.5, to derive the solution for $\phi_0$ near the critical frequency. If $\Gamma \neq 0$, we obtain

$$\phi_0(\vec{x}, \omega) = \frac{F(\vec{x}) \ln|\omega - \omega_c|}{\mathcal{D} + \kappa^2 \Gamma \ln|\omega - \omega_c|} + O(|\omega - \omega_c|) + \text{smaller terms} \qquad |\omega - \omega_c| \ll 1 \tag{6.53}$$

where the function $F$ and the constant $\mathcal{D}$ are independent of frequency $\omega$. Clearly, $\phi_0$ is bounded as $\omega \to \omega_c$. As in two dimensions, the expansion of $\phi_0$ at low frequency can be found by expanding the three-dimensional Green function (Wehausen & Laitone

1960) about $\omega = 0$. The result can be expressed in a symbolic form:

$$\phi_0(\vec{x},\omega) = \phi_{00}(\vec{x}) + \omega^2\phi_{01}(\vec{x}) + \text{smaller terms} \qquad \omega \ll 1\,. \tag{6.54}$$

Substituting (6.53) and (6.54) into (6.48) and upon integration by parts, it follows that

$$\Phi(\vec{x},t) = \frac{U\phi_{00}(\vec{x})}{2} + \frac{\mathcal{D}UF(\vec{x})}{i\pi\omega_c}\left(\frac{e^{i\omega_c t}}{t}\right)\int_0^\epsilon \frac{e^{i\varrho t}}{\varrho(\mathcal{D}+\kappa^2\Gamma\ln\varrho)^2}\,d\varrho$$

$$+ \text{c.c.} + O\left(\frac{1}{t^2}, \frac{e^{-i\omega_c t}}{t^2}\right) \qquad \text{as } t\to\infty. \tag{6.55}$$

The use of the method of steepest decent for the integral in (6.55) leads to

$$\Phi(\vec{x},t) = \frac{U\phi_{00}(\vec{x})}{2} + \frac{\mathcal{D}UF(\vec{x})}{\pi\omega_c}\left(\frac{e^{i\omega_c t}}{t}\right)\int_0^\infty \frac{e^{-\varrho t}/\varrho}{[\mathcal{D}+\kappa^2\Gamma(i\pi/2+\ln\varrho)]^2}\,d\varrho$$

$$+ \text{c.c.} + O\left(\frac{1}{t^2}, \frac{e^{-i\omega_c t}}{t^2}\right) \qquad \text{as } t\to\infty. \tag{6.56}$$

The integral in (6.56) is formally similar to Vortela integral which is known to vanish exponetially as $t\to\infty$. Therefore, we can write (6.56) as:

$$\Phi(\vec{x},t) = \frac{U\phi_{00}(\vec{x})}{2} + \frac{\mathcal{D}UF(\vec{x})}{\pi\omega_c}\left(\frac{e^{-\gamma t}}{t}e^{i\omega_c t}\right) + \text{c.c.} + O\left(\frac{1}{t^2}, \frac{e^{-i\omega_c t}}{t^2}\right) \tag{6.57}$$

as $t\to\infty$, where the constant $\gamma \approx e^{-\frac{\mathcal{D}}{\kappa^2\Gamma}}$ determined from $\mathcal{D}+\kappa^2\Gamma\ln\gamma = 0$. We remark that neglecting the exponential decay, the time dependence of $\Phi$ in (6.57) is identical to that in (6.44).

## 6.5 Numerical confirmation

In this section, we confirm our theoretical results through direct long-time numerical simulations in the time domain.

The first problem we consider is that of a two-dimensional submerged circular

cylinder started impulsively from rest to constant forward speed. We solve this linear problem using the spectral method developed in chapter 2, and obtain accurate transient results. For the case of Froude number $F_r = U/\sqrt{gR} = 1$ and submergence $H/R = 2$, figure 6-1 shows the comparison between the numerical result and the fitted asymptotic solution based on the above analysis for the unsteady wave resistance on the body. The behavior of the decaying transient solution is well corroborated. Figure 6-2 shows the time-dependent behavior of the source strength on the body. For simplicity, only the first (circumferential) Fourier mode is plotted. The comparison between theoretical prediction and numerical result is excellent.

As a second problem we consider the unsteady resistance of a surface-piercing three-dimensional body. Specifically, we choose a Wigley hull with a beam-length ratio of $b/a = 0.1$ and a draft-length ratio of $H/a = 0.0625$ at a Froude number of $F_r = U/\sqrt{ga} = 0.15$. The numerical simulation is performed using a time-domain transient Green function method of Lin & Yue (1990). The comparison between the theoretical asymptotic solution and numerical calculation for the time-dependent resistance is shown in figure 6-3. The agreement is again excellent and confirms the $O(t^{-2})$ approach to steady-state resistance.

Finally, we remark that in deriving the large-time transient solution, exponentially-decaying terms are always neglected. Thus, the theoretical prediction of the decay rate becomes apparent only after these exponential-decay terms become smaller than the leading algebraic asymptotes. As shown in (6.57), the exponential decay is controlled by the dimensionless geometric parameter $\kappa^2\Gamma$ for a three-dimensional body. Clearly, the decay is faster for larger values of $\kappa^2\Gamma$. To see the exponential decay, for the Wigley hull, we increase the Froude number to $F_r = U/\sqrt{ga} = 0.3$. This reduces the wave number $\kappa$ and thus slows down the exponential decay. In figure 6-4, we show the transient wave resistance as a function of time. It is seen that the numerical solution matches $O(e^{-.00242\omega_c t}/t)$ very well. In this case, the leading asymptotic algebraic decay $O(t^{-2})$ will overdominate the exponetial-decay effect after about 540 critical wave periods.

## 6.6 Conclusions

The decay behaviour of the transient solution due to an initial acceleration of a body is addressed. For simplicity in analyses, the body is considered to be impulsively started from rest and then move forward with a constant velocity $U$. The initial-boundary-value problem is directly solved in the time domain using a transient free-surface source distribution on the submerged body surface. The linearized body boundary condition is satisfied exactly on the instantaneous position of the moving body. Based on large-time asymptotic expansions of the single-source potentials, the explicit time-dependence of the transient solution is derived. The result is found to depend on the same body-geometric condition which censors the boundedness of the frequency-domain solution of the classical seakeeping problem at the critical frequency $\omega_c = g/4U$. If the body satisfies the requisite geometric condition ($\Gamma \neq 0$), the unsteady resistance on the body decays like $O(t^{-1}, t^{-\frac{3}{2}}e^{i\omega_c t})$ in two dimensions and $O(t^{-2}, t^{-2}e^{i\omega_c t})$ in three dimensions as $t \to \infty$. Otherwise, the steady linear solution may not be reached. As a theoretical verification of the direct time-domain analysis, the same result is rederived by using the Fourier method based on the frequency-domain solution of the general seakeeping problem. For a submerged circular cylinder and a Wigley hull, direct time-domain numerical simulations are carried out to further confirm the analytical predictions.

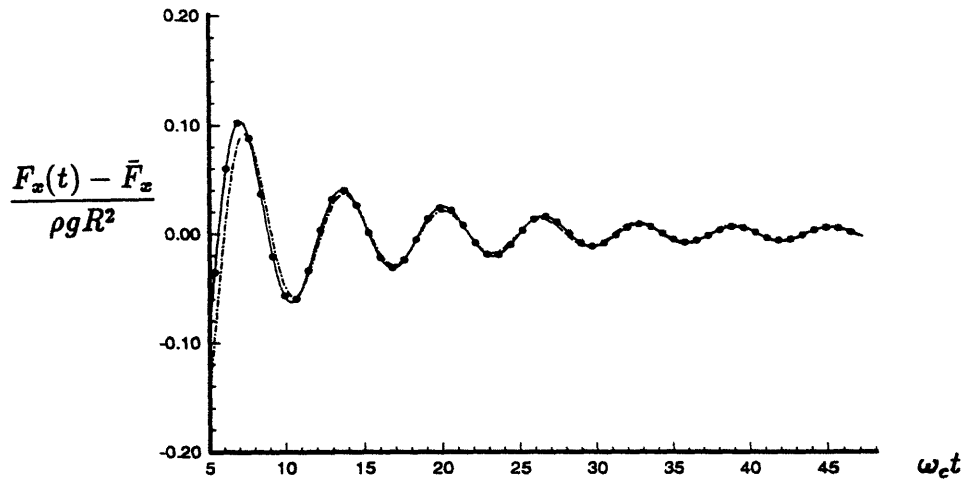


Figure 6-1: Comparison between numerical simulation result (•) and fitted asymptotic solution (— · —) for unsteady wave resistance on the cylinder. ($F_r$=1, $H/R$=2.)

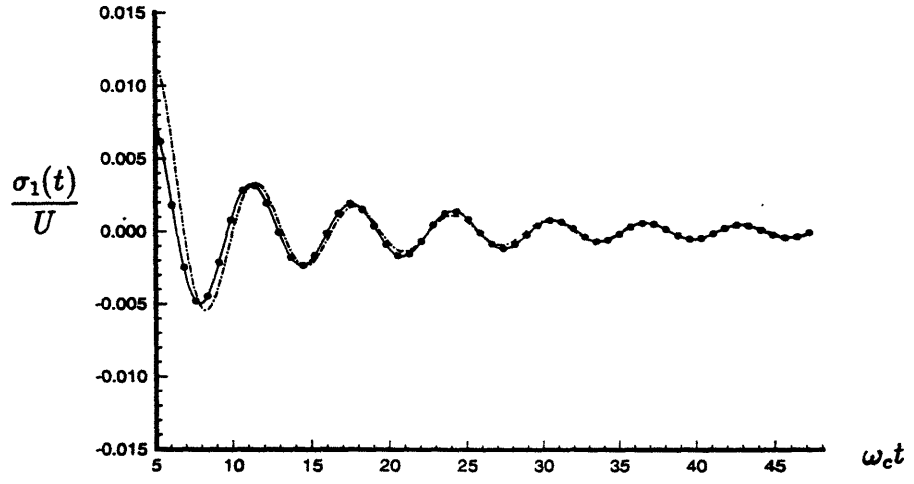


Figure 6-2: Comparison between numerical result (•) and fitted asymptotic solution (— · —) for the first (circumferential) Fourier mode of the source distribution on the cylinder. ($F_r$=1, $H/R$=2.)

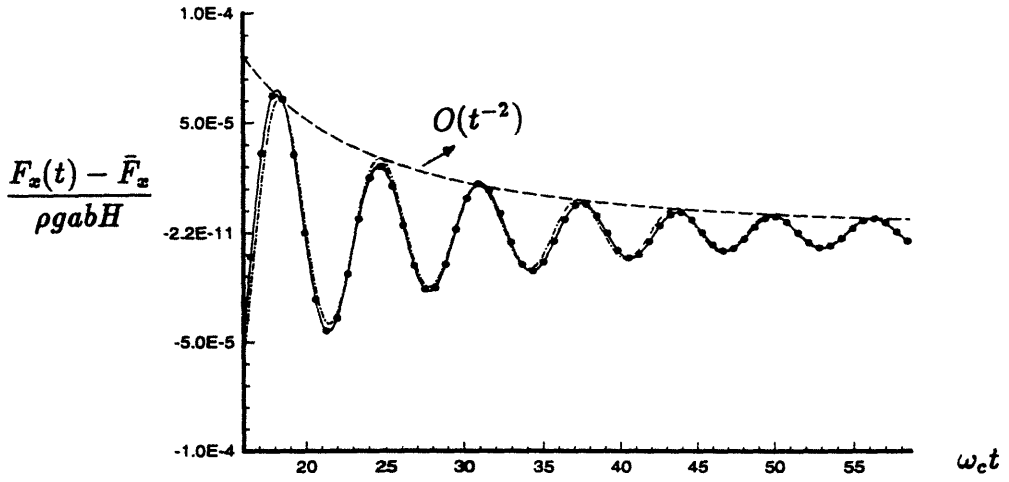


Figure 6-3: Comparison between numerical result (•) and fitted asymptotic solution (— · —) for unsteady wave resistance on the Wigley hull. ($F_r$=0.15, $b/a$=0.1, $H/a$=0.0625.)

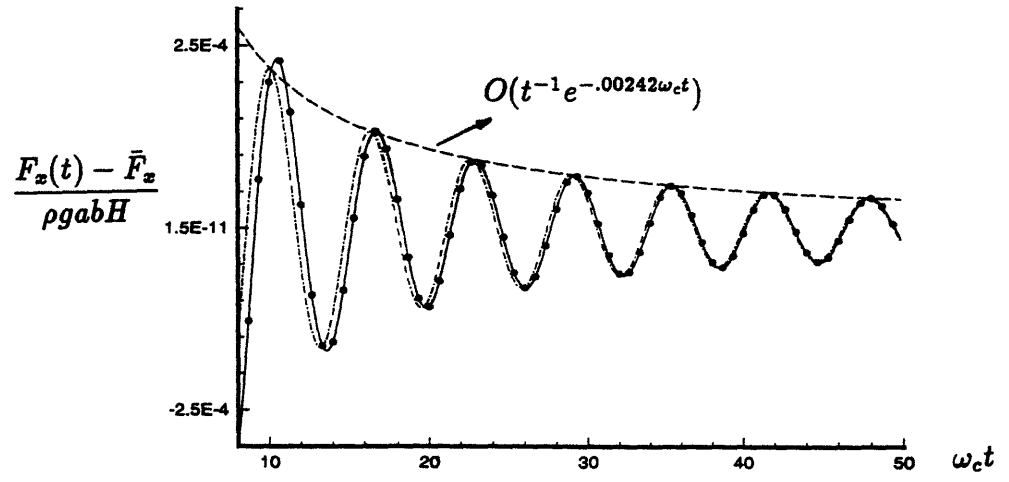


Figure 6-4: Comparison between numerical result (•) and fitted asymptotic solution (— · —) for unsteady wave resistance on the Wigley hull. ($F_r$=0.3, $b/a$=0.1, $H/a$=0.0625.)

# Chapter 7

# Nonlinear motion coefficients near the critical frequency

Having shown that the linear seakeeping solution is bounded at the critical frequency under a simple geometric condition $\Gamma \neq 0$, we next focus on the study of nonlinear solutions in the neighbourhood of $\tau = \frac{1}{4}$. The primary interest is to understand the high-order effects of quadratic and cubic interactions among steady and unsteady surface waves upon body-motion coefficients. As a numerical example, we choose to study nonlinear wave radiation from a submerged circular cylinder in a uniform current using the high-order spectral method.

The linear asymptotic solution (5.52) at $\tau = \frac{1}{4}$ for a submerged circular cylinder shows that the amplitude of the $k_{1,2}$ waves increases exponentially with the body submergence. This implies that coupled interactions of surface waves must play a significant role for the seakeeping solution near the critical frequency for deeply submerged bodies.

On the other hand, the group velocity of the $k_{1,2}$ waves is known to vanish at $\tau = \frac{1}{4}$ according to linearized theory. As a result, the associated wave energy is trapped in the near field of the body. When nonlinear interactions are included, the third-order change in the dispersion relation is generally expected to increase wave radiation through the change of the group velocity. For the case of a single source, this third-order effect has been shown to be critical for obtaining the bounded solution at

the critical frequency (Dagan & Miloh, 1982). For a real physical body, in principle, this nonlinear free-surface effect must also be significant near $\tau = \frac{1}{4}$.

## 7.1 Numerical aspects

We apply the high-order spectral method to study nonlinear wave radiation from a submerged circular cylinder in a uniform current. The body is forced to oscillate periodically in deep water with the frequency near $\tau = \frac{1}{4}$. As initial conditions, the free-surface elevation $\eta(x,0)$ and potential $\Phi^s(x,0)$ are prescribed to be zero. At each time step, the boundary-value problem is solved up to an arbitrary order $M$ in surface wave steepness using the spectral method. With long-time simulations, we obtain steady-state solutions for the radiation force on the body including nonlinear free-surface and body effects. The harmonic components are then extracted via the Fourier transform of steady-state time histories.

In the following, we address several numerical aspects associated with the implementation of the high-order spectral method for the present nonlinear forward speed problem.

### 7.1.1 The base flow

With the high-order spectral method, in principle, any harmonic function can be used for the velocity potential $\bar{\phi}$ of the base flow. In practice, we choose $\bar{\phi}$ to be the leading order solution of the steady problem so that the perturbation potential $\Phi$ can converge rapidly with respect to the order $M$ in computations. For the present study, we use the double-body flow as the base flow. By approximating the circular cylinder with a dipole, we obtain a closed-form solution for $\bar{\phi}$:

$$\begin{aligned}\bar{\phi}(x,z) &= -Ux - \left(\frac{\pi UR^2}{2L}\right)\frac{\sin(\pi x/L)}{\sin^2(\pi x/2L)+\sinh^2[\pi(z+H)/2L]} \\ &\quad - \left(\frac{\pi UR^2}{2L}\right)\frac{\sin(\pi x/L)}{\sin^2(\pi x/2L)+\sinh^2[\pi(z-H)/2L]}\end{aligned} \tag{7.1}$$

where $U$ is the speed of the current, $R$ the radius of the cylinder, $H$ the body submergence, and $2L$ the length of the periodic domain.

### 7.1.2 The body boundary conditions

For heave radiation, the Neumann boundary conditions for perturbation potentials $\Phi^{(m)}$, $m = 1, \cdots, M$, applied on the mean position of the body $\bar{S}_B$ are explicitly given by (cf. 2.12):

$$\Phi_n^{(1)} = -\bar{\phi}_n - \xi_2 \bar{\phi}_{zn} + n_z \frac{d}{dt}\xi_2(t) \,, \tag{7.2}$$

$$\Phi_n^{(m)} = -\frac{\xi_2^m}{m!}\frac{\partial^m}{\partial z^m}\bar{\phi}_n - \sum_{k=1}^{m-1} \frac{\xi_2^k}{k!}\frac{\partial^k}{\partial z^k}\Phi_n^{(m-k)} \,, \quad m = 2, \cdots, M \tag{7.3}$$

where $\xi_2(t)$ denotes the forced heave motion of the body. For sway radiation, the similar boundary conditions can be written as:

$$\Phi_n^{(1)} = -\bar{\phi}_n - \xi_1 \bar{\phi}_{xn} + n_x \frac{d}{dt}\xi_1(t) \,, \tag{7.4}$$

$$\Phi_n^{(m)} = -\frac{\xi_1^m}{m!}\frac{\partial^m}{\partial x^m}\bar{\phi}_n - \sum_{k=1}^{m-1} \frac{\xi_1^k}{k!}\frac{\partial^k}{\partial x^k}\Phi_n^{(m-k)} \,, \quad m = 2, \cdots, M \tag{7.5}$$

where $\xi_1(t)$ is the forced sway motion of the body.

### 7.1.3 Perturbation pressures and radiation forces

Once the boundary-value problem for the potential $\Phi$ is solved up to the specified order $M$, the pressure on the instantaneous body surface, in general, can be obtained from (2.4). To be consistent with the potential calculation, we also expand the pressure in a perturbation series:

$$P(x, z, t) = \sum_{m=1}^{M} P^{(m)}(x, z, t) \,. \tag{7.6}$$

Upon substituting (7.6) and the perturbation expansion of $\Phi$ (2.9) into (2.4) and then expanding (2.4) in Taylor series about the mean body position $\bar{S}_B$, each perturbation

pressure $P^{(m)}$ on the body can be determined in terms of $\Phi^{(m)}$ and the body motion $(\xi_1, \xi_2)$. For heave radiation, we write $P^{(m)}$ evaluated on $\bar{S}_B$ as:

$$\frac{P^{(1)}}{\rho} = -\frac{P_s}{\rho} - \frac{\xi_2}{\rho}(P_s)_z - [\Phi_t^{(1)} + \nabla\bar{\phi}\cdot\nabla\Phi^{(1)}]\,, \tag{7.7}$$

$$\frac{P^{(2)}}{\rho} = -\frac{\xi_2^2}{2\rho}(P_s)_{zz} - \sum_{k=0}^{1}\xi_2^k\frac{\partial^k}{\partial z^k}[\Phi_t^{(2-k)} + \nabla\bar{\phi}\cdot\nabla\Phi^{(2-k)}] - \frac{1}{2}\nabla\Phi^{(1)}\cdot\nabla\Phi^{(1)}\,, \tag{7.8}$$

$$\frac{P^{(3)}}{\rho} = -\frac{\xi_2^3}{6\rho}(P_s)_{zzz} - \sum_{k=0}^{2}\xi_2^k\frac{\partial^k}{\partial z^k}[\Phi_t^{(3-k)} + \nabla\bar{\phi}\cdot\nabla\Phi^{(3-k)}]$$
$$-\nabla\Phi^{(1)}\cdot\nabla\Phi^{(2)} - \frac{\xi_2}{2}(\nabla\Phi^{(1)}\cdot\nabla\Phi^{(1)})_z\,, \tag{7.9}$$

$$\frac{P^{(4)}}{\rho} = -\frac{\xi_2^4}{24\rho}(P_s)_{zzzz} - \sum_{k=0}^{3}\xi_2^k\frac{\partial^k}{\partial z^k}[\Phi_t^{(4-k)} + \nabla\bar{\phi}\cdot\nabla\Phi^{(4-k)}] - \frac{1}{2}\nabla\Phi^{(2)}\cdot\nabla\Phi^{(2)}$$
$$-\nabla\Phi^{(1)}\cdot\nabla\Phi^{(3)} - \frac{\xi_2^2}{4}(\nabla\Phi^{(1)}\cdot\nabla\Phi^{(1)})_{zz} \tag{7.10}$$

where $P_s = \frac{1}{2}(\nabla\bar{\phi}\cdot\nabla\bar{\phi} - U^2)$ depends on the base flow only. Here the solution for $m > 4$ is omitted since the resulting force on the body with $M$ up to 4 is accurate enough for the present study, as demonstrated in §§7.2 and 7.3. For sway radiation, similarly, $P^{(m)}$ can be expressed as:

$$\frac{P^{(1)}}{\rho} = -\frac{P_s}{\rho} - \frac{\xi_1}{\rho}(P_s)_x - [\Phi_t^{(1)} + \nabla\bar{\phi}\cdot\nabla\Phi^{(1)}]\,, \tag{7.11}$$

$$\frac{P^{(2)}}{\rho} = -\frac{\xi_1^2}{2\rho}(P_s)_{xx} - \sum_{k=0}^{1}\xi_1^k\frac{\partial^k}{\partial x^k}[\Phi_t^{(2-k)} + \nabla\bar{\phi}\cdot\nabla\Phi^{(2-k)}] - \frac{1}{2}\nabla\Phi^{(1)}\cdot\nabla\Phi^{(1)}, \tag{7.12}$$

$$\frac{P^{(3)}}{\rho} = -\frac{\xi_1^3}{6\rho}(P_s)_{xxx} - \sum_{k=0}^{2}\xi_1^k\frac{\partial^k}{\partial x^k}[\Phi_t^{(3-k)} + \nabla\bar{\phi}\cdot\nabla\Phi^{(3-k)}]$$
$$-\nabla\Phi^{(1)}\cdot\nabla\Phi^{(2)} - \frac{\xi_1}{2}(\nabla\Phi^{(1)}\cdot\nabla\Phi^{(1)})_x\,, \tag{7.13}$$

$$\frac{P^{(4)}}{\rho} = -\frac{\xi_1^4}{24\rho}(P_s)_{xxxx} - \sum_{k=0}^{3}\xi_1^k\frac{\partial^k}{\partial x^k}[\Phi_t^{(4-k)} + \nabla\bar{\phi}\cdot\nabla\Phi^{(4-k)}] - \frac{1}{2}\nabla\Phi^{(2)}\cdot\nabla\Phi^{(2)}$$
$$-\nabla\Phi^{(1)}\cdot\nabla\Phi^{(3)} - \frac{\xi_1^2}{4}(\nabla\Phi^{(1)}\cdot\nabla\Phi^{(1)})_{xx}\,. \tag{7.14}$$

The instantaneous force on the body can be obtained by integration of the pressure over the body. The harmonic components can be extracted from the steady-state (limit-cycle) time history via the Fourier transform. The conventional added mass

and damping coefficients can be determined from the complex amplitude of the first-harmonic force. For sway oscillation $\xi_1(t) = \xi_x \sin(\omega t)$, for example, the added mass and damping of the body can be calculated by:

$$\left.\begin{aligned} A_{xx} &= 2\Re F_x^{(1)}/\xi_x\omega^2 \,, \qquad A_{zx} = 2\Re F_z^{(1)}/\xi_x\omega^2 \,, \\ B_{xx} &= -2\Im F_x^{(1)}/\xi_x\omega \,, \qquad B_{zx} = -2\Im F_z^{(1)}/\xi_x\omega \,. \end{aligned}\right\} \tag{7.15}$$

where $A_{ij}$ ($B_{ij}$) respresents the added mass (damping) in the $i$-direction due to the body motion in the $j$-direction, and $F_x^{(1)}$ and $F_z^{(1)}$ are corresponding complex amplitudes of the first-harmonic force in the x- and $z$-directions respectively.

### 7.1.4 Evaluation of spatial derivatives of $\Phi^{(m)}$ on the body

For the calculation of body boundary conditions (7.3 and 7.5 ) and perturbation pressures (7.7-7.14), it is necessary to evaluate high spatial derivatives of $\Phi^{(m)}$ accurately. To do that, we transform $(x, z)$-derivatives into cylindrical coordinates $(r, \theta)$ by using chain rules:

$$\frac{\partial}{\partial x} = \cos\theta\frac{\partial}{\partial r} - \sin\theta\frac{\partial}{r\partial\theta} \,, \quad \text{and} \quad \frac{\partial}{\partial z} = \sin\theta\frac{\partial}{\partial r} + \cos\theta\frac{\partial}{r\partial\theta} \,. \tag{7.16}$$

Since $\Phi^{(m)}$ and its $r$-derivatives on the circular cylinder are periodic in $\theta$, their derivatives with respect to $\theta$ can be easily evaluated in the spectral space. Once the first $r$-derivative of $\Phi^{(m)}$ is determined (from the body boundary condition), the second $r$-derivative can be obtained from Laplace's equation:

$$\Phi_{rr}^{(m)} = -\frac{1}{r}\Phi_r^{(m)} - \frac{1}{r^2}\Phi_{\theta\theta}^{(m)} \,, \tag{7.17}$$

and the higher $r$-derivatives follow from the differentiation of (7.17).

### 7.1.5 Enabling long-time simulations

For a computational domain fixed relative to wavelength and body dimensions, the solution in the near field of the body will eventually be distorted due to 'reflections' from the periodic boundaries as the simulation time $T_s$ increases. In general, this error is avoided by successively increasing the length of the periodic domain until the steady-state solution of interest is reached.

For the forward speed problem, however, the steady state is approached very slowly due to the influence of the critical frequency. More seriously, we deal with the seakeeping solution near the critical frequency in the present study. The minimum length of the periodic domain required exceeds the limit allowed by the available computational facilities. In order to obtain steady-state solutions, it is then necessary to develop a procedure which allows for long-time simulations in a fixed computational domain.

To do that, we follow Dommermuth & Yue (1988) and smoothly truncate the free-surface elevation and potential at the longitudinal ends of the computational domain after each time step. Specifically, we multiply $\eta$ and $\Phi^s$ by a tapering function $\Omega(x, \Delta)$ which is equal to one in the middle and smoothly approaches zeros at the ends:

$$\Omega(x,\Delta) = \begin{cases} 1, & |x| < L - \Delta \\ \\ \Pi((|x| - L + \Delta)/\Delta), & L - \Delta \le |x| \le L \end{cases} \tag{7.18}$$

where $\Delta$ measures the width of the tapering region and is a parameter to be chosen. Here the Hermitian polynomial, $\Pi(s)$, $0 \geq s \leq 1$, is defined to be:

$$\Pi(s) = 1 - 462s^6 + 1980s^7 - 3465s^8 + 3080s^9 - 1386s^{10} + 252s^{11} \tag{7.19}$$

where $\Pi(0) = \Pi(1) = 0$, and $(d^k/ds^k)\Pi(0) = (d^k/ds^k)\Pi(1) = 0$ for $k = 1, \cdots, 5$. Note that such smooth tapering function $\Pi(s)$ will not cause Gibb's phenomena. As the numerical tests in §7.2 indicate, this simple tapering procedure is remarkably effective and allows us to carry out very long simulations and obtain steady-state linear and

nonlinear solutions for the radiation force on the body near the critical frequency.

## 7.2 Convergence tests

We need to test the accuracy and convergence of our numerical method with respect to the order $M$, the maximum numbers of body and free-surface modes, $N_B$ and $N_F$. In addition, we also need to determine the tapering parameter $\Delta$ for conducting long-time simulations.

The convergence of numerical time integration is similar to that for the zero speed problem (chapter 3). With the use of fourth-order Runge-Kutta integration scheme, the global error is expected to be $O(\Delta t/T)^4$ provided the boundary-value problem itself is sufficiently accurate. Based on numerical tests in table 3.5 and to be more conservative, we here use $T/\Delta t = 128$ for all of following calculations.

### 7.2.1 Convergence of the boundary-value problem solution

First, we test the high-order solution of the boundary-value problem by considering the steady wave resistance of a submerged circular cylinder at a Froude number of $F_r = U/(gR)^{\frac{1}{2}} = 2.4$. The computational domain is chosen to contain 64 steady wavelengths, i.e., $2L = N_w\lambda_0 = 64\lambda_0$. To minimize the initial disturbance and accelerate the approach of steady states, we multiply the free-surface forcing in (2.8) by a smooth time function, $\tanh(t/3T_c)$, where $T_c$ is the critical wave period. This is equivalent to a smooth start of the body motion in simulations. With this simple procedure, the steady-state solution for wave resistance of the body is reached rapidly after $T_s = 6T_c$.

Table 7.1 shows the convergence of wave resistance of the body with respect to the number of body modes $N_B$ for different order $M$, keeping $N_F$ fixed. Similar to the results at zero forward speed (§3.2), the solution converges to its limit exponentially fast as $N_B$ is increased for any given $M$. For $N_B = 64$, steady resistance of the body shows convergence up to three significant figures.

Similar rapid convergence with respect to the number of free-surface modes $N_F$

| $N_B$ | $M=1$ | $M=2$ | $M=3$ |
|---|---|---|---|
| 32 | 0.2760 | 0.2543 | 0.2527 |
| 64 | 0.2773 | 0.2560 | 0.2540 |
| 128 | 0.2776 | 0.2562 | 0.2538 |

Table 7.1: Convergence of the normalized wave resistance, $|\bar{F}_x|/\rho g R^2$, on a submerged circular cylinder with increasing the number of body modes $N_B$ and order $M$. $F_r$=2.4, $H/R$=4; and $N_w = 64$, $N_F = 32N_w$, $T_c/\Delta t$=128, $T_s = 10T_c$.

| $N_F/N_w$ | $M=1$ | $M=2$ | $M=3$ |
|---|---|---|---|
| 8 | 0.2650 | 0.2460 | 0.2430 |
| 16 | 0.2752 | 0.2545 | 0.2520 |
| 32 | 0.2773 | 0.2560 | 0.2540 |
| 64 | 0.2780 | 0.2563 | 0.2544 |

Table 7.2: Convergence of the normalized wave resistance, $|\bar{F}_x|/\rho g R^2$, on a submerged circular cylinder with increasing the number of free-surface modes $N_F$ and order $M$. $F_r$=2.4, $H/R$=4; and $N_w = 64$, $N_B = 64$, $T_c/\Delta t$=128, $T_s = 10T_c$.

and with order $M$ is displayed in table 7.2. Again, exponential convergence with both $N_F$ and $M$ is achieved. For subsequent computations of wave resistance, we employ $N_w$=64, $N_F/N_w = 32$, $N_B$=64, $T_c/\Delta t = 128$, and $T_s/T_c = 10$. Based on the foregoing numerical tests, we anticipate the maximum error for resistance of the body to be less than 1%.

### 7.2.2 Determination of the tapering parameter $\Delta$

To determine the tapering parameter $\Delta$, we consider sway radiation of a submerged circular cylinder at the critical frequency $\tau = \frac{1}{4}$. For computations, we choose the motion amplitude $\xi_x/R = 0.1$, the submergence $H/R = 2$, and the Froude number $F_r = 1$. For numerical parameters, we use $N_w = 128$ and $N_F/N_w$=16, $N_B = 64$ and $T_c/\Delta t = 128$. Based on convergence tests in tables 7.1 and 7.2, we expect the error of the boundary-value problem solution to be within 5%.

For different values of $\Delta$, we calculate the linear ($M = 1$) first-harmonic force on the body. Table 7.3 shows the results for the horizontal force component at

| $\Delta/\lambda_0$ | $T_s/T_c = 20$ | $T_s/T_c = 30$ | $T_s/T_c = 40$ | $T_s/T_c = 50$ |
|---|---|---|---|---|
| 0.0 | 1.4815 | 1.4970 | 1.5220 | 1.7030 |
| 1.0 | 1.4815 | 1.4970 | 1.5050 | 1.6100 |
| 3.0 | 1.4815 | 1.4971 | 1.5030 | 1.5050 |
| 5.0 | 1.4815 | 1.4971 | 1.5010 | 1.5020 |

Table 7.3: The effect of tapering on the first-harmonic horizontal force, $|F_x^{(1)}|/\rho g \xi_x R$ on a submerged circular cylinder with a forced sway oscillation. $\xi_x/R = 0.1$, $F_\tau = 1.0$, $H/R = 2.0$; and $N_w = 128$, $N_F/N_w = 16$, $N_B = 64$, $T_c/\Delta t = 128$.

different simulation time $T_s$. It is seen that the result without the use of tapering is eventually distorted by the disturbance reflected from the computation boundaries as the simulation time is increased up to $T_s = 40T_c$. On the other hand, the tapered simulations with $\Delta/\lambda_0$=3 and 5 perform quite well and the steady-state solution for the first-harmonic force on the body seems to be achieved when $T_s/T_c = 40 \sim 50$.

Note that for nonlinear computations, in general, the steady state is reached much faster than that in linear simulations, as shown later in figure 7-5. Therefore, the tapering procedure in principle allows for a smaller computational domain. For convenience, we fix the computational domain for both linear and nonlinear calculations and use $N_w = 128$, $\Delta/\lambda_0$=5, $N_F/N_w = 16$, and $N_B = 64$ for all of the following simulations of the wave radiation problem.

## 7.3 Numerical results

Having established the accuracy and convergence of the present method, we apply it to study wave resistance and wave radiation of a submerged circular cylinder in a uniform current, $-U$. Our major concern here is to understand the nonlinear seakeeping solution, particularly near the critical frequency $\tau = \frac{1}{4}$. The primary results include linear and nonlinear solutions for the added mass and damping coefficients as well as wave resistance on the body. The comparisons to theoretical and numerical results are made whenever they are available.

### 7.3.1 Wave resistance

We first study the wave resistance problem. For this problem, there exists an analytic second-order solution obtained by Tuck (1965) who approximated the body with high-order singularities and considered the second-order free-surface effect using the extended Wehausen scheme (Wehausen & Laitone 1960). Due to the second-order free-surface effect, significant nonlinear correction was found for resistance of a circular cylinder at moderate submergence.

We employ the high-order spectral method to solve this problem including nonlinear free-surface effects. The body boundary condition is satisfied exactly. For the submergence $H/R = 4$, we show our linear and nonlinear results for resistance on the body in figure 7-1 as functions of the Froude number, $F_r = U/(gR)^{\frac{1}{2}}$. For comparisons, we reproduce the theoretical solutions of Tuck and also plot them in figure 7-1. Overall, the agreement is very good for both the linear and complete second-order solutions. As noted by Tuck, the high-order correction due to nonlinear free-surface effects is considerable, especially at small Froude numbers. According to regular perturbation theory, linear wave resistance of the body is of first-order in steady wave steepness, while the leading nonlinear correction is of second-order. For this case, the steady wave slope is found to be $k_0 A_0 \approx 0.35$.

Figure 7-2 shows our convergent spectral-method results for the vertical drift force on the body. Similarly, an important high-order correction due to nonlinear free-surface effects is found. Note that the lift force on the body changes its direction from upward to downward as the Froude number increases. Not surprisingly, this phenomenon is associated with the presence of a forward speed.

In general, it is expected that when the body is moved closer to the free surface, steady waves steepen and nonlinear interactions become stronger. For example, our first-order solution ($M = 1$) indicates that when $H/R = 2$, the steady wave steepness $k_0 A_0 \approx 2.0$. For this case, perturbation expansions in both Tuck (1965) and the present method diverge. To obtain reliable prediction of the resistance on the body, a fully nonlinear scheme has to be adopted.

### 7.3.2 Motion coefficients

We now turn to study the problem of wave radiation from a submerged circular cylinder in a uniform current. The body is forced to perform periodic oscillations with the frequency near $\tau = \frac{1}{4}$. The emphasis here is on the understanding of nonlinear solutions for the added mass and damping coefficients near the critical frequency.

It must be noted that in principle, the present method can provide steady-state solutions for both near- and far-field quantities (cf. §3.3) provided that the computational domain is sufficiently large. For the seakeeping problem particularly near the critical frequency, however, this method should be viewed as a near-field scheme since the steady state in far-field is reached very slowly in time-domain simulations. For such a problem, it may not be practical to compute far-field quantities through initial-value simulations. In this study, therefore, we focus on the radiation force on the body only and will not pursue any numerical solution for the wave field.

*Linear solutions*

For the linearized problem, a simple approximate solution for the damping coefficient under deep submergence can be derived by using the far-field formula (Grue & Palm, 1985):

$$B_{xx,zz} = \frac{\rho g}{2\omega \xi_{x,z}^2} \left[ \left( \frac{A_1^2}{k_1} + \frac{A_2^2}{k_2} \right) (1-4\tau)^{\frac{1}{2}} + \left( -\frac{A_3^2}{k_3} + \frac{A_4^2}{k_4} \right) (1+4\tau)^{\frac{1}{2}} \right] \tag{7.20}$$

where $A_{1,2,3,4}$ represents the wave amplitudes corresponding to wavenumbers $k_{1,2,3,4}$. Near $\tau = \frac{1}{4}$, $A_{1,2}$ can be calculated according to our asymptotic solution (5.51). For $\tau$ away from $\frac{1}{4}$, Grue & Palm (1985) obtained:

$$A_{1,2} = \begin{cases} \frac{2\pi (k_{1,2}R)^2 \xi_{x,z}}{(1-4\tau)^{\frac{1}{2}}} \exp(-k_{1,2}H) , & (\tau \leq \frac{1}{4} - \delta^2) ; \\ \\ 0 , & (\tau > \frac{1}{4}) . \end{cases} \tag{7.21}$$

As shown in chapter 5, $A_{3,4}$ are continuous across the critical frequency $\tau = \frac{1}{4}$ and

can be calculated by (Grue & Palm, 1985):

$$A_{3,4} = \frac{2\pi(k_{3,4}R)^2\xi_{x,z}}{(1+4\tau)^{\frac{1}{2}}}\exp(-k_{3,4}H)\,, \quad (0<\tau<\infty)\,. \tag{7.22}$$

As the results shown in figures 7-4, 7-7 and 7-9 indicate, (7.20) together with the use of (5.51), (7.21) and (7.22) for $A_{1,2,3,4}$ gives a fair approximation to the linear damping coefficient for a circular cylinder with moderately deep submergence for $0<\tau<\infty$.

Through rigorous asymptotic analyses in the frequency domain, in chapter 5, we have theoretically shown that the linear solution of the general seakeeping problem at the critical frequency $\tau = \frac{1}{4}$ is always bounded for a submerged body with non-zero volume. Such a finding can actually be further verified by the present initial-value simulations. To do that, we consider sway radiation of a submerged circular cylinder with the submergence $H/R = 2$ at a Froude number of $F_\tau = 1$. For $\xi_x/R = 0.05$, time histories of the linear force ($M = 1$) on the body are shown in figure 7-3. The rapid approach of the steady state after the simulation time $T_s = 10T_c$ indicates that the frequency-domain solution is finite. Due to computational expenses, we are unable to verify the asymptotic solution (5.52) for far-field waves with the present time-domain approach.

For $\tau \neq \frac{1}{4}$, Grue & Palm (1985) numerically solved the integral equation resulting from the application of the boundary-integral equation method in the frequency domain and obtained the linear seakeeping solution for the case of a submerged circular cylinder. To illustrate the efficacy of the present numerical method, we compare our linear solution with their numerical result. For the case of $F_\tau = 0.4$ and $H/R = 3$, the comparison for the sway damping coefficient is shown in figure 7-4 as a function of dimensionless frequency $\tau$, where the approximate solution by (7.20) is also depicted. In general, the agreement between the present solution ($M = 1$) and the numerical result of Grue & Palm (1985) is excellent and thus confirms the validity of the present numerical method. In addition, it is also seen that (7.20) gives a very good approximation in this case.

*Nonlinear solutions*

After understanding the linear solution, we now turn to study the nonlinear problem. Based on a perturbation analysis, it is clear that up to third-order in wave steepness, there are two different interactions which affect the first-harmonic radiation force on the body. One is the quadratic interaction between the steady and unsteady waves which is of second-order. The other is the third-order self-interaction of unsteady waves. To understand the importance of each interaction in the nonlinear solution, we first choose to study sway radiation with parameters $H/R = 6$ and $F_\tau = 0.75$. Under such deep submergence, the steady wave is so small ($k_0 A_0 \approx 0.01$) that its interaction with unsteady waves can be neglected.

Accoding to linearized theory, at the critical frequency $\tau = \frac{1}{4}$, the group velocity of the $k_{1,2}$ waves is known to vanish so that the wave energy associated with these waves is trapped in the region near the body. This implies that the steady-state solution in initial-value simulations is reached very slowly. When nonlinear interactions are included, the third-order change in the dispersion relation makes the group velocity of the $k_{1,2}$ waves different from zero so the radiation of wave energy is increased. As a result, the steady-state nonlinear solution should be approached more rapidly than the linear solution. In figure 7-5, we present time histories of the complex amplitude of the first-harmonic horizontal force on the body oscillating at the critical frequency. The comparisons among numerical results with $M = 1$, 2, and 3 support our expectation that the inclusion of high-order free-surface effects accelerates the approach of steady states in time-domain simulations.

To quantify the influence of self-interactions of unsteady surface waves on wave radiation, we calculate linear and nonlinear solutions for the added mass and damping coefficients at the critical frequency by changing the sway motion amplitude while keeping other parameters fixed. Figure 7-6 shows results for added mass and damping coefficients at $\tau = \frac{1}{4}$ as functions of the body motion amplitdue. Since both normalized linear and nonlinear solutions are independent of the motion amplitude, the nonlinear correction due to cubic self-interactions of unsteady waves is of first-order in wave steepness (or body motion amplitude). This surprising finding can actually be justified by using the nonlinear single-source solution.

By including third-order free-surface nonlinearity, Dagan & Miloh (1982) obtained a nonlinear solution at the critical frequency for a point source. For a source located at $(x', z')$ with a strength of $O(\epsilon)$, the solution of the velocity potential can be formally expressed as: $G_{NL}(x, z; x', z') \sim \epsilon^{\frac{1}{2}} \exp[i\kappa(x - x') + \kappa(z + z')] + O(\epsilon)$. In principle, the nonlinear solution for a physical body can be constructed in terms of a source distribution on the body. Because the leading-order term of $G_{NL}$ has the same space dependence as the singular term of the linear Green's function in (5.12), the analytical procedure in §§5.2 and 5.3 can be applied here to show that for a $O(\epsilon)$ body forcing, the nonlinear seakeeping solution at $\tau = \frac{1}{4}$ is $O(\epsilon)$ for a body satisfying the geometric condition $\Gamma \neq 0$. This is consistent with our numerical results shown in figure 7-6.

Figure 7-7 shows our nonlinear solutions with the order $M$ up to 3 for added mass and damping coefficients in the neighbourhood of $\tau = \frac{1}{4}$. The approximate solution for the damping coefficient based on (7.20) is also plotted there. For both added mass and damping, the linear solutions ($M = 1$) vary sharply near $\tau = \frac{1}{4}$. When nonlinear free-surface and body effects are included, the peaks of added mass and damping are considerably reduced. Such important nonlinear corrections are seen to exist only in a small region near $\tau = \frac{1}{4}$. For $\tau$ away from $\frac{1}{4}$, nonlinear effects are insignificant for this case. Figure 7-8 shows the results for coupling added mass and damping coefficients. Similarly, significant nonlinear free-surface effects are seen near $\tau = \frac{1}{4}$.

To understand the effect of the quadratic interaction between steady and unsteady waves, we change the body submergence to be $H/R = 4$. For this case, the steady wave steepness is found to be $k_0 A_0 \approx 0.2$. Since the second-order wave component generated by this interaction is locked to the steady wave, in general, it does not radiate any wave energy to the far field. In principle, we thus expect that such interaction can influence the added mass only, but not the first-harmonic damping. Figure 7-9 shows our converged numerical results with $M$ up to 3 for added mass and damping coefficients near $\tau = \frac{1}{4}$. In particular, the contribution of the quadratic interaction between steady and unsteady waves is separated from the total nonlinear solution for the added mass and is also presented in figure 7-9. It is seen that this contribution varies very smoothly near $\tau = \frac{1}{4}$. This indicates that the second-order

interaction between steady and unsteady waves does not exert any special effect on the solution near the critical frequency. We also find that such interaction is not important to coupling added mass and damping coefficients, which are presented in figure 7-10.

## 7.4 Conclusions

To elucidate nonlinear seakeeping solution near the critical frequency $\tau = \frac{1}{4}$, we study nonlinear wave radiation of a submerged circular cylinder in a uniform current using an efficient computational method. Through long-time simulations, we obtain nonlinear steady-state (limit-cycle) solution for the radiation force on the body including high-order effects of the free surface and body. Compared to the linear solution, the nonlinear correction due to cubic self-interactions of unsteady waves is shown to be of *first*-order in wave steepness. Such strong nonlinear effect persists only in the neighbourhood of $\tau = \frac{1}{4}$ where the radiation of wave energy is significantly amplified through the change of wave group velocities by free-surface nonlinearity. On the other hand, we find that the quadratic interaction between steady and unsteady waves influences the added mass only, but not the first-harmonic damping.

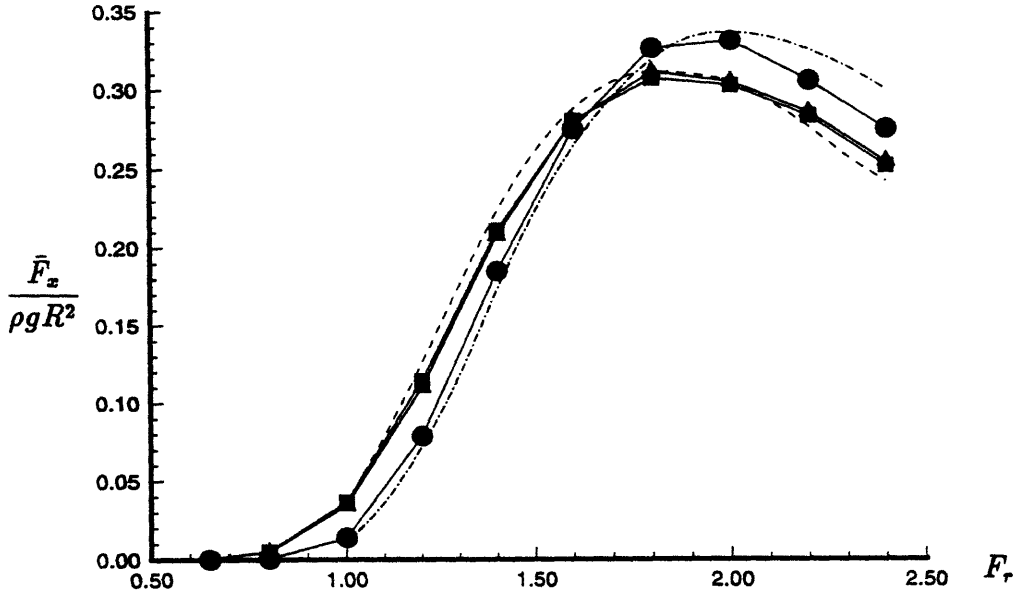


Figure 7-1: Wave resistance on the submerged circular cylinder as a function of the Froude number $F_r = U/(gR)^{\frac{1}{2}}$. Linear (— · —) and complete second-order (- - -) solutions of Tuck (1965), and present numerical results for $M = 1$ (●), $M = 2$ (▲), $M = 3$ (■). $(H/R = 4.)$

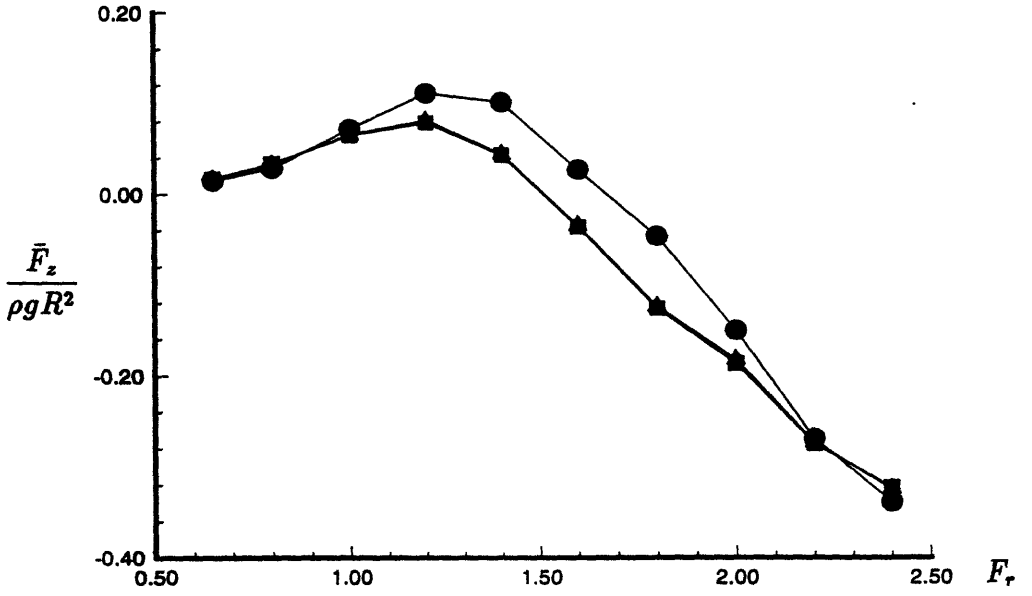


Figure 7-2: Mean vertical force on the submerged circular cylinder as a function of the Froude number $F_r = U/(gR)^{\frac{1}{2}}$. $M = 1$ (●), $M = 2$ (▲), $M = 3$ (■). $(H/R = 4.)$

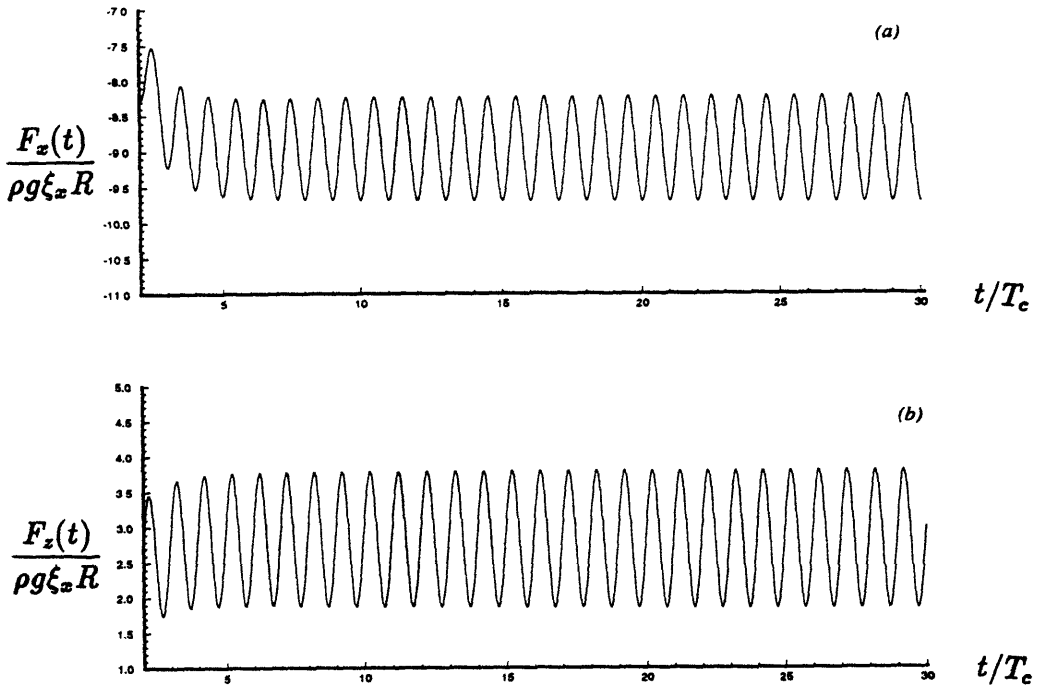


Figure 7-3: Time histories of (a) horizontal and (b) vertical forces on the submerged circular cylinder under sway oscillation. ($H/R = 2.$, $F_r = 1.0$, $\xi_x/R = 0.05$)

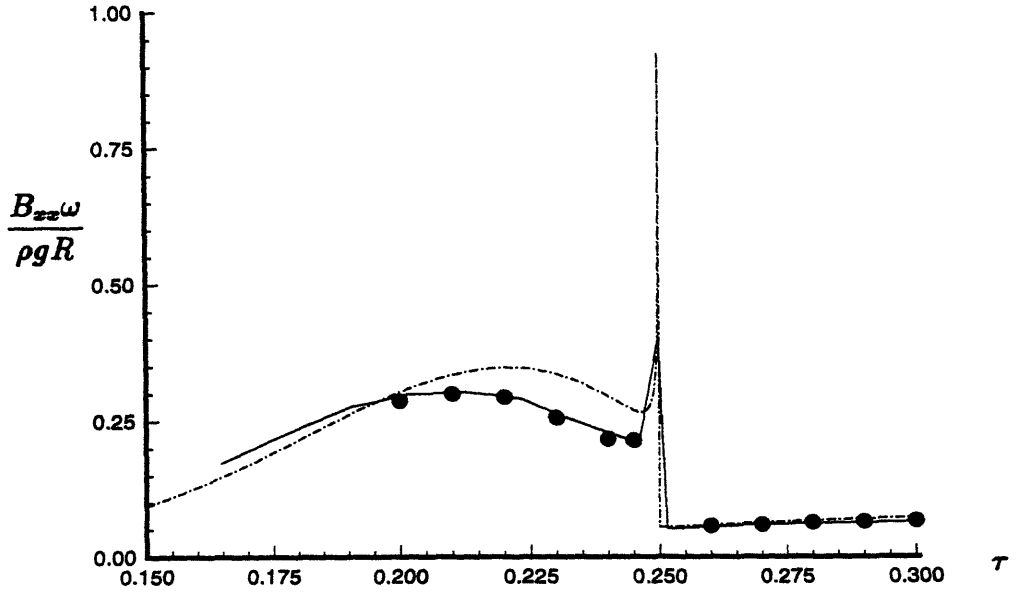


Figure 7-4: Sway damping coefficient as a function of the dimensionless frequency $\tau$. Linear solution of Grue & Palm (1985) (——), approximate solution by (7.20) (— · —), and present numerical result $M = 1$ (●). ($H/R = 3.$, $F_r = 0.4$)

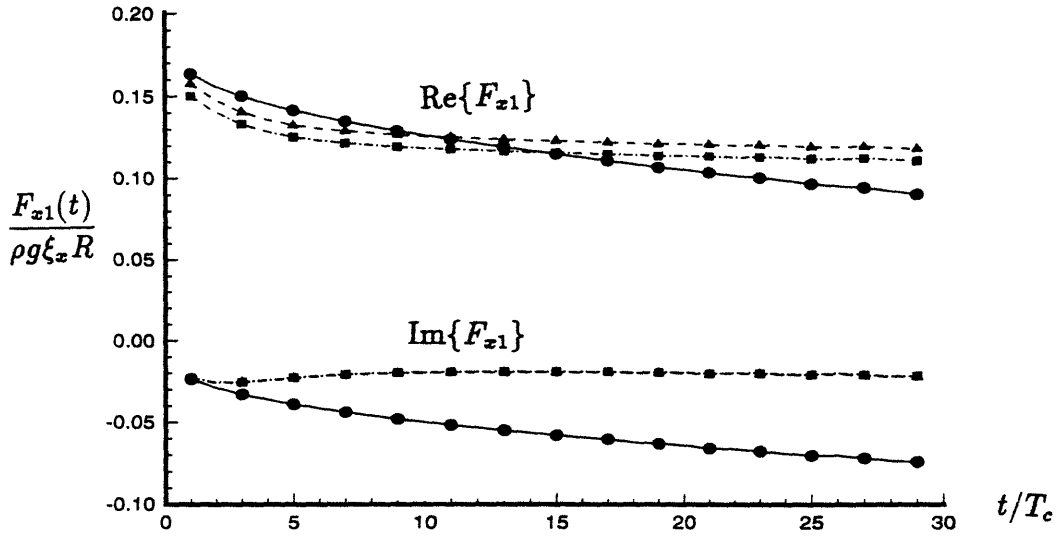


Figure 7-5: Time histories of the complex amplitude of the first-harmonic horizontal force on the submerged circular cylinder. $M = 1$ (●), $M = 2$ (▲), and $M = 3$ (■). $(H/R = 6.,\ F_\tau = 0.75,\ \xi_x/R = 0.075,\ \tau = \frac{1}{4})$

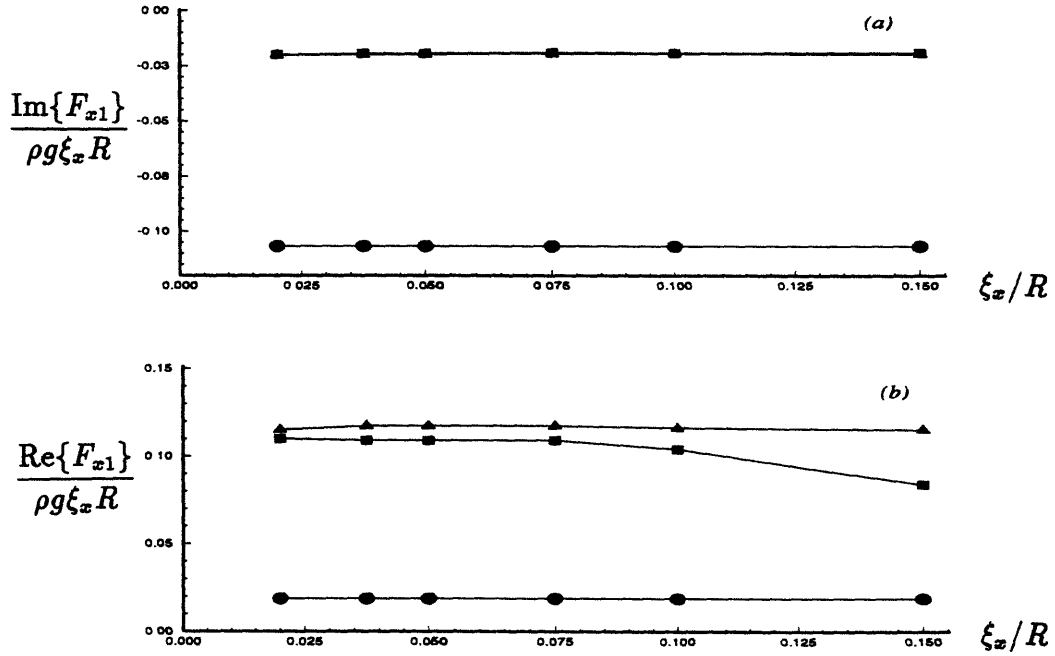


Figure 7-6: (a) Added mass and (b) damping coefficients at the critical frequency $\tau = \frac{1}{4}$ as functions of the body motion. $M = 1$ (●), $M = 2$ (▲), and $M = 3$ (■). $(H/R = 6.,\ F_\tau = 0.75)$

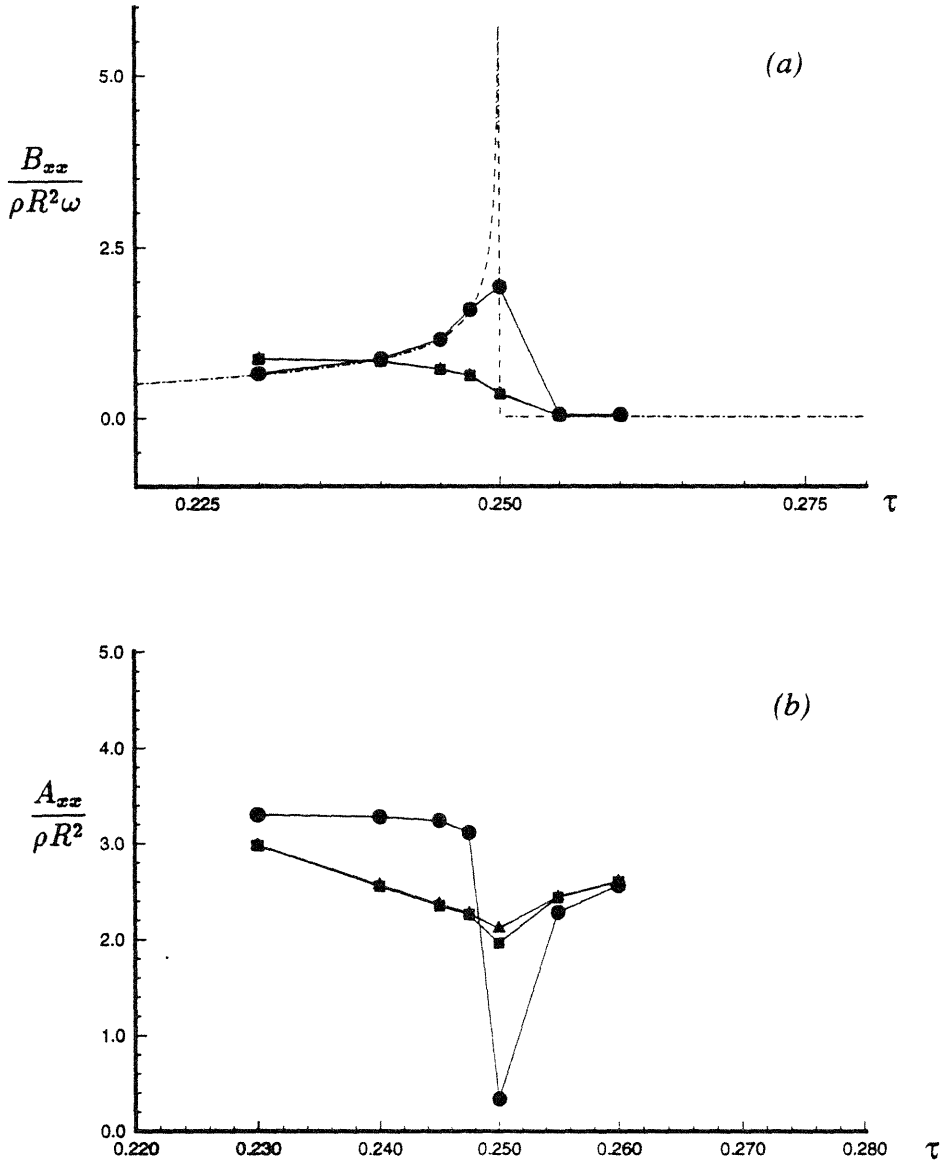


Figure 7-7: (a) Damping and (b) added mass coefficients $B_{xx}$ and $A_{xx}$ as functions of $\tau$. Approximate solution by (7.20) (— · —) and present numerical results for $M = 1$ (●), $M = 2$ (▲), $M = 3$ (■). ($H/R = 6.$, $F_r = 0.75$, $\xi_x/R = 0.05$)

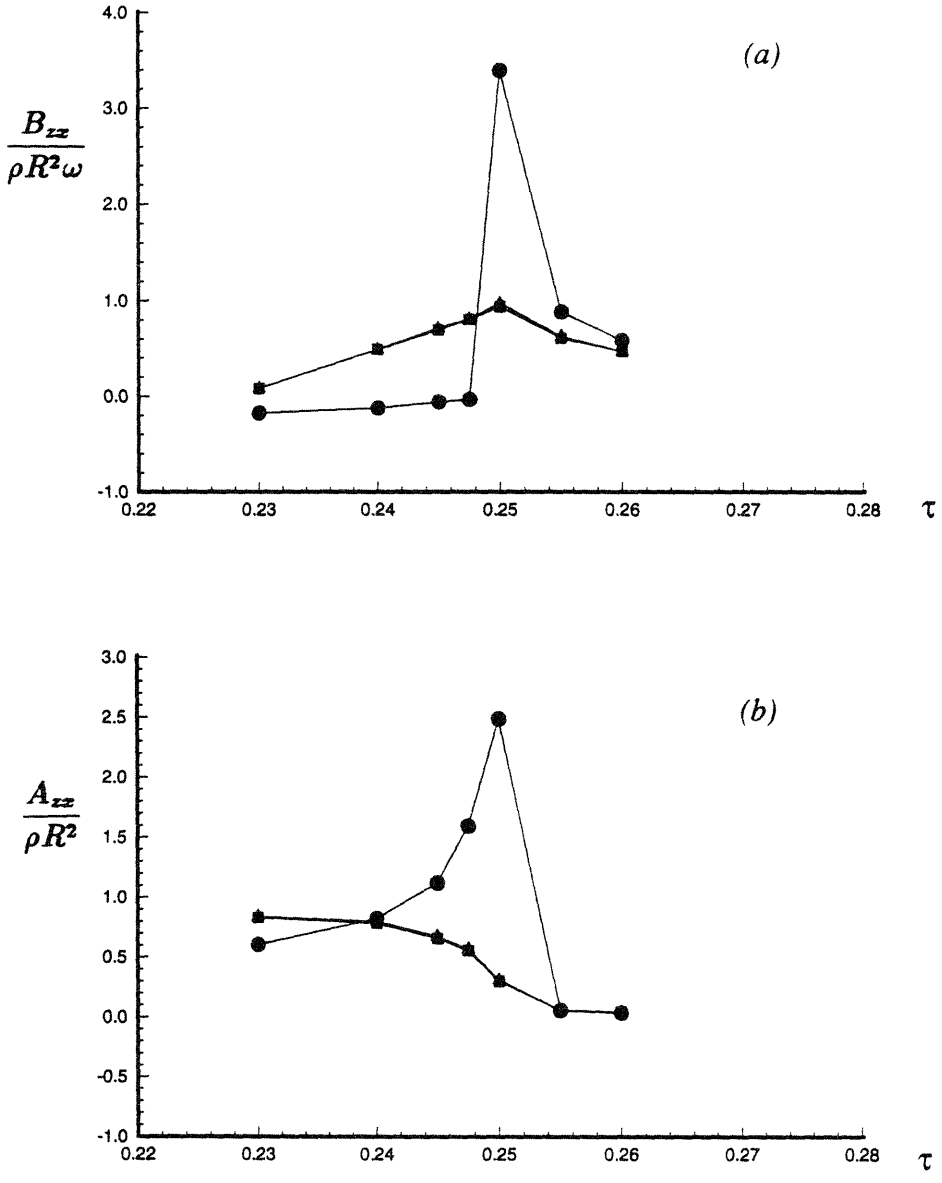


Figure 7-8: (a) Damping and (b) added mass coefficients $B_{zz}$ and $A_{zz}$ as functions of $\tau$. $M = 1$ (●), $M = 2$ (▲), and $M = 3$ (■). ($H/R = 6.$, $F_r = 0.75$, $\xi_x/R = 0.05$)

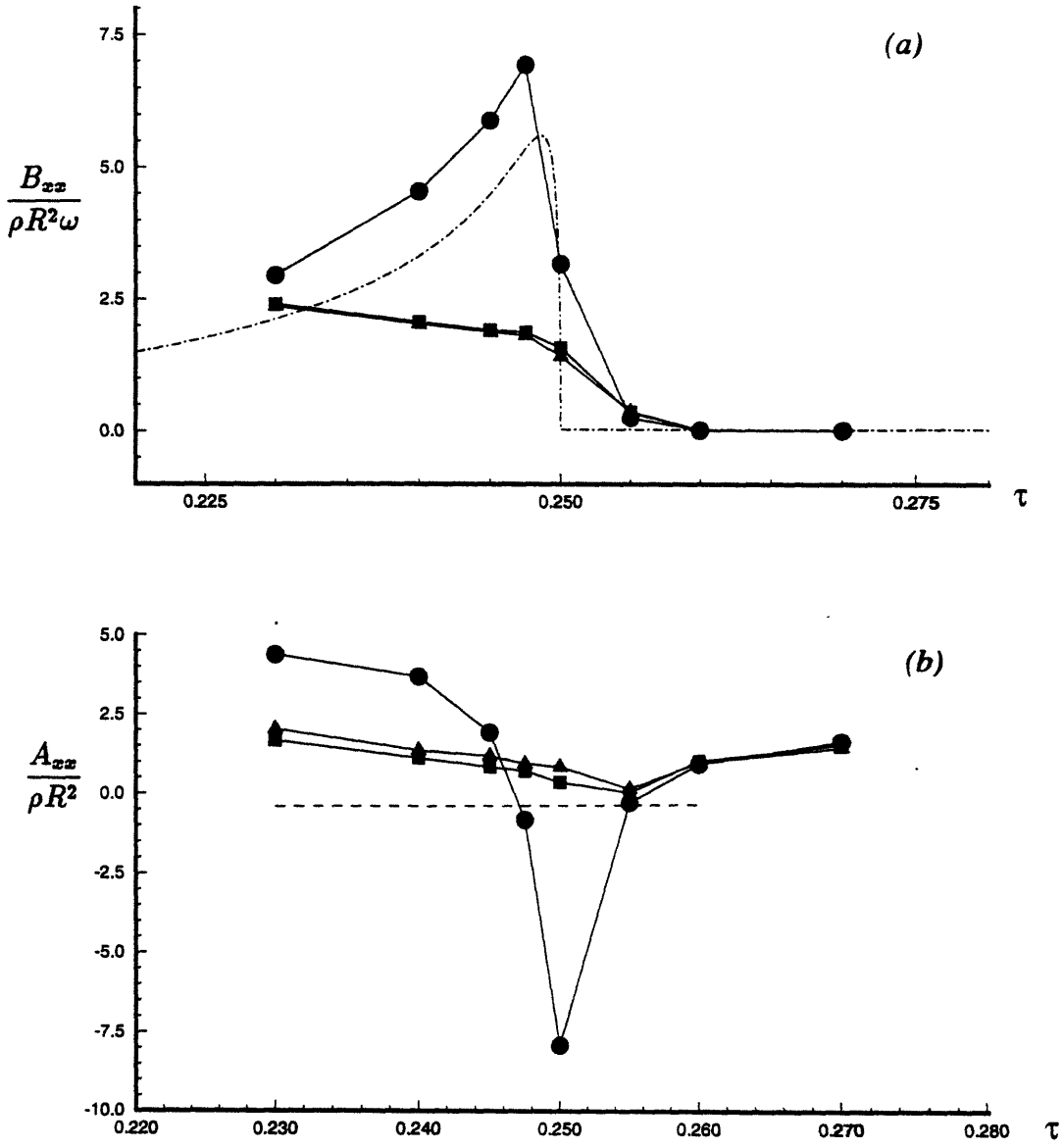


Figure 7-9: (a) Damping and (b) added mass coefficients $B_{xx}$ and $A_{xx}$ as functions of $\tau$. Approximate solution based on (7.20) (— · —) and present numerical results for $M = 1$ (●), $M = 2$ (▲), and $M = 3$ (■). ($H/R = 4.$, $F_\tau = 0.75$, $\xi_x/R = 0.05$)

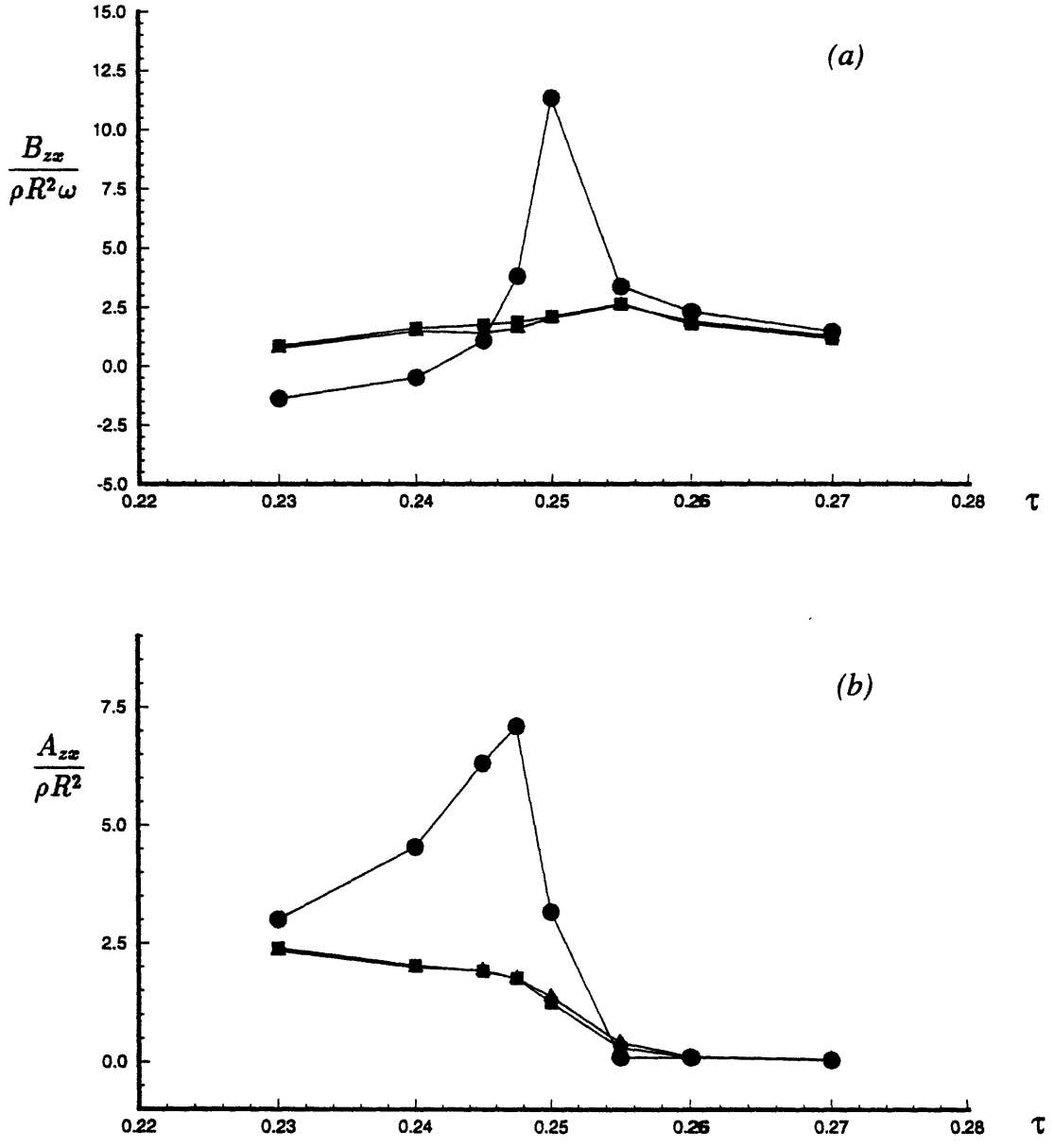


Figure 7-10: (a) Damping and added mass coefficients $B_{zz}$ and $A_{zz}$ as functions of $\tau$. $M = 1$ (●), $M = 2$ (▲), $M = 3$ (■). ($H/R = 4.$, $F_\tau = 0.75$, $\xi_z/R = 0.05$)

# Chapter 8

# Resonant reflection of surface waves traveling over bottom undulations

In this chapter, we develop an efficient computational method to investigate nonlinear resonant reflection of surface waves by an undulated bottom topography. Specifically, we extend the study of the Bragg scattering problem by including nonlinear boundary effects of both the free surface and bottom. The major objective here is to understand and quantify the effect of higher-order Bragg resonances on wave propagations over bottom undulations. This study has significant implications in the prediction of the spectrum of ocean waves in coastal zones and the protection of beaches.

The resonant reflection of surface waves by patches of bottom undulations has been extensively studied recently, owing to its importance in the development of shore-parallel bars. A straightforward perturbation analysis shows that large resonant reflection occurs under a Bragg condition, namely when the bottom undulation has a wavelength half that of the incident waves (Davies 1982). Laboratory experiments of Davies & Heathershaw (1984) confirm this prediction and suggest a possible practical application of this mechanism for the protection of beaches. For mild incident wave and bottom slopes, reflection at or near Bragg resonance is well predicted by perturbation theory based on multiple scales and the assumption of linearized surface

waves (Mei 1985). For small surface waves, this Bragg reflecton can also be predicted by using the boundary-integral-equation method (BIEM) (Dalymple & Kirby 1986) and Miles' (1967) successive-application-matrix model (SAMM) (Guazelli *et al.* 1992; O'Hare & Davies 1993). A notable drawback with these numerical schemes employing direct discretization of bottom surface is that free-surface nonlinearity cannot be accounted for and extension to a two-dimensional bottom topography is difficult and probably infeasible in practice. Based on the extended-mild-slope equation, Kirby (1986) included free-surface nonlinearity and found no significant nonlinear effect on the magnitude of Bragg resonant reflection for steep incident waves. However, the occurrence of higher-order Bragg resonances was not studied.

For moderate to large wave and/or bottom steepnesses, it is generally expected that higher-order Bragg resonance must also occur due to nonlinear interactions between surface waves and bottom undulations. For a bottom containing unidirectional doubly-sinusoidal ripples, significant Bragg reflection corresponding to differences of the bottom ripple wavenumbers is observed in experiments even for small undulation amplitudes (Guazzelli *et al.* 1992). This second-order Bragg resonant reflection can be comparable in magnitude (although not at the same frequency) to that due to linear Bragg effect. Since this phenomenon is a result of higher-order bottom nonlinear effects, in principle, it can be predicted by the BIEM and SAMM, but *not* the theory of Mei (1985).

When nonlinear free-surface effects are included, second-order Bragg resonance corresponding to sums or differences of incident wave frequencies can also exist in principle. The simplest case for such high-order Bragg resonance is when a single incident wave travels over a horizontal bottom with uniformly-sinusoidal ripples. By considering quartet interactions between surface waves and bottom ripples (with the incident wave counted twice), a free superharmonic (double-frequency) wave is generated and reflected. Despite its obvious importance in the development of the spectrum of ocean waves, this nonlinear Bragg phenomenon has not been addressed yet.

In this chapter, we extend the high-order spectral method to study nonlinear wave interactions with bottom ripples. In contrast to existing theories and numer-

ical schemes such as BIEM and SAMM, the present method is able to account for both free-surface and bottom nonlinearities up to an arbitrary order $M$ in surface wave and/or bottom steepness. Upon using spectral expansions for the solution, the method retains exponential convergence with respect to the number of spectral modes $N$. Significantly, with the use of fast transform techniques, the computational effort per time step is linearly proportional to $M$ and $N$. Moreover, the present method can be directly applied to study general three-dimensional wave-bottom problems.

This powerful method is used here to investigate nonlinear resonant reflection of surface waves by patches of bottom undulations. For both normal and oblique incidences, our efficient and high-resolution computations confirm existing theoretical and experimental results. Furthermore, we are able to examine the effect of second-order Bragg resonances due to both free-surface and bottom nonlinearities. For waves propagating over a horizontal bottom containing uniformly sinusoidal undulations, in particular, we obtain accurate prediction for the resonant superharmonic waves. For moderate surface wave and/or bottom slopes, the present numerical result compares well with the analytical prediction based on regular perturbation expansions.

## 8.1 Mathematical formulation

We consider surface wave propagation over a rippled bottom $z = -h + \zeta(\mathbf{x})$ with constant mean water depth $h$. Under the usual assumption of potential flow, the boundary-value problem for the velocity potential $\Phi(\mathbf{x}, z, t)$ consists of Laplace's equation within the fluid, no flux condition on the bottom,

$$\Phi_z(\mathbf{x}, z, t) = \nabla_{\mathbf{x}}\zeta \cdot \nabla_{\mathbf{x}}\Phi \,, \qquad \text{on} \qquad z = -h + \zeta(\mathbf{x}) \,, \tag{8.1}$$

and nonlinear kinematic and dynamic boundary conditions on the free surface. For initial conditions, the free surface elevation $\eta(\mathbf{x}, 0)$ and velocity potential $\Phi(\mathbf{x}, z, 0)$ are prescribed.

For simplicity, we ignore the current effect. Then the free surface boundary con-

ditions (2.8) reduce to:

$$\left.\begin{aligned} &\eta_t + \nabla_{\mathbf{x}}\eta \cdot \nabla_{\mathbf{x}}\Phi^s - (1 + \nabla_{\mathbf{x}}\eta \cdot \nabla_{\mathbf{x}}\eta)\Phi_z(\mathbf{x},\eta,t) = 0 \ , \\ &\Phi^s_t + g\eta + \tfrac{1}{2}\nabla_{\mathbf{x}}\Phi^s \cdot \nabla_{\mathbf{x}}\Phi^s - \tfrac{1}{2}(1 + \nabla_{\mathbf{x}}\eta \cdot \nabla_{\mathbf{x}}\eta)\Phi^2_z(\mathbf{x},\eta,t) = 0 \ . \end{aligned}\right\} \tag{8.2}$$

In a typical initial-value solution scheme, these nonlinear equations are used as evolution equations for $\eta$ and $\Phi^S$ with the surface vertical velocity $\Phi_z(\mathbf{x},\eta,t)$ obtained from the boundary-value problem.

To solve the boundary-value problem, we consider regular perturbation expansions in both the bottom undulation $\zeta(\mathbf{x})$ and the instantaneous free surface $\eta(\mathbf{x},t)$ simultaneously. For simplicity (and without loss of generality), we assume that $\epsilon \ll 1$ measures both the bottom and free-surface wave slopes. Our intention is to solve the problem to arbitrary high order $M$ in $\epsilon$ using the spectral method. To do that, we first write the potential $\Phi$ in a perturbation series up to order $M$, (2.9). In order to find the free-surface and bottom boundary conditions for each perturbation potential $\Phi^{(m)}$, we expand the bottom boundary condition (8.1) and the surface potential $\Phi^S$ in separate Taylor series with respect to the mean surfaces $z = -h$ and 0 respectively. Collecting terms at the respective orders, we finally obtain a sequence of Neumann boundary conditions on $z = -h$:

$$\Phi^{(1)}_z(\mathbf{x},-h,t) = 0,$$

$$\begin{aligned} \Phi^{(m)}_z(\mathbf{x},-h,t) = \sum_{\ell=1}^{m-1} \Bigg\{ &\left[\frac{\zeta^\ell}{\ell!}\frac{\partial^{(\ell-1)}}{\partial z^{(\ell-1)}}\Phi^{(m-\ell)}_x(\mathbf{x},-h,t)\right]_x \\ &+ \left[\frac{\zeta^\ell}{\ell!}\frac{\partial^{(\ell-1)}}{\partial z^{(\ell-1)}}\Phi^{(m-\ell)}_y(\mathbf{x},-h,t)\right]_y \Bigg\}, \quad m = 2,3,\ldots,M \ ; \end{aligned} \tag{8.3}$$

and a sequence of Dirichlet boundary conditions (2.11) on $z = 0$.

At each order $m$, $\Phi^{(m)}$ satisfies Laplace's equation in the mean fluid domain $-h < z < 0$, the Neumann boundary condition (8.3) on $z = -h$, and the Dirichlet boundary condition (2.11) on $z = 0$. In a spectral approach, we represent $\Phi^{(m)}$ in terms of

global basis functions which satisfy the field equation and the homogeneous surface and bottom conditions. To accomplish this, we follow Dommermuth & Yue (1987b) and write $\Phi^{(m)} = \alpha^{(m)} + \beta^{(m)}$, where

$$\alpha^{(m)}(\mathbf{x}, z, t) = \sum_{n=0}^{\infty} \alpha_n^{(m)}(t) \frac{\cosh[|\mathbf{k}_n|(z+h)]}{\cosh(|\mathbf{k}_n|h)} e^{i\mathbf{k}_n \cdot \mathbf{x}} + \text{c.c.}\,, \tag{8.4}$$

$$\beta^{(m)}(\mathbf{x}, z, t) = \beta_0^{(m)} z + \sum_{n=1}^{\infty} \beta_n^{(m)}(t) \frac{\sinh(|\mathbf{k}_n|z)}{|\mathbf{k}_n| \cosh(|\mathbf{k}_n|h)} e^{i\mathbf{k}_n \cdot \mathbf{x}} + \text{c.c.}\,. \tag{8.5}$$

Here, $\mathbf{k}_n = (k_x, k_y)$ is the wavenumber vector, and the summation in $n$ implies summing over all integer values of $k_x$ and $k_y$. In the above, $\alpha^{(m)}$ and $\beta^{(m)}$ respectively satisfy zero Neumann condition on $z = -h$ and zero Dirichlet condition on $z = 0$. The amplitudes of the orthogonal spectral modes, $\alpha_n^{(m)}$ and $\beta_n^{(m)}$, are then determined by taking the inner product of $e^{i\mathbf{k}_n \cdot \mathbf{x}}$ with (2.11) and (8.3) respectively. For smooth (periodic) $\Phi^{(m)}$, $\alpha_n^{(m)}$ and $\beta_n^{(m)}$ decay exponentially with increasing wavenumber $\mathbf{k}_n$.

After the boundary-value problems for $\Phi^{(m)}$ are solved sequentially up to the desired order $M$, the vertical velocity on the free surface can then be determined from (2.15). The overall problem is integrated in time via (8.2) starting from initial conditions.

## 8.2 Conditions for Bragg resonances

If assuming harmonic time dependence, the present problem can be formulated as a boundary-value problem for the amplitude of the velocity potential. For small surface wave and/or bottom slopes, this boundary-value problem can then be solved using regular perturbation expansions. At certain wavenumber combinations of surface waves and bottom ripples, the boundary-value problem becomes degenerate and so-called Bragg resonances occur.

The condition for leading-order Bragg resonance is simple and well known (Davis 1982, Mei 1985), while those for higher-order Bragg resonances are relatively complex and have not been systematically discussed yet. In the following, we derive higher-order Bragg conditions through the relation to those for nonlinear wave resonances

in a multiple-wave dynamic system. To be complete, the linear Bragg condition is rederived here.

*Class I Bragg condition*

Let two surface waves with wavenumbers $\mathbf{k}_1$ and $\mathbf{k}_2$ propagate on a rippled horizontal bottom with wavenumber $\mathbf{k}_r$. The general condition for resonance due to quadratic interactions between the surface waves and the bottom is (Mei 1985):

$$\mathbf{k}_1 \pm \mathbf{k}_2 \pm \mathbf{k}_r = 0 \qquad \text{and} \qquad \omega_1 \pm \omega_2 = 0 \tag{8.6}$$

where $\omega_i$ denotes the frequency corresponding to $\mathbf{k}_i$. For propagating waves, wavenumber $\mathbf{k}_i$ and frequency $\omega_i$ need to satisfy the dispersion relation

$$\omega_i^2 = g|\mathbf{k}_i| \tanh |\mathbf{k}_i| h \qquad (i = 1, 2)\,. \tag{8.7}$$

An apparent combination of $\mathbf{k}_1$, $\mathbf{k}_2$, and $\mathbf{k}_r$ for (8.6) to be satisfied is

$$\mathbf{k}_1 = -\mathbf{k}_2 = \frac{\mathbf{k}_r}{2} \tag{8.8}$$

which is the well-known condition for linear Bragg resonance (Davies 1982). In order to distinguish from those for higher-order Bragg resonances, we call (8.8) class I Bragg condition.

*Class II Bragg condition*

For a bottom containing doubly-sinusoidal undulations with wavenumbers $\mathbf{k}_{r1}$ and $\mathbf{k}_{r2}$, the condition for quartet resonance between the surface waves and bottom undulations reduces to

$$\mathbf{k}_1 \pm \mathbf{k}_2 \pm \mathbf{k}_{r1} \pm \mathbf{k}_{r2} = 0 \qquad \text{and} \qquad \omega_1 \pm \omega_2 = 0 \tag{8.9}$$

where $\mathbf{k}_1$ and $\mathbf{k}_2$ satisfy the dispersion relation (8.7). It is straightforward to verify

that one simple solution to (8.9) is:

$$\mathbf{k}_1 = -\mathbf{k}_2 = \frac{\mathbf{k}_{r1} \pm \mathbf{k}_{r2}}{2} \tag{8.10}$$

which is the (linear) Bragg condition corresponding to the sum or difference of bottom wavenumbers (Guazelli 1992). We call (8.10) class II Bragg condition.

*Class III Bragg condition*

For three surface waves traveling over a horizontal bottom containing uniformly-sinusoidal ripples, the general condition for quartet resonance is:

$$\mathbf{k}_1 \pm \mathbf{k}_2 \pm \mathbf{k}_3 \pm \mathbf{k}_r = 0 \qquad \text{and} \qquad \omega_1 \pm \omega_2 \pm \omega_3 = 0 \,. \tag{8.11}$$

Here wavenumber $\mathbf{k}_3$ and frequency $\omega_3$ must also satisfy the dispersion relation in (8.7). The simplest possible case for this resonance is when $\mathbf{k}_2 = \mathbf{k}_3$. From (8.11), we then have:

$$\mathbf{k}_1 = \pm 2\mathbf{k}_2 \pm \mathbf{k}_r \qquad \text{and} \qquad \omega_1 = \pm 2\omega_2 \,. \tag{8.12}$$

After imposing the dispersion relation to $\mathbf{k}_1$ and $\omega_1$, it follows that

$$4|\mathbf{k}_2| \tanh |\mathbf{k}_2|h = |2\mathbf{k}_2 \pm \mathbf{k}_r| \tanh |2\mathbf{k}_2 \pm \mathbf{k}_r|h \,. \tag{8.13}$$

This resonance condition is new for wave/bottom interactions and called class III Bragg condition. Given any one of $\mathbf{k}_1$, $\mathbf{k}_2$ and $\mathbf{k}_r$, the other two can be determined from (8.12) and (8.13) so that they form a resonant quartet system (with $\mathbf{k}_2$ counted twice).

We remark that in nonlinear wave dynamics, it is well known that quartet resonance does not exist for one-dimensional waves traveling over a flat bottom. If one of surface waves is replaced by bottom ripples, however, we here find that quartet resonance indeed can occur. As shown in §§8.4.4 and 8.5.3, this high-order Bragg resonance can cause significant superharmonic wave reflection by patches of parallel bottom undulations.

## 8.3 Numerical method

### 8.3.1 Implementation

The implementation of the nonlinear spectral method for wave reflection by an undulated bottom is slightly different from that for nonlinear wave-body interactions. The numerical procedure for a problem using $N$ wave modes and retaining nonlinearities up to a specified order $M$ consists of two major parts:

(a) Given the surface elevation $\eta(\mathbf{x},t)$ and potential $\Phi^s(\mathbf{x},t)$ on that surface at some instant of time $t$, the modal amplitudes $\alpha_n^{(m)}$ and $\beta_n^{(m)}$ subject to the Dirichlet condition (2.11) and the Neumann condition (8.3) are solved using a pseudospectral method. Specifically, all spatial derivatives of $\Phi^{(m)}$, $\Phi^s$ and $\eta$ are evaluated in wavenumber space while nonlinear products are calculated in physical space at a discrete set of points $\mathbf{x}_j$. For periodic boundary conditions where the eigenfunctions expansions are represented in Fourier series (8.4 and 8.5), $\mathbf{x}_j$ are equally spaced and fast-Fourier transforms are used to project between the wavenumber and physical domains. At each order, (2.11) and (8.3) are solved in wavenumber space by equating Fourier modes, and the number of operations required is $O(N \ln N)$. For perturbations up to order $M$, the operation count is then $O(MN \ln N)$ per time step.

(b) The evolution equations (8.2) are then integrated in time to obtain the new values $\eta(\mathbf{x},t+\Delta t)$ and $\Phi^s(\mathbf{x},t+\Delta t)$. For the present computations, we use a fourth-order Runge-Kutta integrator with constant time step $\Delta t$.

The two steps (a)-(b) is repeated starting from initial conditions.

### 8.3.2 Convergence tests

To test the accuracy and convergence of the present method, we consider the wave reflection by a patch of uniformly sinusoidal bottom undulations. For numerical calculations, we choose a rippled horizontal bottom with a bed length of $L_0 = 20\pi/k_r$, a bottom slope of $k_r d = 0.31$, and a mean water depth of $h = 6.25d$, where $d$ represents the (bottom) ripple amplitude. As initial conditions, the solution of exact Stoke's

| $N_w$ | $M=2$ | $M=3$ | $M=4$ |
|---|---|---|---|
| 16 | 0.7250 | 0.7080 | 0.7080 |
| 24 | 0.7115 | 0.7111 | 0.7113 |
| 32 | 0.7115 | 0.7112 | 0.7113 |

Table 8.1: Convergence of the amplitude of the reflection coefficient, $|R_1| = |a_r/a_1|$, with increasing number of wavelengths $N_w$ of the periodic domain and for different order $M$. $k = k_r/2$, $kA$=0.05, $L_0 = 20\pi/k_r$, $k_r d$=0.31, $d/h$=0.16; and $N_F$=64$N_w$, $T/\Delta t$=64, $T_s$=20$T$.

wave is used.

As in the simulation of nonlinear wave-body interactions, the radiation condition at the far-filed of bottom undulations is considered by imposing the periodic boundary condition in the horizontal direction. The error due to 'reflection' from the periodic boundaries is avoided by successively increasing the length of the periodic domain until the quantities of interest no longer vary. Table 8.1 shows the results for Bragg resonant reflection by increasing $N_w$, keeping $k_r L_0$, $k_r d$, and $d/h$ fixed. For $N_w = 32$, the amplitude of reflection coefficient, $|R_1|$, shows convergence up to four significant figures.

In practice, the number of spectral modes in (8.4) and (8.5) is truncated at a suitable number $N_F$. Because of the use of orthogonal global basis functions, the convergence of (8.4) and (8.5) with respect to $N_F$ is expected to be exponentially rapid for mild surface wave and bottom slopes. Table 8.2 shows the convergence of Bragg resonant reflection with the number of spectral modes $N_F$ by keeping other parameters fixed. The results in table 8.2 confirm exponential convergence of the solution with respect to $N_F$.

We next show the approach of the steady-state limit (limit-cycle) of Bragg resonant reflection by bottom undulations by considering the convergence of $|R_1|$ with the simulation time $T_s$. This is shown in table 8.3 for different order $M$. The steady-state limit is reached rapidly after $T_s \sim 15T$. Finally, we note that the convergence of the numerical time integration with $\Delta t$ is similar to that for nonlinear wave-body interactions, which has been systematically tested in §3.2. The global error is expected

| $N_F/N_w$ | $M=2$ | $M=3$ | $M=4$ |
|---|---|---|---|
| 16 | 0.7125 | 0.7110 | 0.7155 |
| 32 | 0.7110 | 0.7106 | 0.7107 |
| 64 | 0.7115 | 0.7112 | 0.7113 |

Table 8.2: Convergence of the amplitude of the reflection coefficient, $|R_1| = |a_r/a_1|$, with number of spectral modes $N_F$ for different order $M$. $k = k_r/2$, $kA$=0.05, $L_0 = 20\pi/k_r$, $k_r d$=0.31, $d/h$=0.16; and $N_w$=32, $T/\Delta t$=64, $T_s$=20$T$.

| $T_s/T$ | $M=2$ | $M=3$ | $M=4$ |
|---|---|---|---|
| 11 | 0.7615 | 0.7550 | 0.7510 |
| 12 | 0.7455 | 0.7352 | 0.7320 |
| 13 | 0.7310 | 0.7265 | 0.7250 |
| 14 | 0.7200 | 0.7180 | 0.7170 |
| 15 | 0.7150 | 0.7130 | 0.7125 |
| 16 | 0.7116 | 0.7113 | 0.7112 |
| 17 | 0.7115 | 0.7114 | 0.7111 |
| 18 | 0.7113 | 0.7112 | 0.7112 |
| 19 | 0.7114 | 0.7113 | 0.7112 |
| 20 | 0.7115 | 0.7112 | 0.7113 |

Table 8.3: Convergence of the amplitude of the reflection coefficient, $|R_1| = |a_r/a_1|$, with duration of simulation $T_s$ and perturbation order $M$. $k = k_r/2$, $kA$=0.05, $L_0 = 20\pi/k_r$, $k_r d$=0.31, $d/h$=0.16; and $N_w$=32, $N_F = 64N_w$, $T/\Delta t$=64.

to be $O(\Delta t/T)^4$ due to the use of fourth-order Runge-Kutta scheme as the integrator.

Unless otherwise stated, for all subsequent computations in this chapter, we use $N_w = 32$, $N_F = 64N_w$, $T_s = (15 \sim 25)T$, and $\Delta t = T/64$. Based on foregoing numerical tests, we anticipated the maximum error for $|R_1|$ to be less than 1%.

## 8.4 Normal incidence over a patch of periodic bars

First we study a relatively simple case where a normally incident wave propagates over a patch of parallel bottom undulations. It is well known that Bragg resonant reflection occurs when the bottom undulation has a wavelength half that of the incident waves.

When nonlinear free-surface and bottom effects are included, strong reflection can also occur due to higher-order Bragg resonances (see §8.2). Our primary interest here is to understand the effect of these higher-order Bragg resonances on wave propagations.

### 8.4.1 Calculation of the reflection and transmission coefficients

To determine reflection and transmission of an incident wave by bottom undulations, the approach of Goda & Suzuki (1976) is used here. After factoring out the fast dependences on space and time, we can write the surface elevation $\eta(x,t)$ as:

$$\eta(x,t) = a_r(x)\cos(kx + \omega t + \delta_r) + a_t(x)\cos(kx - \omega t + \delta_t) + \cdots \tag{8.14}$$

where the amplitudes of the reflected and transmitted waves, $a_r(x)$ and $a_t(x)$, vary slowly with space $x$. Through a time harmonic analysis, $\eta(x,t)$ can also be expressed as:

$$\eta(x,t) = \eta_r(x)\cos\omega t + \eta_i(x)\sin\omega t + \cdots \tag{8.15}$$

where the amplitudes, $\eta_r(x)$ and $\eta_i(x)$, have fast dependence on $x$. From (8.14) and (8.15), we have

$$a_r(x)\cos(kx + \omega t + \epsilon_r) + a_t(x)\cos(kx - \omega t + \epsilon_t) = \eta_r(x)\cos\omega t + \eta_i(x)\sin\omega t \tag{8.16}$$

for the first-harmonic wave. Applying (8.16) at two discrete points ($x$ and $x + \Delta x$) and solving for $a_r$ and $a_t$, we obtain:

$$a_r(x) = \frac{1}{2|\sin k\Delta x|}\Big[(\eta_{r2} - \eta_{r1}\cos k\Delta x + \eta_{i1}\sin k\Delta x)^2 + (\eta_{i2} - \eta_{r1}\sin k\Delta x - \eta_{i1}\cos k\Delta x)^2\Big]^{\frac{1}{2}} \tag{8.17}$$

and

$$a_t(x) = \frac{1}{2|\sin k\Delta x|}\Big[(\eta_{r2} - \eta_{r1}\cos k\Delta x - \eta_{i1}\sin k\Delta x)^2 + (\eta_{i2} + \eta_{r1}\sin k\Delta x - \eta_{i1}\cos k\Delta x)^2\Big]^{\frac{1}{2}} \qquad (8.18)$$

where $\eta_{r1} = \eta_r(x)$, $\eta_{r2} = \eta_r(x + \Delta x)$, $\eta_{i1} = \eta_i(x)$, and $\eta_{i2} = \eta_i(x + \Delta x)$. The reflection and transmission coefficients are then defined by $R_1(x) = a_r(x)/a_1$ and $T_1(x) = a_t(x)/a_1$ with $a_1$ representing the first-harmonic amplitude of the incident waves.

Note that since the approximation $a_{r,t}(x) = a_{r,t}(x + \Delta x)$ is applied in deriving (8.17) and (8.18), small $\Delta x$ should be used in practice in order to obtain accurate solutions for $a_r$ and $a_t$.

### 8.4.2 Class I Bragg resonance

Let $\mathbf{k}_2$ represent an incident wave and $\mathbf{k}_1$ the reflected wave. Under class I Bragg condition (8.8), the reflected wave will be resonated due to quadratic interactions between the incident wave and bottom undulations. This resonant reflection by periodic bottom ripples was confirmed by experiments of Davies & Heathershaw (1984). For mild incident wave and bottom slopes, reflection at or near class I Bragg resonance can be well predicted by perturbation theory based on multiple scales and the assumption of linearized surface waves (Mei 1985).

To illustrate the efficacy and usefulness of the present numerical method, we consider a single wave propagation on a horizontal bottom with uniformly sinusoidal ripples and accurately calculate the wave reflection near class I Bragg resonance. Nonlinear solutions are obtained and compared to experiments of Davies & Heathershaw (1984) and perturbation theory (Mei 1985).

In order to compare with experiments, we choose to study a particular case of Davies & Heathershaw (1984) where the horizontal bottom contains 10 sinusoidal ripples with a constant slope of $k_r d$=0.31. In figure 8-1, we show results for the amplitude of the total reflection coefficient in the vicinity of class I Bragg resonance.

The present numerical results with order $M = 3$ are compared to experiments of Davies & Heathershaw (1984) and theoretical solution of Mei (1985). The agreement among them is excellent. By varying incident wave steepness, our numerical solutions indicate that nonlinearity of the free surface has little effect on the amplitude of the reflection coefficient near linear Bragg resonance. This was also found by Kirby (1986) based on the extended-mild-slope equation.

In figure 8-1, peak reflection in experiments and the present numerical results is slightly shifted to the downside of the Bragg point ($2k/k_r = 1$). In general, this can be attributed to high-order boundary effects. Since nonlinearity of the free surface is known to lengthen the incident waves, it moves the peak reflection to the upside of Bragg resonance. Therefore, the downside shift must be caused by nonlinear bottom effects. To understand this, we write the dispersion relation for a small surface wave on a mild-slope bottom as:

$$\omega^2 = gk \tanh k[h + \zeta(x)] \, . \tag{8.19}$$

Since $\zeta \ll h$, we can expand wavenumber $k(x)$ in a perturbation series:

$$k(x) = k_0 + k_1(x) + k_2(x) + \cdots \, . \tag{8.20}$$

Substituting (8.20) into (8.19) and solving for the perturbation wavenumbers, we obtain:

$$\frac{k_1(x)}{k_0} = -\frac{2k_0\zeta(x)}{2k_0h + \sinh 2k_0h} \, , \tag{8.21}$$

and

$$\frac{k_2(x)}{k_0} = \frac{2(k_0\zeta(x))^2}{(2k_0h + \sinh 2k_0h)^3}\left[4k_0h + (3 + \cosh 2k_0h)\sinh 2k_0h\right] \tag{8.22}$$

where $k_0$ is independent of $x$ and is governed by $\omega^2 = gk_0 \tanh k_0h$. After taking space average of $k(x)$, it follows that

$$\bar{k} = k_0 + \frac{(k_0|\zeta(x)|)^2}{(2k_0h + \sinh 2k_0h)^3}\left[4k_0h + (3 + \cosh 2k_0h)\sinh 2k_0h\right] + \cdots \, . \tag{8.23}$$

From (8.23), it is clear that bottom nonlinearity shortens surface waves and thus shifts the peak reflection to the downside (lower frequency) of Bragg resonance.

Figure 8-2 shows the comparisons among the present nonlinear spectral-method solution ($M = 3$), experiments of Davies & Heathershaw (1984), and perturbation theory of Mei (1985) for the amplitude of the reflected waves in the region of bottom ripples. The agreement is very good and thus confirms the validity of the present numerical method for the study of nonlinear wave-bottom interactions.

### 8.4.3 Class II Bragg resonance

For a horizontal bottom consisting of doubly-sinusoidal ripples with wavenumbers $k_{r1}$ and $k_{r2}$, according to (8.10), resonant reflection can also occur if the incident waves satisfy the condition $k = (k_{r1} \pm k_{r2})/2$. This corresponds to the quartet resonance by cubic interactions between surface waves and bottom undulations. In general, the wave reflection due to such high-order Bragg resonance becomes stronger as increasing bottom length and ripple amplitudes while reducing water depth.

In their experiments, Guazzelli *et al.* (1992) observed significant Bragg reflection corresponding to differences of the bottom ripple wavenumbers for mild undulation amplitudes. We here apply the high-order spectral method to calculate resonant wave reflection which we compare to the measurements of Guazzelli *et al.*:

We choose to study a experimental case in Guazzelli *et al.* where the rippled horizontal bottom has a bed length of $L_0 = 16\pi/k_{r1} = 24\pi/k_{r2} = 48$cm, ripple amplitudes of $d_1 = d_2 = 1$cm, and a mean water depth of $h = 4$cm. Nonlinear results with order $M = 3$ are obtained and compared to experiments in figure 8-3, where the solutions near class I Bragg resonances are also shown. Both numerical and experimental results indicate that the nonlinear resonant reflection due to subharmonic (class II) Bragg resonance can be comparable in magnitude (although not at the same frequency) to that due to linear (class I) Bragg effect. The agreement between the present numerical results and the experiments is seen to be very good.

We note that in general, subharmonic resonant reflection is much stronger and more important in practice than that due to superharmonic Bragg resonance ($k =$

$(k_{r1} + k_{r2})/2)$ since the bottom effect is weaker on surface waves with shorter wavelength for a fixed water depth.

### 8.4.4 Class III Bragg resonance

For one-dimensional waves propagating on a flat bottom, it is known that no quartet resonance exists. If the bottom contains a patch of periodic undulations, however, the quartet resonance indeed can occur under the condition (8.11). Despite its obvious significance in predicting the development of the spectrum of ocean waves in coastal zones, such resonance phenomenon has not been addressed yet.

In order to understand the resonance mechanism, we just consider the simplest case where a single surface wave travels over a horizontal bottom with uniformly sinusoidal ripples. Upon accounting for the incident wave twice, the cubic interaction between surface waves and bottom undulations is resonant under the condition (8.13). As a result, the double-frequency (superharmonic) wave component becomes a free (propagating) wave and its amplitude grows as it travels over the rippled bottom by absorbing energy from the incident wave. Although the energy transfer due to quartet resonance is generally of third-order in surface wave and bottom slopes, the free (resonated) superharmonic wave can still be substantially developed over a long patch of bottom undulations.

Depending on the incident waves and bottom topography, in practice, the tertiary (resonated) wave can be either reflected or transmitted over bottom ripples. From (8.13), it follows that the double-frequency wave is transmitted if

$$4k \tanh kh = (2k + k_r) \tanh(2k + k_r)h \ , \tag{8.24}$$

while it is reflected if

$$4k \tanh kh = (k_r - 2k) \tanh(k_r - 2k)h \tag{8.25}$$

with $k_r - 2k > 0$. The simple relations between $k$ and $k_r$ in (8.24) and (8.25) are

plotted in figure 8-4.

For quartet wave resonance in deep water, Longuet-Higgins (1962) derived an analytic solution for the initial growth of the tertiary wave based on a regular perturbation analysis. This solution was later confirmed by the experiments of Longuet-Higgins & Smith (1966). For the present problem, likewise, we can also derive an perturbation solution for the resonant superharmonic waves using the approach of Longuet-Higgins (1962).

*Perturbation solution for resonant superharmonic waves*

For simplicity, we here present the perturbation solution for reflected resonant superharmonic waves only although that for transmitted resonant waves can be easily obtained in a similar way.

Referring to a small parameter $\epsilon$ which measures both free-surface and bottom slopes, we expand the velocity potential $\Phi(x,z,t)$ and the surface elevation $\eta(x,t)$ in perturbation series. Upon expanding nonlinear free-surface and bottom boundary conditions in Taylor series about mean positions $z = 0$ and $-h$ respectively, we obtain a sequence of linear boundary-value problems for perturbation potentials $\Phi^{(m)}$, $m = 1, 2, \cdots$. We write them in a general form as:

$$\Phi^{(m)}_{xx} + \Phi^{(m)}_{zz} = 0 \qquad \text{for} \quad -h < z < 0 \tag{8.26}$$

$$\Phi^{(m)}_{tt} + g\Phi^{(m)}_{z} = F^{(m)}(\Phi^{(1)}, \cdots, \Phi^{(m-1)}) \qquad \text{on} \quad z = 0 \tag{8.27}$$

$$\Phi^{(m)}_{z} = H^{(m)}(\Phi^{(1)}, \cdots, \Phi^{(m-1)}, \zeta) \qquad \text{on} \quad z = -h \tag{8.28}$$

where $\zeta(x) = d\sin(k_r x) = O(\epsilon)$ represents the bottom elevation. Here the free-surface and bottom forcings at $m$-th order, $F^{(m)}$ and $H^{(m)}$, are given in terms of the solutions at lower orders and the boundary-value problems for $\Phi^{(m)}$ can be solved sequentially.

At the first order, we have $F^{(1)} = H^{(1)} = 0$. We choose a right-going progressive wave to be the first-order solution:

$$\Phi^{(1)} = \left(\frac{gA}{\omega}\right)\frac{\cosh k(z+h)}{\cosh kh}\sin(kx - \omega t)\,, \qquad \text{and} \tag{8.29}$$

$$\eta^{(1)} = A\cos(kx - \omega t) \tag{8.30}$$

where $A$ is the incident wave amplitude.

At the second order, the free-surface and bottom forcings are found to be:

$$F^{(2)} = -\left(\frac{3}{2}\right)\frac{g^2(kA)^2}{\omega\cosh^2 kh}\sin(2kx - 2\omega t)\,, \qquad \text{and} \tag{8.31}$$

$$H^{(2)} = \frac{gkAd}{2\omega\cosh kh}\{(k_r + k)\cos[(k_r + k)x - \omega t] + (k_r - k)\cos[(k_r - k)x - \omega t]\}\,. \tag{8.32}$$

The solutions of the second-order potential and surface elevation are then given by:

$$\begin{aligned}\Phi^{(2)} = {} & \left(\frac{gkAd}{2\omega\cosh kh}\right)\left\{\frac{g(k_r - k) - \omega^2\tanh(k_r - k)h}{\omega^2 - g(k_r - k)\tanh(k_r - k)h}\times\right. \\ & \times\cosh(k_r - k)(z + h)\cos[(k_r - k)x + \omega t] \\ & + \sinh(k_r - k)(z + h)\cos[(k_r - k)x + \omega t] \\ & + \sinh(k_r + k)(z + h)\cos[(k_r + k)x - \omega t] \\ & \left. + \frac{g(k_r + k) - \omega^2\tanh(k_r + k)h}{\omega^2 - g(k_r + k)\tanh(k_r + k)h}\cosh(k_r + k)(z + h)\cos[(k_r + k)x - \omega t]\right\} \\ & + \left(\frac{3gkA^2}{4\omega}\right)\frac{\cosh 2k(z + h)}{\sinh 2kh\sinh^2 kh}\sin(2kx - 2\omega t)\,,\end{aligned} \tag{8.33}$$

and

$$\begin{aligned}\eta^{(2)} = {} & -\frac{kA^2}{2\sinh 2kh} + \left(\frac{kA^2}{2}\right)\frac{2 + \cosh 2kh}{\tanh^2 kh\sinh 2kh}\cos(2kx - 2\omega t) \\ & - \frac{Adk(k_r + k)\sin[(k_r + k)x - \omega t]}{k\sinh 2kh\cosh(k_r + k)h - (k_r + k)\cosh kh\sinh 2(k_r + k)h} \\ & + \frac{Adk(k_r - k)\sin[(k_r - k)x + \omega t]}{k\sinh 2kh\cosh(k_r - k)h - (k_r - k)\cosh kh\sinh 2(k_r - k)h}\,.\end{aligned} \tag{8.34}$$

In the third-order free-surface and bottom forcings, there are resonant and non-resonant terms. In the present calculation, we are interested only in the resonant forcing. Omitting others, we have

$$F^{(3)} = \frac{g\omega A^2 d(k_r - k)[(k_r^2 - 6k_r k)\cosh^2 kh + 6k^2]\cos[(k_r - 2k)x + 2\omega t]}{2[(k_r - k)\tanh(k_r - k)h - k\tanh kh]\sinh 2kh \cosh kh \cosh(k_r - k)h} \quad (8.35)$$

and

$$H^{(3)} = \frac{3}{8}k\omega A^2 d(k_r - 2k)\sinh^{-4} kh \cos[(k_r - 2k)x + 2\omega t]\,. \quad (8.36)$$

If we now have $4\omega^2 = g(k_r - 2k)\tanh(k_r - 2k)h$, a solution of equations (8.26)-(8.28) is:

$$\begin{aligned}\Phi^{(3)} &= \frac{gA^2 d\cosh(k_r - 2k)(z+h)}{8\cosh(k_r - 2k)h}\left\{-\frac{3k(k_r - 2k)}{4\cosh(k_r - 2k)h\sinh^4 kh}\right. \\ &\left. + \frac{(k_r - k)[(k_r^2 - 6k_r k)\cosh^2 kh + 6k^2]\cosh^{-1}(k_r - k)h}{[(k_r - k)\tanh(k_r - k)h - k\tanh kh]\sinh 2kh\cosh kh}\right\} \times \\ &\times t\sin[(k_r - 2k)x + 2\omega t] \quad (8.37)\end{aligned}$$

which represents a wave whose amplitude grows in time. The corresponding wave amplitude is given by:

$$\begin{aligned}|\eta^{(3)}| &= \frac{\omega t A^2 d}{4}\left|\frac{3k(k_r - 2k)}{4\cosh(k_r - 2k)h\sinh^4 kh}\right. \\ &\left. - \frac{(k_r - k)[(k_r^2 - 6k_r k)\cosh^2 kh + 6k^2]\cosh^{-1}(k_r - k)h}{[(k_r - k)\tanh(k_r - k)h - k\tanh kh]\sinh 2kh\cosh kh}\right|\,. \quad (8.38)\end{aligned}$$

which becomes unbounded as $t \to \infty$.

If the incident waves interact bottom undulations for an unlimited time but over only a finite distance $L_x$, measured in the direction of propagation of the resonated wave, it is necessary only to replace $t$ in (8.38) by $L_x/C_g$, where $C_g$ is the group velocity of the resonated wave.

*Nonlinear spectral-method solution*

To study class III Bragg resonance, as an numerical example, we consider a horizontal bottom with a bed length of $L_0 = 72\pi/k_r = 27.25\pi h$ and a ripple amplitude of $d = 0.0946h$. For incident waves with wavenumber $k = 0.6/h$, the superharmonic wave is resonated and reflected according to (8.25). With a fixed incident wave steepness $kA = 0.04$, we accurately calculate nonlinear wave reflection by varying incident wavenumber $k$. The present numerical results with order $M = 3$ and 4 for the amplitude of superharmonic reflection coefficient, $|R_2| = |a_2/a_1|$, near class III Bragg resonance are shown in figure 8-5. The maximum amplitude of the resonated superharmonic waves reaches up to 30% of that of the incident wave. Due to nonlinear bottom effects, the peak reflection is again slightly shifted to the downside of the resonance point ($kh = 0.6$).

For small incident waves and bottom undulations, the initial growth of the reflected superharmonic wave due to quartet resonant interactions between the incident waves and bottom undulations can be analytically calculated from (8.38). For a finite patch of bottom ripples, the final amplitude of the superharmonic wave can simply be obtained by replacing the time in (8.38) by $L_0/C_g$. For above case, we obtain the amplitude of the reflected superharmonic wave over bottom undulations:

$$\frac{|a_2|}{|a_1|} = 0.00577k(\frac{L_0}{2} - x)\,, \qquad -\frac{L_0}{2} < x < \frac{L_0}{2}\,. \tag{8.39}$$

In figure 8-6, our numerical results ($M = 3$ and 4) at peak reflection for the amplitude of the superharmonic wave over the bottom undulations are compared to that of small-amplitude perturbation theory (8.39). The agreement is seen to be excellent and thus supports the present numerical simulations.

We summarize that according to perturbation theory and the present numerical calculations, the amplitude of the resonant superharmonic wave due to class III Bragg resonance is linearly proportional to bed length and (bottom) ripple amplitude, while it is of second-order in surface wave steepness.

## 8.5 Oblique incidence over a strip of parallel bars

In this section, we study Bragg resonant reflection of oblique incident waves by parallel bottom undulations lying within the strip $-L_0/2 < x < L_0/2$ on a sea of constant mean water depth $h$. Compared to the case of normal incidence, the important concern here is to understand the effect of oblique angle $\theta$ on the resonant wave reflection.

### 8.5.1 Class I Bragg resonance

For an oblique incident wave propagating on a horizontal bottom containing infinitely-long parallel ripples, linear Bragg resonance can also occur when the $x-$component of incident wavenumber ($k_x = k\cos\theta$) satisfies the class I Bragg condition, i.e., $k\cos\theta = k_r/2$. Here the oblique angle $\theta$ is measured by rotating the $x-$axis to the incident wave ray in the horizontal $x$-$y$ plane.

To simulate oblique wave interactions with parallel bottom undulations, the doubly-periodic computational domain is chosen to be $N_{wx}\lambda_x$ long and $N_{wy}\lambda_y$ wide, where $\lambda_x = \lambda/\cos\theta$ and $\lambda_y = \lambda/\sin\theta$, for incident waves at an oblique angle $\theta$=$\tan^{-1}(N_{wy}/N_{wx})$. Since the reflection and transmission coefficients are independent of $y$, they can again be calculated by using (8.17) and (8.18) with an arbitrarily selected $y$.

To illustrate the dependence of linear Bragg reflection on oblique angle, as an example, we consider a rippled horizontal bottom with a bed length of $L_0 = 20\pi/k_r$, a ripple amplitude of $d = 0.16h$, and a mean water depth of $h = 0.3125\lambda_r$. This bottom configuration is identical to that used for normal incidence in §8.4.2. For a fixed incident wave steepness $kA = 0.05$, we calculate the reflection coefficient, $|R_1| = |a_r/a_1|$, including nonlinear free-surface and bottom effects by varying incident wavenumber and oblique angle.

In figure 8-7, numerical results for the amplitude of the reflection coefficient under the exact Bragg condition are shown as a function of incidence angle $\theta$. The comparison is made to the perturbation theory of Mei *et al.* (1988). Agreement is seen to be excellent. A noticeable result is that at the critical incidence angle $\theta = \pi/4$, the

bottom ripples lose all effects on surface waves.

In figure 8-8, the amplitude of the reflection coefficient in the neighbourhood of class I Bragg resonance ($k_x = k_r/2$) is presented for a fixed incidence angle $\theta = 19.47^o$. The agreement between the present numerical results and the perturbation theory of Mei *et al.* (1988) is again excellent.

### 8.5.2 Class II Bragg resonance

For an oblique incident wave traveling over a horizontal bottom containing parallel double-sinusoidal undulations, the reflected wave is resonated due to subharmonic Bragg resonance under the class II Bragg condition, i.e., $k_x = (k_{r1} - k_{r2})/2$. To study the influence of an incidence angle $\theta$ upon the resonant reflection, we consider a rippled bottom with a bed length of $L_0 = 72\pi/k_{r1} = 48\pi/k_{r2}$, ripple amplitudes of $d_1/h = d_2/h = 0.125$, and a constant mean water depth of $h = 2\pi/k_{r1}$. With the $x-$component of incident wavenumber fixed by the subharmonic Bragg condition, we calculate nonlinear wave reflection by varying incidence angle $\theta$.

Figure 8-9 shows a plot of the amplitude of the reflection coefficient due to subharmonic Bragg resonance as a function of incidence angle $\theta$. Numerical solutions are convergent with respect to the perturbation order $M$. For a fixed bottom configuration, the effect of the subharmonic resonance on surface waves releases slightly as the oblique angle increases.

### 8.5.3 Class III Bragg resonance

For oblique incidence over a patch of infinitely-long parallel ripples, class III Bragg resonance occurs if the incident waves satisfy the condition:

$$4|\mathbf{k}| \tanh |\mathbf{k}|h = |2\mathbf{k} \pm k_r \mathbf{e}_1| \tanh |2\mathbf{k} \pm k_r \mathbf{e}_1|h \tag{8.40}$$

where $\mathbf{e}_1$ is the unit vector in the $x-$direction. As a result, the superharmonic (double-frequency) wave with its wavenumber vector given by $2\mathbf{k} \pm k_r \mathbf{e}_1$ is resonated and its amplitude grows with the time for which the incident waves interact with bot-

tom ripples. For given bottom configurations, the solution of (8.40) for the incident wavenumber vector $\mathbf{k}$ is plotted in figure 8-10.

To study the effect of an oblique angle upon class III Bragg resonance, the same bottom configuration as that for normal incidence in §8.4.4 ($L_0 = 72\pi/k_r$, $k_r d = 0.25$, and $k_r h = 2.642$) is used here. For numerical calculations, an incidence angle $\theta = 19.47^o$ is chosen. With such a bottom configuration and at this incidence angle, according to (8.40), class III Bragg resonance occurs when $kh = 0.62443$ and the resonated superharmonic wave is reflected with the wavenumber vector given by $\mathbf{k}_r h = (-1.4646, 0.4163)$. For an incident wave steepness $kA = 0.04$, we calculate the amplitudes of the resonated superharmonic waves near class III Bragg resonance, which are shown in figure 8-11. Compared to the result in normal incidence, the peak reflection at class III Bragg resonance is reduced for oblique incident waves.

## 8.6 Conclusions and discussions

An efficient computational method is developed for the study of nonlinear wave-bottom interactions. The method employs spectral basis functions and numerically accounts for arbitrarily high order expansions in *both* the free surface steepness and bottom slope. For moderately steep slopes, the method retains exponential convergence of the solution with both the number of spectral modes and the order of the expansions. With the use of fast transform techniques, the computational burden is only linearly proportional to the number of spectral modes and to the free surface and bottom perturbation orders.

This powerful method is used to predict Bragg resonant reflection of surface waves by patches of periodic bottom undulations including nonlinear free-surface and bottom effects. For both normal and oblique incidences over a stripe of parallel bars, we confirm existing theoretical and experimental results for both linear and subharmonic Bragg resonances. When free-surface nonlinearity is accounted for, we find a new superharmonic Bragg mechanism associated with quartet resonant interactions between surface waves and bottom undulations. Based on a perturbation analysis

and the present computations, the amplitude of the resonant superharmonic waves is found to be linearly proportional to bed length and ripple amplitude, while it is of second-order in surface wave steepness. Even for small bottom undulations, the reflected superharmonic wave can be comparable in magnitude to the incident waves. This new high-order Bragg effect must play a important role in the evolution of the spectrum of ocean waves in nearshore areas.

Having shown basic mechanisms associated with linear and high-order Bragg resonances and demonstrated the computational capability of the nonlinear spectral method for general three-dimensional problems, it is of interest to study the following three general cases:

- propagation of multiple surface waves over a strip of parallel sinusoidal bars;
- travelling of a single surface wave over a bottom containing two-dimensional sinusoidal ripples;
- propagation of multiple surface waves over a two-dimensional undulated bottom topography;

Finally, we remark that for a bottom containing disordered ripples, localization of surface waves has been predicted by theory (Devillard *et al.* 1988) and observed in experiments (Belzons *et al.* 1988). The present efficient method will be useful for the study of this localization phenomenon for providing an alternative for the protection of beaches.

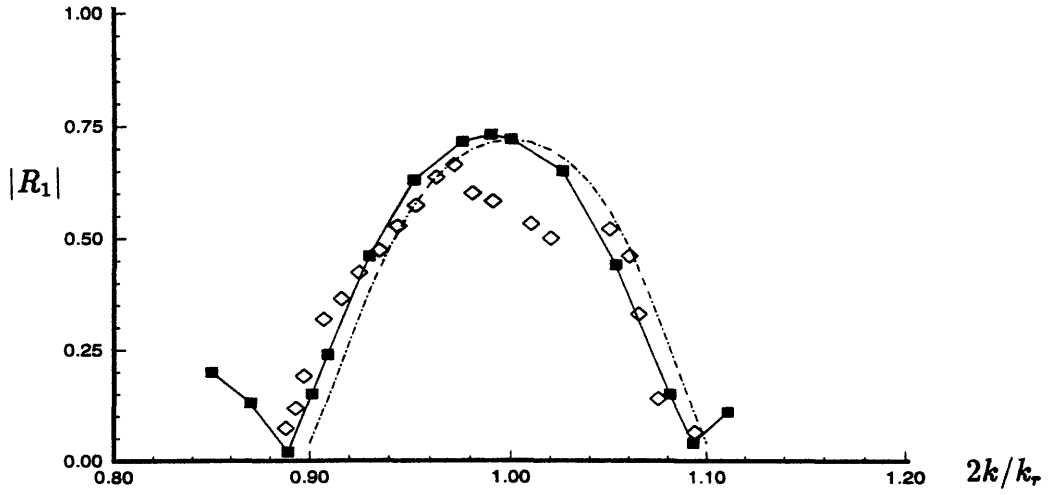


Figure 8-1: Reflection coefficient near Bragg resonance ($2k/k_r = 1$). Experiments (Davies & Heathershaw 1984) ($\diamond$); perturbation theory (Mei 1985) (— · —); and present high-order results for $M = 3$ ($\blacksquare$). ($kA = 0.05$, $k_r d = 0.31$, $d/h = 0.16$, $d \equiv$ ripple amplitude)

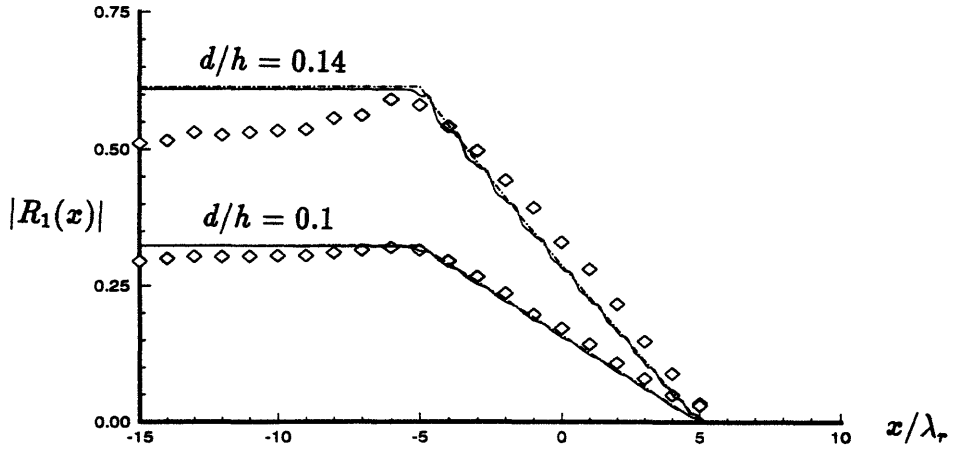


Figure 8-2: Variation of the reflection coefficient over the bottom ripples under Bragg condition ($2k/k_r = 1$). Experiments (Davies & Heathershaw 1984) ($\diamond$); perturbation theory (Mei 1985) (— · —); and present high-order results for $M = 3$ (——). $x \equiv$ distance along the direction of incident waves. $\lambda_r \equiv$ ripple wavelength. The bottom ripples are from $x = -5\lambda_r$ to $x = 5\lambda_r$. ($kA = 0.05$, $k_r d = 0.31$)

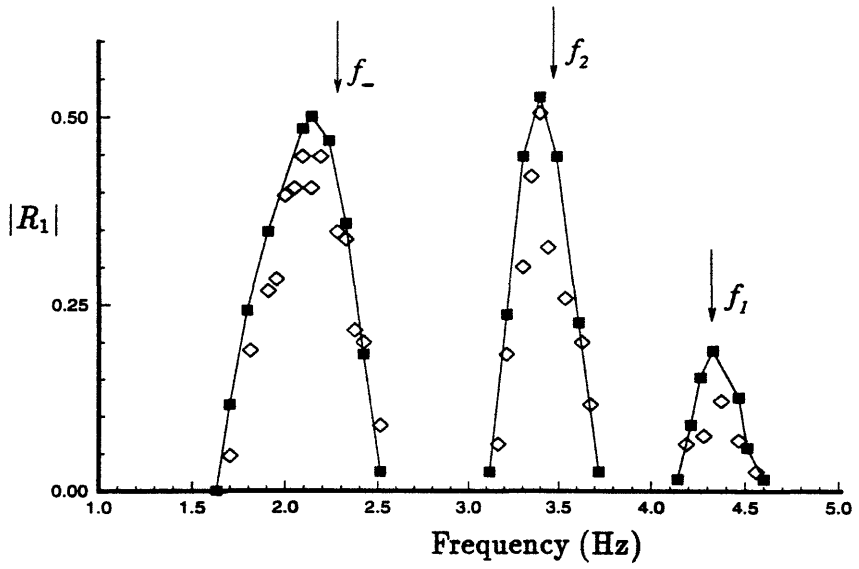


Figure 8-3: Comparison between the present numerical results for $M = 3$ (■) and the experiments (Guazzelli *et al.* 1992) (◇) for the resonant reflection coefficient. $f_1$: $k = k_{r1}/2$; $f_2$: $k = k_{r2}/2$; and $f_-$: $k = (k_{r1} - k_{r2})/2$. ($kA = 0.05$)

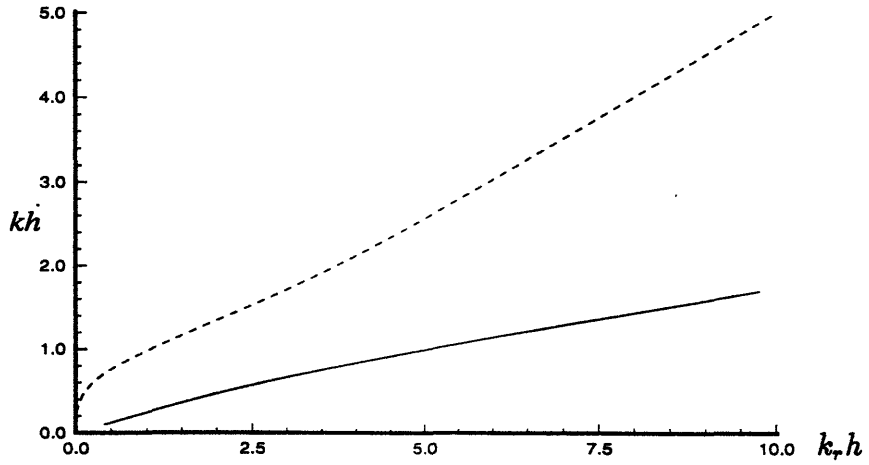


Figure 8-4: Dimensionless incident wavenumber $kh$ under class III Bragg condition as a function of dimensionless bottom wavenumber $k_r h$ with the tertiary wave transmitted (- - -) or reflected (——).

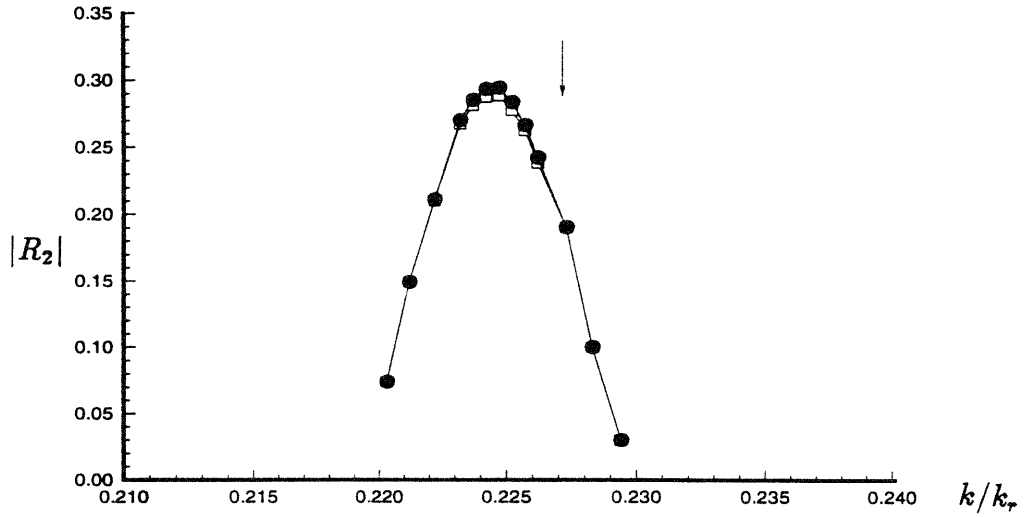


Figure 8-5: Reflection coefficient of the superharmonic wave near class III Bragg resonance. $M = 3$ ($\square$) and $M = 4$ ($\bullet$). ($kA = 0.04$, $k_r d = 0.25$, $k_r h = 2.642$)

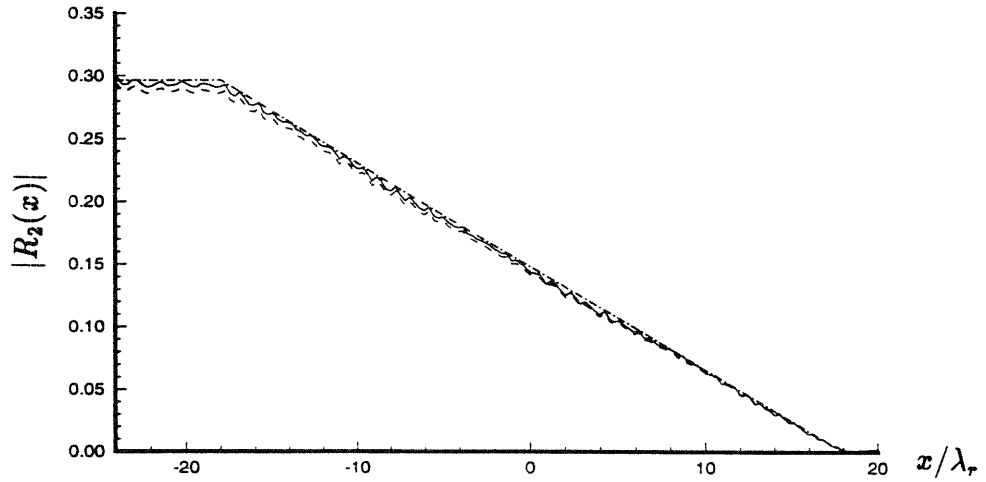


Figure 8-6: Variation of the amplitude of the reflected superharmonic wave over the bottom undulations. The perturbation theory (— · —), and the present numerical results for $M = 3$ (- - -) and $M = 4$ (——). $x \equiv$ distance along the direction of incident waves. $\lambda_r \equiv$ ripple wavelength. The periodic undulations are from $x = -18\lambda_r$ to $x = 18\lambda_r$. ($kA = 0.04$, $k_r h = 2.642$, $k_r d = 0.250$, $k/k_r = 0.225$)

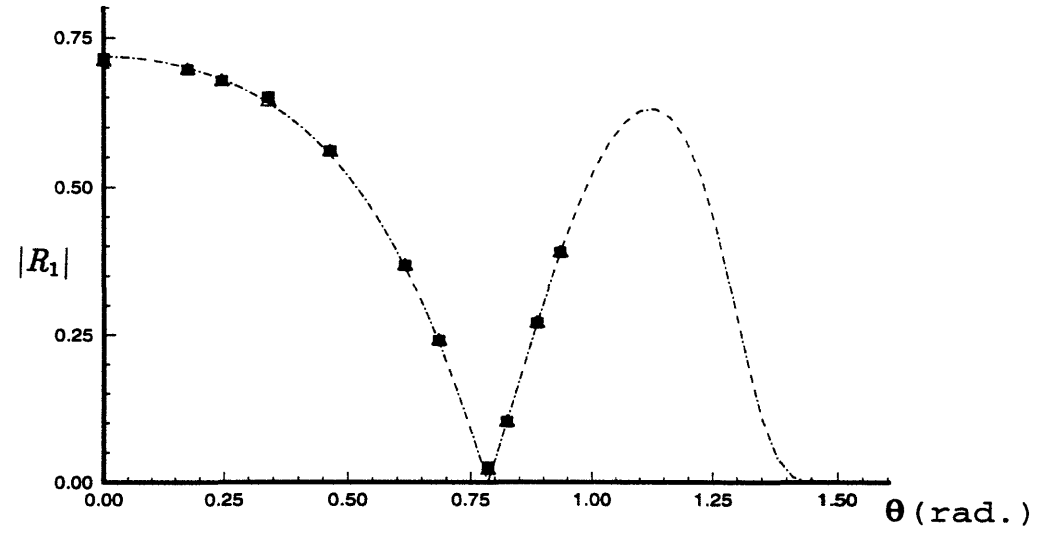


Figure 8-7: Reflection coefficient as a function of incidence angle $\theta$ at Bragg resonance ($2k_x/k_r = 1$). Perturbation theory (Mei *et al.* 1988) (— · —); and present high-order numerical results for $M = 2$ (△), and $M = 3$ (■). ($kA = 0.05$, $k_r d = 0.31$, $d/h = 0.16$)

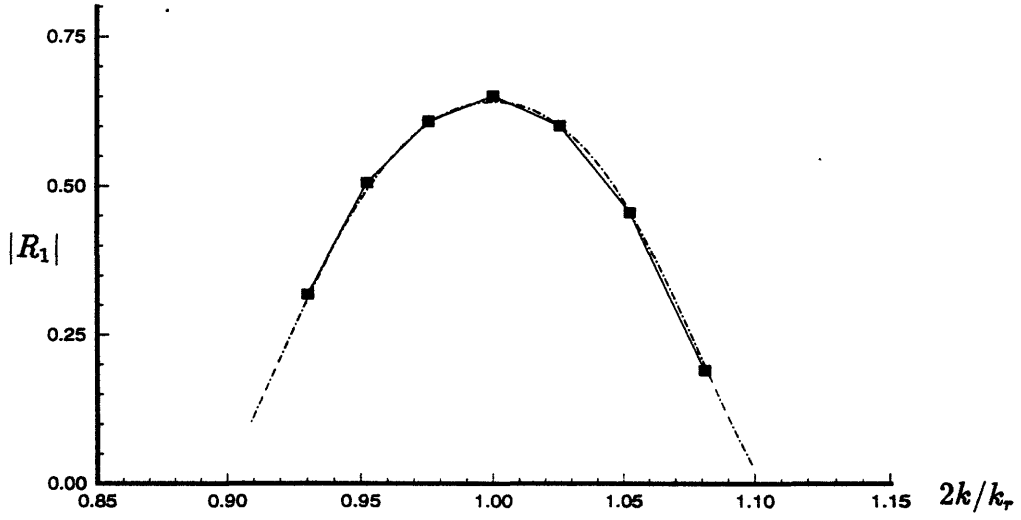


Figure 8-8: Reflection coefficient near Bragg resonance ($2k_x/k_r = 1$) for fixed incidence angle $\theta = 19.47°$. Perturbation theory (Mei *et al.* 1988) (— · —); and present high-order numerical results for $M = 3$ (■). ($kA = 0.05$, $k_r d = 0.31$, $d/h = 0.16$)

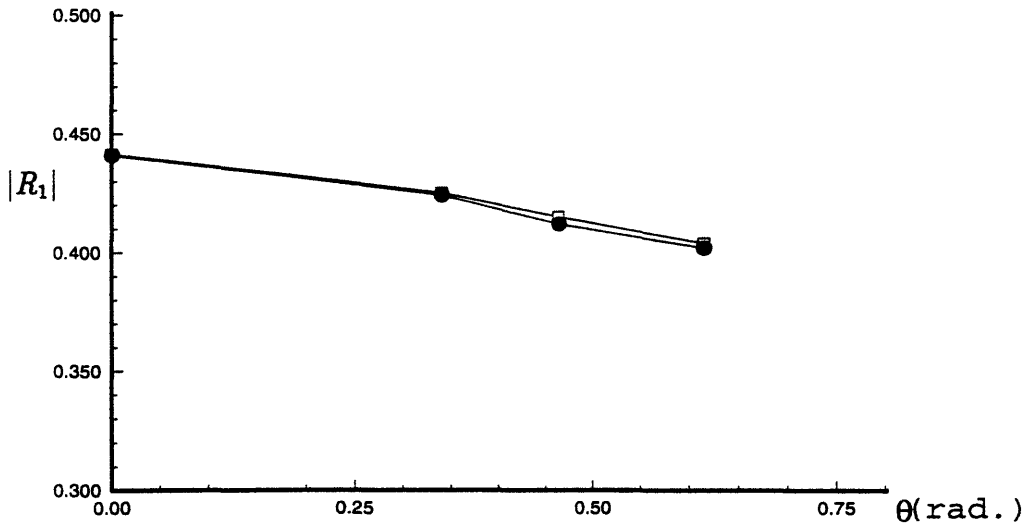


Figure 8-9: Reflection coefficient as a function of incidence angle $\theta$ at subharmonic Bragg resonance ($2k_x/(k_{b1} - k_{b2}) = 1$). $M = 3$ (□) and $M = 4$ (●). ($kA = 0.05$, $L_0 = 72\pi/k_{r1} = 48\pi/k_{r2}, d_1/h = d_2/h = 0.125$, $h = 2\pi/k_{r1}$)

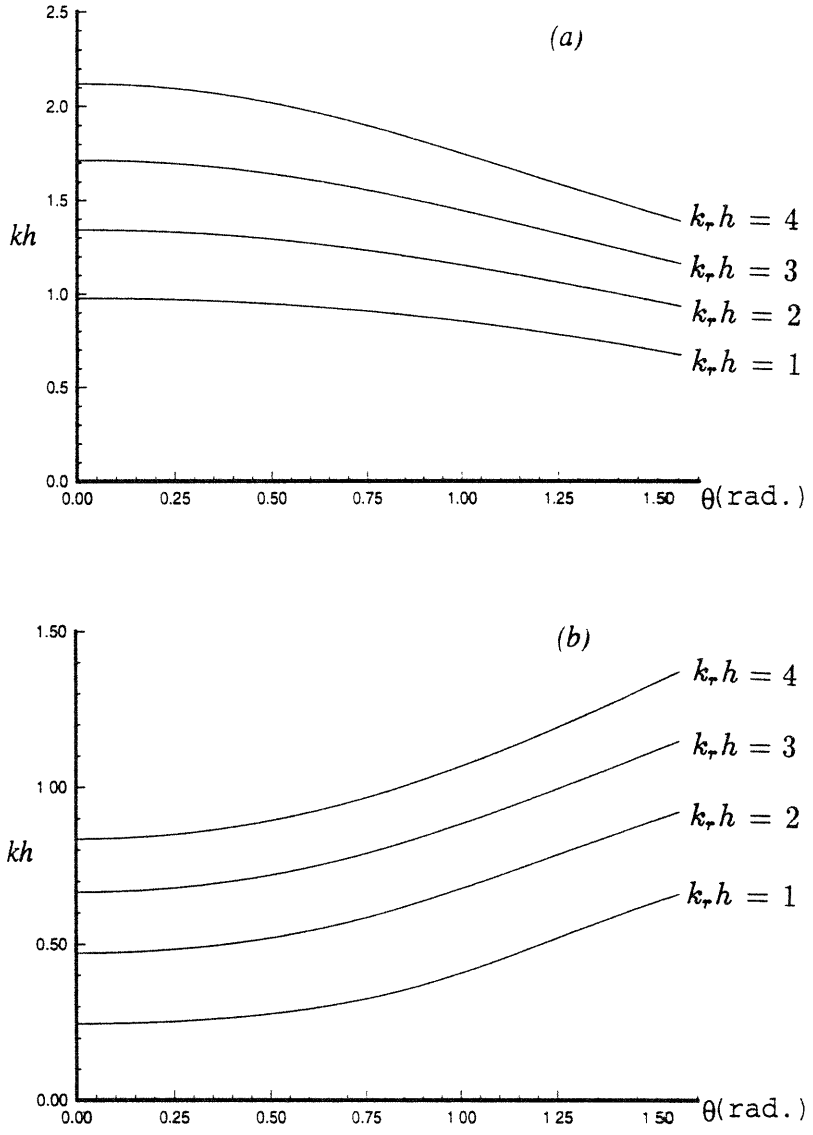


Figure 8-10: Dimensionless incident wavenumber $kh$ under class III Bragg condition (8.40) as a function of incidence angle $\theta$. (a) solution with plus sign in (8.40) and (b) solution with minus sign in (8.40).

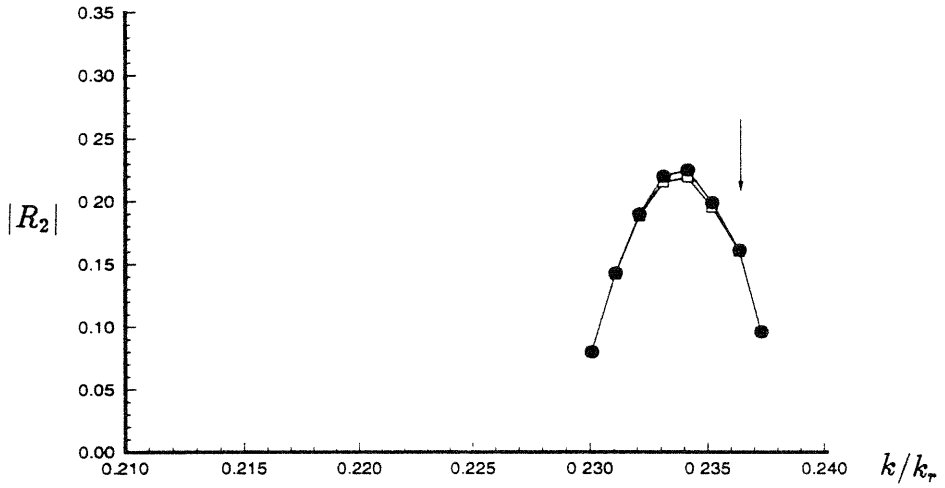


Figure 8-11: Reflection coefficient of the superharmonic wave near class III Bragg resonance for incidence angle $\theta = 19.47°$. $M = 3$ ($\square$) and $M = 4$ ($\bullet$). ($kA = 0.04$, $k_r d = 0.25$, $k_r h = 2.642$)

# Chapter 9

# Conclusions and further studies

This chapter summarizes the conclusions of this thesis and offers some suggestions for further studies.

## 9.1 Conclusions

This thesis focuses on the study of nonlinear wave-body/bottom interaction problems of theoretical interest and practical importance. The body can be either stationary or undergoing imposed oscillatory or steady motions. Nonlinear solutions are obtained through careful numerical simulations using an extended efficient high-order spectral method. To assist us in understanding the nonlinear seakeeping solution, theoretical analyses regarding the linear-solution behaviours near the critical frequency corresponding to $\tau \equiv \omega_c U/g = 1/4$ as well as the decay of the transients associated with the abrupt motions of a body are included. For simplicity of the numerical simulation, we consider submerged bodies only.

The principal contributions of this work include:

1. the discovery of the following critical high-order effects in nonlinear surface wave interactions with bodies and/or bottoms that:

    - the quadratic interaction between the first- and third-order (first-harmonic) waves produces a significant fourth-order negative horizontal drift force on

a submerged circular cylinder;

- nonlinear free-surface and linear three-dimensional effects produce comparable (in magnitude) and opposing (in direction) mean pitch moments on a submerged spheroid in head seas;
- the third-order change in the dispersion relation due to free-surface nonlinearity causes first-order corrections to the motion coefficients of the seakeeping problem near the critical frequency $\tau = \frac{1}{4}$;
- the resonant quartet interactions between surface waves and bottom undulations generate significant superharmonic reflected and/or transmitted waves;

2. analytic proofs that the linear seakeeping solution at the critical frequency $\tau = \frac{1}{4}$ is actually bounded for a geneal class of submerged and floating bodies, and that the decay of the transient solution due to an initial acceleration of a submerged or floating body is an order of magnitude faster than classical theory predictions;

3. successful extension of the high-resolution nonlinear spectral method to the study of wave interactions with general two- and three-dimensional submerged bodies which can be either stationary or undergoing imposed oscillatory or steady motions.

### (I) Nonlinear wave diffraction by a submerged circular cylinder

For wave diffraction by a fixed and submerged circular cylinder, high-resolution nonlinear solutions for the force on the body and the diffracted wave field are obtained. Comparisons to available measurements as well as existing theoretical/computational predictions are in good agreement. The most important result is the quantification of the negative horizontal drift force on the cylinder which is fourth-order in the incident wave steepness. It is found that the dominant contribution of this force is a result of the quadratic interaction of first- and third-order waves rather than the self-interaction of second-order waves which in fact reduces the negative drift force. To correctly predict this force, third-order wave effects must be considered.

### (II) The mean force and pitch moment on a submerged spheroid

To understand the effect of similar interactions on a three-dimensional body, we consider the mean force and pitch moment on a submerged near-surface spheroid. If nonlinear interactions are included, both the horizontal drift force in beam seas and the mean pitch moment in head seas change their directions as the surface waves steepen or when the body is moved closer to the free surface. Based on systematic simulations, the dominant nonlinear corrections for both the mean force and pitch moment are found to be due to the quadratic interaction of the first- and third-order waves. The linear solution and high-order correction are generally of opposite signs such that for a given body in an ambient wave field, there must be a particular submergence at which the horizontal drift force or the mean pitch moment is minimized. For the mean pitch moment, in particular, a simple formula for the estimation of such a special position is established.

### (III) The linear seakeeping solution near the critical frequency

To study the nonlinear seakeeping problem, it is necessary to understand the linear solution, particularly near the critical frequency $\tau = \frac{1}{4}$. Through rigorous asymptotic analyses in the frequency domain, we offer a formal proof that the linear solution of the seakeeping problem is finite if and only if a certain geometric condition is satisfied. This is in contrast to existing theories based upon the single-source result. For a submerged body, a necessary and sufficient condition is that the body must have non-zero volume. For a surface-piercing body, a sufficient condition is derived which has a geometric interpretation similar to that of John (1950). As an illustration, we provide an analytic (closed-form) solution for the case of a submerged circular cylinder oscillating near $\tau = \frac{1}{4}$, which compares well with the calculations of Grue & Palm (1985). Also, we identify the underlying difficulties of existing approximate theories and numerical computations near $\tau = \frac{1}{4}$, and offer a simple remedy for the latter.

### (IV) The time-dependence of the wave resistance of a body

An immediate implication of the frequency-domain result is that with the removal of the $\tau = \frac{1}{4}$ singularity, the actual decay of the transients associated with the abrupt motions of a floating body must necessarily be an order faster than the single-source predictions for a body which satisfies the requisite geometric condition. We are able to prove this in a thorough analysis of the time-dependence of the wave resistance of a body starting from rest. The exact decay rate is found to be proportional to $t^{-\frac{3}{2}}$ and $t^{-2}$ for two- and three-dimensional bodies in contrast to $t^{-\frac{1}{2}}$ (Havelock 1949) and $t^{-1}$ (Wehausen 1963) obtained by approximating a body using sources at a particular point or on a special plane. These theoretical results are confirmed by our direct time-domain simulations.

### (V) Nonlinear wave radiation near the critical frequency

After understanding the linear solution completely, the nonlinear seakeeping problem near the critical frequency is studied. To elucidate the basic nonlinear mechanism, we consider the nonlinear wave radiation of a submerged circular cylinder in a uniform current. With long-time simulations, nonlinear steady-state (limit-cycle) solutions for the radiation force on the body are obtained including high-order effects of the free surface and body. Compared to the linear solution, it is found that the nonlinear correction due to cubic self-interactions of unsteady waves is of *first*-order in the wave slope. Such strong nonlinear effect persists only in the neighbourhood of $\tau = \frac{1}{4}$ where the radiation of wave energy is significantly amplified through the first-order change of wave group velocities due to free-surface nonlinearity. On the other hand, the quadratic interaction between steady and unsteady waves is found to influence the added mass only, but not the first-harmonic damping.

### (VI) Nonlinear wave reflection by an undulated bottom topography

To study a problem for which nonlinear effects are amplified due to a near-periodic placement of weak scatterers, we consider surface wave propagation over patches of

bottom undulations. Because of strong Bragg resonance, large wave reflection can occur for certain incident waves. In addition to the confirmation of existing theoretical and experimental results associated with linear and subharmonic Bragg resonances, we discover a new Bragg mechanism corresponding to superharmonic transmitted and/or reflected waves. We obtain this by including free-surface nonlinearity and considering resonant quartet interactions between surface waves and bottom undulations. For moderately steep waves and mild bottom slopes, the amplitude of the resonant superharmonic wave is linearly proportional to the bed length and the ripple amplitude, whereas it is of second-order in the surface wave slope.

**(VII) The extended high-order spectral method**

The numerical scheme used in this thesis is an extension of the high-order spectral method of Dommermuth & Yue (1987b) for nonlinear wave-wave interactions. This method allows interactions between surface waves and the body/bottom up to an arbitrary order $M$ in wave steepness, and exhibits exponential convergence with respect to M and the number of spectral modes $N$. Significantly, with fast transform techniques, the computational effort is only linearly proportional to $M$ and $N$. The efficiency and accuracy of the present nonlinear spectral method allows us to perform high-resolution calculations for nonlinear wave-body/bottom interaction problems of practical importance.

## 9.2 Further studies

We present three suggestions for the extension of the present study:

1. For the problem of wave propagation over an undulated bottom topography, we have found the basic Bragg resonance mechanisms and demonstrated the computational capability of the nonlinear spectral method for the general three-dimensional problem. It is now of interest to study the solutions of the following general cases:

- propagation of multiple surface waves over a strip of parallel sinusoidal bars;
- normal incidence of a single wave over a rippled bottom containing two-dimensional sinusoidal ripples.
- travelling of multiple surface waves over a two-dimensional undulated bottom topography.

2. The extension of the efficient high-order spectral method to a surface-piercing body should be very useful for practical problems. The key difference from the case of a submerged body is that the free surface is now not continuous at the intersection with the body. As a result, the surface elevation and velocity potential cannot be expanded in Fourier series. To retain rapid convergence, the solutions must be represented in terms of spectral functions such as Chebyshev or Legendre polynomials, whose exponential convergence is independent of the end conditions.

3. Traditional mode-coupling theories are generally known to be incapable of describing the long-short wave interactions because the expansion of the velocity potential on the free surface about a reference surface diverges as a product of the long-wave amplitude and short-wave number. However, the key in using the high-order spectral method for the study of nonlinear long-short wave interactions is the accurate evaluation of the vertical velocity on the free surface. Following Brueckner and West (1988), in appendix D, we are able to analytically cancel out all divergent terms in the expansion of the vertical velocity on the free surface and obtain a convergent series in terms of products of the short-wave amplitude and long-wave number. Because of this, we can avoid the numerical summation of divergent terms in calculations and are able to extend the high-order spectral method to the study of long-time evolution of an ocean wave field including long-short wave interactions.

# Appendix A

# The velocity potential at large distances

In this appendix, we consider the behavior of the solution in the limit $|\vec{x}| \to \infty$ such that $\kappa|\vec{x}|\delta \to \infty$ while $\delta \ll 1$. For simplicity, we consider the case of a two-dimensional submerged body.

As $|x| \to \infty$, $G_0$ vanishes and the principle-value integrals in (5.6) to (5.9) can be integrated analytically via contour integration. For $x \to +\infty$, $G_1$, $G_3$, and $G_4$ vanish, while

$$G_2 \sim \frac{i2\pi}{\sqrt{1-4\tau}} e^{k_2[-i(x-x')+(z+z')]} . \tag{A.1}$$

For $x \to -\infty$, $G_2$ vanishes, while

$$G_1 \sim \frac{i2\pi}{\sqrt{1-4\tau}} e^{k_1[-i(x-x')+(z+z')]} , \tag{A.2}$$

$$G_{3,4} \sim \frac{\mp i2\pi}{\sqrt{1+4\tau}} e^{k_{3,4}[i(x-x')+(z+z')]} . \tag{A.3}$$

Substitution of (A.1)-(A.3) into (5.14) gives

$$\phi(x,z) \sim \frac{i2\pi}{\delta} e^{k_2(-ix+z)} \int_{S_B} \sigma(x',z') e^{k_2(ix'+z')} ds' \tag{A.4}$$

for $x \to +\infty$, and

$$\phi(x,z) \sim \frac{i2\pi}{\delta} e^{k_1(-ix+z)} \int_{S_B} \sigma(x',z') e^{k_1(ix'+z')} ds' + \int_{S_B} \sigma(x',z')(G_3+G_4) ds' \quad \text{(A.5)}$$

for $x \to -\infty$. In the neighborhood of $\delta \ll 1$, we expand the kernel $e^{k_{1,2}(ix'+z')}$ in Taylor series about $k_{1,2} = \kappa$:

$$e^{k_{1,2}(ix'+z')} = e^{\kappa(ix'+z')}[1 \pm 2\kappa(ix'+z')\delta + O(\delta^2)] \,, \qquad \delta^2 \ll 1 \,. \quad \text{(A.6)}$$

After substituting (A.6) into (A.4) and (A.5), we obtain

$$\phi(x,z) \sim i2\pi(\alpha_1/\delta - \alpha_3) e^{k_2(-ix+z)} + O(\delta) \quad \text{(A.7)}$$

for $x \to +\infty$, and

$$\phi(x,z) \sim i2\pi(\alpha_1/\delta + \alpha_3) e^{k_1(-ix+z)} + \int_{S_B} \sigma(x',z')(G_3+G_4) ds' + O(\delta) \quad \text{(A.8)}$$

for $x \to -\infty$. Here, the constant $\alpha_3$ is given by

$$\alpha_3 = 2\kappa \int_{S_B} (ix'+z') \sigma(x',z') e^{\kappa(ix'+z')} ds' \,, \quad \text{(A.9)}$$

and can formally be at most $O(1)$ for finite $\sigma$. For $\Gamma \neq 0$, $\alpha_1/\delta = O(1)$ and $\sigma = O(1)$. Thus the potentials in (A.7) and (A.8) are bounded as $\delta \to 0$.

We remark that the $k_{1,2}$ potentials in (A.8) and (A.7) respectively approach the same finite limit as $\delta \to 0$. This is due to the fact that $\alpha_3$ is $O(\delta)$ which can be shown starting from just before (5.12). The analysis itself is a detail and is omitted here.

# Appendix B

# Large-time expansions of single-source potentials

In this appendix, we derive asymptotic expansions of single-source potentials $\Psi$ and $\Xi$ for a variety of source functions under $\frac{|\vec{x}-\vec{x'}|}{Ut} = o(1)$ as $t \to \infty$.

## B.1 Two-dimensional sources

Given time dependence of a two-dimensional source, the large-time asymptotic expansion of the corresponding potential $\Psi$ can be derived starting from equation (6.7).

**Case I: $\sigma(t) = q_0 = 1$ for $t > 0$ and $q_0 = 0$ elsewhere**

For $\sigma(t) = 1$, the integration with respect to $\tau$ in (6.7) can be carried out to give

$$\Psi(\vec{x}, \vec{x'}, q_0) = \ln\left(\frac{r}{r_1}\right) + 2\fint_0^\infty \left(\frac{1}{k-k_0} - \frac{1}{k}\right) \mathrm{e}^{k(z+z')} \cos k(x-x')\, \mathrm{d}k$$

$$+ 2\int_0^\infty \left(\frac{1}{m} - \frac{1}{m+m_0}\right) \mathrm{e}^{m^2\psi + \mathrm{i}(m^2U + mg^{\frac{1}{2}})t}\, \mathrm{d}m + \text{c.c.}$$

$$+ \fint_{-\infty}^\infty \left(\frac{1}{m} - \frac{1}{m-m_0}\right) \mathrm{e}^{m^2\psi + \mathrm{i}(m^2U - mg^{\frac{1}{2}})t}\, \mathrm{d}m + \text{c.c.} \qquad \text{(B.1)}$$

where $k_0 = g/U^2$, $m_0 = k_0^{\frac{1}{2}}$. Here Cauchy principal-value integrals are indicated and the first integral in (B.1) is independent of time.

At large time, the second integral in (B.1), denoted by $I_2$, is dominated by the integration near $m = 0$. By use of the method of steepest decent, the integration path can be changed to the line of steepest decent (namely, the line $m = \mathrm{i}\varrho/g^{\frac{1}{2}}$). Upon expanding the integrand in Taylor series about $\varrho = 0$, we have

$$I_2 \simeq 2\int_0^{\epsilon} \left[\frac{1}{\varrho} - \frac{\mathrm{i}}{Um_0^2} + O(\varrho)\right] \mathrm{e}^{-\varrho t}\, \mathrm{d}\varrho + \text{c.c.} \qquad \text{as } t \to \infty \tag{B.2}$$

where $\epsilon$ is a small positive number. After Changing variable with $\lambda = \varrho t$, it follows that

$$I_2 \simeq 4\int_0^{\infty} \frac{e^{-\lambda}}{\lambda}\, \mathrm{d}\lambda + O\left(\frac{1}{t^2}\right) \qquad \text{as } t \to \infty\,. \tag{B.3}$$

Note that although the integral in (B.3) diverges, it can be dropped in the expansion of $\Psi(\vec{x}, \vec{x'}, q_0)$ as an arbitrarily-large constant.

The last integral ($I_3$) in (B.1) possesses a saddle point at $m = tg^{\frac{1}{2}}/2\xi$ with $\xi = x - x' + Ut$, and two poles at $m = 0$ and $m = m_0$. Since we seek for the large-time expansion of $\Psi$ under $\frac{|\vec{x}-\vec{x'}|}{Ut} = o(1)$, $\xi$ can be considered positive. Deforming the path of integration to the lines of steepest decent given by $m_{1,2} = tg^{\frac{1}{2}}/2\xi \pm \varrho \mathrm{e}^{\mathrm{i}\frac{\pi}{4}}$, we obtain

$$I_3 = 2\pi \mathrm{e}^{k_0(z+z')} \sin k_0(x - x')$$

$$+\, m_0 \mathrm{e}^{\mathrm{i}(\frac{\pi}{4} - \frac{gt^2}{4\xi})} \int_0^{\infty} \left[\frac{\mathrm{e}^{m_1^2(z+z')}}{m_1(m_0 - m_1)} + \frac{\mathrm{e}^{m_2^2(z+z')}}{m_2(m_0 - m_2)}\right] e^{-\xi\varrho^2}\, \mathrm{d}\varrho + \text{c.c.}\,. \tag{B.4}$$

For large $\xi$, the integral in (B.4) can be evaluated by using Laplace's method. By expanding the terms inside square-brackets in Taylor series about $\varrho = 0$, it follows that

$$I_3 \simeq 2\pi \mathrm{e}^{k_0(z+z')} \sin k_0(x - x') + \frac{8m_0\xi^2}{tg^{\frac{1}{2}}(2\xi m_0 - tg^{\frac{1}{2}})} \times$$

$$\times e^{i(\frac{\pi}{4}-\frac{gt^2}{4\xi})+\frac{gt^2}{4\xi^2}(z+z')}\int_0^{\epsilon}\left[1+O(\varrho^2)\right]e^{-\xi\varrho^2}\,d\varrho+\text{c.c.}\quad\text{as }\xi\to\infty\,. \tag{B.5}$$

Extending the upper limit of the integration to infinity and carrying out the resulting integral, we obtain

$$I_3 = 2\pi e^{k_0(z+z')}\sin k_0(x-x')$$

$$+\frac{4\xi^{\frac{3}{2}}(\pi/g)^{\frac{1}{2}}}{t(2\xi-Ut)}e^{i(\frac{\pi}{4}-\frac{gt^2}{4\xi})+\frac{gt^2}{4\xi^2}(z+z')}\left[1+O\left(\frac{1}{t}\right)\right]+\text{c.c.}\qquad\text{as }\xi\to\infty\,. \tag{B.6}$$

Substituting $\xi = x-x'+Ut$ for (B.6) and applying the condition $\frac{|x-x'|}{Ut}=o(1)$, we can further expand (B.6) in a simpler form:

$$I_3 = \quad 2\pi e^{k_0(z+z')}\sin k_0(x-x')$$

$$+4\left(\frac{\pi}{\kappa Ut}\right)^{\frac{1}{2}}e^{\kappa\psi-i\omega_c t+i\frac{\pi}{4}}+\text{c.c.}+O\left(\frac{e^{-i\omega_c t}}{t^{\frac{3}{2}}}\right)\qquad\text{as } t\to\infty \tag{B.7}$$

where $\kappa = k_0/4$ and $\omega_c = g/4U$.

In summary, the expansion of $\Psi$ can be written as:

$$\Psi(\vec{x},\vec{x'},q_0)=\bar{G}(\vec{x},\vec{x'})+C_0\frac{e^{-i\omega_c t}}{t^{\frac{1}{2}}}e^{\kappa\psi}+\text{c.c.}+O\left(\frac{e^{-i\omega_c t}}{t^{\frac{3}{2}}}\right)\quad\text{as } t\to\infty \tag{B.8}$$

where the constant $C_0 = 8(\frac{\pi U}{g})^{\frac{1}{2}}e^{i\frac{\pi}{4}}$ and the time-independent function $\bar{G}$ is given by

$$\bar{G}(\vec{x},\vec{x'})=\ln(rr_1)+2\pi e^{k_0(z+z')}\sin k_0(x-x')+2\int_0^{\infty}\frac{\cos k(x-x')}{k-k_0}e^{k(z+z')}dk\,. \tag{B.9}$$

**Case II: $\sigma(t)=\tilde{\sigma}(t)\neq 0$ for $t\in(0,t_0)$ and $\tilde{\sigma}(t)=0$ elsewhere**

If a source is suddenly turned on at $t=0$ and turned off at $t=t_0$, the resulting potential for $t>t_0$ can be expressed as:

$$\tilde{\Psi}(\vec{x},\vec{x'},\sigma(t))=i2g^{\frac{1}{2}}\int_0^{\infty}dm\,e^{m^2\psi+i(m^2U+mg^{\frac{1}{2}})t}\int_0^{t_0}\tilde{\sigma}(\tau)e^{-i(m^2U+mg^{\frac{1}{2}})\tau}\,d\tau+\text{c.c.}$$

$$-\mathrm{i}g^{\frac{1}{2}}\int_{-\infty}^{\infty}\mathrm{d}m\,\mathrm{e}^{m^2\psi+\mathrm{i}(m^2U-mg^{\frac{1}{2}})t}\int_0^{t_0}\tilde{\sigma}(\tau)\mathrm{e}^{-\mathrm{i}(m^2U-mg^{\frac{1}{2}})\tau}\,\mathrm{d}\tau+\mathrm{c.c.}\,. \quad \text{(B.10)}$$

Assuming $\tilde{\sigma}(\tau)$ a smooth and continueous function of $\tau$, the integrals with respect to $\tau$ in (B.10) are generally regular. At large time, the integrals with respect to $m$ are dominated by the integration near the stationary phase point at $m = m_0/2$. Upon using the method of stationary phase, we obtain

$$\tilde{\Psi}(\vec{x},\vec{x'},\tilde{\sigma}(t))=\tilde{W}(\vec{x'})\frac{\mathrm{e}^{-\mathrm{i}\omega_c t}}{t^{\frac{1}{2}}}\mathrm{e}^{\kappa\psi}+\mathrm{c.c.}+O\left(\frac{1}{t}\right)\qquad \text{as } t\to\infty \quad \text{(B.11)}$$

where the time-independent function $\tilde{W}$ is given by

$$\tilde{W}(\vec{x'})=\left(\frac{g\pi}{U}\right)^{\frac{1}{2}}e^{-i\frac{\pi}{4}}\int_0^{t_0}\tilde{\sigma}(\tau)\mathrm{e}^{\mathrm{i}\omega_c\tau}\,\mathrm{d}\tau\,. \quad \text{(B.12)}$$

**Case III: $\sigma(t)=q_1=t^{-\frac{1}{2}}\mathrm{e}^{-\mathrm{i}\omega_c t}$ for $t>t_0$ and $q_1=0$ elsewhere**

By substituting $\sigma(\tau)=\tau^{-\frac{1}{2}}\mathrm{e}^{-\mathrm{i}\omega_c\tau}$, for $\tau>t_0$ into (6.7), the resulting velocity potential for $t>t_0$ can be written as:

$$\Psi(\vec{x},\vec{x'},q_1)=\frac{\mathrm{e}^{-\mathrm{i}\omega_c t}}{t^{\frac{1}{2}}}\ln\left(\frac{r}{r_1}\right)$$

$$+\,\mathrm{i}2g^{\frac{1}{2}}\int_0^{\infty}e^{m^2\psi+\mathrm{i}(m^2U+mg^{\frac{1}{2}})t}\,\mathrm{d}m\int_{t_0}^{t}\tau^{-\frac{1}{2}}\mathrm{e}^{-\mathrm{i}(m^2U+mg^{\frac{1}{2}}+\kappa U)\tau}\,\mathrm{d}\tau \quad \text{(B.13)}$$

$$-\,\mathrm{i}2g^{\frac{1}{2}}\int_0^{\infty}e^{m^2\psi^*-\mathrm{i}(m^2U+mg^{\frac{1}{2}})t}\,\mathrm{d}m\int_{t_0}^{t}\tau^{-\frac{1}{2}}\mathrm{e}^{\mathrm{i}(m^2U+mg^{\frac{1}{2}}-\kappa U)\tau}\,\mathrm{d}\tau \quad \text{(B.14)}$$

$$-\,\mathrm{i}g^{\frac{1}{2}}\int_{-\infty}^{\infty}e^{m^2\psi+\mathrm{i}(m^2U-mg^{\frac{1}{2}})t}\,\mathrm{d}m\int_{t_0}^{t}\tau^{-\frac{1}{2}}\mathrm{e}^{-\mathrm{i}(m^2U-mg^{\frac{1}{2}}+\kappa U)\tau}\,\mathrm{d}\tau \quad \text{(B.15)}$$

$$+\,\mathrm{i}g^{\frac{1}{2}}\int_{-\infty}^{\infty}\mathrm{e}^{m^2\psi^*-\mathrm{i}(m^2U-mg^{\frac{1}{2}})t}\,\mathrm{d}m\int_{t_0}^{t}\tau^{-\frac{1}{2}}\mathrm{e}^{\mathrm{i}(m^2U-mg^{\frac{1}{2}}-\kappa U)\tau}\,\mathrm{d}\tau\,. \quad \text{(B.16)}$$

In order to determine the integration with respect to $\tau$ in (B.13)-(B.16), we first evaluate the following integral

$$\int_{t_0}^{t} \frac{\mathrm{e}^{\pm \mathrm{i}\nu\tau}}{\tau^{\frac{1}{2}}}\,\mathrm{d}\tau = \frac{W_{1,2}}{\nu^{\frac{1}{2}}} \pm \frac{\mathrm{e}^{\pm \mathrm{i}\nu t}}{\mathrm{i}\nu t^{\frac{1}{2}}} + O\left(\frac{\mathrm{e}^{\pm \mathrm{i}\nu t}}{t^{\frac{3}{2}}}\right) \quad \text{as } t \to \infty \tag{B.17}$$

where $\nu$ is a positive constant and $W_{1,2}$ are regular functions of $\nu$ and given by

$$W_{1,2}(\nu) = \int_{\nu t_0}^{\infty} \frac{1}{\lambda^{\frac{1}{2}}}(\cos\lambda \pm \mathrm{i}\sin\lambda)\,\mathrm{d}\lambda\ . \tag{B.18}$$

After carrying out the integration with respect to $\tau$, (B.13) can be written as:

$$I_1 = \mathrm{i}2m_0U^{\frac{1}{2}} \int_0^{\infty} W_2[(m+m_0/2)^2U] \frac{\mathrm{e}^{m^2\psi + \mathrm{i}(m^2U + mg^{\frac{1}{2}})t}}{m+m_0/2}\,\mathrm{d}m$$

$$- 2m_0 \frac{\mathrm{e}^{-\mathrm{i}\omega t}}{t^{\frac{1}{2}}} \int_0^{\infty} \frac{e^{m^2\psi}}{(m+m_0/2)^2}\,\mathrm{d}m + O\left(\frac{\mathrm{e}^{-\mathrm{i}\omega_c t}}{t^{\frac{3}{2}}}\right) \quad \text{as } t \to \infty\ . \tag{B.19}$$

Upon integration by parts, it is clear that the first term of $I_1$ is $O(\frac{1}{t})$ for large $t$. The large-time asymptotic expansion of $I_1$ can then be expressed as:

$$I_1 = -2m_0 \frac{\mathrm{e}^{-\mathrm{i}\omega_c t}}{t^{\frac{1}{2}}} \int_0^{\infty} \frac{\mathrm{e}^{m^2\psi}}{(m+m_0/2)^2}\,\mathrm{d}m + O\left(\frac{1}{t}\right) \quad \text{as } t \to \infty\ . \tag{B.20}$$

After using (B.17), we can write (B.14) as:

$$I_2 = -\mathrm{i}2m_0U^{\frac{1}{2}} \left\{ \int_0^{m_2} \frac{W_2}{(m_2-m)^{\frac{1}{2}}} + \int_{m_2}^{\infty} \frac{W_1}{(m-m_2)^{\frac{1}{2}}} \right\} \frac{\mathrm{e}^{m^2\psi^* - \mathrm{i}(m^2U + mg^{\frac{1}{2}})t}}{(m+m_1)^{\frac{1}{2}}}\,\mathrm{d}m$$

$$-2m_0 \frac{\mathrm{e}^{-\mathrm{i}\omega_c t}}{t^{\frac{1}{2}}} \int_0^{\infty} \frac{e^{m^2\psi^*}}{(m+m_1)(m-m_2)}\,\mathrm{d}m + O\left(\frac{\mathrm{e}^{-\mathrm{i}\omega_c t}}{t^{\frac{3}{2}}}\right) \quad \text{as } t \to \infty \tag{B.21}$$

where $m_{1,2} = m_0(\sqrt{2}\pm 1)/2$, and the path of integration is indented to pass below the pole at $m = m_2$. The integrals inside the brackets have neither pole nor stationary phase point for $m \in (0,\infty)$. As $t \to \infty$, they are dominated by the integration near end points. Using the method of steepest decent, it can be shown that the integration from the interval near $m = 0$ is $O(1/t)$, while it is $O(1/t^{\frac{1}{2}})$ near $m = m_2$. Omitting

detailed derivation, we write the expansion for $I_2$ as:

$$I_2 = -\frac{e^{-i\omega_c t}}{t^{\frac{1}{2}}}\Big\{i\sqrt{2\pi}\left[W_1(0)e^{-i\frac{\pi}{4}} + W_2(0)e^{i\frac{\pi}{4}}\right]e^{m_2^2\psi^*}$$

$$+ 2m_0 \oint_0^\infty \frac{e^{m^2\psi^*}}{(m+m_1)(m-m_2)}\,dm\Big\} + O\left(\frac{1}{t}\right) \qquad \text{as } t \to \infty\ . \quad \text{(B.22)}$$

For (B.15), we can rewrite the integral with respect to $\tau$ in terms of error functions:

$$I_3 = -e^{i\frac{\pi}{4}} m_0 (\pi U)^{\frac{1}{2}} e^{-i\omega_c t} \int_{-\infty}^{\infty} \frac{e^{m^2\psi + i(m-m_0/2)^2 Ut}}{|m - m_0/2|} \times$$

$$\left[erf(e^{i\frac{\pi}{4}}(Ut)^{\frac{1}{2}}|m-m_0/2|) - erf(e^{i\frac{\pi}{4}}(Ut_0)^{\frac{1}{2}}|m-m_0/2|)\right]\,dm\ . \quad \text{(B.23)}$$

Since the error function tends to zero as $m \to m_0/2$, the integral in (B.23) is regular. The main contribution to this integral comes from the interval near the stationary phase point ($m = m_0/2$). Replacing the first error function in (B.23) by its series expansion and applying the method of steepest decent, we obtain the asymptotic expansion for $I_3$:

$$I_3 = e^{-i\frac{\pi}{4}} m_0 U^{\frac{1}{2}} \left[\sum_{n=0}^{\infty} \frac{\Gamma(n+\frac{1}{2})}{(2n+1)n!} - 2\left(\frac{\pi t_0}{t}\right)^{\frac{1}{2}}\right] e^{-i\omega_c t} e^{\kappa\psi} + O\left(\frac{e^{-i\omega_c t}}{t}\right) \qquad \text{(B.24)}$$

as $t \to \infty$, where the series can be shown to be convergent as $n \to \infty$.

After using (B.17) for the integration with respect to $\tau$, (B.16) can be written as:

$$I_4 = im_0 U^{\frac{1}{2}} \int_{-\infty}^{-m_2} W_1 \frac{e^{m^2\psi^* - i(m^2U - mg^{\frac{1}{2}})t}}{(m_1-m)^{\frac{1}{2}}(-m-m_2)^{\frac{1}{2}}}\,dm$$

$$+ im_0 U^{\frac{1}{2}} \int_{-m_2}^{m_1} W_2 \frac{e^{m^2\psi^* - i(m^2U - mg^{\frac{1}{2}})t}}{(m_1-m)^{\frac{1}{2}}(m+m_2)^{\frac{1}{2}}}\,dm$$

$$+ im_0 U^{\frac{1}{2}} \int_{m_1}^{\infty} W_1 \frac{e^{m^2\psi^* - i(m^2U - mg^{\frac{1}{2}})t}}{(m-m_1)^{\frac{1}{2}}(m+m_2)^{\frac{1}{2}}}\,dm$$

$$+ m_0 \frac{\mathrm{e}^{-\mathrm{i}\omega_c t}}{t^{\frac{1}{2}}} \int_{\mathcal{L}} \frac{e^{m^2\psi^*}}{(m-m_1)(m+m_2)}\,\mathrm{d}m + O\left(\frac{\mathrm{e}^{-\mathrm{i}\omega_c t}}{t^{\frac{3}{2}}}\right) \qquad \text{as } t \to \infty \quad \text{(B.25)}$$

where the contour $\mathcal{L}$ extends from $-\infty$ to $+\infty$ in the complex $m$-plane and is indented to pass above the pole at $m = -m_2$ and below the pole at $m = m_1$. Clearly, no pole exists in the first three integrals of $I_3$. The main contribution to these integrals thus comes from the region near the stationary phase point ($m = m_0/2$) and the end points of the integration ($m = m_1, -m_2$). These contributions can be easily determined by using the method of steepest decent. The final result can be expressed as:

$$I_4 = \mathrm{e}^{\mathrm{i}\frac{\pi}{4}}\sqrt{2\pi}W_2(m_0^2U/2)\,\frac{\mathrm{e}^{\mathrm{i}\omega_c t}}{t^{\frac{1}{2}}}\mathrm{e}^{\kappa\psi^*}$$

$$+ \mathrm{i}\sqrt{\frac{\pi}{2}}\left[W_1(0)e^{-i\frac{\pi}{4}} + W_2(0)\mathrm{e}^{\mathrm{i}\frac{\pi}{4}}\right]\frac{\mathrm{e}^{-\mathrm{i}\omega_c t}}{t^{\frac{1}{2}}}\left\{\mathrm{e}^{m_1^2\psi^*} + \mathrm{e}^{m_2^2\psi^*}\right\}$$

$$+ m_0\frac{\mathrm{e}^{-\mathrm{i}\omega_c t}}{t^{\frac{1}{2}}}\int_L \frac{\mathrm{e}^{m^2\psi^*}}{(m-m_1)(m+m_2)}\,\mathrm{d}m + O\left(\frac{\mathrm{e}^{-\mathrm{i}\omega_c t}}{t^{\frac{3}{2}}}\right) \qquad \text{as } t \to \infty \quad \text{.(B.26)}$$

In summary, the large-time expansion of the velocity potential due to a varying source $q_1$ can be expressed as:

$$\Psi(\vec{x}, \vec{x'}, q_1) = (C_1 t^{\frac{1}{2}} + \bar{C}_1)\frac{\mathrm{e}^{-\mathrm{i}\omega_c t}}{t^{\frac{1}{2}}}e^{\kappa\psi} + \hat{C}_1\frac{\mathrm{e}^{\mathrm{i}\omega_c t}}{t^{\frac{1}{2}}}e^{\kappa\psi^*}$$

$$+H(\vec{x}, \vec{x'})\frac{\mathrm{e}^{-\mathrm{i}\omega_c t}}{t^{\frac{1}{2}}} + O\left(\frac{1}{t}, \frac{\mathrm{e}^{-\mathrm{i}\omega_c t}}{t}\right) \qquad \text{as } t \to \infty \qquad \text{(B.27)}$$

where the constants $C_1$, $\bar{C}_1$, and $\hat{C}_1$ are given by

$$C_1 = \mathrm{e}^{-\mathrm{i}\frac{\pi}{4}} m_0 U^{\frac{1}{2}} \sum_{n=0}^{\infty} \frac{\Gamma(n+\frac{1}{2})}{(2n+1)n!}\,, \qquad \text{(B.28)}$$

$$\bar{C}_1 = -2\mathrm{e}^{-\mathrm{i}\frac{\pi}{4}} m_0 (\pi U t_0)^{\frac{1}{2}}\,, \qquad \hat{C}_1 = \mathrm{e}^{\mathrm{i}\frac{\pi}{4}}\sqrt{2\pi}W_2(m_0^2U/2) \qquad \text{(B.29)}$$

and the time-independent function $H$ is given by

$$H(\vec{x},\vec{x'}) = \ln\left(\frac{r}{r_1}\right) + \mathrm{i}\sqrt{\frac{\pi}{2}}\left[W_1(0)\mathrm{e}^{-\mathrm{i}\frac{\pi}{4}} + W_2(0)\mathrm{e}^{\mathrm{i}\frac{\pi}{4}}\right]\left\{\mathrm{e}^{m_1^2\psi^*} - e^{m_2^2\psi^*}\right\}$$

$$+ m_0\left\{-2\int_0^\infty \frac{e^{m^2\psi}}{(m+m_0/2)^2}\,\mathrm{d}m - \oint_0^\infty \frac{e^{m^2\psi^*}}{(m+m_1)(m-m_2)}\,\mathrm{d}m\right.$$

$$\left. + \int_L \frac{e^{m^2\psi^*}}{(m-m_1)(m+m_2)}\,\mathrm{d}m\right\}. \qquad \text{(B.30)}$$

## B.2 Three-dimensional sources

In three dimensions, the velocity potential $\Xi$ due to a source located at $\vec{x'}$ with a strength of $\sigma(t)$ can be expressed as (Wehausen & Laitone 1960):

$$\Xi(\vec{x},\vec{x'},\sigma(t)) = \sigma(t)\left(\frac{1}{R} - \frac{1}{R_1}\right) - \frac{\mathrm{i}}{4\pi}\int_{-\pi}^{\pi}\mathrm{d}\theta\int_0^\infty (gk)^{\frac{1}{2}}\mathrm{e}^{k[(z+z')+\mathrm{i}\varpi(\theta)]}\times$$

$$\times\left\{\mathrm{e}^{\mathrm{i}t(gk)^{\frac{1}{2}}}\int_0^t \sigma(\tau)\mathrm{e}^{-\mathrm{i}[(gk)^{\frac{1}{2}}+kU\cos\theta]\tau}\,\mathrm{d}\tau\right.$$

$$\left. -\mathrm{e}^{-\mathrm{i}t(gk)^{\frac{1}{2}}}\int_0^t \sigma(\tau)\mathrm{e}^{\mathrm{i}[(gk)^{\frac{1}{2}}-kU\cos\theta]\tau}\,\mathrm{d}\tau\right\}\mathrm{d}k + \text{c.c.} \qquad \text{(B.31)}$$

in which $R^2, R_1^2 = (x-x')^2 + (y-y')^2 + (z\mp z')^2$ and $\varpi(\theta) = \xi\cos\theta + (y-y')\sin\theta$. Reducing the range of integration from $(-\pi,\pi)$ to $(0,\pi/2)$ and changing variable with $k = m^2$, we can rewrite (B.31) as:

$$\Xi(\vec{x},\vec{x'},\sigma(t)) = \sigma(t)\left(\frac{1}{R} - \frac{1}{R_1}\right)$$

$$-\frac{\mathrm{i}4g^{\frac{1}{2}}}{\pi}\int_0^{\frac{\pi}{2}}\mathrm{d}\theta\int_0^\infty \chi(m,\theta)\,\mathrm{e}^{\mathrm{i}mtg^{\frac{1}{2}}}\,\mathrm{d}m\int_0^t \sigma(\tau)\,\mathrm{e}^{-\mathrm{i}(mg^{\frac{1}{2}}+m^2U\cos\theta)\tau}\,\mathrm{d}\tau + \text{c.c.}$$

$$+\frac{\mathrm{i}2g^{\frac{1}{2}}}{\pi}\int_0^{\frac{\pi}{2}}\mathrm{d}\theta\int_{-\infty}^\infty \chi(m,\theta)\,\mathrm{e}^{-\mathrm{i}mtg^{\frac{1}{2}}}\,\mathrm{d}m\int_0^t \sigma(\tau)\,\mathrm{e}^{\mathrm{i}(mg^{\frac{1}{2}}-m^2U\cos\theta)\tau}\,\mathrm{d}\tau + \text{c.c.} \qquad \text{(B.32)}$$

in which $\chi(m,\theta) = m^2\cos[m^2(y-y')\sin\theta]\mathrm{e}^{m^2(z+z')+\mathrm{i}m^2\xi\cos\theta}$.

**Case I: $\sigma(t) = q_0 = 1$ for $t > 0$ and $q_0 = 0$ elsewhere**

After carrying out the integration with respect to $\tau$ in (B.32), we get

$$\Xi(\vec{x},\vec{x'},q_0) = \frac{1}{R} - \frac{1}{R_1}$$

$$-\frac{4k_0}{\pi}\int_0^{\frac{\pi}{2}}\mathrm{d}\theta\!\!\!\!\!\!\int_0^{\infty}\mathrm{e}^{k(z+z')}\cos[k(y-y')\sin\theta]\frac{\cos[k(x-x')\cos\theta]}{k\cos^2\theta - k_0}\,\mathrm{d}k \qquad \text{(B.33)}$$

$$-\frac{4m_0}{\pi}\int_0^{\frac{\pi}{2}}\mathrm{d}\theta\int_0^{\infty}m\mathrm{e}^{m^2(z+z')}\cos[m^2(y-y')\sin\theta]\frac{\mathrm{e}^{\mathrm{i}(m^2\xi\cos\theta+mtg^{\frac{1}{2}})}}{m\cos\theta+m_0}\,\mathrm{d}m + \text{c.c.} \qquad \text{(B.34)}$$

$$+\frac{2m_0}{\pi}\int_0^{\frac{\pi}{2}}\mathrm{d}\theta\!\!\!\!\!\!\int_{-\infty}^{\infty}m\mathrm{e}^{m^2(z+z')}\cos[m^2(y-y')\sin\theta]\frac{\mathrm{e}^{\mathrm{i}(m^2\xi\cos\theta-mtg^{\frac{1}{2}})}}{m\cos\theta-m_0}\,\mathrm{d}m + \text{c.c.}\,. \qquad \text{(B.35)}$$

From (B.33) to (B.35), it is clear that $\Xi(\vec{x},\vec{x'},q_0)$ is symmetric about $y-y'=0$. Thus we only need to consider the case $y-y'>0$.

(B.33) is independent of time and thus a part of the steady solution. Its evaluation has been investigated by Newman (1987) and is omitted here. For the integration with respect to $m$ in (B.34), we see that there exists neither a pole nor a stationary phase point within the range of integration. The leading contribution to this integral comes from the end region $m \in (0,\epsilon)$. Changing the path of integration to the line of steepest decent ($m = \mathrm{i}\varrho/g^{\frac{1}{2}}$) and making an expansion of the integrand around $\varrho = 0$, (B.34) becomes

$$\mathcal{I}_2 \simeq -\frac{8}{\pi}\int_0^{\frac{\pi}{2}}\mathrm{d}\theta\int_0^{\infty}\left[-\frac{\varrho}{m_0^2U^2}+O(\varrho^2)\right]\mathrm{e}^{-\varrho t}\,\mathrm{d}\varrho = \frac{4}{k_0(Ut)^2}+O\left(\frac{1}{t^3}\right) \qquad \text{(B.36)}$$

as $t\to\infty$.

In order to evaluate the integrals in (B.35), we first rewrite (B.35) as:

$$\mathcal{I}_3 = \frac{m_0}{\pi}\int_0^{\frac{\pi}{2}}\sec\theta\,[\Theta(\zeta_1,\theta)+\Theta(\zeta_2,\theta)]\,\mathrm{d}\theta + \text{c.c.} \qquad \text{(B.37)}$$

where $\zeta_{1,2} = \xi \cos\theta \pm (y - y') \sin\theta$ and the function $\Theta$ is defined by

$$\Theta(\zeta, \theta) = \oint_{-\infty}^{\infty} \frac{m}{m - \vartheta} \, \mathrm{e}^{m^2(z+z') + \mathrm{i}(m^2\zeta - mtg^{\frac{1}{2}})} \, \mathrm{d}m \tag{B.38}$$

with $\vartheta = m_0 \sec\theta$. We notice that as long as $\theta \neq \frac{\pi}{2}$, $\zeta_{1,2}$ are definitely positive for $\frac{|\vec{x} - \vec{x'}|}{Ut} = o(1)$ as $t \to \infty$ . We thus only need to consider the case $\zeta > 0$ in evaluating $\Theta$. From (B.38), it is seen that $\Theta$ is dominated not only by the pole at $m = \vartheta$ but also by the stationary phase point located at $m = tg^{\frac{1}{2}}/2\zeta$. To obtain the complete asymptotic expansion for $\Theta$ at large time, the method of steepest decent is again used. After changing the path of integration to the line of steepest decent given by $m_{1,2} = tg^{\frac{1}{2}}/2\zeta \pm \varrho \mathrm{e}^{\mathrm{i}\frac{\pi}{4}}$, it follows that

$$\Theta(\zeta, \theta) = \mathrm{i}\pi\vartheta e^{\vartheta^2(z+z') + \mathrm{i}(\vartheta^2\zeta - \vartheta tg^{\frac{1}{2}})}$$

$$+ \mathrm{e}^{\mathrm{i}(\frac{\pi}{4} - \frac{gt^2}{4\zeta})} \int_0^{\infty} \left[ \frac{m_1 \mathrm{e}^{m_1^2(z+z')}}{m_1 - \vartheta} + \frac{m_2 \mathrm{e}^{m_2^2(z+z')}}{m_2 - \vartheta} \right] \mathrm{e}^{-\zeta\varrho^2} \, \mathrm{d}\varrho \tag{B.39}$$

in which the first term results from the residue at the pole $m = \vartheta$. By use of Laplace's method, we can carry out the integral in (B.39) to obtain

$$\Theta(\zeta, \theta) = \mathrm{i}\pi\vartheta \mathrm{e}^{\vartheta^2(z+z') + \mathrm{i}(\vartheta^2\zeta - \vartheta tg^{\frac{1}{2}})}$$

$$+ \frac{t(\pi g)^{\frac{1}{2}}}{tg^{\frac{1}{2}} - 2\vartheta\zeta} \mathrm{e}^{\mathrm{i}(\frac{\pi}{4} - \frac{gt^2}{4\zeta}) + \frac{gt^2}{4\zeta^2}(z+z')} \left[ \frac{1}{\zeta^{\frac{1}{2}}} + O\left( \frac{1}{\zeta^{\frac{3}{2}}} \right) \right] \quad \text{as } \zeta \to \infty \, . \tag{B.40}$$

Substitution of (B.40) into (B.37) gives

$$\mathcal{I}_3 = -4 \int_0^{\frac{\pi}{2}} \vartheta^2 \sin[m_0\vartheta(x - x')] \cos[\vartheta^2 \sin\theta(y - y')] e^{\vartheta^2(z+z')} \, \mathrm{d}\theta$$

$$+ te^{\mathrm{i}\frac{\pi}{4}} \left( \frac{g}{\pi} \right)^{\frac{1}{2}} \int_0^{\frac{\pi}{2}} \vartheta \left\{ \frac{\mathrm{e}^{-\mathrm{i}\frac{gt^2}{4\zeta_1} + \frac{gt^2}{4\zeta_1^2}(z+z')}}{\zeta_1^{\frac{1}{2}}(tg^{\frac{1}{2}} - 2\vartheta\zeta_1)} + \frac{\mathrm{e}^{-\mathrm{i}\frac{gt^2}{4\zeta_2} + \frac{gt^2}{4\zeta_2^2}(z+z')}}{\zeta_2^{\frac{1}{2}}(tg^{\frac{1}{2}} - 2\vartheta\zeta_2)} \right\} \times$$

$$\left[1+O\left(\frac{1}{\zeta_1},\frac{1}{\zeta_2}\right)\right]\,\mathrm{d}\theta+\text{c.c.}\qquad\text{as }\zeta_1,\zeta_2\to\infty\,. \tag{B.41}$$

After plugging $\zeta_1$ and $\zeta_2$ into (B.41), it becomes clear that the terms inside the brackets have neither pole nor stationary phase point for $\theta\in(0,\pi/2)$. It can be easily shown that this integral is dominated by the integration in the region near $\theta=0$. After taking the end expansion around $\theta=0$ and extending the range of integration to infinity, the resulting integral can be integrated to give

$$\begin{aligned}\mathcal{I}_3 &= -4\int_0^{\frac{\pi}{2}}\vartheta^2\sin[m_0\vartheta(x-x')]\cos[\vartheta^2\sin\theta(y-y')]\mathrm{e}^{\vartheta^2(z+z')}\,\mathrm{d}\theta\\ &+2m_0\frac{(2Ut/\xi)^{\frac{1}{2}}}{tg^{\frac{1}{2}}-2\xi m_0}\mathrm{e}^{-\mathrm{i}\frac{gt^2}{4\xi}+\frac{gt^2}{4\xi^2}(z+z')}\left[1+O\left(\frac{1}{\xi},\frac{1}{t}\right)\right]+\text{c.c.}\qquad\text{as } t\to\infty\,.\end{aligned} \tag{B.42}$$

Substituting $\xi$ for (B.42) and taking Taylor expansion about $\frac{|x-x'|}{Ut}=o(1)$, $\mathcal{I}_3$ can be expressed as:

$$\begin{aligned}\mathcal{I}_3 &= -4\int_0^{\frac{\pi}{2}}\vartheta^2\sin[m_0\vartheta(x-x')]\cos[\vartheta^2\sin\theta(y-y')]\mathrm{e}^{\vartheta^2(z+z')}\,\mathrm{d}\theta\\ &-\frac{2\sqrt{2}}{U}\frac{\mathrm{e}^{-\mathrm{i}\omega_c t}}{t}\mathrm{e}^{\kappa\psi}+\text{c.c.}+O\left(\frac{\mathrm{e}^{-\mathrm{i}\omega_c t}}{t^2}\right)\qquad\text{as } t\to\infty\,.\end{aligned} \tag{B.43}$$

The asymptotic expansion of $\Xi(\vec{x},\vec{x'},q_0)$ is summarized as follows:

$$\Xi(\vec{x},\vec{x'},q_0)=\bar{\mathcal{G}}(\vec{x},\vec{x'})+\mathcal{C}_0\frac{\mathrm{e}^{-\mathrm{i}\omega_c t}}{t}\mathrm{e}^{\kappa\psi}+\text{c.c.}+O\left(\frac{\mathrm{e}^{-\mathrm{i}\omega_c t}}{t^2}\right)\qquad\text{as } t\to\infty \tag{B.44}$$

in which the constant $\mathcal{C}_0=-\frac{2\sqrt{2}}{U}$, and the time independent part $\bar{\mathcal{G}}$ is given by

$$\begin{aligned}\bar{\mathcal{G}}(\vec{x},\vec{x'}) &= \frac{1}{R}-\frac{1}{R_1}-\frac{4k_0}{\pi}\int_0^{\frac{\pi}{2}}\mathrm{d}\theta\int_0^{\infty}\mathrm{e}^{k(z+z')}\cos[k(y-y')\sin\theta]\frac{\cos[k(x-x')\cos\theta]}{k\cos^2\theta-k_0}\,\mathrm{d}k\\ &-4k_0\int_0^{\frac{\pi}{2}}\sec^2\theta\sin[k_0\sec\theta(x-x')]\cos[k_0\sec^2\theta\sin\theta(y-y')]\mathrm{e}^{k_0\sec^2\theta(z+z')}\,\mathrm{d}\theta\,.\end{aligned} \tag{B.45}$$

**Case II:** $\sigma(t) = \tilde{\sigma}(t) \neq 0$ **for** $t \in (0, t_0)$ **and** $\tilde{\sigma}(t) = 0$ **elsewhere**

If a source in the fluid is turned on at $t = 0$ and turned off at $t = t_0$, the resulting velocity potential at large time can be expanded as:

$$\tilde{\Xi}(\vec{x}, \vec{x'}, \tilde{\sigma}(t)) = \tilde{\mathcal{W}}(\vec{x'}) \frac{\mathrm{e}^{-\mathrm{i}\omega_c t}}{t} \mathrm{e}^{\kappa\psi} + \text{c.c.} + O\left(\frac{1}{t^2}\right) \qquad \text{as } t \to \infty \tag{B.46}$$

where $\tilde{\mathcal{W}}$ is independent of time and is given by

$$\tilde{\mathcal{W}}(\vec{x'}) = \mathrm{i}2\sqrt{2}\kappa \int_0^{t_0} \tilde{\sigma}(\tau) \mathrm{e}^{\mathrm{i}\omega_c \tau} \, \mathrm{d}\tau \, . \tag{B.47}$$

**Case III:** $\sigma(t) = q_1 = t^{-1}\mathrm{e}^{-\mathrm{i}\omega_c t}$ **for** $t > t_0$ **and** $q_1 = 0$ **elsewhere**

For a source of variable strength given by $t^{-1}\mathrm{e}^{-\mathrm{i}\omega_c t}$ for $t > t_0$, the resulting velocity potential at large time can be expanded as:

$$\begin{aligned} \Xi(\vec{x}, \vec{x'}, q_1) = (\mathcal{C}_1 \ln t + \bar{\mathcal{C}}_1) \frac{\mathrm{e}^{-\mathrm{i}\omega_c t}}{t} e^{\kappa\psi} + \hat{\mathcal{C}}_1 \frac{\mathrm{e}^{\mathrm{i}\omega_c t}}{t} e^{\kappa\psi^*} \\ + \frac{\mathrm{e}^{-\mathrm{i}\omega_c t}}{t} \mathcal{H}(\vec{x}, \vec{x'}) + O\left(\frac{1}{t^2}, \frac{\mathrm{e}^{-\mathrm{i}\omega_c t}}{t^2}\right) \qquad \text{as } t \to \infty \end{aligned} \tag{B.48}$$

where the constants $\mathcal{C}_1 = \mathrm{i}2\sqrt{2}\kappa$, $\bar{\mathcal{C}}_1$ and $\hat{\mathcal{C}}_1$ are given by

$$\bar{\mathcal{C}}_1 = \mathrm{i}2\sqrt{2}\kappa \left( -\ln t_0 + \pi^{-\frac{1}{2}} \sum_{n=1}^{\infty} \frac{\Gamma(n + \frac{1}{2})}{n! n} \right) , \qquad \hat{\mathcal{C}}_1 = -i2\sqrt{2}\kappa \int_{\frac{k_0 U t_0}{2}}^{\infty} \frac{\mathrm{e}^{-\mathrm{i}\lambda}}{\lambda} d\lambda \tag{B.49}$$

and the time-independent function $\mathcal{H}$ is given by

$$\begin{aligned} \mathcal{H}(\vec{x}, \vec{x'}) = \frac{1}{R} - \frac{1}{R_1} + \mathrm{i}2 \int_0^{\frac{\pi}{2}} \frac{\cos\theta}{(1 + \cos\theta)^{\frac{1}{2}}} [\mathcal{F}(\mathcal{M}_2) - \mathcal{F}(\mathcal{M}_1)] \, \mathrm{d}\theta \\ + \frac{4m_0}{\pi} \int_0^{\frac{\pi}{2}} \mathrm{d}\theta \int_0^{\infty} \frac{\mathcal{F}^*(m)}{m m_0 + m^2 \cos\theta + \kappa} \, \mathrm{d}m \\ + \frac{4m_0}{\pi} \int_0^{\frac{\pi}{2}} \mathrm{d}\theta \int_0^{\infty} \frac{\mathcal{F}(m)}{(m + \mathcal{M}_1)(m - \mathcal{M}_2)} \, \mathrm{d}m \end{aligned}$$

$$-\frac{2m_0}{\pi}\int_0^{\frac{\pi}{2}} \mathrm{d}\theta \int_L \frac{\mathcal{F}(m)}{(m-\mathcal{M}_1)(m+\mathcal{M}_2)}\,\mathrm{d}m \tag{B.50}$$

with wave numbers $\mathcal{M}_{1,2}$ and function $\mathcal{F}$ given by

$$\mathcal{M}_{1,2} = \frac{(1+\cos\theta)^{\frac{1}{2}} \pm 1}{2\cos\theta} m_0 \,, \tag{B.51}$$

$$\mathcal{F}(m) = m^2 \cos[m^2(y-y')\sin\theta] e^{m^2[(y-y')-\mathrm{i}(x-x')\cos\theta]} \,. \tag{B.52}$$

# Appendix C

# Nonlinear wave-body interactions in finite depth

In this appendix, we extend the high-order spectral method for nonlinear wave-body interactions to include the effect of finite depth.

In finite depth, the velocity potential $\Phi$ needs to satisfy the zero Neumann boundary condition $\Phi_z = 0$ on the bottom $z = -h$, where the water depth $h$ is assumed to be constant. In principle, this requires the consideration of the image of the body with respect to the bottom.

With the high-order spectral method, the bottom condition can be treated as an essential boundary condition for the basis functions. In the construction of these global basis functions, the images of singularity distributions on the body and the mean free surface with respect to the bottom must be considered. This can be easily accomplished by replacing the deep-water Green function $G$ in (3.3), (3.4), (4.3), and (4.4) by the finite-depth Green function $G_h$. Here $G_h$ satisfies the zero Neumann boundary condition on the bottom and is simply given by:

$$G_h(\mathbf{x}, z; \mathbf{x}', z') = G(\mathbf{x}, z; \mathbf{x}', z') + G(\mathbf{x}, z; \mathbf{x}', -z' - 2h) \,. \tag{C.1}$$

To study the effect of finite depth, as an example, we choose to study the wave diffraction force on a fixed and submerged circular cylinder. With parameters $kA =$

| $h/R$ | $\bar{F}_x/\rho g\epsilon^2 A^2$ | $\bar{F}_z/\rho g A^2$ |
|---|---|---|
| $\infty$ | -12.0075 | 0.6737 |
| 4.0 | -7.2700 | 0.6628 |
| 3.5 | 1.2574 | 0.6310 |

Table C.1: The mean horizontal and vertical forces on the fixed and submerged circular cylinder for different water depth $h$. $\epsilon = kA = 0.04, kR = 0.4, H/R = 1.5$; and $N_w$=32, $N_F$=64$N_w$, $N_B = 256$, $T/\Delta t$=64, $\tau_0$=5$T$.

0.04, $kR = 0.4$ and $H/R = 1.5$ fixed, table C.1 shows the nonlinear results with order $M = 4$ for the mean horizontal and vertical forces on the body for a range of water depth. The decrease of the water depth reduces the magnitude of the negative horizontal drift force and eventually changes the sign of the drift force to be positive. The mean vertical force is also reduced as the water depth becomes smaller.

# Appendix D

# Evaluation of the vertical surface velocity in long-short wave interactions

In this appendix, we present explicit formulae for the evaluation of the vertical surface velocity in extending the high-order spectral method to the study of long-short wave interactions.

As shown in the evolution equation (2.8), the key to the success of time simulations of nonlinear wave-wave/body interactions is the accurate and efficient evalutation of the vertical surface velocity $\Phi_z(\mathbf{x}, \eta(\mathbf{x}, t), t)$.

With the high-order spectral method, at a given instant of time, we first solve boundary-value problems for the perturbation potentials $\Phi^{(m)}$ up to a specified order $M$ and then calculate $\Phi_z(\mathbf{x}, \eta(\mathbf{x}, t), t)$ in terms of its Taylor series expansion about the mean free surface $z = 0$.

In a mode-coupling approach, it is known that the surface potential expansion diverges as the perturbation order increases when two different length scales are encountered. Therefore, the high-order spectral method is believed to fail in the presence of long-short wave interactions. However, Brueckner and West (1988) recently showed that the perturbation expansion for $\Phi_z(\mathbf{x}, \eta(\mathbf{x}, t), t)$ on the free surface is convergent with respect to the order $M$ although that for the surface potential $\Phi(\mathbf{x}, \eta(\mathbf{x}, t), t)$ is

divergent. This implies that the high-order spectral method is actually valid for the study of long-short wave interactions if the vertical surface velocity can directly be evaluated (i.e. not through the calculation of the perturbation potentials).

Base on the surface potential expansion and through theoretical analyses, we derive the following explicit formulae for the direct calculation of the vertical surface velocity in terms of known surface elevation $\eta(\mathbf{x},t)$ and potential $\Phi^s(\mathbf{x},t)$:

$$\Phi_z(\mathbf{x},\eta(\mathbf{x},t),t) = W^{(1)} + W^{(2)} + W^{(3)} + \cdots \,, \tag{D.1}$$

where the perturbation velocities are given by

$$W^{(1)} = \frac{\partial \Phi^s}{\partial z} \,, \qquad z = 0 \,; \tag{D.2}$$

$$W^{(2)} = (\eta\frac{\partial}{\partial z} - \frac{\partial}{\partial z}\eta)W^{(1)} \,, \qquad z = 0 \,; \tag{D.3}$$

$$\begin{aligned} W^{(3)} &= (\eta\frac{\partial}{\partial z} - \frac{\partial}{\partial z}\eta)W^{(2)} \\ &+\frac{1}{2}\left[\eta(\eta\frac{\partial}{\partial z} - \frac{\partial}{\partial z}\eta) - (\eta\frac{\partial}{\partial z} - \frac{\partial}{\partial z}\eta)\eta\right]\frac{\partial^2\Phi^s}{\partial z^2} \,, \qquad z = 0 \,. \end{aligned} \tag{D.4}$$

In a typical mode-coupling approach, $\eta$ and $\Phi^s$ are expanded in Fourier series:

$$\eta(\mathbf{x},t) = \sum_n \eta_n(t) e^{i\mathbf{k}_n\mathbf{x}} \,; \tag{D.5}$$

$$\Phi^s(\mathbf{x},t) = \sum_n \phi^s_n(t) e^{i\mathbf{k}_n\mathbf{x}} \,, \tag{D.6}$$

and the z-derivatve of $\Phi^s$ is calculated by

$$\Phi^s_z(\mathbf{x},t) = \sum_n |\mathbf{k}_n| \phi^s_n(t) e^{i\mathbf{k}_n\mathbf{x}} \,. \tag{D.7}$$

# Bibliography


[1] M. Abramowitz and I. A. Stegun. *Handbook of Mathematical Functions.* Dover Press, New York, 1964.

[2] T. R. Akylas. On the excitation of nonlinear water waves by a moving pressure distribution oscillating at resonant frequency. *Phys. Fluids*, 27:2803-2807, 1984.

[3] J. A. Aranha, D. K. P. Yue, and C. C. Mei. Nonlinear waves near a cut-off frequency in an acoustic duct – a numerical study. *J. Fluid Mech.*, 121:465-485, 1982.

[4] G. R. Baker, D. I. Meiron, and S. A. Orszag. Generalized vortex methods for free-surface flow problems. *J. Fluid Mech.*, 123:477-501, 1982.

[5] D. J. Benney. Nonlinear gravity wave interactions. *J. Fluid Mech.*, 14:577-589, 1962.

[6] M. Belzons, E. Guazzelli, and O. Parodi. Gravity waves on a rough bottom: experimental evidence of one-dimensional localization. *J. Fluid Mech.*, 186:539-558, 1988.

[7] H. B. Bingham. *Simulating ship motions in the time domain.* PhD thesis, Massachusetts Institute of Technology, Cambridge, Massachusetts, 1994.

[8] R. Brard. The representation of a given ship form by singularity distributions when the boundary condition on the free surface is linearized. *J. Ship Res.*, 16:79-92, 1972.

[9] K. A. Brueckner and B. J. West. Vindication of mode-coupled descriptions of multiple-scale water wave fields. *J. Fluid Mech.*, 196:585-592, 1988.

[10] R. Cointe. Nonlinear simulation of transient free surface flows. In *5th Intl. Conf. on Numerical Ship Hydro.*, Hiroshima, Japan, 1989.

[11] J. R. Chaplin. Nonlinear forces on a horizontal cylinder beneath waves. *J. Fluid Mech.*, 147:449-464, 1984.

[12] D. R. Crawford, B. M. Lake, P. G. Saffman, and H. C. Yuen. Stability of weakly nonlinear deep-water waves in two and three dimensions. *J. Fluid Mech.*, 105:177-191, 1981.

[13] D. Dagan and T. Miloh. Free-surface flow past oscillating singularities at resonant frequency. *J. Fluid Mech.*, 120:139-154, 1982.

[14] R. A. Dalrymple and J. T. Kirby. Water waves over ripples. *J. Waterways, Port, Coastal Ocean Engng*, 112:309-319, 1986.

[15] A. G. Davies. The reflection of wave energy by undulations on the seabed. *Dyn. Atmos. Oceans*, 6:207-232, 1982.

[16] A. G. Davies and A. D. Heathershaw. Surface-wave propagation over sinusoidally varying topography. *J. Fluid Mech.*, 144:419-443, 1984.

[17] C. R. De Prima and T. Y. Wu. On the theory of generating of surface waves on water by moving obstacles. In *9th Intl. Conf. of Applied Mech.*, Brussels, Belgium, 1956.

[18] W. R. Dean. On the reflection of surface waves by a submerged circular cylinder. *Proc. Camb. Phil. Soc.*, 44:483-491, 1948.

[19] J. Dern. Existence, uniqueness and regularity of the solution of Neumann-Kelvin problem for two or three dimensional submerged bodies. *Proc. 13th Symp. Naval Hydro.*, Tokyo, Japan, pages 57-77, 1980.

[20] P. Devillard, F. Dunlop, and B. Souillard. Localization of gravity waves on a channel with a random bottom. *J. Fluid Mech.*, 186:521-538, 1988.

[21] D. G. Dommermuth, W. M. Lin, D. K. P. Yue, R. J. Rapp, E. S. Chan, and W. K. Melville. Deep water plunging breakers: a comparison between potential theory and experiments. *J. Fluid Mech.*, 189:423-442, 1988.

[22] D. G. Dommermuth and D. K. P. Yue. Numerical simulations of nonlinear axisymmetric flows with a free surface. *J. Fluid Mech.*, 178:195-219, 1987a.

[23] D. G. Dommermuth and D. K. P. Yue. A high-order spectral method for the study of nonlinear gravity waves. *J. Fluid Mech.*, 184:267-288, 1987b.

[24] D. G. Dommermuth and D. K. P. Yue. Nonlinear three-dimensional wave-wave interactions using a high-order spectral method. In *Symposium on Nonlinear Wave Interactions in Fluids*, Boston, USA, 1987c.

[25] D. G. Dommermuth and D. K. P. Yue. The nonlinear three-dimensional waves generated by a moving surface disturbance. *Proc. 17th Symp. on Naval Hydro.*, Hague, Netherlands, 1988.

[26] O. J. Emmerhoff and P. D. Sclavounos. The slow-drift motion of arrays of vertical cylinders. *J. Fluid Mech.*, 242:31-50, 1992.

[27] B. Fornberg and G. B. Whitham. A numerical and theoretical study of certain nonlinear wave phenomena. *Phil. Trans. R. Soc. Lond.*, A289:373-404, 1978.

[28] A. Friis. A second order diffraction forces on a submerged body by a second order Green function method. In *5th Intl. Workshop on Water Waves and Floating Bodies*, Manchester, UK, 1990.

[29] Y. Gota and Y. Suzuki. Estimation of incident and reflected waves in randaom wave experiments. *Coastal Eng.*, pages 828-845, 1976.

[30] J. Grue. Nonlinear water waves at a submerged obstacle or bottom topography. *Preprint Series of Institute of Mathematics, University of Oslo*, 2:1-21, 1991.

[31] J. Grue and E. Palm. Wave radiation and wave diffraction from a submerged body in a uniform current. *J. Fluid Mech.*, 151:257-278, 1985.

[32] E. Guazzelli, V. Rey, and M. Belzon. Higher-order Bragg reflection of gravity surface waves by periodic beds. *J. Fluid Mech.*, 245:301-317, 1992.

[33] T. Hanaoka. Theoretical investigation concerning ship motion in regular waves. *Proc. Symp. on the Behaviour of Ships in a Seaway*, Netherland, pages 266-285, 1957.

[34] M. D. Haskind. The hydrodynamic theory of ship oscillations in rolling and pitching. *Prikl. Mat. Mekh*, 10:33-66, 1946. (Engl. transl., *Tech. Res. Bull.*, 1-12:3-43, Soc. Nav. Archit. Mar. Eng., New York, 1953.)

[35] M. D. Haskind. On wave motion of a heavy fluid. *Prikl. Mat. Mekh.*, 18:15-26, 1954.

[36] K. Hasselmann. On the nonlinear energy transfer in a gravity wave spectrum. Part I: General theory. *J. Fluid Mech.*, 12:481-500, 1962.

[37] K. Hasselmann. On the nonlinear energy transfer in a gravity wave spectrum. Part II: Conservation theorems; wave particle analogy; Irreversibility. *J. Fluid Mech.*, 15:273-281, 1963a.

[38] K. Hasselmann. On the nonlinear energy transfer in a gravity wave spectrum. Part III: Evaluation of the energy flux and sea-swell interaction for a Neumann spectrum. *J. Fluid Mech.*, 15:385-398, 1963b.

[39] T. H. Havelock. The resistance of a submerged cylinder in accelerated motion. *Quart. J. Mech. Appl. Math.*, 2:419-427, 1949.

[40] T. H. Havelock. The effect of speed of advance upon the damping of heave and pitch. *Quarterly Transaction of the Institution of Naval Architects*, 100:131-135, 1958.

[41] R. Inoue and Y. Kyozuka. On the nonlinear wave forces acting on submerged cylinders. *J. Soc. Nav. Arch.*, Japan, 156;115-127, 1984.

[42] R. Jefferys. A slender body model of ringing. In *8th Intl. Workshop Water Waves & Floating Bodies*, St. John's, Newfoundland, 1993.

[43] F. John. On the motion of floating bodies. Part II, *Comm. Pure Appl. Math.*, 3:45-101, 1950.

[44] M.-H. Kim and D. K. P. Yue. The nonlinear sum-frequency wave excitation and response of a tension-leg platform. In *5th Intl. Conf. Behaviour Offshore Structures*, Norway, 1988.

[45] M.-H. Kim and D. K. P. Yue. The complete second-order diffraction solution for an axisymmetric body. Part 1: monochromatic incident waves. *J. Fluid Mech.*, 200:235-264, 1989.

[46] M.-H. Kim and D. K. P. Yue. The complete second-order diffraction solution for an axisymmetric body. Part 2: bichromatic incident waves and body motions. *J. Fluid Mech.*, 211:257-293, 1990.

[47] J. T. Kirby. A general wave equation for waves over rippled beds. *J. Fluid Mech.*, 162:171-186, 1986.

[48] N. E. Kochin. On the wave-making resistance and lift of bodies submerged in water. *Central Aero-Hydrodynamical Institute, Moscow*, pages 65-134, 1937. (Engl. transl., *Tech. Res.*, Bull. No. 1-8, Soc. Nav. Archit. Mar. Eng., New York, 1952.)

[49] F. T. Korsmeyer, C.-H. Lee, J. N. Newman, and P.D. Sclavounos. The analysis of wave interactions with tension leg platforms. In *OMAE Conference*, Houston, Texas, 1988.

[50] C.-H. Lee and J. N. Newman. First- and second-order wave effects on a submerged spheroid. *J. Ship Res.*, 35:183-190, 1991.

[51] C.-H. Lee, J. N. Newman, M.-H. Kim, and D. K. P. Yue. The computation of second-order wave loads. In *OMAE Conference*, Stavanger, Norway, 1991.

[52] C.-M. Lee and J. N. Newman. The vertical mean force and moment of submerged bodies under waves. *J. Ship Res.*, 15:231-245, 1971.

[53] W. M. Lin and D. K. P. Yue. Time-domain analysis for floating bodies in mild-slope waves of large amplitude. *Proc. 18th Symp. on Naval Hydro.*, Ann Arbor, Michigan, 1990.

[54] Y. Liu, D. G. Dommermuth, and D. K. P. Yue. A high-order spectral method for nonlinear wave-body interactions. *J. Fluid Mech.*, 245:115-136, 1992.

[55] Y. Liu and D. K. P. Yue. On the solution near the critical frequency for an oscillating and translating body in or near a free surface. *J. Fluid Mech.*, 254:251-266, 1993.

[56] Y. Liu and D. K. P. Yue. The mean pitch moment on a submerged spheroid. *Submitted for publication*, 1994a.

[57] Y. Liu and D. K. P. Yue. The time-dependence of the wave resistance of a body. *Submitted for publication*, 1994b.

[58] Y. Liu and D. K. P. Yue. The nonlinear seakeeping solution near the critical frequency. *Submitted for publication*, 1994c.

[59] Y. Liu and D. K. P. Yue. Resonant reflection of surface waves travelling over bottom undulations. *Submitted for publication*, 1994d.

[60] M. S. Longuet-Higgins. Resonant interactions between two trains of gravity waves. *J. Fluid Mech.*, 12:321-332, 1962.

[61] M. S. Longuet-Higgins. The mean forces exerted by waves on floating or submerged bodies with applications to sand bars and wave power machines. *Proc. R. Soc. Lond.*, A352:463-480, 1977.

[62] M. S. Longuet-Higgins and E. D. Cokelet. The deformation of steep surface waves on water. I a numerical method of computation. *Proc. R. Soc. Lond.*, A350:1-26, 1976.

[63] M. S. Longuet-Higgins and N. D. Smith. An experiment on third-order resonant wave interactions. *J. Fluid Mech.*, 25:417-435, 1966.

[64] J. K. Lunde. On the linearized theory of wave resistance for displacement ships in steady and accelerated motion. *Trans. of the Society of Naval Arch. and Marine Eng.*, pages 1-61, 1951.

[65] H. Maruo. The drift force of a body floating on waves. *J. Ship Res.*, 4(4):1-10, 1960.

[66] H. Maruo. Application of the slender body theory to the longitudinal motion of ships among waves. *Bull. Fac. Eng., Yokohama Natl. Univ.*, 16:29-61, 1967.

[67] M. McIver and P. McIver. Second-order wave diffraction by a submerged circular cylinder. *J. Fluid Mech.*, 219:519-529, 1990.

[68] C. C. Mei. Numerical methods in water-wave diffraction and radiation. *Ann REv. Fluid Mech.*, 10:393-416, 1978.

[69] C. C. Mei. *The applied dynamics of ocean surface waves.* John Wiley & Sons, New-York, 1983.

[70] C. C. Mei. Resonant reflection of surface water waves by periodic sand-bars. *J. Fluid Mech.*, 152:315-335, 1985.

[71] C. C. Mei, T. Hara, and M. Naciri. Note on Bragg scattering of water waves by parallel bars on the seabed. *J. Fluid Mech.*, 186:147-162, 1988.

[72] J. W. Miles. Surface-wave scattering matrix for a shelf. *J. Fluid Mech.*, 28:755-767, 1967.

[73] H. Miyata, G. Khalil, Y.-G. Lee, and M. Kanai. An experimental study of the Nonlinear forces on horizontal cylinders. *J. Kansai Soc. N.A.*, Japan, 209:11-23, 1988.

[74] A. Mo and E. Palm. On radiated and scattered waves from a submerged elliptic cylinder in a uniform current. *J. Ship Res.*, 31:23-33, 1987.

[75] D. E. Nakos and P. D. Sclavounos. Steady and unsteady ship wave patterns. *J. Fluid Mech.*, 215:265-288, 1990.

[76] J. N. Newman. The damping and wave resistance of a pitching and heaving ship. *J. Ship Res.*, 3:1-19, 1959.

[77] J. N. Newman. *Marine Hydrodynamics.* M. I. T. Press, Cambridge, Mass., 1977.

[78] J. N. Newman. The theory of ship motions. *Adv. Appl. Mech.*, 18:221-283, 1978.

[79] J. N. Newman. Evaluation of the wave-resistance Green function. Part 1: the double integral. *J. Ship Res.*, 31:79-90, 1987.

[80] J. N. Newman. The Green function for potential flow in a rectangular channel. *J. Eng. Maths.*, 26:51-59, 1992.

[81] J. N. Newman. Wave-drift damping of floating bodies. *J. Fluid Mech.*, 249:241-259, 1993.

[82] J. N. Newman. *Private communication*, 1994.

[83] T. F. Ogilvie. First and second-order forces on a cylinder submerged under a free surface. *J. Fluid Mech.*, 16:451-472, 1963.

[84] T. F. Ogilvie. Second-order hydrodynamic effects on ocean platforms. In *Intl Workshop ship & Platform Motion*, Berkeley, pages 205-265. 1983.

[85] T. F. Ogilvie and E. O. Tuck. A rational strip theory for ship motions, Part I. Technical Report 013, The Department of Naval Architecture and Marine Engineering, The University of Michigan, Ann Arbor, Michigan, 1969.

[86] T. J. O'Hare and A. G. Davies. A comparison of two models for surface-wave propagation over rapidly varying topography. *Appl. Ocean Res.*, 15:1-11, 1993.

[87] S. A. Orszag. Numerical simulation of incompressible flows within simple boundaries: accuracy. *J. Fluid Mech.*, 49:75-112, 1971.

[88] E. Palm. Non-linear wave reflection from a submerged circular cylinder. *J. Fluid Mech.*, 233:49-63, 1991.

[89] O. M. Phillips. On the dynamics of unsteady gravity waves of finite amplitude. Part 1. The elementary interactions. *J. Fluid Mech.*, 9:193-217, 1960.

[90] D. Resio and W. Perrie. A numerical study of nonlinear energy fluxes due to wave-wave interactions. Part I: Methodology and basic results. *J. Fluid Mech.*, 223:603-629, 1991.

[91] S. H. Salter, D. C. Jeffrey, and J. R. M. Taylor. The architecture of nodding duck wave power generators. *The Naval Arch.*, pages 21-24, 1976.

[92] L. W. Schwartz. Computer extension and analytic continuation of Stokes' expansion for gravity waves. *J. Fluid Mech.*, 62:553-578, 1974.

[93] P. K. Stansby and A. Slaouti. On non-linear wave interaction with cylindrical bodies: a vortex sheet approach. *Appl. Ocean Res.*, 6:108-115, 1983.

[94] T. Stokka. A third-order wave model. Technical Report 93-2071, DET Norske Veritas Research AS, Norway, 1994.

[95] E. O. Tuck. The effect of nonlinearity at the free surface on flow past a submerged cylinder. *J. Fluid Mech.*, 22:401-414, 1965.

[96] F. G. Tricomi. *Integral Equations.* Dover Press, New York, 1957.

[97] F. Ursell. Surface waves on deep water in the presence of a submerged circular cylinder I. *Proc. Camb. Phil. Soc.*, 46:141-152, 1950.

[98] F. Ursell. The decay of the free motion of a floating body. *J. Fluid Mech.*, 19:305-319, 1964.

[99] F. Ursell. On head seas travelling along a horizontal cylinder. *J. Inst. Maths. Applics.*, 4:414-427, 1968.

[100] F. Ursell. Mathematical notes on the two-dimensional Kelvin-Neumann problem. *Proc. 13th Symp. on Naval Hydro.*, Tokyo, pages 245-255, 1980.

[101] T. Vada. A numerical solution of the second-order wave-diffraction problem for a submerged cylinder of arbitrary shape. *J. Fluid Mech.*, 174:23-37, 1987.

[102] T. Vinje and P. Brevig. Numerical calculations of forces from breaking waves. *Intl. Symp. Hydro. Ocean Eng.*, Norway, 1981.

[103] J. V. Wehausen. Effect of the initial acceleration upon the wave resistance of ship models. *J. Ship Res.*, 8:38-50, 1964.

[104] J. V. Wehausen. The wave resistance of ships. *Adv. Appl. Mech.*, 13:93-245, 1973.

[105] J. V. Wehausen and E. V. Laitone. Surface Waves. In *Handbuch der Physik*, pages 446-778. Springer, 1960.

[106] G. X. Wu. On the second order wave reflection and transmission by a horizontal cylinder. *Appl. Ocean Res.*, 13:58-62, 1991.

[107] G. X. Wu and R. Eatock Taylor. The exciting force on a submerged spheroid in regular waves. *J. Fluid Mech.*, 182:411-426, 1987.

[108] G. X. Wu and R. Eatock Taylor. Radiation and diffraction of water waves by a submerged sphere at forward speed. *Proc. R. Soc. Lond.*, A417:433-461, 1988.

[109] H. Xu and D. K. P. Yue. Computations of fully-nonlinear three-dimensional water waves. *Proc. 19th Symp. on Naval Hydro.*, Seoul, Korea, 1992.

[110] V. E. Zakharov. Stability of periodic waves of finite amplitude on the surface of a deep fluid. *J. Appl. Mech. and Tech. Phys.*, 9:190-194, 1968 (English Trans.).

[111] S. J. Zaroodny and M. D. Greenberg. On a vortex sheet approach to the numerical calculation of water waves. *J. Comp. Phys.*, 11:440-446, 1973.